2015

Life-Cycle Management of Civil and Marine Structures under Fatigue and Corrosion Effects

Mohamed Soliman
Lehigh University

Life-Cycle Management of Civil and Marine Structures under Fatigue and Corrosion Effects

by

Mohamed Soliman

A Dissertation

Presented to the Graduate Research Committee

of Lehigh University

in Candidacy for the Degree of Doctor of Philosophy

in

Structural Engineering

Lehigh University

January 2015

January 2015

Approved and recommended for acceptance as a dissertation in partial fulfillment of the requirements for the degree of Doctor of Philosophy.

Date

Dr. Dan M. Frangopol
Dissertation Advisor
Professor of Civil and Environmental Engineering, Lehigh University

Accepted Date

Committee Members:

Dr. John L. Wilson
Committee Chairperson
Professor of Civil and Environmental Engineering, Lehigh University

Dr. Ben T.Yen
Member
Emeritus Professor of Civil and Environmental Engineering, Lehigh University

Dr. Clay J. Naito
Member
Associate Professor of Civil and Environmental Engineering, Lehigh University

Dr. Liang Cheng
Member
Associate Professor of Computer Science and Engineering, Lehigh University

ACKNOWLEDGEMENTS

First of all, I would like to express my appreciation to my advisor Prof. Dan M. Frangopol for his guidance, endless patience and continuous support throughout my Ph.D. pursuit. I am grateful to Prof. Frangopol for providing me the opportunity to co-author seventeen papers for publication in reputable scientific journals and for selecting me to participate in multiple tasks to develop my capabilities as a researcher, teacher, and professional engineer. I also appreciate his patience and how he kindly tolerated my special personal circumstances. Moreover, his frequent and critical, yet friendly, guidance kept me on track. As a result, ten journal papers have already been published, and seven are under review, in addition to three book chapters, more than twenty five conference and keynote papers, and a paper that won the 2014 prestigious J. James R. Croes Medal of the American Society of Civil Engineers. Additionally, I was awarded the P.C. Rossin Fellowship of Lehigh University in 2012. My gratitude is extended to Professors Wilson, Yen, Naito, and Cheng who served on my Ph.D. committee and evaluated my work.

I gratefully acknowledge the support by grants from (a) the National Science Foundation (NSF) Award CMS-0639428, (b) the Commonwealth of Pennsylvania, Department of Community and Economic Development, through the Pennsylvania Infrastructure Technology Alliance (PITA) through several contracts, (c) the U.S. Federal Highway Administration (FHWA) Cooperative Agreement Award DTFH61-07-H-00040, (d) the U.S. Office of Naval Research (ONR) Awards N00014-08-1-0188 and N00014-12-1-0023, and (e) the National Aeronautics and Space Administration (NASA) Award NNX10AJ20G.

I would like to thank my former and current colleagues Dr. Sunyong Kim, Dr. Kihyon Kwon, and Alysson Mondoro for their contributions to parts of this study. I thank Dr. Paolo Bocchini, Dr. Alberto Decò, Dr. Duygu Saydam, and You Dong for their constructive discussions and comments to improve this study, and their warm friendship. Special thanks to my office mates Benjin Zhu and Samatha Sabatino for their assistance, encouragement and warm friendship. I would also like to thank Dr. Giorgio Barone for his contribution to this study during his post-doctoral work at Lehigh University.

Finally and most importantly, I sincerely thank my wife Hebatallah for her love, support, patience, and understanding. I would also like to thank my parents Soliman and Soheir, and my sons Yassin, Moustafa, and Omar.

TABLE OF CONTENTS

LIST OF TABLES

LIST OF FIGURES

ABSTRACT

Infrastructure systems are under continuous deteriorating effects due to various environmental and mechanical stressors. These effects can be generated by sudden threats such as earthquakes, tornadoes, blast, and fire, or gradual deterioration due to fatigue and corrosion. Moreover, as indicated in the 2013 American Society of Civil Engineers (ASCE) Report Card of America's Infrastructure, the United States' infrastructure systems are highly deteriorating with a required estimated investment of 3.6 trillion USD to improve their condition within the next seven years. Given the limited financial resources, rational methodologies are required to support the optimum budget allocation while maintaining maximum possible safety levels. Uncertainties associated with the performance prediction, damage initiation and propagation, damage detection capabilities, and the effect of maintenance and retrofit on the structural performance add more challenges to this allocation process. In this context, life-cycle engineering provides rational means to optimize budget allocation and manage an infrastructure system starting from the initial design and construction to dismantling and replacing the system at the end of its service life.

This study provides novel management methodologies which support the decision-making process for civil and marine large-scale structural systems under fatigue and corrosion deterioration. Multi-objective optimization models that seek the optimal trade-offs between conflicting life-cycle management (LCM) aspects such as the life-cycle cost and the projected service life are proposed. These models provide the optimum intervention schedules (e.g., inspections and maintenance actions) which fulfil the LCM goals. For the first time in the field of life-cycle management, an approach capable of

establishing the optimum inspection, monitoring, and repair actions simultaneously is proposed. Maximizing the expected service life, minimizing the total life-cycle cost, minimizing the maintenance delay, and maximizing the probability of damage detection are examples of the considered optimization goals. It is shown that the implementation of optimum solutions resulting from the proposed management plans can significantly reduce the life-cycle cost. A methodology for planning inspection actions for bridges with multiple critical fatigue details is proposed. This is considered a step forward from the traditional approaches which are only capable of considering one critical fatigue detail. Additionally, this study provides methodologies for the reliability-based performance evaluation of structures under fatigue deterioration. Furthermore, rational approaches which make use of structural health monitoring (SHM) and non-destructive inspection information for the near real-time decision making for deteriorating structures are proposed. Specifically, an approach to obtain the fatigue reliability of aluminium high-speed naval vessels based on SHM information is proposed. By using the proposed approach, the effect of individual operational conditions encountered by the ship on the overall fatigue damage accumulation can be quantified. This quantification is not possible by using the traditional fatigue life estimation methods. Probabilistic reliability methods and Monte Carlo simulation are implemented to account for uncertainties associated with different aspects of the LCM process. Existing large-scale structural systems are analysed to demonstrate the feasibility and effectiveness of the proposed methodologies.

CHAPTER 1 INTRODUCTION

1.1 Overview

Structures and infrastructure systems play a significant role in improving the economic, social, and environmental welfare of nations. These systems are subjected to deterioration due to aging effects (e.g., corrosion), natural hazards (e.g., seismic events and hurricanes), and man-made extreme events (e.g., collisions and terrorist attacks). A sudden failure or loss of functionality of these systems may have severe economic, social, and environmental impacts. Recent studies suggest that the consequences of failure are significantly more than just the cost of rebuilding or replacing the dysfunctional components, especially if the social and environmental impacts are included (Bocchini *et al.* 2014; Dong *et al.* 2013). Moreover, it has been shown that structural failures may have significant long-term consequences. Therefore, in order to minimize the number of failures and their consequences, infrastructure managers adopt various activities to maintain the adequate long-term performance and functionality while satisfying financial constraints. These activities include periodic inspections, maintenance, retrofit actions, in addition to structural health monitoring (SHM), which can provide an accurate indication on the actual structural responses and aid in predicting the performance and evaluating future maintenance needs.

Although these activities assist in maintaining the performance of a system within acceptable limits, they may create a major financial burden. Accordingly, these activities should be rationally scheduled along the life-cycle of the structural system within an integrated framework capable of simultaneously considering various conflicting

economic and safety requirements. Additionally, uncertainties associated with the performance prediction, damage initiation and propagation, damage detection capabilities, and the effect of maintenance and retrofit on the structural performance should be included for the proper life-cycle management (LCM).

Since most infrastructure management decisions are made under strict budgetary constraints, optimization is an essential tool for the LCM. By employing optimization techniques, trade-offs between conflicting LCM criteria such as minimizing the life-cycle cost and maximizing the expected service life can be identified. Indeed, this process can be computationally demanding, especially when performed on a probabilistic basis. However, recent increase in the computational capabilities permitted conducting complex large-scale simulations and paved the road for advanced probabilistic techniques to be applied for infrastructure management problems (Okasha & Frangopol 2010c, 2011).

An ultimate comprehensive LCM framework will be in the form of integrated modules responsible for performing various management computational tasks. These tasks include performance prediction under uncertainty, optimization of interventions, and reliability- and cost-informed decision making, among others. An attempt to formulate such framework is presented in Frangopol (2011) and Frangopol *et al.* (2012). This framework has been applied to various types of structural systems such as bridges and naval vessels. The development of such framework required a parallel development of an integrated computational platform which combines different modules of the life-cycle framework to establish the optimum life-cycle decisions. The platform consists of a central user interface (e.g., MATLAB® (MathWorks Inc. 2014b) or VisualScript (VisualScript 2006)) responsible for the data flow to/from separate computational

modules which perform different tasks of the life-cycle analysis such as the structural analysis (e.g., ABAQUS (ABAQUS 2009)), reliability analysis (e.g., RELSYS (Estes & Frangopol 1998)), and structural optimization (e.g., MATLAB® (MathWorks Inc. 2014a)), among others. This framework has been introduced through several studies which handle the infrastructure management of multiple types of structural systems including bridges (Kim & Frangopol 2011b,2012; Kwon & Frangopol 2011; Okasha & Frangopol 2010a,b,2012) and naval vessels (Kim & Frangopol 2011a,c; Kwon & Frangopol 2012a,b; Okasha *et al.* 2010, 2011). Several of these studies aimed to investigate the life-cycle performance of deteriorating systems, while others focused on evaluating the life-cycle cost considering maintenance and repair actions, in addition to scheduling these actions to yield optimum life-cycle decisions. Despite the large number of studies related to the LCM framework presented in Frangopol (2011), several enhancements to the available framework are still required. Specifically, more methodologies are needed to (a) aid in the accurate estimation of the deteriorating structural performance and the life-cycle cost under uncertainty, (b) optimally plan inspection, monitoring, and maintenance actions along the service life of a structure, (c) support the efficient integration of SHM information for enhancing the LCM and decision making capabilities, and (d) reduce the gap between theory and practice in the LCM field. Accordingly, several of these enhancements are addressed in this study.

1.2 Objectives

The objectives of this study are:

1- Develop probabilistic approaches that aid in the accurate estimation of the deteriorating structural performance under uncertainty.

2- Develop approaches to simultaneously schedule inspection, monitoring, and maintenance activities for deteriorating structures in a life-cycle context.
3- Develop optimization methodologies to assist the LCM of structures deteriorating at multiple locations.
4- Develop an approach to integrate field inspection data into the LCM framework for enhanced decision making.

1.3 Summary of the Proposed Approach

In this study, analyses have been performed to enhance the capabilities of the LCM framework proposed in Frangopol (2011) and Frangopol *et al.* (2012). A modified version of this framework, shown schematically in Figure 1.1, is formulated as the combination of seven interconnected modules. Each of these modules is responsible for performing a certain task and contributes to the fulfillment of the overall LCM goal, (i.e., providing the optimal management decisions for the analyzed structure). The framework starts with analyzing the structure under investigation to determine the deteriorating mechanisms affecting the structure (i.e., Module 1). As shown in Figure 1.1, the proposed life-cycle analysis scheme can be applied to bridges or naval vessels. Time-variant structural performance and reliability are next assessed (i.e., in Module 3) to determine the current condition of the analyzed components or the entire structure. Multiple performance measures can be used to study the performance of the component or system under investigation. Uncertainty in modeling and randomness in loading, requiring the use of probability-based concepts for quantifying the structural performance, are considered in this module. Examples of such measures include, but are not limited to, reliability, redundancy, robustness, risk, and vulnerability, in addition to the performance

measures based on lifetime functions (Leemis 1995). In this study, focus is placed on estimating the structural performance in terms of reliability, probabilistic damage level (i.e., time-variant crack size, or corrosion depth), and lifetime functions (e.g., the probability density function (PDF) of the time to failure). Using the damage level as the performance measure facilitates decision making and interpretation of the results; thus, it aids in the real-world implementation of the management plans. Performance prediction is performed at this stage to forecast the future damage evolution and project the performance level of the structure up to the end of its service life. Time-dependent damage propagation and hazard sources, such as the fatigue crack propagation, corrosion penetration, and increasing traffic loads are included in this process.

Since the performance prediction is the foundation of the LCM, it is desirable to increase the accuracy of this process to ensure a reliable management process. SHM provide information about the actual structural responses under service loads which can be used to enhance the accuracy of the LCM process. Inspection information provides an indication on the actual damage level at the inspected location. As shown in Figure 1.1, whenever available, information provided by previous inspection or health monitoring is implemented in the structural performance assessment process (i.e., Module 2). This information is incorporated to enhance the quality of the performance prediction process. SHM information can be especially useful for fatigue assessment and service life prediction of structural details. SHM in this case provides an estimate of the stress range and the average number of cycles occurring at the detail. In this study, probabilistic fatigue assessment based on the *S-N* (i.e., stress-life) (Fisher *et al.* 1998) approach and SHM data are proposed to find the fatigue reliability of critical bridge and high speed

ship details. Additionally, stress range and cycle count prediction based on SHM data are used to study the crack growth at several steel bridge details. For these details, Monte Carlo simulation (Robert & Casella 1999) is implemented to find the PDF of the time to failure for the investigated bridge details.

Optimization is next applied to obtain the optimal inspection/monitoring/ maintenance schedules which fulfill the LCM goals. These goals include minimizing the life-cycle cost, maximizing the structural performance during service life of deteriorating structures, and maximizing the service life of the structure. Moreover, multiple goals can be included simultaneously in the optimization scheme, where the results come in the form of a Pareto-optimal solution set (Arora 2012). Each point belonging to the Pareto-optimal solution set represents an optimum inspection/monitoring/maintenance strategy that satisfies the optimization constraints. Results of the optimization process are used by decision makers to find the optimal management strategy that best suits their needs, as well as any other practical considerations regarding this specific application.

Next, as shown in Figure1.1, the selected optimum management plan is applied to the structure under investigation. At any point in time through the structure life-cycle, if SHM or inspection information becomes available, this information can be used to update the load and/or resistance parameters to yield more accurate prediction models (i.e., through Modules 5 and 6). The updated performance prediction will result in an updated intervention schedule. Performance updating based on SHM and inspection information has been an active line of research. In this study, a Bayesian updating approach, in which information from inspections is used to represent the likelihood function, is adopted. This function is combined with the prior information on model parameters to find their

posterior distributions, and ultimately, updated time-variant performance profiles. The approach is used to enhance the decision making process for the management of fatigue critical structures.

1.4 Contributions of the Proposed Approach

This study adds several enhancements to the capabilities of the LCM framework; especially, with respect to the optimization of management activities along the life-cycle and the integration of inspection and SHM information to improve the decision making abilities. The following are the main contributions of this study:

1- Propose an approach which provides optimum inspection times and types for a structure with multiple deteriorating locations. The approach provides the optimal inspection times and optimum inspection methodology that should be used for each location during an inspection.

2- Propose a novel integrated approach for optimizing the times and types of inspection, monitoring, and maintenance activities along the service life of a deteriorating structure. The approach can be applied under several types of deterioration such as fatigue, corrosion of steel girders, and uniform and pitting corrosion of reinforcing steel in reinforced concrete (RC) members. This approach is considered as a step forward since it handles three types of interventions (i.e., inspection, monitoring, and maintenance), whereas available approaches in literature can only handle one type of interventions.

3- Formulate a probabilistic framework for integrating field inspection information to enable updating the management plans and to support the informed real-time decision making under uncertainty.

4- Propose a reliability-based approach based on bi-linear *S-N* relationships to investigate the possible further improvement of the current AASHTO *S-N* specifications.

5- Formulate a reliability-based methodology which integrates SHM data to enable investigating the individual effects of the different operational conditions on the fatigue reliability of high-speed aluminum naval vessels. The approach also enables the reliability-based quantification of the fatigue life under a complete operational profile. Additionally, a simplified, yet accurate, methodology is proposed to find the reliability-based remaining fatigue life.

1.5 Outline

- **Chapter 1** serves as introduction.
- **Chapter 2** presents general performance prediction and optimization methods used throughout the subsequent chapters of the study. An introduction to probabilistic and reliability concepts for performance evaluation of components and systems is presented. Methodologies for predicting the initiation and propagation of uniform and pitting corrosion damage in RC members are discussed. Additionally, a brief review of the *S-N* approach and the application of linear elastic fracture mechanics (LEFM) for fatigue performance evaluation is presented. Furthermore, the general concepts of intervention (i.e., inspection, monitoring, and/or maintenance) scheduling using multi-criteria optimization are provided.
- **Chapter 3** proposes a method for fatigue assessment and service life prediction for existing steel bridge details by integrating SHM into a probabilistic bi-linear *S-N* approach. The *S-N* lines have different slopes above and below constant amplitude

fatigue threshold (CAFT). The aim of the study is to investigate the possible implementation of the bi-linear *S-N* approach in the current AASHTO *S-N* specifications. SHM information is used to build stress range bin histograms. Next, the best fit for the PDF of the stress range is identified and used to find an estimate of the time-variant fatigue reliability. The effect of the second slope and its probabilistic properties on the fatigue reliability is investigated. The resulting reliability profile is used to find the reliability-based fatigue service life. The work in this chapter is mainly related to Modules 2 and 3 of the LCM framework (see Figure 1.1).

- **Chapter 4** presents a reliability-based fatigue life estimation approach for aluminum high-speed naval vessels. The approach utilizes SHM data collected during seakeeping trials to obtain the fatigue damage accumulation with respect to the ship's operational condition. The operational condition is defined in terms of the navigation speed, heading angle, and sea conditions. The obtained damage accumulation is next used to find the time-variant fatigue reliability, using the second order reliability method (SORM), and the reliability-based fatigue life. This approach can be effectively used to adjust the safe operational envelope of the ship. Additionally, formulations which provide an approximate value for the reliability-based fatigue life are proposed. This chapter also aims at improving the performance prediction (i.e., Modules 2 and 3 in Figure 1.1) capabilities of the framework.
- **Chapter 5** proposes a methodology for establishing the optimum inspection, monitoring, and maintenance scheduled which minimizes the life-cycle cost and maximizes the service life of structures subjected to fatigue and corrosion deterioration. The approach accounts for uncertainties associated with the

performance prediction, damage initiation and propagation, the relationship between the degree of damage and the probability of damage detection, and the effect of maintenance activities on the service life. An event tree model which provides the probabilities of different outcomes of an inspection action is established and used for obtaining the expected service life, life-cycle cost, and the delay associated with maintenance plans. Several applications analyzing bridges and ships under fatigue and corrosion deterioration are presented. This chapter is mainly related to Modules 3 and 4 of the LCM framework.

- **Chapter 6** presents an approach for integrating information collected during inspections into the LCM framework. Based on the difference between the predicted and the measured damage level at the time of the inspection, a Bayesian updating approach is implemented to find updated damage propagation model parameters. Damage level measurements obtained during an inspection are used to construct the likelihood function which is next implemented to establish the posterior distributions of the damage propagation model parameters. An updated and more accurate damage propagation model results from this process which is next implemented to find updated LCM plans. The work in this chapter spans across Modules 3 to 7 shown in Figure 1.1.
- **Chapter 7** proposes a methodology for inspection scheduling for bridges subjected to fatigue and corrosion at multiple locations. Based on SHM data, Monte Carlo simulation is performed to draw samples from the PDF of time to failure of each of the critical locations. These PDFs are integrated into an event tree model to compute the probability of detection at each of the inspected locations. Next, an optimization

scheme is formulated to find the optimum inspection times which maximize the probability of damage detection at all the inspected location and minimizes the total inspection cost. The approach provides the optimum inspection times, as well as the best inspection method that should be used at each of the inspected locations. The work in this chapter covers Modules 2, 3, and 4 of the framework in Figure 1.1.

- **Chapter 8** proposes a system-based methodology to plan for future inspection and maintenance actions for bridges subjected to corrosion and time-dependent increasing traffic loads. The bridge model is constructed using the series-parallel system formulations and the time-variant performance profile is established. An optimization model is constructed to find the optimum inspection and maintenance schedule which minimizes the maximum expected annual system failure rate and minimizes the expected total inspection and maintenance cost. This chapter focuses on Modules 3 and 4 of the framework in Figure 1.1.
- **Chapter 9** presents a computational procedure to integrate sustainability measures into the LCM framework and estimate the effect of indirect economic, social, and environmental costs arising from bridge maintenance activities on the life-cycle cost of steel bridges. In most of LCM studies, the total life-cycle cost is considered to be composed of inspection, monitoring, and maintenance cost. In this chapter, it is shown that these indirect costs can be substantial. The chapter also compares the computed life-cycle cost of an existing steel bridge constructed using conventional painted carbon steel to that of a similar bridge constructed using corrosion resistant steel. This chapter generally serves the whole framework.

- **Chapter 10** summarizes this study, draws conclusions, and recommends future research directions.

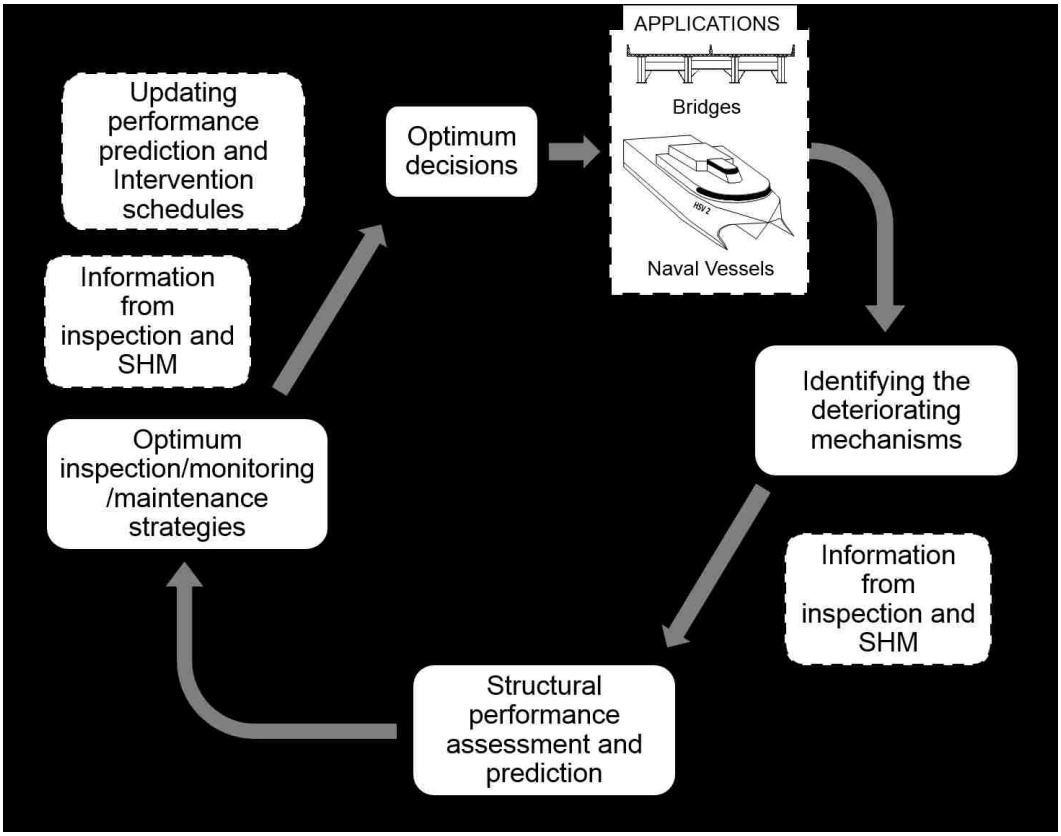

Figure 1.1 Life-cycle management framework

CHAPTER 2 BACKGROUND

2.1 Overview

This chapter presents the general methods used for the LCM of civil and marine structures throughout this study. An introduction to probability and reliability concepts for time-variant performance evaluation of components and systems is presented. A brief review of the *S-N* approach and the application of LEFM for fatigue performance evaluation is presented. Additionally, methodologies for predicting the initiation and propagation of uniform and pitting corrosion damage in RC members are discussed. The general concepts of intervention (i.e., inspection, monitoring, and/or maintenance) scheduling using multi-criteria optimization are also discussed. Finally, the role of SHM information in the damage diagnosis and prognosis, and in supporting the goals of the LCM is presented.

2.2 Time-variant Performance Prediction

Time-dependent structural deterioration processes such as corrosion, fatigue, and increase in demand (e.g., increase in traffic volume) impose continuous aging effects on infrastructure systems. These effects, individually or when combined with those arising from extreme events such as earthquakes and hurricanes, can cause catastrophic consequences. Time-dependent deterioration significantly alters the resistance of the structure and reduces the initial structural load carrying capacity (Barone & Frangopol 2013a,b). Accordingly, the life-cycle of infrastructure systems should be clearly analyzed taking into consideration various aging effects.

The complexity of this type of analysis may increase due to the presence of various aleatory and epistemic uncertainties (Ang & Tang 2007) associated with structural damage occurrence and propagation, as well as, the damage detection processes. These uncertainties should be considered in the life-cycle analysis throughout the integrated life-cycle framework for management of the aging infrastructures. Reliability-based methods for performance assessment of structures offer the means for integrating uncertainties associated with the resistance and load effects. The service life can also be computed based on the reliability threshold. Additionally, these methods provide a rational way to assess the overall structural safety; in contrast to commonly employed methods of designing and evaluating structural systems on component basis. In the next subsections, the main concepts for computing the reliability of components and structural systems are presented.

2.2.1 Structural reliability analysis

In general, the reliability of a structural component can be related to the probability of failure, defined as the probability of violating a certain limit state $g = 0$. The performance function g is defined as

$$g = R - Q \tag{2.1}$$

where R and Q are, respectively, the random capacity and demand of the structure. Based on the defined limit state function, the probability of failure P_f can be defined as

$$P_f = P(g \leq 0) \tag{2.2}$$

The PDFs of R, S, and g as well as the probability of failure P_f are represented in Figure 2.1 Thus, the reliability index β can be defined as

$$\beta = \Phi^{-1}(1 - P_f) \tag{2.3}$$

where $\Phi^{-1}(\cdot)$ denotes the inverse standard normal cumulative distribution function (CDF).

For cases where *R* and *S* are statistically independent random variables following the normal or lognormal distributions, exact expressions for calculating the reliability index can be formulated (Ditlevsen & Madsen 2007). For more complex problems, where *R* and *S* follow a PDF other than normal or lognormal, efficient reliability techniques can be used to evaluate the component reliability, such as the first order method (FORM), second order method (SORM), and Monte Carlo simulation (Ang & Tang 1984, 2007; Melchers 1999). The FORM and SORM have been widely employed in many structural reliability problems and various software packages, such as RELSYS (Estes & Frangopol 1998) and CalREL (Liu *et al.* 1989), to calculate the reliability indices of structural components and systems.

System reliability concepts

System-based reliability can be thought of as an extension of the component reliability or single failure mode evaluation to cover multiple components or failure modes of the system under consideration. In these methods, complex interactions within the system are taken into account to evaluate the overall system performance. Different system configurations such as the series, parallel, or series-parallel system interactions, shown in Figure 2.2, can be considered.

For this type of analysis, regardless of the system configuration, the system reliability is expressed in terms of the component reliabilities. For a series system (i.e., Figure 2.1 (a), in which the failure of any component will lead to the system failure, the system probability of failure is defined as

$$P_{fsys} = P_f(g_1 \leq 0 \cup g_2 \leq 0 \cup ..... \cup g_n \leq 0) \tag{2.4}$$

where g_n represents the performance function of the *n*th component. On the other hand, for a parallel system, in which the system failure occurs with the failure of all components, the system failure probability is defined as

$$P_{fsys} = P_f(g_1 \leq 0 \cap g_2 \leq 0 \cap ..... \cap g_n \leq 0) \tag{2.5}$$

Similarly, the system probability of failure for different series-parallel configurations can be formulated. For more complex systems, different methods such as the cut-set method can be used to represent the system performance (Rausand & Høyland 2004).

System reliability in a life-cycle context

For life-cycle analysis, the evolution of the damage levels and system reliability with time should to be evaluated. Thus, the component limit state becomes a function of time as

$$g(t) = R(t) - Q(t) = 0 \tag{2.6}$$

and the instantaneous probability of failure is defined as (Ellingwood 2005; Frangopol 2011)

$$P_f(t) = \int_0^\infty F_R(x,t)\, f_S(x,t) dx \tag{2.7}$$

where $F_R(x,t)$ is the instantaneous CDF of the resistance and $f_S(x,t)$ is the instantaneous PDF of the load effects at time *t*.

Measures for the reliability of systems over a given period of time has been defined by researchers such as the time-dependent reliability indicator defined by Mori & Ellingwood (1993). This performance indicator provides the probability of survival of a structural system subjected to a sequence of discrete loading events described by a

Poisson's process with mean occurrence rate of λ_o during a period of time t_L. Thus the calculated reliability can be considered as time-dependent reliability. Computer programs such as RELTSYS (Enright & Frangopol 2000) were developed to quantify the reliability of general series-parallel systems by using the reliability function proposed by Mori & Ellingwood (1993).

2.2.2 Performance assessment based on lifetime functions

Lifetime functions (Leemis 1995) offers multiple performance indicators for the structural reliability of components and systems. These indicators have been successfully used for the LCM of bridges under corrosion deterioration (see Yang *et al*. 2004, Okasha & Frangopol 2009, 2010a,b,c; Orcesi & Frangopol 2011b). Multiple lifetime functions can be defined, including the time to failure PDF, cumulative probability of failure, survivor function, hazard function, and cumulative hazard function. Each of these functions has different interpretation and represents a distinctive feature that can be implemented within the general LCM framework. Three of these functions, defined in this section, will be used later in this study.

Time to failure probability density function.

The random time to failure T of a component, is defined as the time elapsing from placing the component into operation until it fails for the first time (Rausand & Høyland 2004). The PDF of the time to failure can be found through the statistical information of the damage propagation model and it is the first step to calculate the rest of the lifetime reliability measure. For small time interval Δt and a given time t, this PDF provides the

probability that the failure will occur between the time t and $(t+\Delta t)$. Therefore, it has the following probabilistic interpretation (Leemis 1995)

$$f_T(t)\Delta t = P\left(t \le T \le (t+\Delta t)\right) \tag{2.8}$$

where $P(\cdot)$ represents the probability of occurrence of the event between parentheses.

Cumulative probability of failure and Survivor function.

The cumulative probability of failure $F_T(t)$ represents the probability that component is not functioning at time t and is expressed as

$$F_T(t) = P(T \le t) = \int_0^t f(x)dx \tag{2.9}$$

The survivor function $S_T(t)$, on the other hand, represents the probability that the component will be functioning at time t, and it is calculated as the complement of the cumulative probability of failure

$$S_T(t) = 1 - F_T(t) = P(T \ge t) = \int_t^\infty f(x)dx \tag{2.10}$$

The survivor function provides a measure of the reliability of the component since it constitutes the definition that the structure is functioning at time t (Leemis 1995). Figure 2.3 represents schematically the relationship between $f_T(t)$, $F_T(t)$, and $S_T(t)$. As shown, at a certain time t_i, the cumulative probability of failure value $F_T(t_i)$ is represented by the area A_1, whereas the survivor function value $S_T(t_i)$ is represented by the area $A_2 = 1 - A_1$. In this study, lifetime functions have been used to model the structural performance under corrosion and fatigue deterioration.

2.2.3 Fatigue assessment of civil and marine structures

Fatigue is one of the major concerns in steel and aluminum structures (e.g., bridges and ships). Fatigue damage can exist in mild environments as well as aggressive ones, in which the latter is known as corrosion-induced fatigue. For a component subjected to elastic stress fluctuations, fatigue damage may accumulate at regions of stress concentration where the local stress exceeds the yield limit of the material. Stress concentrations can occur at the component due to the presence of initial flaws in the material, welding process, or fabrication. Initiation and propagation of cracks in the plastic localized region occurs due to the cumulative damage acting over a certain number of stress fluctuations. These cracks can eventually cause the fracture of the component. This process can be minimized by adopting better details, avoiding stress concentrations and decreasing the number of welded attachments, among others. Currently, design specifications provide guidelines for maximizing the fatigue life and offer means for selecting details associated with higher fatigue resistance (Barsom & Rolfe 1999).

Fatigue for civil and marine structures can generally be assessed by the *S-N* approach and the fracture mechanics approach (also known as the crack growth approach). The former gives relationship between the stress acting on the detail and the predicted number of stress cycles to failure while the latter provides a theoretical model to calculate the crack size in relation to the number of cycles acting on the detail. A brief discussion on both approaches is given in the next subsections.

The S-N approach

In the *S-N* approach, the fatigue life of a certain detail is determined in a laboratory test by applying constant or variable amplitude stress cycles to the detail until a crack with predefined size grows through the detail. The test is repeated for several specimens and for different stress amplitudes. Next, the stress range amplitude is plotted versus the number of cycles to failure in a logarithmic scale plot, as shown in Figure 2.4, and a linear or multi-linear fitting of the data is performed yielding the mean *S-N* lines. Due to the variability in test results, a design line is usually defined by codes in which the mean line is shifted to the left by a certain amount sufficient to achieve a satisfactory probability of survival for designed structures. For example, the AASHTO LRFD design specifications (AASHTO 2014) shift the mean line to the left by two standard deviations indicating that approximately 95% of the specimens would survive the associated number of cycles (Fisher *et al.* 1998). The resulting *S-N* relationship of the detail can be expressed, for a single slope *S-N* relation, as

$$S = \left(\frac{A}{N} \right)^{\frac{1}{m}} \tag{2.11}$$

in which S is the stress range (i.e., fatigue resistance), A is a fatigue detail coefficient for each category, N is the number of cycles, and m is a material constant defining the value of the slope of the *S-N* line.

Details in civil and marine structures are normally subjected to variable amplitude stress range cycles; therefore, an equivalent constant amplitude stress range is needed for fatigue assessment. Miner's rule (Miner 1945) is widely used to quantify the fatigue damage accumulation at details subjected to variable amplitude loading with a known

stress range histogram. By assuming a linear damage accumulation, Miner's damage accumulation index D is

$$D = \sum_{i=1}^{n_{ss}} \frac{n_i}{N_i} \tag{2.12}$$

where n_{ss} is the number of stress range bins in a stress-range histogram, n_i is the number of stress cycles in the ith bin with stress range S_i, and N_i is the number of cycles to failure under the stress range S_i. According to Miner's damage accumulation rule, the failure of the detail occurs when D = 1.0. However, research showed that this value is subjected to significant variability, and, up to date, no value is widely accepted by all research communities.

Based on Miner's damage accumulation rule, an equivalent constant amplitude stress range can be defined as

$$S_{re} = \left[\sum_{i=1}^{n_{ss}} \frac{n_i}{N_T} \cdot S_i^{\,m} \right]^{\frac{1}{m}} \tag{2.13}$$

where $N_T = \sum_{i=1}^{n_{ss}} n_i$. S_{re} can be alternatively calculated using the PDF $f_S(s)$ of the stress range S as

$$S_{re} = \left[\int_0^{\infty} s^{m_1} \cdot f_S(s) \cdot ds \right]^{\frac{1}{m_1}} \tag{2.14}$$

For structural details, the stress range can follow lognormal, Rayleigh, or Weibull distributions. The three-parameter PDFs of these distributions, including the cut-off threshold s_c, are expressed, respectively, as

$$f_S(s) = \frac{1}{(s - s_c)\cdot\zeta\cdot\sqrt{2\pi}} \cdot \exp\left[-\frac{1}{2}\cdot\left(\frac{\ln(s - s_c) - \lambda}{\zeta}\right)^2\right] \tag{2.15}$$

$$f_S(s) = \left(\frac{s - s_c}{S_{ro}^2}\right)\cdot\exp\left[-\frac{1}{2}\left(\frac{s - s_c}{S_{ro}}\right)^2\right] \tag{2.16}$$

$$f_S(s) = \frac{\kappa}{\alpha}\cdot\left(\frac{s - s_c}{\alpha}\right)^{\kappa-1}\cdot\exp\left[-\left(\frac{s - s_c}{\alpha}\right)^{\kappa}\right] \tag{2.17}$$

where $s > s_c$, α and κ are the scale and shape parameters of the Weibull distribution, respectively, λ and ζ are the location parameter and scale parameters of the lognormal distribution, respectively, and S_{ro} is the mode of the Rayleigh distribution. The cut-off threshold s_c is the lowest stress level considered in the stress range bin histogram (Fatemi & Yang 1998). In many cases, depending on the stress range bin histogram, a two-parameter PDF can be used considering $s_c = 0$.

-Using the equivalent constant amplitude stress range, fatigue life, measured as the number of cycles to failure, is calculated as

$$N = \frac{A}{S_{re}^m} \tag{2.18}$$

This number of cycles can be used in conjunction with the average annual number of cycles N_{avg} to estimate the fatigue life in years using the following equation

$$t_l(years) = \frac{N}{N_{avg}} \tag{2.19}$$

The *S-N* approach has been widely used for fatigue assessment of steel and aluminum structural details. Multiple design specifications and research reports are available for

fatigue design and assessment fatigue critical details by using the *S-N* approach (e.g., BS 5400 1980; ABS 2010; DNV 1997, 2010; Eurocode 3 2010; Eurocode 9 2009). Since the estimation of the resistance and demand terms in the *S-N* approach is straightforward, this approach has been successfully used for the reliability-based fatigue assessment of bridges and ships. For bridges, Kwon & Frangopol (2010) investigated the effect of the PDF of the equivalent stress range on the time-dependent fatigue reliability profile. They performed fatigue reliability prediction using the AASHTO *S-N* (AASHTO 2002) approach while making use of the available monitoring data of two bridges, the Birmingham Bridge and the Neville Island Bridge, located in Pittsburg, Pennsylvania, USA, which were monitored by personnel form the ATLSS Center at Lehigh University. The study focused on studying the effect of the stress range distribution type on the calculated fatigue reliability. It was concluded that the adopted probability distribution function for fatigue assessment has a great impact on the time-dependent reliability of the detail. The study compared three probability density functions for the use in modeling the stress range distribution of the studied detail: Weibull, Lognormal, and Gamma distributions. The effect of truncating the recorded stress range histograms generated from the field monitoring, as well as the annual increase rate of the number of cycles on the computed reliability profiles were also quantified. Kwon *et al.* (2012) investigated probabilistically the AASHTO *S-N* approach for the possible implementation of the bi-linear *S-N* lines. In this approach the *S-N* lines have a different slope above and below the CAFT. The study considered a slope above and below the CAFT to be 3.0 and 4.

For ship structures, Ayyub *et al.* (2002) proposed reliability-based design guidelines for fatigue of ship details. They briefly discussed the available fatigue

assessment methods for ship structures and their associated parameters. Kwon *et al.* (2013) conducted fatigue reliability assessment, based on SHM data, by estimating the probabilistic lifetime sea loads for high-speed ship structures. The British Standards *S-N* relationships (BS 5400 1980) were used in their approach.

The *S-N* approach is implemented in Chapters 3 and 4 to estimate the fatigue reliability and service life of bridge and ship details.

The fracture mechanics approach

Although the *S-N* approach is widely used for the fatigue assessment of structural details, it cannot be used to study the crack condition at a given detail since it does not provide a direct relation between the crack size and the number of cycles affecting the detail. The approach based on fracture mechanics, on the other hand, can be used to study the crack conditions and stability at a damaged detail. In this method, the stresses near the crack tip, which are responsible for the crack propagation, are related to the stress intensity factor *K*. LEFM can be applied through Paris' equation (Paris & Erdogan 1963) for assessing fatigue behavior of steel details. This equation relates the crack growth rate to the range of the stress intensity factor as follows

$$\frac{da}{dN} = C \cdot (\Delta K)^m \tag{2.20}$$

where a is the crack size, N is the number of cycles, and ΔK is the range of the stress intensity factor. C and m are material parameters. The values for C and m can be found through experimental reports or code specifications. The range of the stress intensity factor can be expressed as

$$\Delta K = Y(a) \cdot S \cdot \sqrt{\pi a} \tag{2.21}$$

Where S is the stress range and $Y(a)$ is a correction factor which depends on the crack orientation and shape. This correction factor takes into account the effects of the elliptical crack shape, free surface, finite width (or thickness), and non-uniform stress acting on the crack. More detailed empirical and exact solutions for these correction factors can be found in Tada *et al.* (2000).

Using Equations (2.20) and (2.21), the number of cycles associated with a growth in the crack size from an initial size of a_o to a size of a_t can be calculated as

$$N = \frac{1}{C \cdot S^m} \cdot \int_{a_o}^{a_t} \frac{1}{\left(Y(a) \cdot \sqrt{\pi a}\right)^m} da \tag{2.22}$$

By setting a_t in Equation (2.22) as the critical crack size a_f, the number of cycles to failure of the detail is obtained. This approach can also be implemented in the probabilistic fatigue life assessment and inspection and monitoring planning. For instance, Kim & Frangopol (2011c) used this approach to find the optimum inspection times which minimize the damage detection delay in fatigue critical steel details.

2.2.4 Performance evaluation of structures under corrosion

Corrosion in steel bridges

Corrosion deterioration of steel girders occurs mainly due to salt water exposure, resulting from the use of de-icing salts on the roads, and atmospheric corrosion of the metal (Estes & Frangopol 1999). Corrosion reduces the original thickness of the webs and flanges of steel girders. If undetected over an extended period of time, corrosion will weaken steel girder webs and flanges and possibly lead to structural failures. Corrosion is usually assumed to penetrate the top and sides of the bottom flanges, in addition to each

side of the web in the pattern shown in Figure 2.5. Due to heavier exposure to leaking salt water, corrosion can be assumed to occur throughout the web height at the supports, whereas only at the bottom quarter of the web height along the rest of the girder length including the mid-span location (Akgül & Frangopol 2004). Due to reductions in web and flange thicknesses, the values of time-variant properties of a steel girder (i.e., section modulus and web area) must be computed based on a corrosion penetration predicting model. If the steel section qualifies as compact, the plastic section modulus is used for determining flexural capacity of the section; otherwise, elastic section modulus is used. Estes & Frangopol (1999) applied such a formulation for modeling the corrosion of the steel girders of Colorado highway bridge E-17-AH. For compact sections, Akgül (2002) computed the plastic section modulus for interior regions of the span in terms of the corroded cross sectional area. In these studies, determination of the corrosion penetration depth over time was based on a corrosion penetration model for steel reported by McCuen & Albrecht (1995).

Severity of steel corrosion, in general, depends on the metal (composition of alloys in metal), local atmosphere (important environmental conditions affecting steel corrosion include temperature and relative humidity), and exposure conditions such as initial climate, sheltering, orientation, angle of exposure, time of wetness, atmospheric pollutants, deicing salt, and debris (Albrecht & Naeemi 1984). Models developed to predict time-variant corrosion penetration in steel are usually empirical formulae intending to capture the actual corrosion process. In most studies, a power function for the corrosion model is used. For example, McCuen & Albrecht (1995) proposed the following formula

$$p = b_o \cdot t^{b_1} \tag{2.23}$$

where b_o and p = the corrosion losses after one and t years, respectively, and b_1 is the slope of the logarithmic transformation of Equation (2.23). The values of different variables in the prediction model represented by Equation (2.23) can be found in McCuen & Albrecht (1995).

Corrosion of Concrete Bridges

Corrosion of steel reinforcement is one of the main factors causing the deterioration in RC structures. Its effect is accelerated when the member is subjected to de-icing salt spray. Corrosion can damage the RC member in various ways such as cracking, spalling, and loss of steel section, among others. Corrosion of reinforcement mainly occurs due to concrete carbonation and chloride penetration. This study considers chloride penetration as the main corrosion driving process. Chloride diffusion in reinforced concrete can be modeled by Fick's second law for nonsteady state diffusion (Stanish *et al*. 1997).

$$\frac{\partial C_c}{\partial t} = D_c \frac{\partial^2 C_c}{\partial x^2} \tag{2.24}$$

where C_c is the concentration of chloride ions (mass/volume), x is the distance from outer surface of the solid, and t represents the time (years). Crank's solution (Crank 1975) of this partial differential equation, using the boundary condition $C_c(x = 0,\ t > 0) = C_0$, initial condition $C_c(x > 0,\ t=0) = 0$, and the infinite point condition $(x = \infty,\ t > 0) = 0$, is

$$C_c(x,t) = C_0\left[1 - \text{erf}\left(\frac{x}{\sqrt{4D_c t}}\right)\right] \tag{2.25}$$

where C_0 is the chloride concentration on concrete surface and erf is the error function. The time t required to reach the chloride concentration $C(x, t)$ at a distance x from the

surface is obtained from Equation (2.25). The time $t = T_I$ required to reach a threshold level of chloride concentration C_{cr} at which the corrosion process will start is the corrosion initiation time.

For uniform corrosion (i.e., general), following the corrosion initiation the corrosion process is assumed to uniformly reduce the cross-sectional area of the steel reinforcement. This reduction is assumed to be constant along the entire surface area of the reinforcing bars. The reinforcement area $A_s(t)$ at time t is found as (Kim and Frangopol 2011b)

$$A_s(t) = \begin{cases} \dfrac{n_s \pi \, d_o^2}{4} & \text{for } 0 \le t \le T_I \\ \dfrac{n_s \pi \, (d_o - r_{corr}(t - T_I))^2}{4} & \text{for } t > T_I \end{cases} \tag{2.26}$$

where n_s = number of rebars subjected to corrosion effect; d_o = initial diameter of rebars (*mm*); and r_{corr} = rate of corrosion (*mm*/year).

According to Gonzalez *et al.* (1995) and Stewart (2004), corrosion can be highly localized, and the probability of failure due to the localized pitting corrosion is larger than that associated with the general corrosion model. The maximum penetration of pitting $PT(t)$ at time t is (Val & Melchers 1997)

$$PT(t) = r_{corr} R_c (t - T_I) \qquad \text{for } t > T_I \tag{2.27}$$

where r_{corr} = rate of corrosion (*mm*/*year*), R_c = ratio of maximum pit depth to average pit depth, and T_I = corrosion initiation time (*year*). The range of R is generally between 4 and 8 (Gonzalez *et al.* 1995). The remaining cross sectional area $A_r(t)$ of reinforcement can be expressed as (Val & Melchers 1997)

$$A_r(t) = \frac{\pi d_o^{\,2}}{4} - \frac{1}{2}\left[\theta_1\left(\frac{d_0}{2}\right)^2 - a\left|\frac{d_0}{2} - \frac{PT(t)^2}{d_0}\right|\right] - \frac{PT(t)^2}{2}\left[\theta_2 - \frac{a}{d_0}\right] \quad \text{for } PT(t) \le \frac{\sqrt{2}\,d_0}{2} \tag{2.28-a}$$

$$A_r(t) = \frac{1}{2}\left[\theta_1\left(\frac{d_0}{2}\right)^2 - a\left|\frac{d_0}{2} - \frac{PT(t)^2}{d_0}\right|\right] - \frac{PT(t)^2}{2}\left[\theta_2 - \frac{a}{d_0}\right] \quad \text{for } \frac{\sqrt{2}\,d_0}{2} < PT(t) \le d_0 \tag{2.28-b}$$

$$A_r(t) = 0 \quad \text{for } PT(t) > d_0 \tag{2.28-c}$$

where d_0 is the initial diameter of the reinforcement (*mm*), and

$$\theta_1 = 2\,arcsin\left(\frac{a}{d_0}\right) \quad \text{and} \quad \theta_2 = 2\,arcsin\left(\frac{a}{2PT(t)}\right) \tag{2.29-a}$$

$$a = 2PT(t)\left[1 - \left(\frac{PT(t)}{d_0}\right)^2\right]^{0.5} \tag{2.29-b}$$

The reinforcement area computed by using Equations (2.26) and (2.28) can be next used to find the ultimate capacity of the RC cross-section and its time-variant reliability. Akgül & Frangopol (2005a, b) analyzed three concrete bridges located in a bridge network in Colorado. Statistical descriptors of the three random variables (i.e. C_0, D_c, and C_{cr}) were determined based on the concrete mix design parameters, results of site-specific chloride content surveys, and values reported in Hutter & Donnelly (1977). They reported that the use of mix designs for calculating the diffusion coefficients for different strength concretes can provide a realistic representation of actual chloride penetration process of the reinforced concrete slabs and girders in existing bridges.

Along the same line, Marsh & Frangopol (2008) developed a reliability model incorporating temporal and spatial variations of probabilistic corrosion rate sensor data. Biondini *et al*. (2006) and Biondini & Frangopol (2008) proposed a structural performance framework for durability analysis of reinforced concrete structures subjected to the diffusive attack from external aggressive agents. Akiyama *et al.* (2012) proposed an approach for integration of the effects of airborne chlorides into reliability-based durability design of reinforced concrete structures in a marine environment.

Corrosion in ships

Several types of corrosion wastage in mild and low alloy steels in marine environments exist, such as uniform (general) corrosion, pitting corrosion, stress corrosion, and galvanic corrosion. For corrosion management and control, both localized and general corrosion must be considered. The former can cause oil or gas leaks, while the latter, which spreads over the surface of the affected area, is more likely to lead to structural strength problems. Stress corrosion occurs to some alloys when exposed to corrosive environments while mechanically stressed. Furthermore, when two different metals are physically connected, galvanic accelerated corrosion occurs to the less noble metal (ISSC 2009). Factors affecting marine immersion corrosion include the type of structural material, corrosion protection method (e.g., coating, cathodic protection), type of cargo or stored material, cycles of loading/unloading of cargo or stored material, humidity, and temperature (ISSC 2006).

In recent years, extensive work has been performed to investigate different parameters affecting the general corrosion wastage and to formulate corrosion wastage prediction models (Paik *et al.* 2003a,b; Melchers 2002, 2003a,b, 2004c, 2006; Guedes

Soares and Garbatov 1999a, Guedes Soares *et al.* 2005). For example, Guedes Soares *et al.* (2005) investigated the influence of salt content, water temperature, dissolved oxygen, PH value, and water velocity on the general corrosion rate and included these effects in the non-linear corrosion wastage model proposed in Guedes Soares & Garbatov (1999a). Their model consists of three corrosion loss stages. The first is penetration of the water particles through the corrosion coating, the second is the formation of the two-dimensional monolayer oxide film, and the third is the start and growth of the three-dimensional oxide nuclei. In this model, the first two stages represent the coating effectiveness period where the corrosion depth at any time t can be found as (Guedes Soares *et al.* 2005)

$$d(t) = d_{\infty}\left(1 - e^{\frac{-(t-\tau_c)}{\tau_t}}\right) \quad \text{for } t > \tau_c \tag{2.30-a}$$

$$d(t) = 0 \qquad \text{for } t \le \tau_c \tag{2.30-b}$$

where $d(t)$ is the time dependent corrosion depth, d_{∞}, τ_c, and τ_t are model parameters depending on the coating type, operational and environmental conditions.

Melchers (2003a, 2003b, 2006) developed a corrosion wastage prediction model consisting of the following phases of average corrosion loss: (a) short-term initial phase in which the corrosion is governed by the chemical kinetics, (b) approximated linear function dependent on the oxygen diffusion from surrounding water, (c) non-linear function governed by oxygen diffusion through corrosion product layer, (d) anaerobic bacterial corrosion phase, and (e) linearly approximated long-term anaerobic bacterial corrosion phase.

Research work has also been performed to model pitting corrosion. However, the scarcity of corrosion depth measurements for this type of corrosion compared to the general corrosion poses additional challenges. In this context, Melchers (2004a, 2004b) proposed a multiphase model for pitting corrosion loss as a function of exposure time.

Due to the importance of the corrosion assessment and repair topic, multiple classification societies issued recommendations and regulations for corrosion coating, prevention, inspection and repair of corroded steel ships (e.g., DNV 1998, 1999; IACS 2003). Corrosion wastage prediction is a process covered by various uncertainties; thus, it has to be conducted probabilistically. Although many corrosion models are available, these models are based on statistical data collected from different vessels; as new construction techniques and materials emerge, these models should be updated and refined.

Time-dependent corrosion losses have an effect on the structural resistance of the ship and should be considered in its life-cycle performance assessment (Kwon & Frangopol 2012a). Corrosion losses may cause reduction in the hull structural resistance, reduction in the local strength, and increase in the fatigue crack propagation within the affected areas. Considering general corrosion, multiple studies have been performed to predict the time-variant hull structural resistance by estimating the loss in the hull girder section modulus due to corrosion (e.g., Ayyub *et al.* 2000; Paik & Wang 2003; Okasha *et al.* 2010; Decò *et al.* 2011, 2012). It is observed that most of the analytical studies tend to overestimate the effect of corrosion on the hull girder strength. In an attempt to address this point, Wang *et al.* (2008) presented a statistical study showing the loss in the hull

girder section modulus in a database of 222 steel ships. This type of analysis can support the verification and calibration of the hull resistance prediction models.

Aluminum alloys used in ship construction, mainly 5xxx-series alloy, have excellent corrosion resistance in marine environment. Part of the corrosion resistance of aluminum is attributed to the formation of a thin oxide layer which prevents the core metal from any further corrosion. This layer is hard and renews itself almost instantly in case of any mechanical abrasion. It is very stable under most conditions except for extreme PH values where it may lose its stability; additionally, the self-renewal may not be fast enough to prevent further corrosion. However, since aluminum is a very active metal, it is highly prone to galvanic corrosion if not properly isolated. Galvanic action, especially at areas where both steel and aluminum are connected, makes the aluminum vulnerable to corrosion. The corrosion damage in this case may be very fast (ISSC 2009). An example of this type of problem is the USS Independence LCS-2, a 127.4 meters, high-speed trimaran capable of speeds up to 44 knots, in which corrosion initiated at the locations where the aluminum hull was in contact with the steel propulsion system (O'Rourke 2012). However, this mode of corrosion can be easily prevented by the use of appropriate isolations or cathodic protection systems.

Another mode of deterioration of aluminum ships is sensitization, which is a degradation mode that occurs in high-magnesium aluminum alloys (e.g., 5083, 5086, 5456, and 5383) when exposed to elevated temperature (Sielski 2007). Under certain conditions, these alloys may suffer intergranular corrosion due to the precipitation of the beta-phase (Mg_2Al_3) on the grain boundaries. This precipitate is electromechanically more active than the aluminum matrix and can cause further intergranular corrosion with

the continued grain boundary migration. Furthermore, this process increases the material susceptibility to stress corrosion cracking, exfoliation, and decreased ductility. Recent studies were carried out to find the time required to sensitize the material based on the thermal profile of the ship. However, this is directly related to the location of the plate within the ship as it is heavily dependent on the stress profile acting on the studied location (Sielski *et al.* 2012).

2.3 Life-cycle Optimization

After evaluating the structural performance and based on the severity of the deterioration, decisions regarding repair or strengthening the managed structural systems have to be made. However, due to the large number of these deteriorating structures, financial resources are usually not available to meet all the maintenance and repair needs. On the other hand, it is known that in some cases, the cost of maintaining the infrastructures might be more than the cost of building new ones (Miyamoto *et al.* 2000). Therefore, the reduction of maintenance costs is a challenge that must be addressed in the integrated maintenance management framework. The proper allocation of the available maintenance and management budgets can be done through the life-cycle optimization process.

For service life extension, maintenance interventions are scheduled to either extend the time required for the structure to reach its performance threshold or to improve the performance of the structure if its threshold is reached. Thus, maintenance types may be categorized into two general groups: preventive (PM) and essential (EM) (Kong & Frangopol 2003a,b, Frangopol & Soliman 2014b). PM actions are usually time-based, that is, they are applied at pre-specified time instants over the life-cycle of the structure.

In contrast, EM actions are performance-based in that they are applied when some performance indicators reach pre-defined target values. The effect of both maintenance types on the performance profile of a structure is shown in Figure 2.6. After obtaining the time-variant structural performance profile, threshold-based EM application times can be obtained as shown in the following example.

2.3.1 Example 2.1

To illustrate the EM planning and reliability concepts for fatigue assessment of a steel structures, consider a detail subjected to stress range which follows Weibull distribution with mean 12.57 MPa and standard deviation 7.91 MPa and an average annual number of cycles of 1.5×10^{6}. Additionally, the detail is classified under fatigue category F of the BS 5400 (1980) specifications,

The material constant *m* for this detail is 3.0, while the constant *A* (see Equation 2.18) is assumed to follow a lognormal distribution with mean of 6.29×10^{11} MPa^3 and a coefficient of variation of 0.54 (Kwon *et al.* 2013). Based on Equation (2.14), the equivalent constant amplitude stress range S_{re} is 17.64 MPa. To account for uncertainty in this value, S_{re} is assumed to follow a lognormal distribution with mean 17.64 MPa and coefficient of variation 0.1.

In order to study the fatigue reliability of the detail, a performance function can be defined as the safety margin

$$g(t) = \Delta - D(t) \tag{2.31}$$

where Δ = Miner's critical damage accumulation index, indicating the allowable accumulated damage and assumed lognormal distributed with mean 1.0 and coefficient of

variation (COV) 0.3 (Wirsching 1984); $D(t)$ = Miner's damage accumulation index, which can be expressed as

$$D(t) = \frac{N(t)}{A} \cdot S_{re}^{m} \tag{2.32}$$

Based on Equations. (2.31) and (2.32) and assuming that the random variables S_{re}, A, and Δ are also lognormally distributed, the fatigue reliability index β can be computed as (Kwon & Frangopol 2010)

$$\beta(t) = \frac{\lambda_{\Delta} + \lambda_{A} - m \cdot \lambda_{S_{re}} - \ln N(t)}{\sqrt{\zeta_{\Delta}^{2} + \zeta_{A}^{2} + (m \cdot \zeta_{S_{re}})^{2}}} \tag{2.33}$$

where λ and ζ are the parameters associated with different random variables. Using Equation (2.33), the reliability profile of the detail can be found as shown in Figure 2.7 (a). The fatigue life of the detail can be calculated by setting a threshold for the reliability index. For structural details subjected to fatigue, a reliability index threshold ranging from 2.0 to 4.0 is appropriate (Mansour *et al.* 1996). For this example, this threshold is set to be 3.0 yielding a fatigue life without maintenance of 9.4 years.

Threshold-based EM, in which the performance is restored to the initial level, can be applied to extend the service life. As shown in Figure 2.7 (b), EM can be performed at 9.4 and 18.8 years yielding a total service life of 28.2 years (i.e, life extension of 18.8 years).

Although the maintenance planning provided in this example is straightforward, other cases of maintenance optimization are not as simple. Especially if multiple maintenance actions of varying types are applied to the structure and each of them yields its own service life extension. In this case, probabilistic optimization techniques should be used efficiently to solve such problems. Therefore, optimization is an essential tool for

providing best decision support in the LCM framework. Components of this framework rely on this computationally intensive process to find the best solution fulfilling the objectives and satisfying the predefined constraints. This describes optimization as the core of infrastructures management process. All elements of this process interact and sometimes conflict, calling for the use of multi-criteria optimization that can extract the best solution among conflicting elements (Frangopol 2011). Different objectives for the life-cycle optimization have been included in recent research work such as, extending the service life of the structure, minimizing damage detection delay, and minimizing the life-cycle cost, among others. Moreover, different conflicting objectives can also be considered simultaneously yielding a Pareto-optimal solution set. Figure 2.8 provides an example of such Pareto fronts in which an optimization problem is solved to find the optimum intervention schedule which maximizes the service life and minimizes the expected life-cycle cost. Each of the points on the solutions front represents an optimum management plan which has its own optimum inspection and/or maintenance times which provide the optimal trade-offs among the conflicting objectives.

Genetic algorithms (GAs) have been used in this study to solve such complex optimization problems mainly due to: (a) the use the objective function directly and not its derivatives, which is, in many cases, difficult or impossible to obtain, (b) the ease of handling discrete variables, (c) the search from a population of points rather than from a single point, and (d) the ease of implementation in a parallel computing environment, which significantly reduces the computational effort. The topic of intervention optimization is covered in detail in Chapters 5-8 of this study.

2.4 Role of Structural Health Monitoring and Non-destructive Inspection

Inspection and SHM play a great role in the damage identification and assessment of civil and marine structures. Departments of transportation across the United States are mandated to inspect their bridges on regular basis (FHWA 2012). These inspections are performed biannually or annually depending on many factors such as the volume of the traffic, age of the bridge, and the bridge condition. Bridges are then rated depending on various performance indicators. However, these inspections are usually performed visually and in some cases they are performed by personnel who can give misleading information regarding the condition of the bridge deeming the inspection to be ineffective. Catbas *et al.* (2007) reported that more than 50% of the visually inspected bridges can be misclassified. Factors affecting inspection errors include, visual acuity and color vision, inspector rushed level, and accessibility (FHWA 2001). In fact, visual inspections may not ensure that fatal problems will be detected (Swartz & Lynch 2008). An example of these cases is the I-35W Mississippi River Bridge which was classified to be structurally deficient and yet was still open for traffic when it collapsed in 2007. Additionally, visual inspection for fatigue damage has significant limitations; especially for sub-surface corrosion and fatigue cracks. For this reason, critical bridges are better evaluated using special non-destructive inspection (NDI) methods such as ultrasonic inspection. NDI based inspections can give more reliable information about the current condition of the examined locations. Moreover, integrating the outcomes of these inspections with the knowledge about the loads and stresses in the tested locations of the structure can help predict the future damage propagation.

The quality of an inspection method can be represented by the probability of detection (*PoD*) function which gives the probability that, given the inspection method, a certain flaw size can be detected. Due to the direct relationship between the inspection outcomes and the maintenance decisions, it is crucial to make sure that the inspections have the highest quality and performed at the optimum times (Kim & Frangopol 2011a).

On the other hand, NDI methods, such as ultrasonic inspection, face more challenges arising from the large scale of the structure and number of locations requiring inspection. In addition, the exact location of damage is generally required to apply this type of inspections; which is generally not the case. Research in the field of NDI and SHM methods that can identify the location and damage level is very active. These methods mostly rely on installing sensors that continuously monitor and record the structural response or emissions and attempting to identify and localize the damage based on the recorded data. These systems include regular strain gauges, accelerometers, and acoustic emission sensors. In general, monitoring systems can be used on multiple fronts such as the validation of design assumptions, monitoring the structural response under normal operation, damage detection and diagnosis, prognosis and useful life estimation, and repair effectiveness assessment. Information from such systems can also be used to update and calibrate performance prediction and damage propagation models to achieve more reliable and accurate performance assessment process (Zhu & Frangopol 2013a,b). In the next subsection, the recent developments in damage identification using NDI and SHM are briefly discussed.

2.4.1 Structural damage detection

Damage detection techniques based on SHM such as vibration-based methods are under continuous development for use in civil and marine structures. Vibration-based methods use advanced signal processing techniques such as the Empirical Mode Decomposition and Hilbert-Huang transform (Huang & Shen 2005) to detect the damage by determining the change in the dynamic properties of the structure. This is based on the fact that a change in the mode shapes or frequencies would suggest that a change has occurred to the physical properties of the structure (Salvino & Brady 2008). Due to the inherent randomness associated with the monitoring outcomes, it is necessary to integrate those uncertainties in the damage detection technique (Okasha *et al.* 2011). Methods such as vector autoregressive modeling can be used for the detection and localization of damage in structures. In this method, the vibration signal obtained from the structure as a reference signal is modeled and this model is fitted to the measured structural response. The parameters of this model are the damage sensitive features (Okasha *et al.* 2011). The model is assumed to provide an accurate prediction of the structural response; thus, an increase in the difference between the model data and the data measured in the future is interpreted as an indication of structural damage. Mattson & Pandit (2006) proposed a vector based model which allow a signal to be described in terms of its own past values as well as the past values of other sensors.

A measure of the goodness of fit can be used to select the order of the auto regressive model which is a function of the predicted signal and the measured one. An application of such method was conducted by Mattson & Pandit (2006) on an experimental set-up. Additionally, the feasibility of application of this model for ships

has been tested in Okasha *et al.* (2011). Although the damage detection using vibration-based statistical methods is found to be a promising approach, more research is still required for verification, validation, and statistical quantification of such models in order to be reliably applied to SHM of large-scale civil and marine structures.

Within the last decade, acoustic emission technique has received considerable attention for its use in the fatigue and corrosion damage detection, monitoring, and localization, specifically, for ship structures. In this approach, stress waves emitted by the material during sudden changes in the internal structure are recorded using special sensors and used to detect structural damage such as crack initiation and growth, fracture, plastic deformation, corrosion, and stress corrosion cracking, among others (Anastasopoulos *et al.* 2009). In general, a uniform steel specimen with no stress raisers will start emitting acoustic emissions when stressed to a level of 60% of its yield stress (Anastasopoulos *et al.* 2009). During the action of normal operation loads on the structure, these emissions can be continuously detected and recorded such that structural damage can be monitored. This approach has been successfully applied to different types of structures such as bridges, pressure vessels and pipelines. Recently, research programs in Europe (see e.g. Baran *et al.* 2012; Tscheliesnig 2006) and the United States (see e.g., Wang *et al.* 2010) have shown the feasibility of such approach in detecting corrosion and crack damage in ship structures. In these research programs, the results of controlled laboratory testing of specimens subjected to fatigue and accelerated corrosion as well as oil tankers showed the feasibility of the approach. Since acoustic emission signals can be very weak, especially for corrosion detection, the damage detection may be significantly affected by the noise arising from the normal ship operation. The research in this area

also aimed to evaluate and isolate the noise under real operation conditions. Special pattern recognition techniques can be used to filter the noise (Baran *et al.* 2012). Multiple damage detection approaches have been developed, along with their necessary hardware. Some approaches use immersed sensors to detect the acoustic waves travelling through liquids in tankers, while others use sensors attached directly to the structure. The results of such research programs show that using acoustic emissions for the continuous application for the real-time monitoring of damage due to fatigue or corrosion is a promising approach. Accordingly, in this study, an approach for scheduling acoustic emission crack monitoring activities along the service life of a structure is proposed.

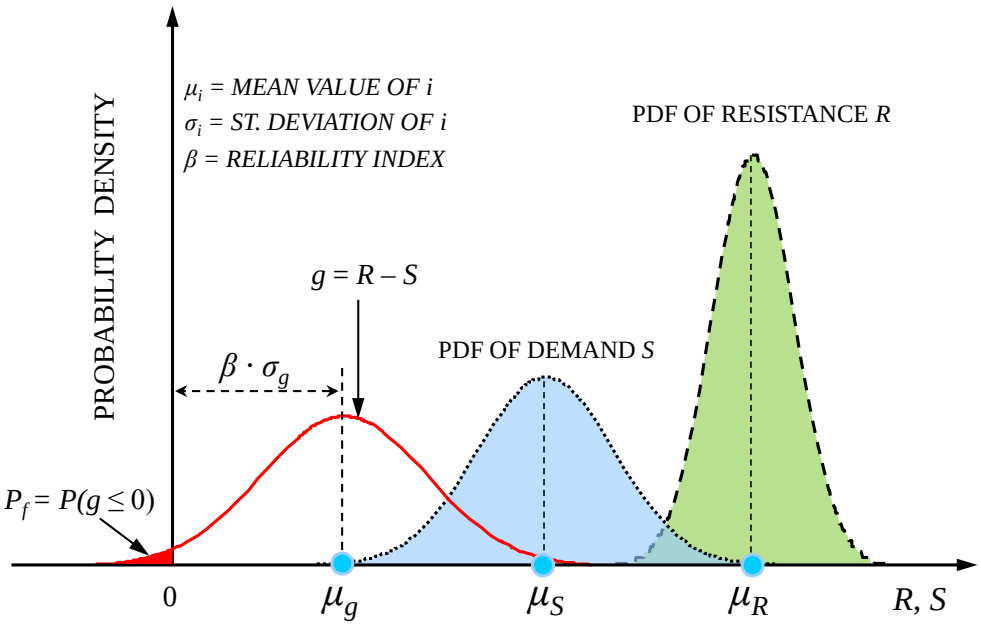

Figure 2.1 Schematic showing probability of failure concept

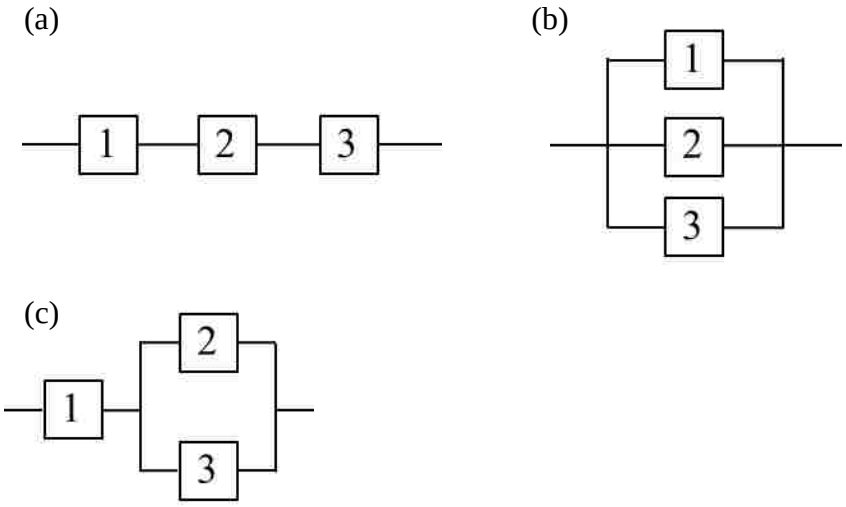

Figure 2.2 Different system configurations, (a) series system, (b) parallel system, and (c) series-parallel system

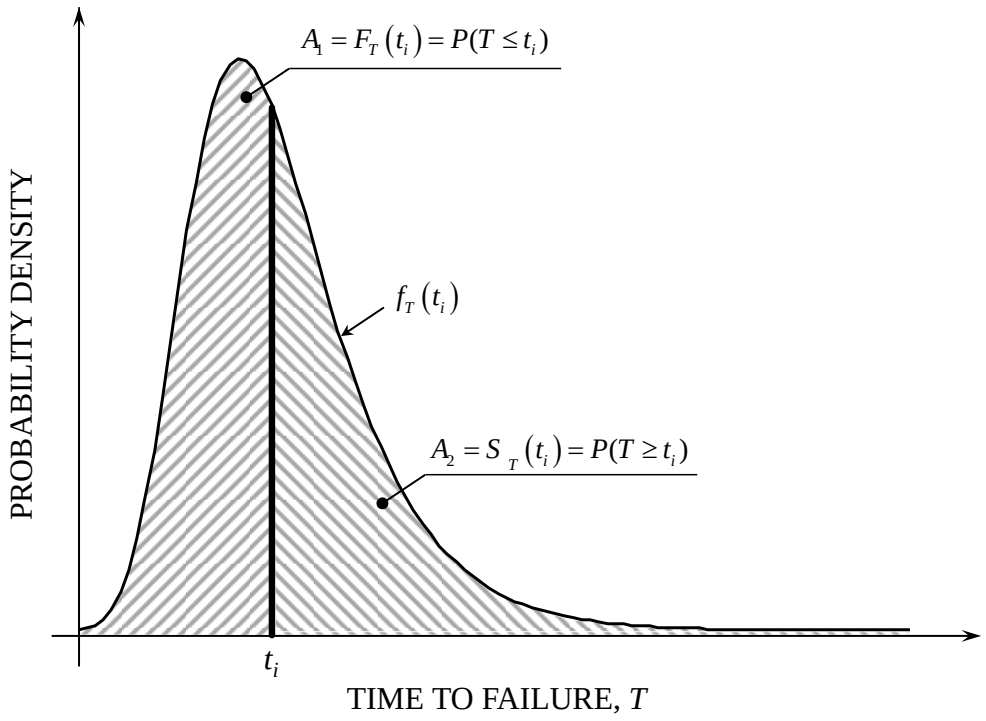

Figure 2.3 Relationship between the PDF of the time to failure $f_T(t)$, the survivor function $S_T(t)$; and the cumulative probability of failure $F_T(t)$

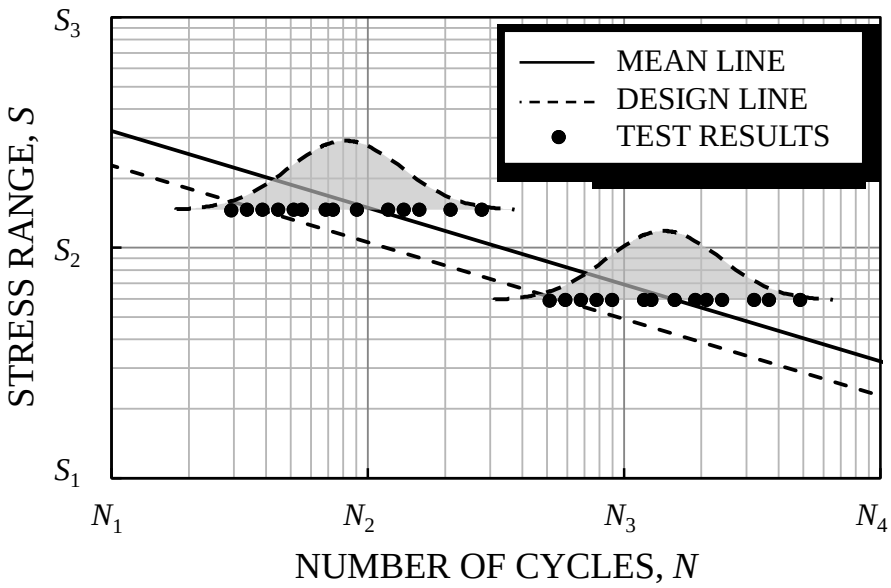

Figure 2.4 *S-N* lines and the PDF of the number of cycles to failure at different stress values

(a)

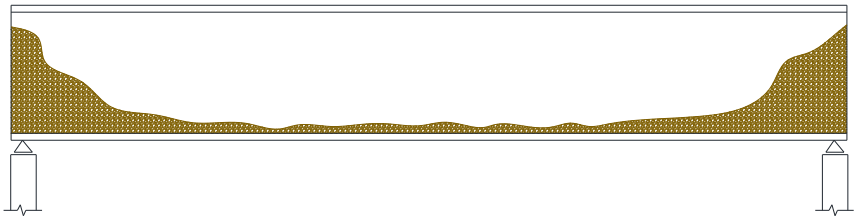

ELEVATION OF THE GIRDER

(b)

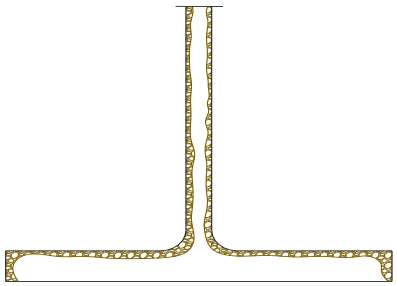

LOWER PART OF THE
CROSS SECTION

Figure 2.5 Typical corrosion pattern adopted by Estes & Frangopol (1999)

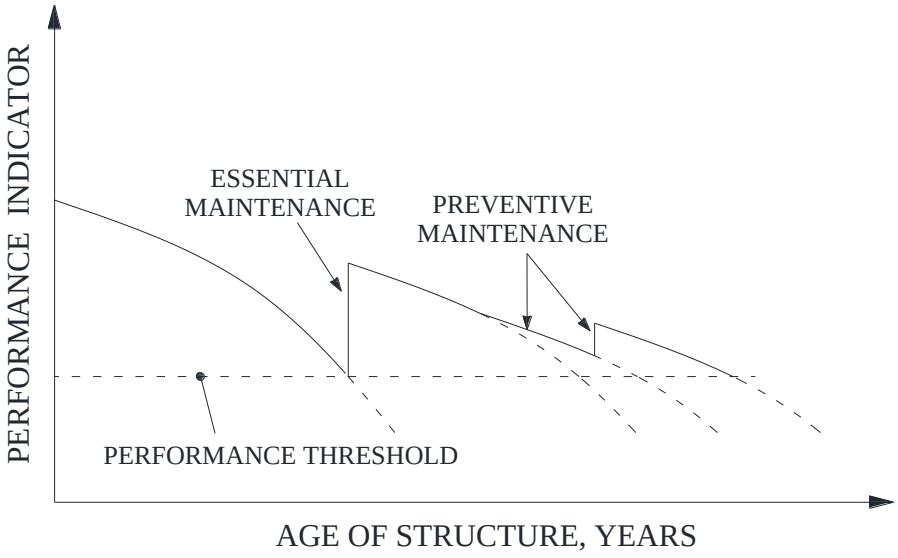

Figure 2.6 Effect of different maintenance types on the performance of the structure

(a)

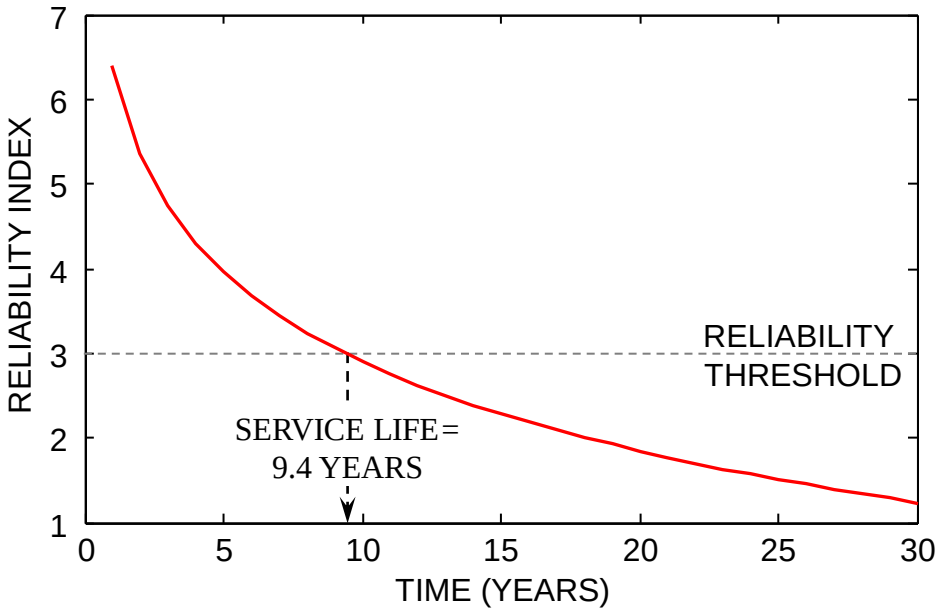

(b)

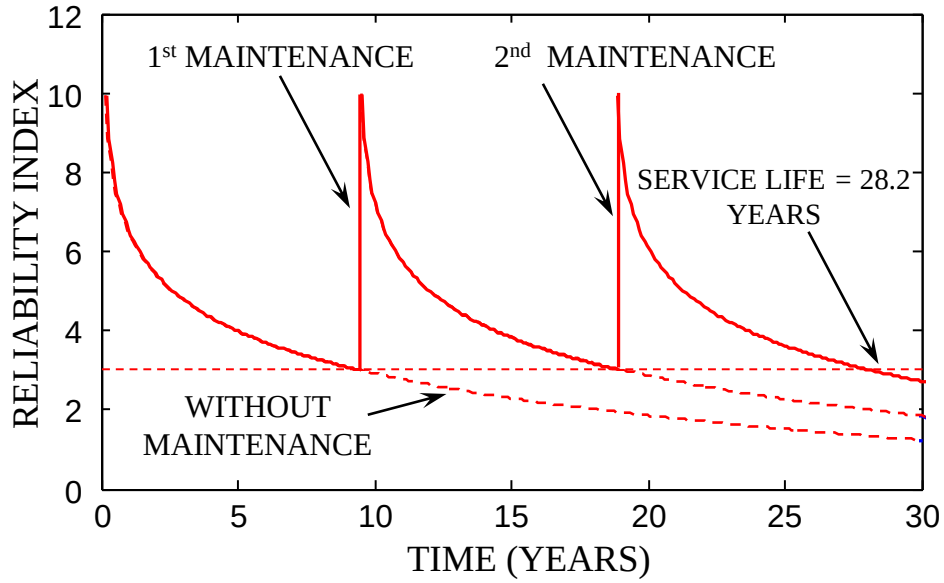

Figure 2.7 Fatigue reliability (a) without maintenance and (b) with EM

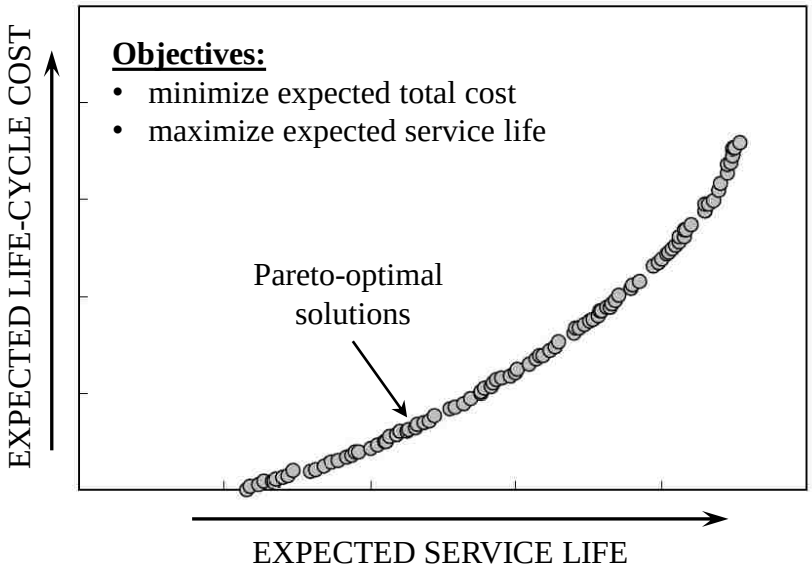

Figure 2.8 A typical Pareto-optimal solution set intervention optimization problem (the axes arrow indicates the direction of increase of the quantity of interest)

CHAPTER 3 PROBABILISTIC FATIGUE LIFE ESTIMATION BASED ON SHM AND A BI-LINEAR *S-N* APPROACH

3.1 Overview

This chapter addresses the fatigue assessment and service life prediction of existing fatigue-prone steel bridge details by integrating SHM data into a probabilistic bi-linear *S-N* approach. The main objective is to enhance the accuracy of current probabilistic fatigue life estimation methodologies. Fatigue assessment of several steel bridge details, having equivalent stress range below the CAFT, showed that many of these details are free of cracks, although the remaining life calculations predicted that they should have already been cracked. This shows that the current methods for predicting fatigue remaining life of steel bridges may be conservative and can lead to unnecessary retrofit and rehabilitation actions. For a better fatigue life prediction, a bi-linear *S-N* approach has been proposed. In this approach, the bi-linear *S-N* lines have different slopes above and below CAFT. The effect of changing the value of the slope of the AASHTO *S-N* lines below the CAFT on the fatigue reliability and remaining life is investigated in this chapter. In addition, an existing steel bridge is used to illustrate the proposed probabilistic approach.

The work in this chapter is based on the published papers Kwon *et al*. (2012) and Soliman *et al*. (2013c).

3.2 Background

The current procedure for fatigue life estimation of steel bridges, adopted by the AASHTO specifications (AASHTO 2014), extends the *S-N* lines with a single slope of 3

for the different detail categories below the CAFT. This approach, in some cases, may be conservative and cab lead to an increase in the maintenance costs due to unnecessary repairs actions. This has been shown by the results of a large number of SHM programs recently performed on bridges. A large number of details have been found to be free of cracks although the fatigue assessment results showed them to have negative remaining fatigue life, implying that they should have already been cracked (Connor *et al.* 2005, Yen *et al.* 2009). As a result, a bi-linear *S-N* approach was proposed by Crudele and Yen (2006) Yen *et al.* (2009, 2013). This approach suggests that the *S-N* lines below the CAFT have a gentler slope than that of the lines above the CAFT.

Currently, SHM techniques are widely implemented in fatigue assessment of steel bridges. Connor *et al.* (2005) and Mahmoud *et al.* (2005) used SHM to conduct full fatigue evaluation and service life prediction for two bridges, the Neville Island Bridge and the I-39 Bridge over Wisconsin River, respectively. In both studies, fatigue critical locations in the investigated bridges were identified and instrumented. Controlled live load testing and long-term monitoring were performed and stress range histogram data for different fatigue details were collected. Additionally, recommendations for future interventions were made. Li *et al*. (2001) and Chan *et al*. (2001) performed fatigue damage evaluation and life prediction for the Tsing Ma Bridge in Hong Kong. The authors used the strain monitoring data of the bridge in a continuum damage mechanics based model. The proposed approach provides a nonlinear fatigue damage curve which covers the crack initiation and propagation phases. In addition, the model enables updating the fatigue damage model once new stress history is available.

Although the above studies successfully handled the fatigue assessment problem, they did not consider the uncertainties inherent in the fatigue evaluation process. These uncertainties are found in both, the SHM results (i.e. stresses, strains, and recorded number of cycles) and the fatigue resistance prediction models. The uncertainties in the later are found in the design values of the *S-N* curve or the parameters of the crack growth model used in the fatigue evaluation. To address these uncertainties, Yazdani & Albrecht (1987) developed a model based on fracture mechanics for determining the probability of fatigue failure of steel bridges. They used Monte Carlo simulation to calculate the probability of fatigue failure considering uncertainties in the crack growth rate, fracture toughness, initial crack size, and loading history. Liu *et al*. (2010) performed a reliability based study to evaluate the effectiveness of the softening approach for retrofitting distortion-induced cracking of steel details. The study was based on the data collected from field monitoring in conjunction with finite element modeling of the floorbeam connection detail. The AASHTO *S-N* approach was used in their study as the resistance prediction model. Kwon & Frangopol (2010) used the field monitoring data to perform fatigue reliability assessment of steel bridges by using PDFs of equivalent stress range. Ni *et al.* (2010) presented a fatigue reliability model which integrates the probability distribution of hot spot stress range, provided by long-term monitoring data of the Tsing Ma Bridge, with a continuous formulation of the Miner's damage cumulative rule.

However, the mentioned studies considered only a single slope *S-N* approach for their prediction models. The bi-linear *S-N* approach was examined by Crudele & Yen (2006) and Yen *et al.* (2009, 2013). They studied the AASHTO *S-N* lines and proposed a

slope of 4 for the *S-N* lines below the CAFT for assessing fatigue of steel details. Their study was based on the concept of decreasing fatigue constant amplitude threshold. Kwon *et al*. (2012) addressed the same issue in a probabilistic framework by studying the improvement in the predicted fatigue life when adopting a slope of 4 below the CAFT. It should be noted that some international design guides adopt a multi-linear approach for fatigue resistance calculations. For example, the Eurocode 3 (EC3) (Eurocode 2010) uses a tri-linear approach with a slope of 3 above the CAFT, slope of 5 below CAFT and a horizontal line after the cut-off fatigue limit. A typical EC3 *S-N* line is shown in Figure 3.1.

This chapter examines the bi-linear approach for fatigue assessment of structural details using reliability-based methods. The fatigue reliability index provides the tool for quantifying the remaining fatigue life. The main goal of this chapter is to improve the fatigue service life prediction process under uncertainty by integrating SHM data into a probabilistic bi-linear *S-N* approach. Additionally, it focuses on examining the effect of the slope below the CAFT, defined herein as m_2 (the second slope of the *S-N* line), on the predicted fatigue life. Needless to say, this goal is not easy to achieve through experimental investigations as it involves a very large number of cycles, which is impractical to be performed even in a long-term experimental work. This fact suggests the need of an effective theoretical approach that can make use of the available SHM data to achieve the research goals. Attempting to address this issue, a parametric study showing the effect of m_2 on the fatigue life of the details is performed. The slope of the *S-N* lines below the CAFT, ranging from 3 to 5, is studied and the reliability index profiles with respect to the different slopes of the *S-N* lines below CAFT are generated. In

addition, the effect of the slope below CAFT on the fatigue life is examined under different target reliability indices. Furthermore, an existing bridge detail is used to illustrate the proposed probabilistic bi-linear *S-N* approach.

3.3 Fatigue Assessment

As previously indicated, fatigue assessment of structural details can be performed by means of two approaches; the crack growth and the *S-N* approaches. In the *S-N* approach, adopted in this study, the *S-N* lines provide the fatigue resistance based on the expected number of stress cycles acting on the detail. This means that the key parameters that can lead to a reliable fatigue life prediction are the stress range acting on the detail and the number of stress cycles. The cumulative number of cycles can be found, during assessment, by means of SHM techniques, while during design phase, the AASHTO specifications (AASHTO 2014) can provide an estimate for the number of cycles depending on the bridge location, bridge geometry, and the location of the detail within the bridge. For the load effect, the stress range acting on the detail can be calculated using the standard fatigue truck analysis. Alternatively, SHM results can provide more accurate estimate of the stress ranges acting on the detail. The data collected during the SHM are processed using an appropriate cycle counting algorithm, such as the rainflow algorithm (Downing & Socie 1982), to construct the stress range bin histogram for each monitored structural detail, which is used afterwards for the fatigue assessment and remaining life prediction.

3.4 Fatigue Resistance

According to the AASHTO LRFD Bridge Design Specifications (AASHTO 2014), a detail can have an infinite or finite fatigue life based on the value of the stress range experienced by the detail. The AASHTO finite fatigue life equation for single slope *S-N* lines is

$$\Delta F = \left(\frac{A}{N}\right)^{\frac{1}{m}} \tag{3.1}$$

in which ΔF is the fatigue resistance (i.e., stress range), A is the fatigue detail coefficient for each category, N is the number of cycles, and m is a material constant defining the value of the single slope of the *S-N* line. This value is considered to be equal to 3 for steel details.

For the bi-linear *S-N* approach, Equation (3.1) for fatigue resistance estimation can be written as

$$\Delta F = \begin{cases} \left(\frac{A_1}{N}\right)^{\frac{1}{m_1}} & for \quad N \le \frac{A_1}{CAFT^{\,m_1}} \\ \left(\frac{A_2}{N}\right)^{\frac{1}{m_2}} & for \quad N > \frac{A_1}{CAFT^{\,m_1}} \end{cases} \tag{3.2}$$

where m_1 and m_2 are the slopes of the *S-N* lines above and below the CAFT respectively, A_1=A and $A_2 = A_1 \cdot CAFT^{(m_2 - m_1)}$. A_1 and A_2 are the fatigue detail coefficients above and below the CAFT, respectively. The values of A_1 and the CAFT are shown in Table 3.1 for the AASHTO design specifications (AASHTO 2014) predefined structural details. Table 3.2 gives the values of A_2 for different details and for different values of m_2.

3.5 Equivalent Constant Amplitude Stress Range

Since bridges are subjected to variable amplitude stress range cycles, the equivalent constant amplitude stress range needs to be calculated for the fatigue assessment. For the linear *S-N* approach, Miner's rule (Miner 1945) can be used to find the equivalent constant amplitude stress range, S_{re}, as follows

$$S_{re} = \left[\sum \frac{n_i}{n_{total}} \cdot S_{ri}^{m_1} \right]^{\frac{1}{m_1}} \tag{3.3}$$

where n_i is the number of cycles in the predefined stress range bin S_{ri} and n_{total} is the total number of cycles. To improve the flexibility of the prediction models, S_{re} can alternatively be calculated using the PDF of the stress range as follows

$$S_{re} = \left[\int_0^\infty s^{m_1} \cdot f_S(s) \cdot ds \right]^{\frac{1}{m_1}} \tag{3.4}$$

where $f_s(s)$ is the PDF of the distribution of the stress range , S. For structural steel bridge details, this PDF can be considered to be Lognormal or Weibull. The three-parameter PDFs of these distributions, including cut-off threshold, s_c, are respectively given by Equation (2.15) and (2.17) in Chapter 2.

On the other hand, S_{re} can be calculated for the bi-linear *S-N* approach as (Kosteas 1999, Yen *et al*. 2013)

$$S_{re} = \begin{cases} \left[\dfrac{\sum \left(n_i^o \cdot S_{ri}^{m_1} \right) + \left(CAFT^{m_1 - m_2} \right) \cdot \sum \left(n_j^o \cdot S_{rj}^{m_2} \right)}{\sum (n_i^o) + \sum (n_j^o)} \right]^{\frac{1}{m_1}} & \text{for } S_{re} \geq \text{CAFT} \\ \left[\dfrac{\left(CAFT^{m_2 - m_1} \right) \cdot \sum \left(n_i^o \cdot S_{ri}^{m_1} \right) + \sum \left(n_j^o \cdot S_{rj}^{m_2} \right)}{\sum (n_i^o) + \sum (n_j^o)} \right]^{\frac{1}{m_2}} & \text{for } S_{re} \leq \text{CAFT} \end{cases} \tag{3.5}$$

in which n_i^o is the number of cycles in the stress range bin S_{ri} greater than CAFT, n_j^o is the number of cycles in the stress range bin S_{rj} less than CAFT, $\sum(n_i^o)+\sum(n_j^o)$ is the total number of cycles to failure, and m_1 and m_2 are the slopes of the *S-N* line above and below the CAFT, respectively.

Alternatively, using the bi-linear *S-N* approach, S_{re} can be calculated using the PDF of the stress range as follows

$$S_{re}=\begin{cases}\left[\int_0^{CAFT}(CAFT^{m_1-m_2})\cdot S^{m_2}\cdot f_S(s)\cdot ds+\int_{CAFT}^{\infty}S^{m_1}\cdot f_S(s)\cdot ds\right]^{\frac{1}{m_1}} & \text{for } S_{re}\geq \text{CAFT}\\ \left[\int_0^{CAFT}S^{m_2}\cdot f_S(s)\cdot ds+\int_{CAFT}^{\infty}(CAFT^{m_2-m_1})\cdot S^{m_1}\cdot f_S(s)\cdot ds\right]^{\frac{1}{m_2}} & \text{for } S_{re}\leq \text{CAFT}\end{cases} \tag{3.6}$$

3.6 Fatigue Life

Fatigue life, measured as the number of cycles to failure, is commonly calculated as

$$N=\frac{A_1}{S_{re}^{m_1}} \tag{3.7}$$

for the single slope *S-N* approach. While for the case of bi-linear approach, it can be calculated as

$$N=\frac{A_2}{S_{re}^{m_2}}\quad \text{for } S_{re}\leq \text{CAFT} \tag{3.8}$$

This number of cycles can be used in conjunction with the average daily number of cycles N_{avg}, provided by the SHM results, to estimate the bridge detail fatigue life in years using the following equation

$$t = \frac{N}{365 \times N_{avg}} \tag{3.9}$$

The calculated fatigue life can be used to find the remaining fatigue life T_{rem} as

$$T_{rem} = t - t_s \tag{3.10}$$

where t_s is the number of elapsed service years of the bridge. However, Equation (3.9) for calculating the fatigue life neglects the annual traffic increase rate and assumes that the average daily number of cycles, N_{avg} , remains constant since the opening of the bridge, which can decrease the accuracy of the fatigue life calculation. This is better addressed using the actual vehicle count data, as discussed later in this chapter.

3.7 Fatigue Reliability Analysis

Reliability index has been widely accepted as a structural performance measure. The reliability index calculation involves the calculation of the probability of failure, $P_{f,}$ as the probability of violating a certain limit state. Therefore the reliability index can be defined as follows

$$\beta = \Phi^{-1}\left(1 - P_f\right) \tag{3.11}$$

in which $\Phi^{-1}\left(\cdot\right)$ is the inverse of the standard normal cumulative distribution function.

For assessing the remaining fatigue life in a probabilistic manner, a reliability approach is developed based on the bi-linear *S-N* fatigue resistance model. The performance function used in developing the fatigue reliability model can be expressed as

$$g\left(t\right) = \Delta - D\left(t\right) \tag{3.12}$$

where Δ = Miner's critical damage accumulation index, indicates the resistance and it is assumed to be lognormal with mean value of 1.0 and coefficient of variation (COV) of

0.3 (Wirsching 1984), and $D(t)$ = Miner's damage accumulation index which can be expressed as

$$D(t) = \begin{cases} \dfrac{N(t)}{A_1} \cdot (S_{re})^{m_1} & \text{for } S_{re} \geq \text{CAFT} \\ \dfrac{N(t)}{(CAFT^{m_2 - m_1} \cdot A_1)} \cdot (S_{re})^{m_2} & \text{for } S_{re} \leq \text{CAFT} \end{cases} \tag{3.13}$$

where S_{re} is the equivalent constant amplitude stress ranges calculated using the bi-linear *S-N* approach. In this chapter, the values of m_1, CAFT, and the number of cycles obtained from the monitoring program $N(t)$ are considered to be deterministic. On the other hand, the stress range S_{re} and the fatigue detail coefficient A_1 are considered random. Two separate cases will be considered for m_2; first it will be treated as a deterministic parameter and next as a random variable.

Equations (3.12) and (3.13) can be used to calculate the reliability index using computer software such as RELSYS (Estes & Frangopol 1998) or CalREL (Liu *et al.* 1989). The discussed procedure for fatigue assessment is summarized in the flowchart shown in Figure 3.2.

3.7.1 Effect of m_2 on fatigue life

A parametric study has been performed to study the effect of the second slope, m_2, on the fatigue life of structural steel details. In order to calculate the mean of the equivalent constant amplitude stress range, S_{re}, the variable amplitude stress range, S_r, is assumed to be a lognormal distributed random variable. Different mean values and COVs of S_r are used to generate different stress range spectra. Given that this investigation deals with the

details experiencing equivalent stress range below the CAFT, the mean value of S_r is assumed to be 0.5 CAFT and 0.75 CAFT. These two values, which were obtained by reviewing statistically a wide range of bridge details monitored by the ATLSS Center at Lehigh University, are used in the parametric study to understand the effect of the mean value of S_r on the fatigue reliability. For these mean values, three COVs (i.e. 0.3, 0.4 and 0.5) are considered. However, to calculate the fatigue reliability index, S_{re}, is assumed to be log-normally distributed with COV of 0.1 (Ayyub *et al*. 2002 and Kwon *et al*. 2011).

3.7.2 Effect of m_2 on the reliability profile

To study the fatigue reliability deterioration over time, detail category "C" is selected and the average daily truck traffic (ADTT) is assumed, following the AASHTO specifications (AASHTO 2014), to be 1290 truck per day. This value is used as the number of cycles per day assuming that each truck passage produces only one stress cycle at the detail. The number of cycles is then projected and the reliability indices versus the number of cycles to failure, for detail category "C", are calculated and plotted in Figures 3.3 (a), (b), and (c) for the different COVs of S_r. In Figure 3.3 (d), the reliability profile for m_2= 4 is compared for different values of COV of S_r.

Figure 3.3 clearly shows that the increase in the value of m_2 significantly improves the reliability index and, accordingly, the fatigue life of the detail. This figure also shows that for a low number of stress cycles, the increase in the reliability index when adopting a slope m_2 of 5 instead of 3 may not be significant; however, for higher numbers of stress cycles, this increase is significant and the reliability index is doubled after 60 million cycles. This can be attributed to the nature of the bi-linear *S-N* lines, for low number of stress cycles, the increase in the allowable stress that is gained when

adopting a slope m_2= 5 instead of m_2= 3 is low, while for large number of stress cycles, this increase in the allowable stress is high, and it is almost 46% at 60 million cycles. This is clearly shown, for detail class "C", in Figure 3.4.

3.7.3 Effect of the mean value of the variable amplitude stress range

To study the effect of the mean value of S_r on the reliability profile, the number of cycles versus the reliability index is plotted in Figure 3.5 for COV (S_r) = 0.4 and two different values for the mean value of S_r. The plot shows the significant effect of the mean value of S_r on the fatigue reliability; a 50% increase in the stress range level can produce a substantial decrease of the fatigue performance of a detail.

3.7.4 Reliability indices for a given target fatigue life

The reliability index is then plotted against the different values of m_2 for different target fatigue life. The results are shown in Figure 3.6 (a), (b), and (c) for different values of COV of S_r. Figure 3.6 (d) shows the reliability index versus the slope m_2 for different COVs of S_r and a target life of 35 million cycles, which is equivalent to the AASHTO 75 years design life for a detail of category "C" using the previous assumption of 1290 cycles per day and 1.0 stress cycle per truck passage. The results show that the increase in the reliability index at the end of the 75 years of service life, when adopting a slope m_2 of 5, is 86%, 72%, and 62% for COVs 0.3, 0.4, and 0.5, respectively, while for m_2 of 4, the respective increase is 45%, 39%, and 34%.

3.7.5 Fatigue life for different target reliability indices

Next, the expected fatigue life is plotted versus the slope below the CAFT for different target reliability indices, the results for COV (S_r) = 0.4 are shown in Figure 3.7. Since the

reliability profiles, shown in Figure 3.3, have the tendency to flatten near the end of the service life, the fatigue life for the combinations that have a high value of m_2 and a low value of the target reliability index can indeed produce an infinite fatigue life. This is clearly expressed in Figure 3.7 for the case with a target reliability index of 2. This figure shows that the increase in the service life with respect to the value of m_2 is much more significant for low target reliability indices.

3.7.6 Effect of m_2 on different detail categories

The previous parametric studies are next applied on other AASHTO (AASHTO 2014) detail categories. The AASHTO parameters of each category are used and the 75 years AASHTO ADTT corresponding to infinite fatigue life is adopted. Figure 3.8 compares the reliability profiles for category "C" and "E". It is shown that different categories yield identical fatigue reliability profiles for a given stress range level (i.e. 0.5 CAFT or 0.75 CAFT) when using the AASHTO 75 years number of cycles.

3.8 Case Study

The fatigue life of a shelf plate detail in an existing bridge, the I-39 Northbound Bridge over the Wisconsin River, is investigated for different values of m_2. Fatigue assessment of the detail is performed using the previously discussed approach with the aid of the monitoring data of this detail. The monitoring data was collected during the field monitoring of the bridge performed by the ATLSS Engineering Research Center at Lehigh University in 2004 (Mahmoud *et al*. 2005).

3.8.1 Bridge description

The I-39 Bridge is located near Wausau, Wisconsin and carries US 51 and I-39 northbound over the Wisconsin River. The bridge is a five span continuous steel girder bridge and was opened to traffic in 1961. The bridge is symmetrical about the midpoint of the third span and has a total length of 194.78 m (639 ft). The length of the first, second, and third spans are 33.41 m (109.6 ft), 42.64 m (139.9 ft), and 42.66 m (140 ft), respectively. The bridge crosses the Wisconsin River from the Village of Rothschild on the southeast, to the town of Weston, Marathon County on the Northwest side. Figure 3.9 shows an elevation of the bridge.

The long-term monitoring was performed on 26 different details of the bridge. This long-term monitoring was conducted from July 29, 2004 through November 3, 2004, for a total of approximately 95 days. Personal communication with Wisconsin department of transportation (WisDOT) revealed that the bridge was completely rehabilitated in 2006 and that the work was finished in 2008. The rehabilitation actions included replacing the existing deck, widening the piers and abutments, and adding more girders in addition to retrofitting the existing steel girders.

3.8.2 Equivalent stress range

The detail at Channel 1 is investigated in this study. This detail is a connection between a lateral shelf plate and the bottom flange of one of the main girders. This detail is shown in Figure 3.9.

For the classified AASHTO categories, the detail at Channel 1 is classified as category E with CAFT of 31 MPa (4.5 ksi). The value of A_1 for this category is 3.61×10^{11} MPa^3 (11×10^8 ksi^3) as shown in Table 3.1.

The monitoring data for Channel 1 is used in this study to generate the stress range bin histogram using the rainflow cycle counting algorithm (Downing & Socie 1982). The maximum stress range of the detail at Channel 1 is found to be 103.5 MPa (15 ksi). This value is higher than the defined AASHTO (AASHTO 2014) CAFT, implying that the detail should experience finite fatigue life. A cut-off threshold of 6.9 MPa (1.0 ksi) was selected for truncating the stress range histogram data. This cut-off threshold approximately corresponds to 0.25 CAFT of the studied details which was found to be an appropriate value for this type of details (Mahmoud *et al*. 2005, Connor and Fisher 2006). Based on the truncated stress range histogram, a goodness-of-fit test, using Anderson and Darling (Anderson & Darling 1952) method, was conducted to select the best fit among the Weibull and Lognormal distributions. As shown in Figure 3.10, the three-parameter Weibull distribution offers the best fit for the stress range data obtained from the field monitoring. The parameters of the PDF are 1.145 and 0.771 for the scale and shape parameters respectively, while the distribution threshold is 6.9 MPa (1.0 ksi). The stress range bin histogram and the proposed distribution are shown in Figure 3.11 (a). Using these parameters and Equation (3.6), the values of S_{re} are calculated for different values of m_2.

3.8.3 Number of cycles

Based on the rainflow data, the average number of cycles per day at Channel 1 is found to be 2857. Using this number of cycles as the daily number of cycles since the bridge was opened to traffic may give a conservative life estimate, as it does not take into account the considerable traffic volume growth that has been developing since the opening of the bridge. In addition, since the values of S_{re} are higher than 0.5 CAFT, the detail is

expected to have a finite fatigue life and it is important to calculate the cumulative number of cycles accurately to get a more refined prediction model. For this reason, the actual vehicle count obtained from WisDOT and discussed in Mahmoud *et al.* (2005) is used to develop a traffic growth model. This traffic growth model is then adjusted to give the same number of cycles found by the rainflow data in 2004, which is 2857 cycles per day.

The traffic logs provided by WisDOT are in the form of discrete Average Daily Traffic (ADT) count. It was recorded in selected years from 1964 to 2001. However, the number of cycles should be calculated using the ADTT rather than the ADT, this is due to the fact that lighter vehicles have little effect on fatigue damage (Moses *et al.* 1987). In this study the ADTT is assumed to be 12 % of the ADT (Mahmoud *et al*. 2005). In order to obtain a function for estimating the annual ADTT, a linear fitting is developed to fit the discrete ADTT data. The discrete ADTT, calculated as 12 % of the recorded ADT, and the fitting are shown in Figure 3.11 (b). However, due to the large variability in the data recorded before 1978, the largest recorded ADT from 1964 to 1978 is used and assumed to be constant during this period. Using this approach, the ADTT is projected up to the year 2004.

It is also known that the number of cycles should not be considered the same as the ADTT, as each truck can produce more than one cycle. To estimate the number of cycles per day at Channel 1 from the ADTT data, the projected ADTT of the year 2004 is correlated to the number of cycles per day greater than 6.9 MPa (1.0 ksi), which is obtained from the SHM results. This is done by dividing the number of cycles per day obtained from the monitoring data by the projected ADTT at the year 2004. For this

detail, the number of cycles/day obtained from the monitoring results is found to be 2,857 and The ADTT for 2004 is estimated to be 1,889. Using the two values, the number of cycles per day can be estimated to be 1.512 times the ADTT.

3.8.4 Fatigue reliability profiles

Based on the calculated values of S_{re}, the cumulative number of cycles, and Equation (3.12), the fatigue reliability profile of the detail is produced using the software RELSYS (1998). These reliability profiles are plotted in Figure 3.11 (c) for values of m_2 ranging from 3.0 to 5.0. The coefficient of variation of the S_{re} is assumed to be 0.1.

The fatigue service life of the detail is then plotted versus the target reliability index for different values of m_2; the plot is shown in Figure 3.12 (a). The last year in the fatigue service life is shown in Table 3.3 for different values of m_2 and for different target reliability indices. The use of the values in the hatched area of Table 3.3 predicts that the detail should be already cracked, which is not true for this case. This shows that the values of m_2 and β_{target} defined in the hatched region are conservative and should not be used in fatigue life estimation. Figure 3.12 (b) shows the increase in service life due to an increase of m_2 from 3 to 5 and from 3 to 4 for different target reliability indices. Given that a reasonable target reliability index for the fatigue problem under consideration would range from 2.0 to 3.5 (Moses *et al.* 1987), it is shown from Figure 3.12 and Table 3.3 that an increase in m_2 from 3 to 5 will give a corresponding increase of 22%, 17.8% and 14.3% in the fatigue service life for β_{target} of 2.5, 3.0 and 3.5, respectively. Additionally, considering m_2 to be 4 instead of 3 will give an increase in the fatigue life of 11%, 7.2% and 6% for the previously mentioned respective target reliability indices.

Since the value of the slope below the CAFT carries significant uncertainty, it was of interest to the authors to study the fatigue reliability profile of Channel 1 considering the uncertainty inherent in the value of m_2. For this study, three different distribution models are assumed for the value of m_2. The first distribution, Distribution I, considers m_2 to be triangularly distributed random variable ranging from 2.5 to 5 with a median equal to 3. Distribution II is also triangular ranging from 2.5 to 5 but with a median of 4, while for Distribution III, the value of m_2 is considered to be uniformly distributed between 2.5 and 5. These distributions are used in a Monte Carlo simulation, using Equation (3.12), to calculate the probability of fatigue failure of the detail. Values of m_1, CAFT and the number of cycles are considered to be deterministic throughout the simulation, while the values of A_1 and Δ are considered to be log-normally distributed random variables. A mean of 1.0 and a COV of 0.3 are adopted for Δ (Wirsching 1984). On the other hand, a mean value of 1.44×10^{13} MPa^3 (4.4×10^{10} ksi^3) and a COV of 0.45 are considered for the variable A_1 (Kwon & Frangopol 2010). In order to calculate S_{re} for each simulated sample, Equation (3.6) is integrated numerically and embedded in the simulation code. A number of 10 million simulations is chosen based on comprehensive convergence studies. A sample convergence plot is shown in Figure 3.13. This number of simulations is performed for each number of cycles starting from 12.1 million cycles, the number of cycles at the CAFT and corresponds to the year 1995, up to the year 2040, four years after the 75 years of service life of the bridge which will be reached in 2036. The resulting reliability profiles is plotted in Figures 3.14 (a), (b) and (c) with the previously generated reliability profiles considering m_2 to be a deterministic variable ranging from 3 to 5. Figure 3.14 (d) compares the reliability profile for the three

distributions of m_2. The last year for fatigue service life estimated by the three distribution models of m_2 is also listed in Table 3.3. The fatigue service life extracted from the reliability profiles of the three distributions is almost identical with a difference of three years for target reliability indices of 3 and 3.5.

3.9 Conclusions

This chapter investigates the effect of the slope of the *S-N* lines below the CAFT, m_2, on the remaining fatigue life of structural steel details. A probabilistic approach was used to calculate the fatigue remaining life. This approach is based on the bi-linear fatigue *S-N* lines, in which the *S-N* lines have different slopes above and below the CAFT. The AASHTO detail categories and their associated parameters were used in this investigation. A parametric study was performed to study the effect of the value of m_2 on the fatigue reliability and the fatigue remaining life. The study considered different values for the mean and the COV of the stress range. A case study was analyzed in this chapter, in which the data from the long-term monitoring of a detail in an existing bridge, the I-39 Bridge over the Wisconsin River, was used to establish stress range histogram. The equivalent stress range, for different values of m_2, was calculated using this histogram and a fatigue reliability study was performed on this detail. The fatigue remaining life was calculated for different values of m_2. In addition, the slope below the CAFT was considered to be a random variable and the fatigue life estimation is performed for three different distributions of m_2. The following conclusions can be drawn:

1. The use of the bi-linear *S-N* approach always predicts longer fatigue life compared to the life calculated using the single slope AASHTO *S-N* lines. Additionally, increasing

the value of m_2 from 3 to 5 results in a significant increase in the remaining life especially for target reliability indices ranging from 2.0 to 3.5.

2. For a low number of stress cycles, the increase in the reliability index when increasing the slope below the CAFT may not be significant; however, for higher numbers of stress cycles, this increase is significant and in some cases the reliability index can be doubled
3. The fatigue reliability is very sensitive to the mean value of the variable amplitude stress range.
4. Using recorded vehicle count data provides additional information for improving the accuracy of the fatigue life assessment.
5. Modeling m_2 as a random variable during fatigue assessment of details is a rational approach; however, more studies are required to find the appropriate statistical characteristics of this variable. This can be achieved by making use of the available bridge inspection and monitoring results and will help improving the fatigue life assessment process of bridges.
6. This approach improves the fatigue life assessment process under uncertainty and can be effectively integrated into the LCM framework shown in Figure 1.1.

Table 3.1 *S-N* values based on the AASHTO fatigue categories (AASHTO 2014)

Detail category	CAFT MPa (ksi)	Values of constant A_1 MPa^3 (ksi^3)
A	165 (24)	82.0×10^{11} (250×10^8)
B	110 (16)	39.3×10^{11} (120×10^8)
B'	82.7 (12)	20.0×10^{11} (61×10^8)
C	69 (10)	14.4×10^{11} (44×10^8)
C'	82.7 (12)	14.4×10^{11} (44×10^8)
D	48.3 (7)	7.21×10^{11} (22×10^8)
E	31 (4.5)	3.61×10^{11} (11×10^8)
E'	17.9 (2.6)	1.28×10^{11} (3.9×10^8)

[redacted]

Detail category	Values of constant A_2 MPa$^{3.5}$ (ksi$^{3.5}$) $m_2 = 3.5$	Values of constant A_2 MPa^{4} (ksi^{4}) $m_2 = 4.0$	Values of constant A_2 MPa$^{4.5}$ (ksi$^{4.5}$) $m_2 = 4.5$	Values of constant A_2 MPa^{5} (ksi^{5}) $m_2 = 5.0$
A	$105.3\times10^{12}(122\times10^{9})$	$135.3\times10^{13}(60\times10^{10})$	$173.8\times10^{14}(294\times10^{10})$	$223\times10^{15}(144\times10^{11})$
B	$41.22\times10^{12}(48\times10^{9})$	$43.23\times10^{13}(19.2\times10^{10})$	$45.34\times10^{14}(76.8\times10^{10})$	$47.6\times10^{15}(30.7\times10^{11})$
B'	$18.20\times10^{12}(21.1\times10^{9})$	$16.54\times10^{13}(7.32\times10^{10})$	$15.04\times10^{14}(25.4\times10^{10})$	$13.7\times10^{15}(8.78\times10^{11})$
C	$11.96\times10^{12}(13.9\times10^{9})$	$9.94\times10^{13}(4.4\times10^{10})$	$8.25\times10^{14}(13.9\times10^{10})$	$6.86\times10^{15}(4.4\times10^{11})$
C'	$13.1\times10^{12}(15.2\times10^{9})$	$11.91\times10^{13}(5.28\times10^{10})$	$10.83\times10^{14}(18.3\times10^{10})$	$9.85\times10^{15}(6.34\times10^{11})$
D	$5.01\times10^{12}(5.82\times10^{9})$	$3.48\times10^{13}(1.54\times10^{10})$	$2.42\times10^{14}(4.07\times10^{10})$	$1.68\times10^{15}(1.08\times10^{11})$
E	$2.01\times10^{12}(2.33\times10^{9})$	$1.12\times10^{13}(0.49\times10^{10})$	$0.623\times10^{14}(1.05\times10^{10})$	$0.347\times10^{15}(0.223\times10^{11})$
E'	$0.541\times10^{12}(0.63\times10^{9})$	$0.229\times10^{13}(0.101\times10^{10})$	$0.964\times10^{13}(0.164\times10^{10})$	$0.41\times10^{14}(0.264\times10^{10})$

Table 3.3 Predicted end of service life of the detail at Channel 1

m_2	End of fatigue service life*†				
	β_{target} = 2.5	β_{target} = 3.0	β_{target} = 3.5	β_{target} = 4.0	β_{target} = 5.0
3.0	2024	2017	2010	2004	1994
3.5	2028	2019	2012	2005	1995
4.0	2031	2021	2013	2006	1995
4.5	2034	2024	2015	2008	1996
5.0	2038	2027	2017	2009	1993
Distribution I	2029	2021	2015	2009	1993
Distribution II	2032	2024	2017	2011	1995
Distribution III	2029	2021	2014	2007	1997

* Bridge opened in 1961; the highlighted area indicates that the detail should be cracked

† Bridge was rehabilitated in 2006

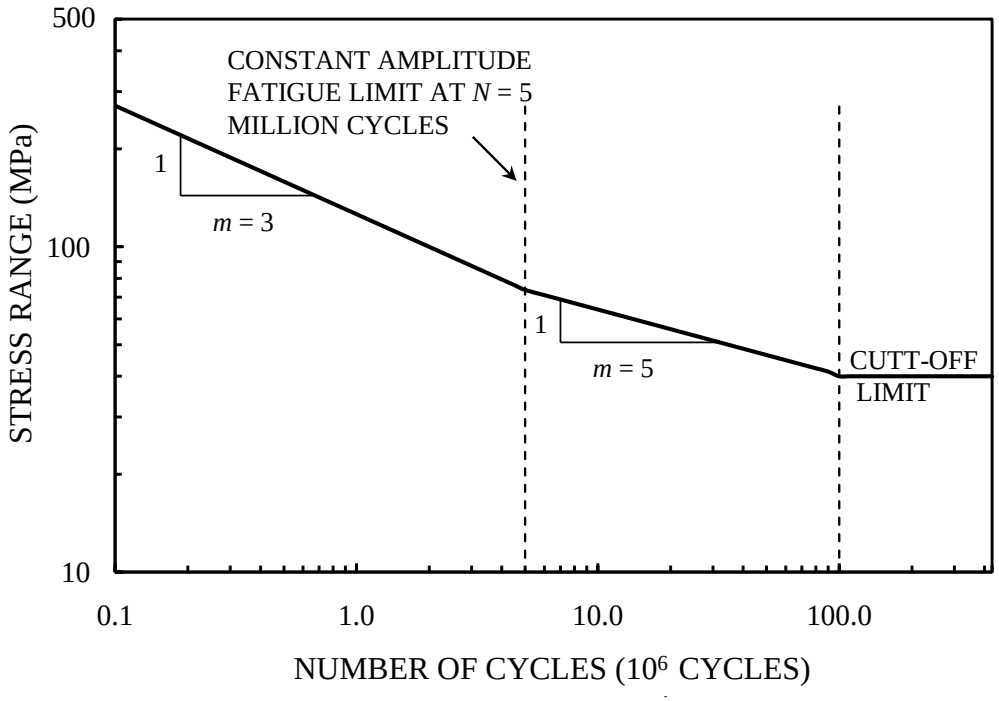

Figure 3.1 EC3 (Eurocode 2010) typical fatigue strength curve for normal stress range

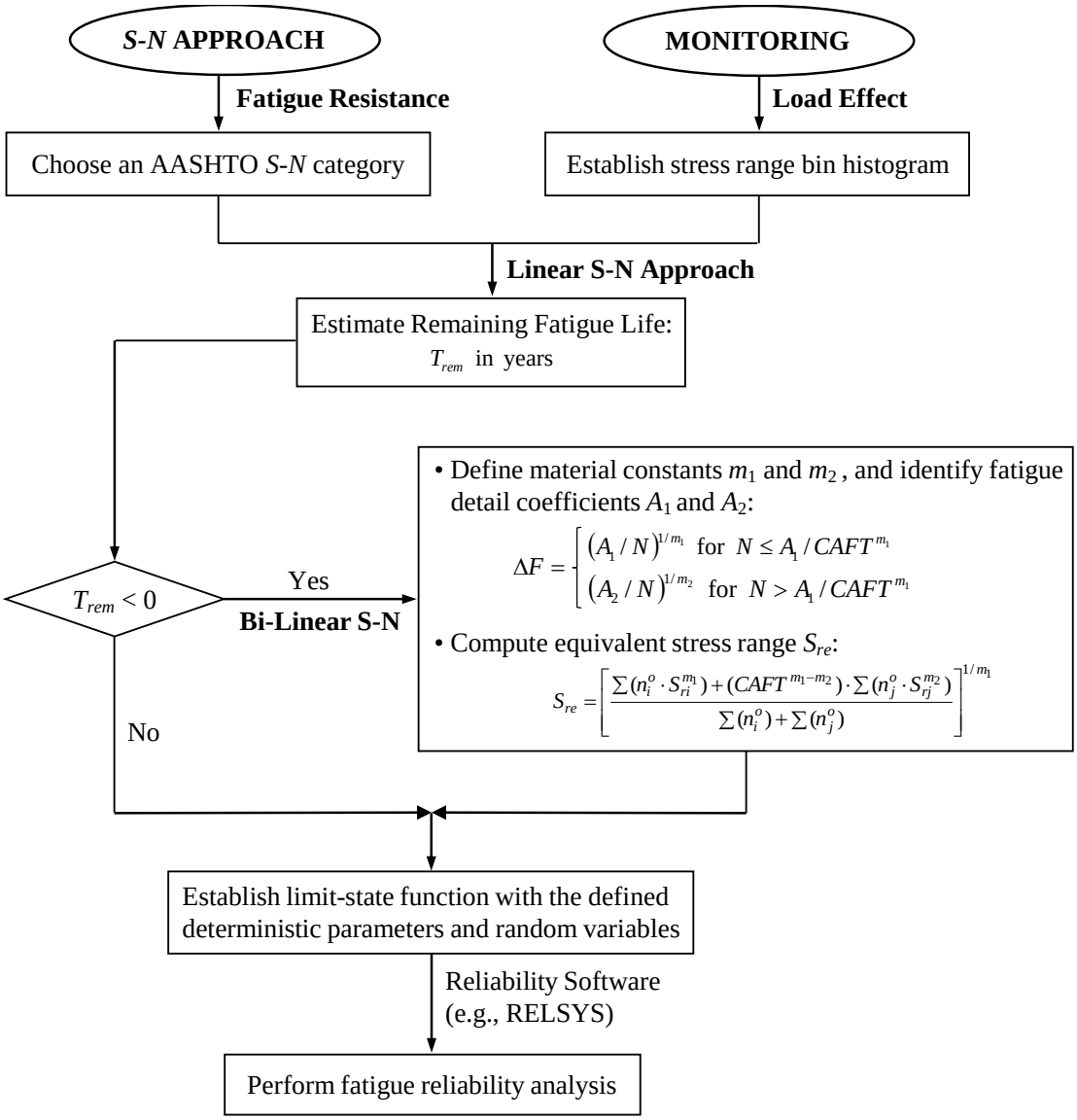

Figure 3.2 Fatigue assessment flowchart

(a)

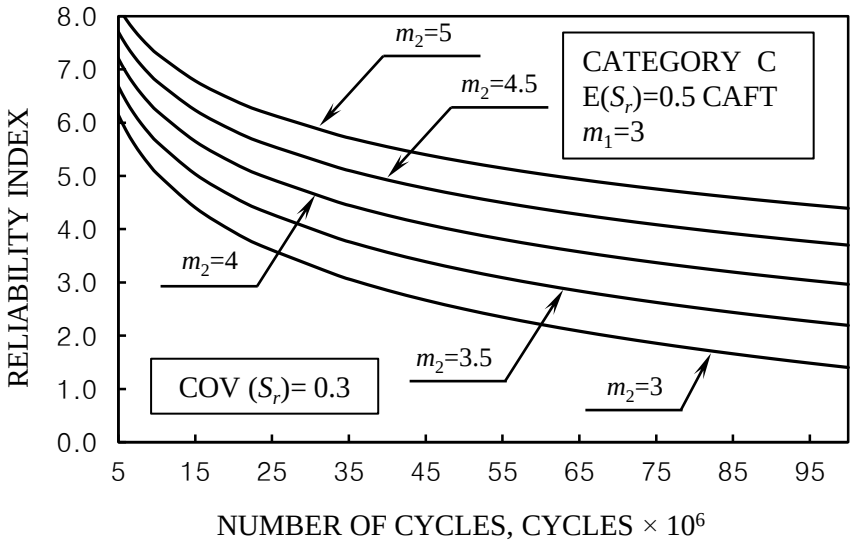
RELIABILITY INDEX
8.0
7.0
6.0
5.0
4.0
3.0
2.0
1.0
0.0
5
15
25
35
45
55
65
75
85
95
m_2=5
m_2=4.5
m_2=4
m_2=3.5
m_2=3
CATEGORY C
E(S_r)=0.5 CAFT
m_1=3
COV (S_r)= 0.3
NUMBER OF CYCLES, CYCLES × 10^6

(b)

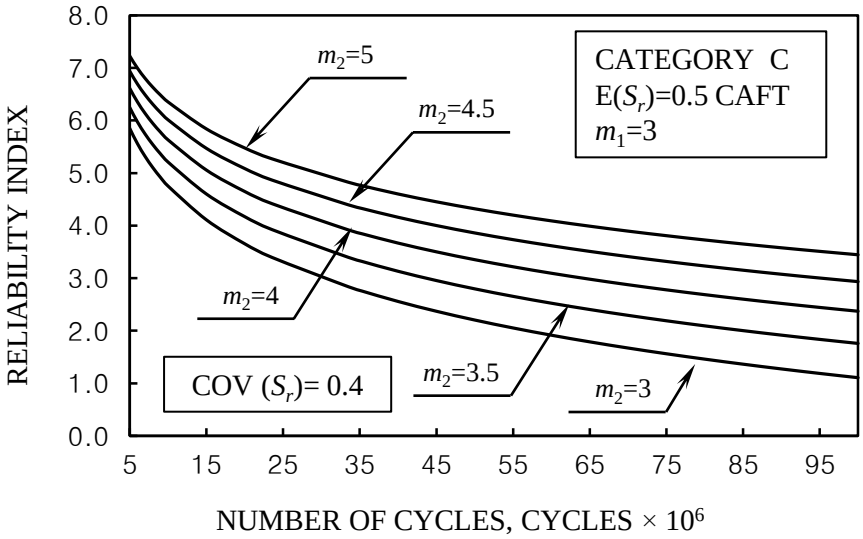
RELIABILITY INDEX
8.0
7.0
6.0
5.0
4.0
3.0
2.0
1.0
0.0
5
15
25
35
45
55
65
75
85
95
m_2=5
m_2=4.5
m_2=4
m_2=3.5
m_2=3
CATEGORY C
E(S_r)=0.5 CAFT
m_1=3
COV (S_r)= 0.4
NUMBER OF CYCLES, CYCLES × 10^6

(c)

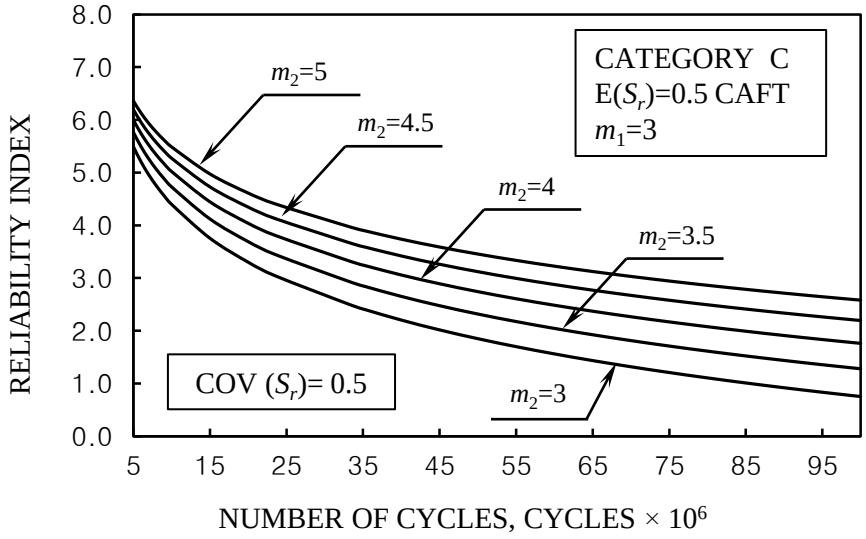

(d)

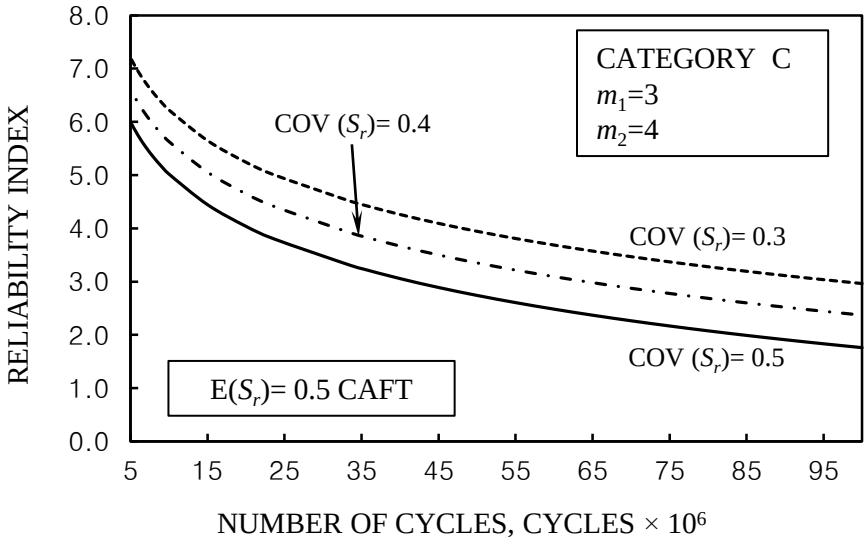

Figure 3.3 Reliability Index versus number of cycles for different values of m_2: (a) COV (S_r) = 0.3, (b) COV (S_r) = 0.4, (c) COV (S_r) = 0.5, and (d) for different values of COV (S_r) with m_1=3 and m_2=4

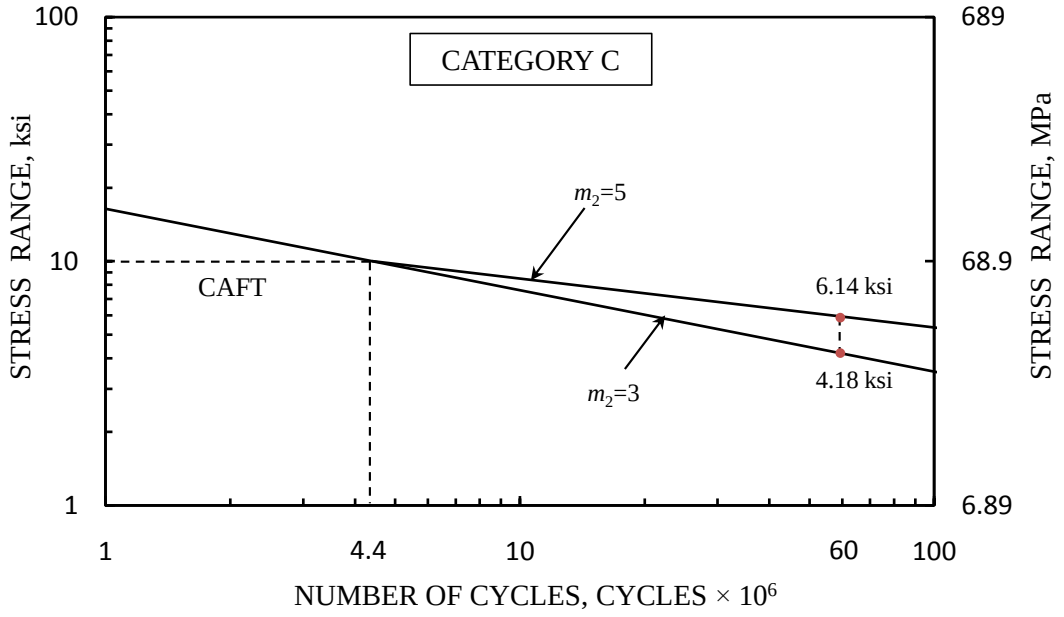

Figure 3.4 *S-N* lines for AASHTO (AASHTO 2014) category "C" with m_2 = 3 and 5

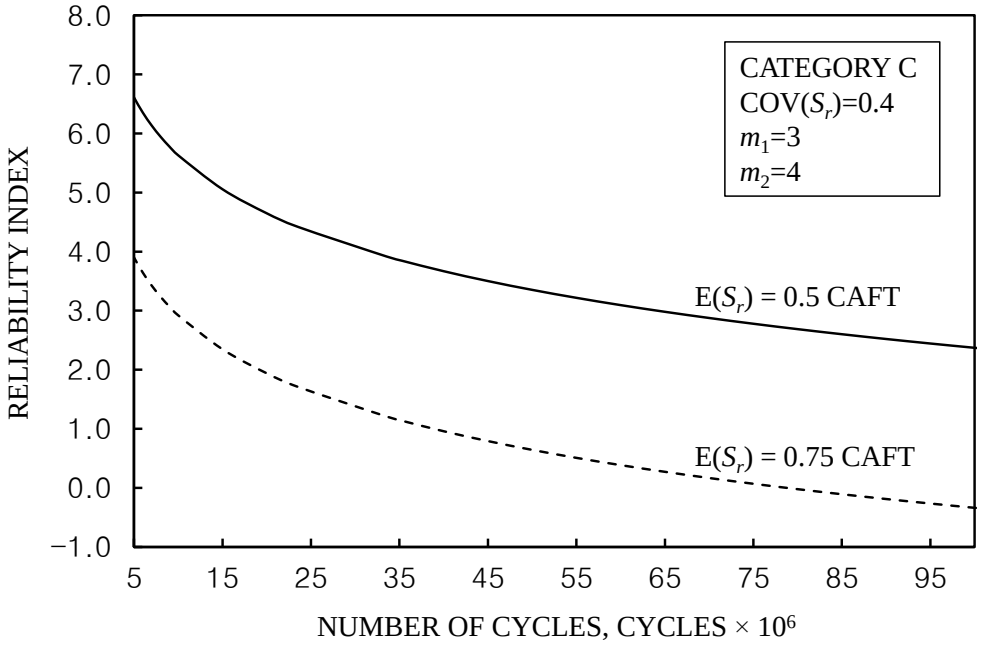

Figure 3.5 Reliability Index versus number of cycles for different mean values of the variable amplitude stress range with COV (S_r) = 0.4 and m_2 = 4

(a)

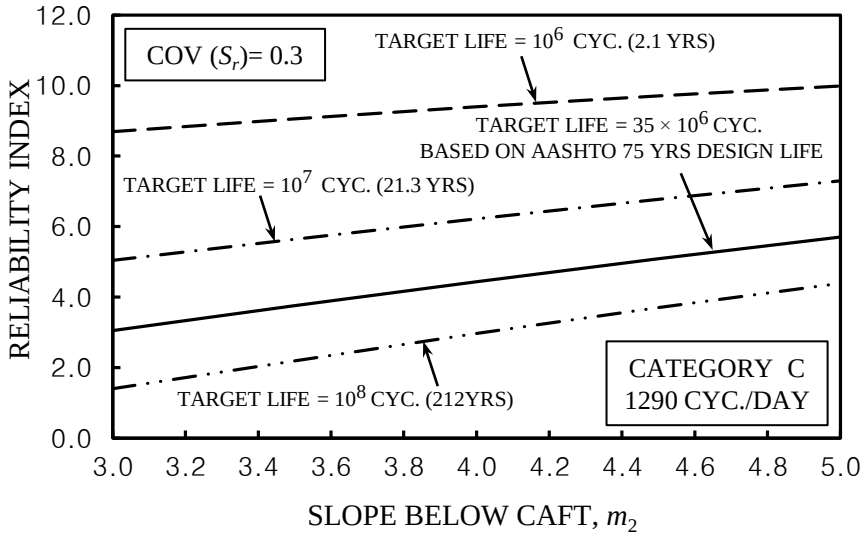
COV (S_r)= 0.3
TARGET LIFE = 10^6 CYC. (2.1 YRS)
TARGET LIFE = 35×10^6 CYC.
BASED ON AAHSTO 75 YRS DESIGN LIFE
TARGET LIFE = 10^7 CYC. (21.3 YRS)
TARGET LIFE = 10^8 CYC. (212YRS)
CATEGORY C
1290 CYC./DAY
RELIABILITY INDEX
SLOPE BELOW CAFT, m_2
12.0
10.0
8.0
6.0
4.0
2.0
0.0
3.0 3.2 3.4 3.6 3.8 4.0 4.2 4.4 4.6 4.8 5.0

(b)

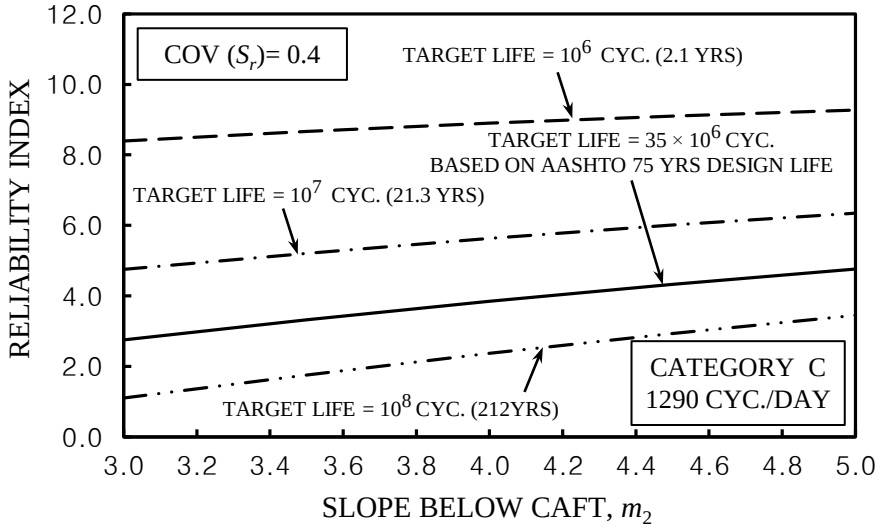
COV (S_r)= 0.4
TARGET LIFE = 10^6 CYC. (2.1 YRS)
TARGET LIFE = 35×10^6 CYC.
BASED ON AAHSTO 75 YRS DESIGN LIFE
TARGET LIFE = 10^7 CYC. (21.3 YRS)
TARGET LIFE = 10^8 CYC. (212YRS)
CATEGORY C
1290 CYC./DAY
RELIABILITY INDEX
SLOPE BELOW CAFT, m_2
12.0
10.0
8.0
6.0
4.0
2.0
0.0
3.0 3.2 3.4 3.6 3.8 4.0 4.2 4.4 4.6 4.8 5.0

(c)

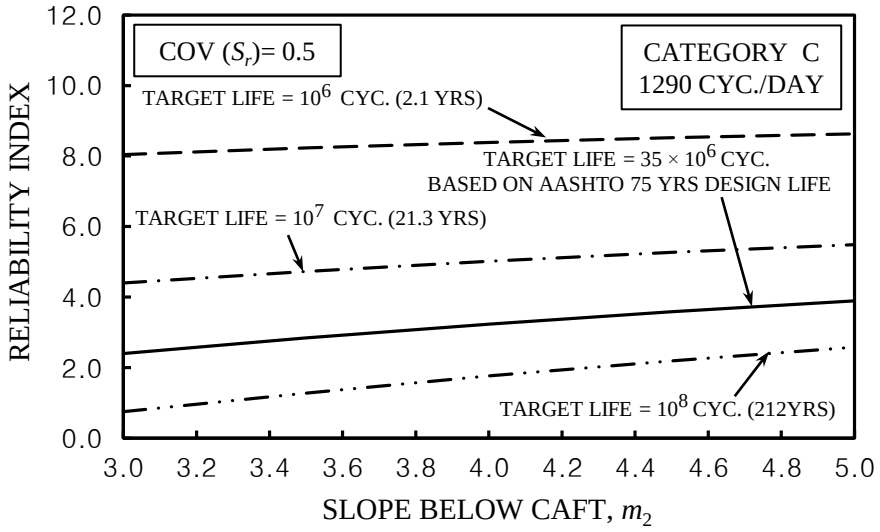

(d)

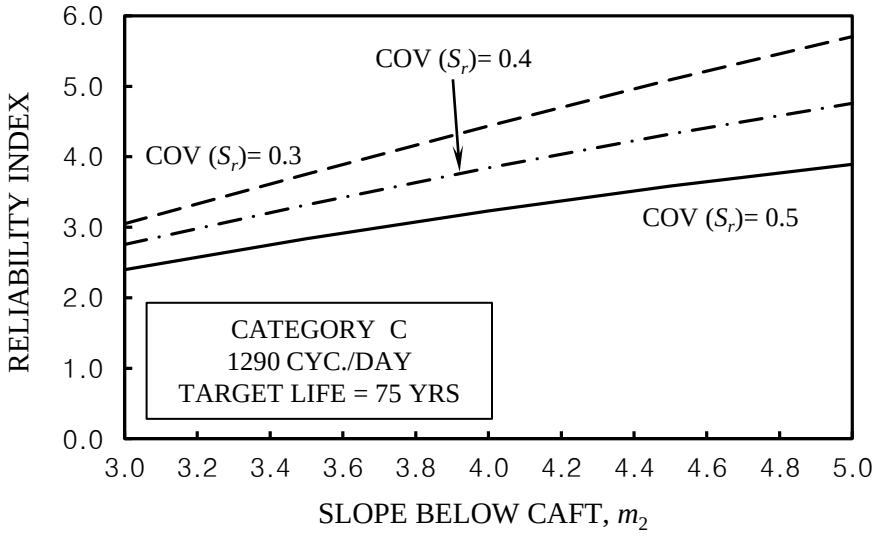

Figure 3.6 Reliability Index versus the slope below the CAFT for different target fatigue life: (a) COV (S_r) = 0.3 (b) COV (S_r) = 0.4, (c) COV (S_r) = 0.5, and (d) for different COVs and a target life of 35 million cycles

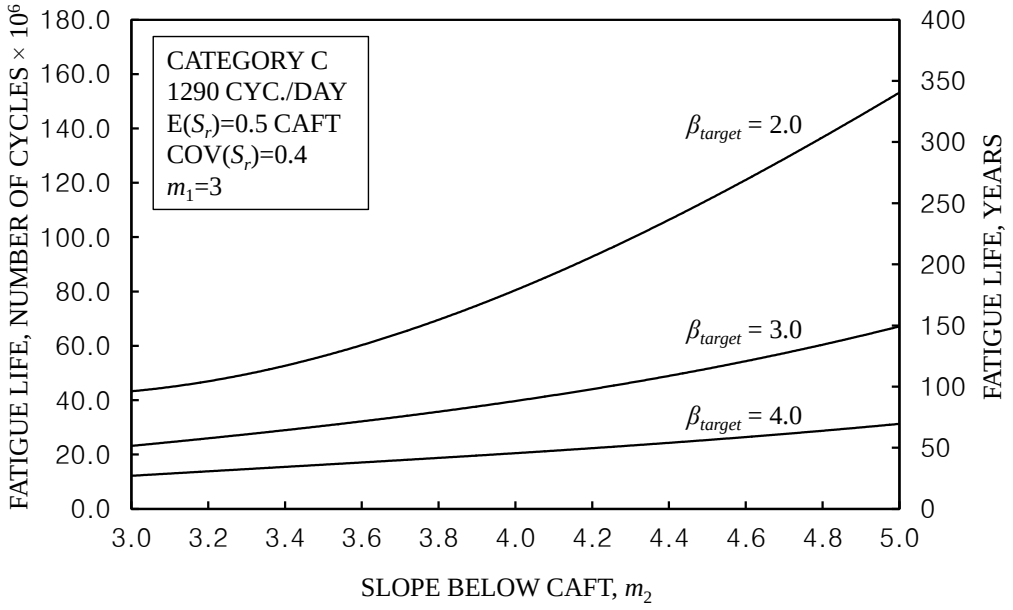

Figure 3.7 Expected fatigue life versus the slope below CAFT for COV (S_r) = 0.4 and different target reliability indices

(a)

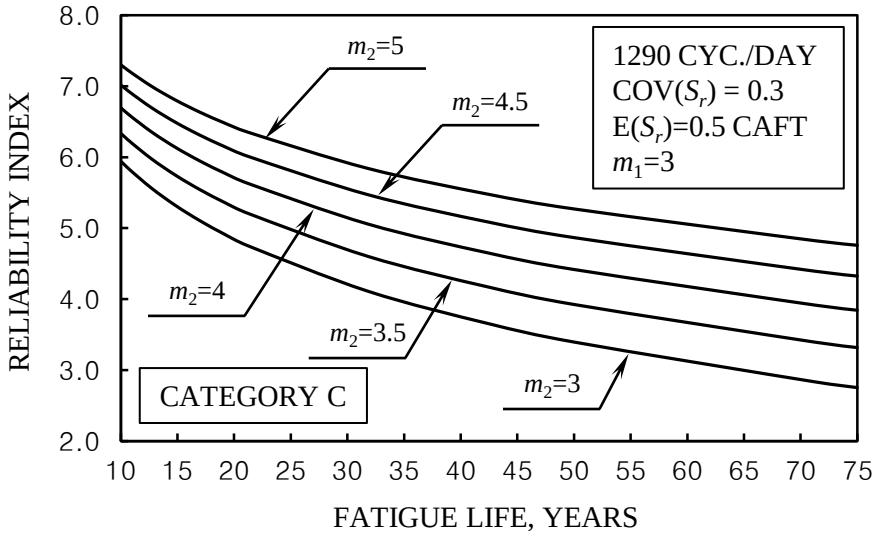

(b)

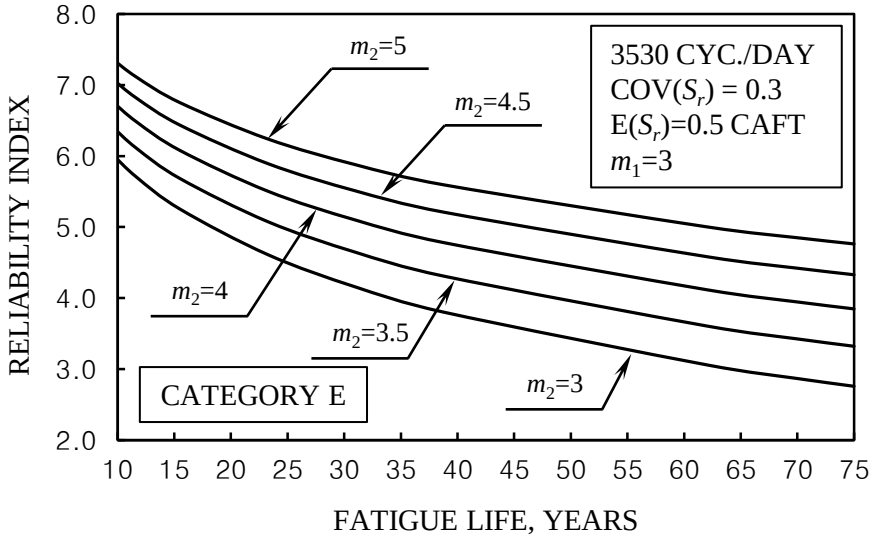

Figure 3.8 Reliability Index versus number of cycles from 10 years to 75 years: (a) Category “C” and (b) Category “E”

(a)

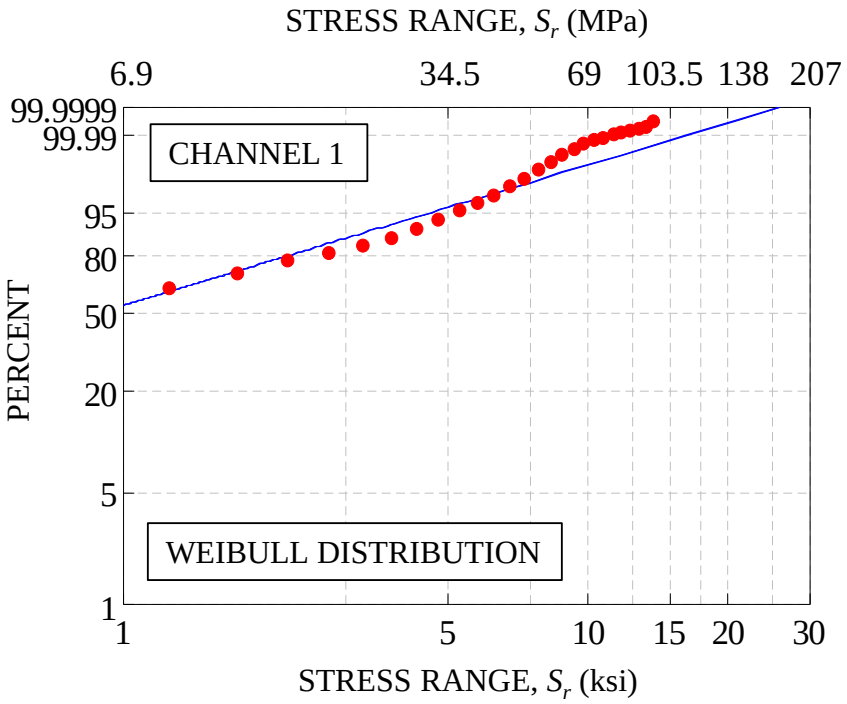

(b)

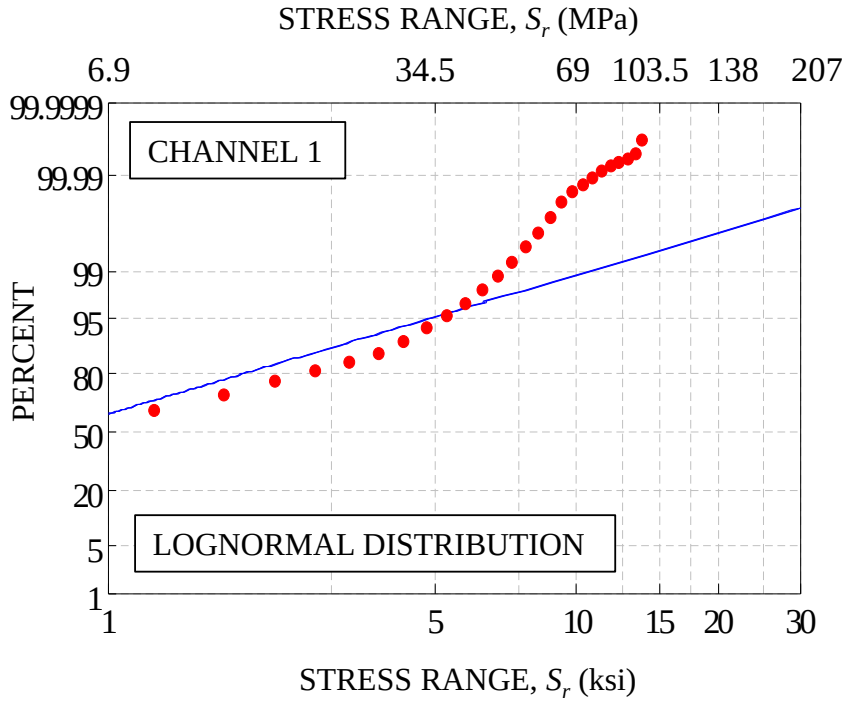

Figure 3.10 Goodness-of-fit tests at Channel 1: (a) Weibull distribution and (b) Lognormal distribution

(a)

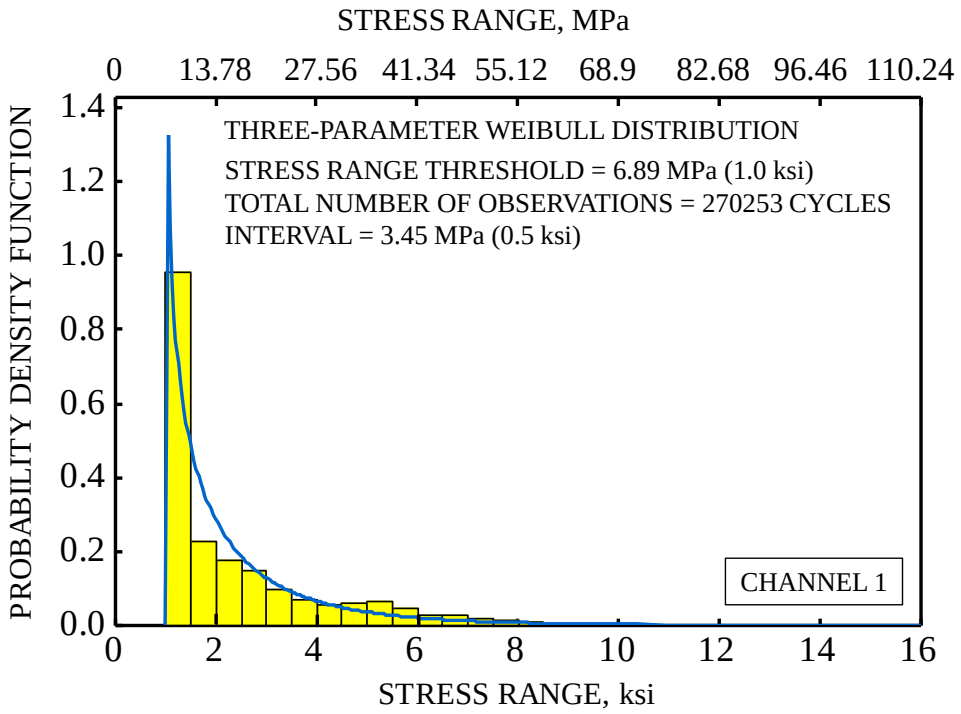
STRESS RANGE, MPa
0
13.78
27.56
41.34
55.12
68.9
82.68
96.46
110.24
PROBABILITY DENSITY FUNCTION
1.4
1.2
1.0
0.8
0.6
0.4
0.2
0.0
THREE-PARAMETER WEIBULL DISTRIBUTION
STRESS RANGE THRESHOLD = 6.89 MPa (1.0 ksi)
TOTAL NUMBER OF OBSERVATIONS = 270253 CYCLES
INTERVAL = 3.45 MPa (0.5 ksi)
CHANNEL 1
0
2
4
6
8
10
12
14
16
STRESS RANGE, ksi

(b)

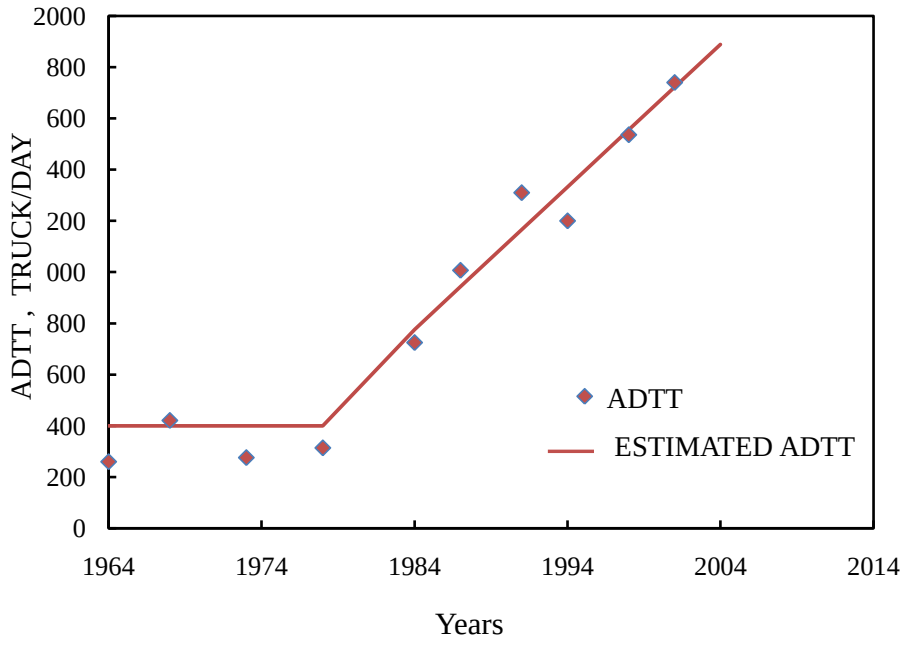
2000
800
600
400
200
000
800
600
400
200
0
ADTT , TRUCK/DAY
ADTT
ESTIMATED ADTT
1964
1974
1984
1994
2004
2014
Years

(c)

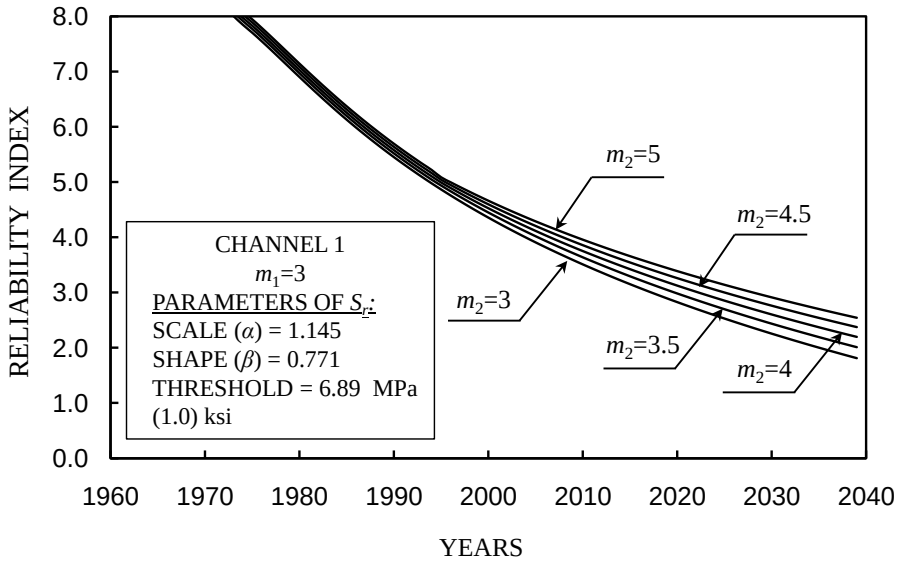

Figure 3.11 Fatigue reliability of the detail at Channel 1: (a) Stress range histogram and its PDF at Channel 1, (b) Estimation of the ADTT from 1978 to 2004, and (c) Reliability profiles of the detail

(a)

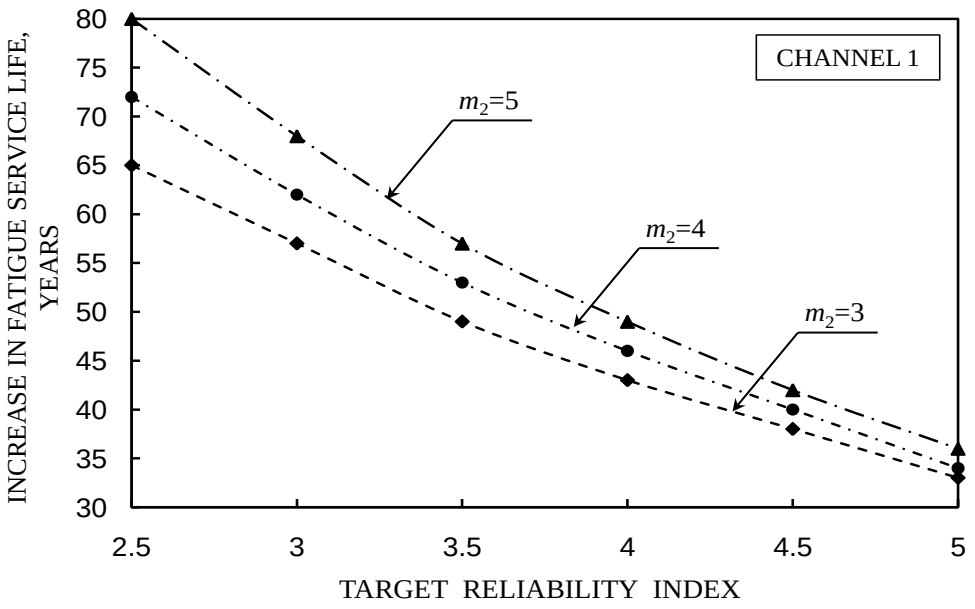

(b)

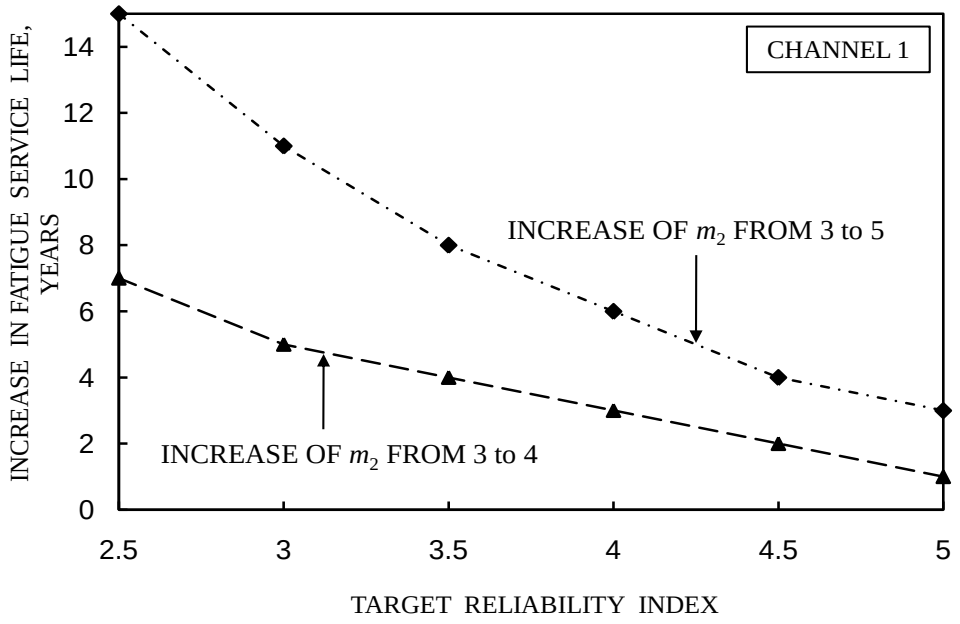

Figure 3.12 Fatigue life prediction of the detail at Channel 1: (a) Fatigue service life of the detail versus the target reliability index for different values of m_2, and (b) Increase in service life of the detail for different values of m_2

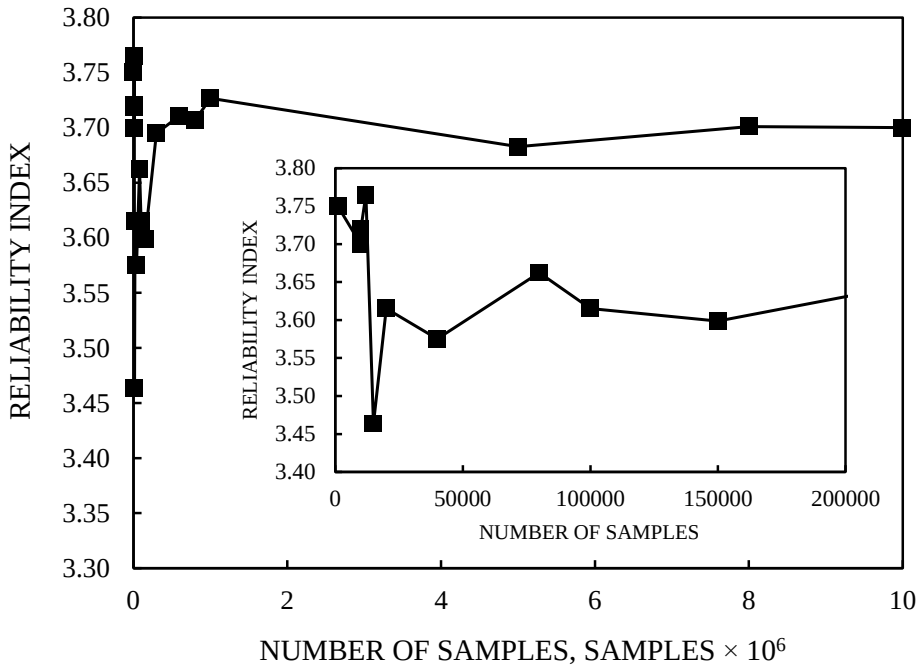

Figure 3.13 A sample convergence plot for the reliability index at the year 2010

(a)

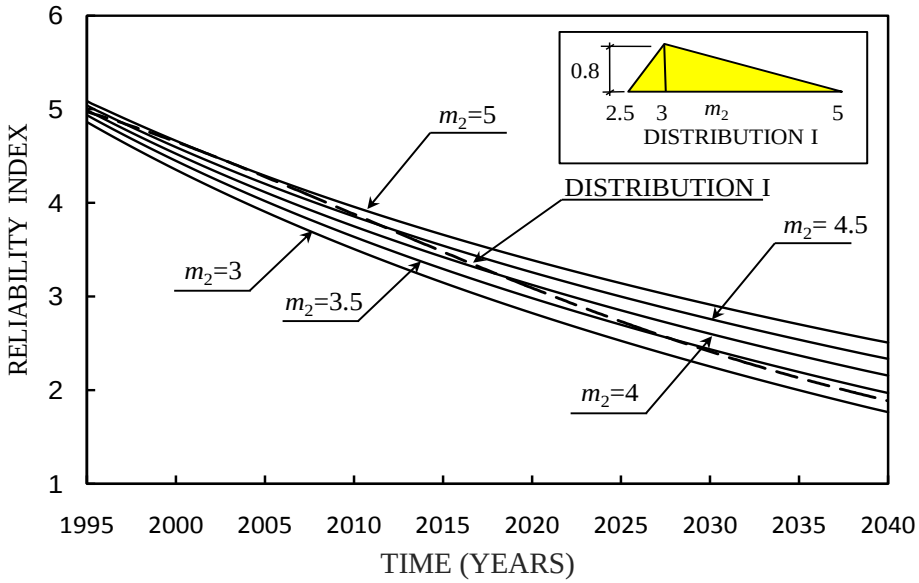
RELIABILITY INDEX
TIME (YEARS)
0.8
2.5
3
m_2
5
DISTRIBUTION I
DISTRIBUTION I
m_2=5
m_2= 4.5
m_2=3
m_2=3.5
m_2=4

(b)

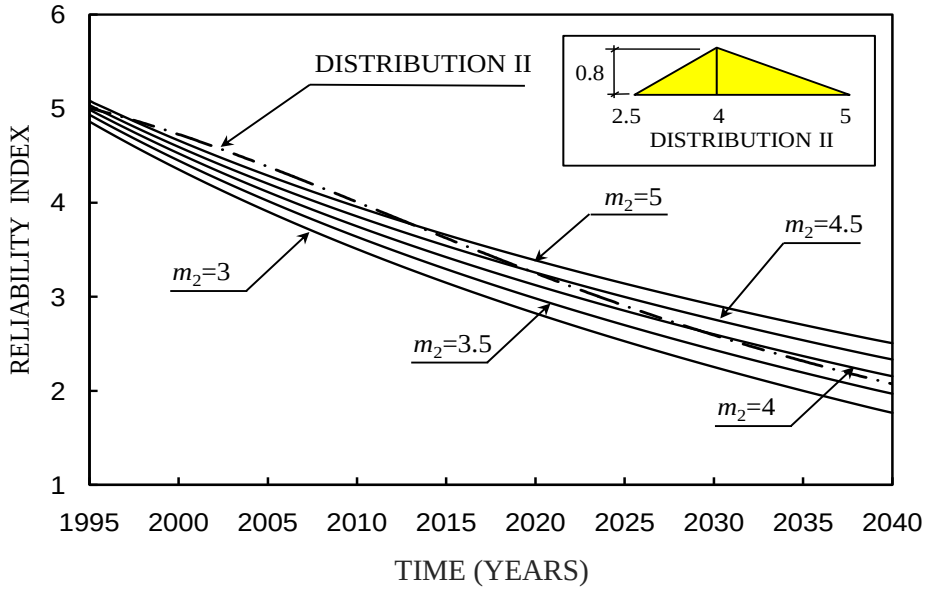
RELIABILITY INDEX
TIME (YEARS)
0.8
2.5
4
5
DISTRIBUTION II
DISTRIBUTION II
m_2=5
m_2=4.5
m_2=3
m_2=3.5
m_2=4

(c)

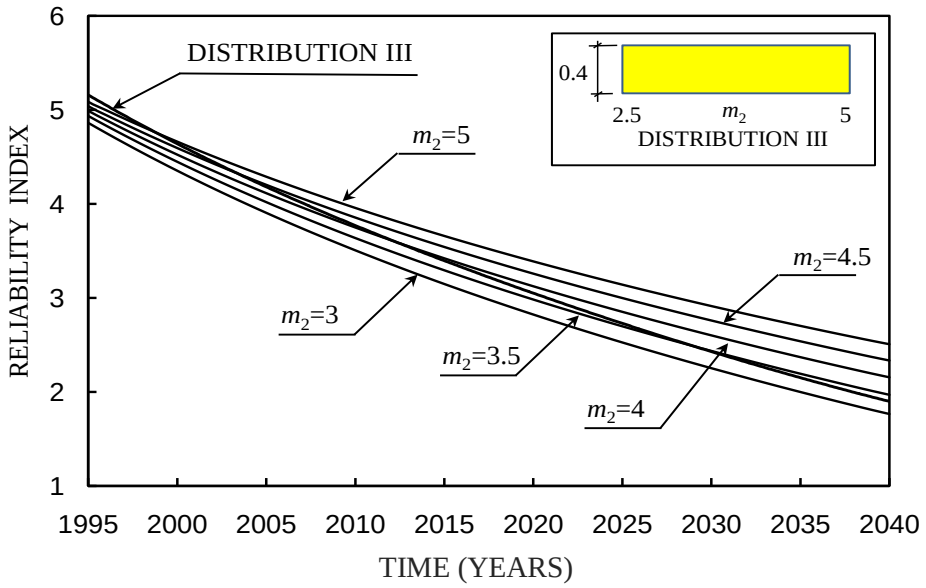

(d)

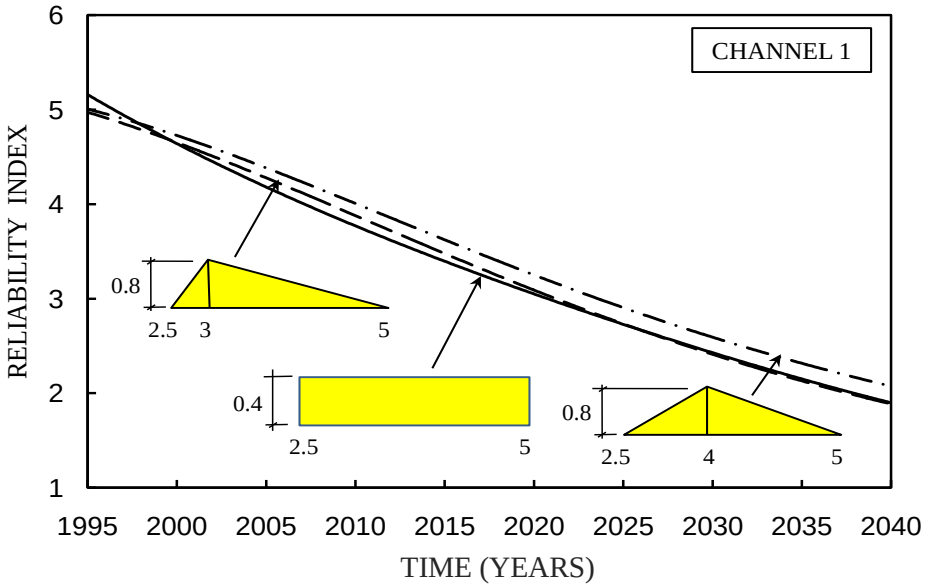

Figure 3.14 Fatigue reliability simulation results compared to the previous ones: (a) Distribution I, (b) Distribution II, (c) Distribution III, and (d) simulation results of the three distributions

CHAPTER 4 FATIGUE RELIABILITY ESTIMATION OF ALUMINUM SHIP DETAILS BASED ON SHM

4.1 Overview

The evolution of naval vessels towards high-speed crafts subjected to severe sea conditions has promoted an increasing interest in lightweight high-strength materials. Due to its strength and weight characteristics, aluminum has been proven especially suitable as construction material for hull structures, as well as other vessel parts. However, fatigue in aluminum naval crafts needs to be effectively addressed for the proper life-cycle assessment. SHM systems constitute effective tools for measuring the structural response and assessing the structural performance under actual operational conditions.

In this chapter, an approach for using SHM information in the fatigue reliability analysis and service life prediction of aluminum naval vessels is presented. The accumulated fatigue damage and the fatigue reliability are quantified based on SHM data acquired under different operational conditions, specified by the ship speeds, sea states, and heading angles. Additionally, an approach for estimating the reliability-based fatigue life under a given operational profile is presented. Seakeeping trial data of an aluminum high-speed naval vessel are used to illustrate the proposed approach. This chapter, along with the previous one, aims to improve the capabilities of the performance prediction module of the LCM framework shown in Figure 1.1 with respect to fatigue critical structures.

The work in this chapter is based on the papers Soliman & Frangopol (2013a, 2014c) and Soliman *et al*. (2014a).

4.2 Background

The use of aluminum in modern naval ships has been recently growing. This is due to its competitive weight and strength characteristics which make it preferable, over conventional steel, to comply with the rapid increase in speed and load requirements. Recently, researchers and designers have been investigating various properties of aluminum as a construction material, including the ultimate carrying capacity of stiffened panels, corrosion resistance, and fatigue behavior of aluminum details. Additionally, this material has been used for innovative structural details whose behavior may still not be well understood. As a result, methodologies for predicting aluminum ship behavior are still topics of active research, focusing especially on the hull capacity, performance in aggressive environments and fatigue resistance (Sielski 2007).

Fatigue damage is one of the main concerns in naval engineering. It occurs at different locations of the ship structure, where stress concentrations or fabrication defects may exist. Fluctuations of stress levels during regular ship operation may cause crack initiation and propagation at these locations. The resulting reduction of the capacity of the affected region may cause failure at load levels well below the service ones. As a result, structures subjected to fatigue damage accumulation require frequent inspections and maintenance actions which can significantly raise the operational cost of the vessel. Fatigue assessment of steel ships and their life-cycle fatigue behavior have been widely investigated (Paik & Frieze 2001; Ayyub *et al.* 2002), and several established design

guides and technical reports have been produced (Munse *et al.* 1982; Glen *et al.* 1999b; ABS 2010; DNV 2010). For aluminum structures, various design guides provide rules for the fatigue design and assessment of structural details, such as the Eurocode 9 (Eurocode 2009) and the DNV (DNV 1997). However, design guidance for fatigue life estimation in high speed naval vessels is still lacking the level of support and detail present in steel ships, and many of the structural details adopted in aluminum ships are still not included in the design codes (Collette 2005). Even for steel ships designed using the appropriate *S-N* specifications, cracks are commonly found to initiate and propagate long before the anticipated fatigue service life is reached (Hess 2007). This suggests the need for more research and refinements in the current fatigue design and assessment approaches to accurately understand the actual ship fatigue behavior under normal operational conditions.

Structural response of ships under sea loading is subjected to randomness inherent in the load conditions, material properties, damage propagation and cross-sectional dimensions. In this context, SHM is an important tool for the reduction of uncertainties, providing information on the real-time structural response (Okasha *et al.* 2011). For fatigue studies, SHM data can be used for calculating the fluctuating stress levels acting on the details at different operational conditions. This task could be theoretically performed through a comprehensive finite element analysis (FEA) coupled with spectral analysis of the actual ship properties (Violette 1998). However, this process is more suited towards the design stage as it consists of significant assumptions and simplifications that can be dropped by using SHM.

Reliability analysis provides a unified measure of the structural performance that takes into account both aleatory and epistemic uncertainties (Frangopol 2011), an attractive feature for fatigue analysis. Moreover, it can give an adjusted service life based on the required safety level for the ship, which is a function of the ship importance, age, and use, among others (Kwon & Frangopol 2012). Although reliability-based fatigue evaluation of steel ship details is well established (see Paik & Frieze (2001) and Ayyub *et al.* (2002)), it is still an active research area for aluminum ones. Most of the studies in this field predict the unified long-term probability density function (PDF) of the ship loading based on the anticipated ship operational conditions which assumes a specific combination of speeds, heading angles, and wave conditions (Brady 2004a; Collette & Incecik 2006; Hess 2007; Kwon *et al.* 2013). This adds significant uncertainties in the fatigue life estimation especially for littoral combat vessels which do not have a well-defined route and are required to operate in a wide range of operational conditions (Hess 2007; Salvino & Brady 2008). Additionally, this approach leaves no room to investigate the effect of different operational conditions on the fatigue damage accumulation. As a result, it is not possible to isolate those operational conditions causing severe fatigue damage from the ship operational profile. This operational profile, developed based on the operational conditions encountered by the ship, is defined in the form of discretized blocks of constant sea-state, speed, and relative heading. Each block has a probability which represents the fraction of the navigation time spent in that operational condition (Brady 2004a). Moreover, this load profile cannot be easily updated, should the ship operational profile change at any point in its life-cycle.

This chapter presents a reliability-based approach to quantify the long-term reliability and fatigue service life based on the short-term SHM data collected during seakeeping trials. The fatigue reliability and damage accumulation are assessed with respect to various operational conditions, including the significant wave height, encountered wave period, navigation speed, and heading angle. The effect of automated ride control systems at various operational conditions on the fatigue performance and reliability is also investigated. The results can be effectively integrated within the LCM framework to support the decision making process with regards to the safe operational conditions. Moreover, it can assist in the evaluation of the current design and assessment guidelines under the effect of large number of cycles that are normally not reached in laboratory testing. Additionally, a computationally efficient approach for the reliability-based estimation of the fatigue service life, based on the SHM data collected either during seakeeping trials or normal ship operation, is proposed. After the initial data analysis, the proposed approach gives the possibility to non-technical crew personnel to estimate the fatigue life at critical details. The approach is applied to the SHM data collected during seakeeping trials performed on an aluminum high-speed naval vessel (the HSV-2) in 2004.

4.3 Fatigue Damage

As previously mentioned, fatigue is considered as a major threat for metallic structures in general, and for ships in particular, since the vessel is subjected to a large number of stress cycles throughout its service life. This is more endangering in the case of aluminum high-speed vessels. Despite their competitive corrosion resistance and strength to weight ratio, aluminum structures have a crack propagation rate considerably higher

than steel structures (Sielski 2007), and therefore a shorter expected fatigue life. This is clearly represented in Figure 4.1 where the *S-N* diagrams of the same details made of aluminum and steel are compared. These *S-N* lines are adapted from the Eurocode 3 (Eurocode 2010) and the Eurocode 9 (Eurocode 2009) for steel and aluminum constructions, respectively. Figure 4.1 (a) depicts the *S-N* relations for rolled or extruded aluminum and steel members, while Figure 4.1 (b) illustrates the same relations for a welded member. As shown, for any stress level, the fatigue life of the aluminum members is considerably reduced compared to the steel ones, and the difference is significantly larger in the case of welded structures. In this chapter, the *S-N* relation given by Equation (2.11) is used.

4.3.1 Stress range

Different stress analysis methods can be used for the fatigue assessment of aluminum details, namely the nominal stress, structural hot spot stress, and notch stress (Maddox 2003; Ye & Moan 2008). The choice of the stress type and its corresponding *S-N* relationships mainly depends on the available data. The nominal stress approach is adopted by several design and assessment guides such as the Eurocode 9 (Eurocode 2009). This method uses the stress acting on the considered location neglecting the stress concentration arising from both the structural configuration and the weld effect. These effects are inherently considered within the *S-N* line definition. The main advantage of using this approach is the ease of application since the nominal stress calculation is usually straightforward. On the other hand, to assess the fatigue damage for a specific detail using this approach, a similar match in the design guide has to be found, and this is not always possible for ship structures.

The structural hot spot stress approach uses the stress induced in the proximity of the weld, including the stress concentration due to the structural configuration but not due to the weld itself. This stress is next compared to *S-N* lines which, instead, incorporate the effect of weld stress concentration. The calculation of the structural stress requires more advanced structural analysis than the nominal stress case. To exclude the stress concentration due to the weld, a single reference point at a prescribed distance from the weld toe can be used; otherwise the structural stress can be extrapolated by measurement performed at multiple reference points (Radaj 2006). The advantage of such approach is that a lower number of *S-N* curves needs to be evaluated compared to the nominal stress case.

The last method, the notch stress, uses the total stress acting at the crack initiation location, which includes the stress concentration due to both the structural configuration and the weld geometry. The notch stress is usually more difficult to obtain; however, it can be used to find the fatigue life of the structural detail using the *S-N* curve for a base non-welded metal. A representation of the three stress types is shown schematically in Figure 4.2.

When dealing with SHM data, it is not practical to find the stress concentration at the weld toe using strain measurement, due to the high stress gradient at this location. Thus, depending on the available data, the nominal stress approach can be used if a similar detail can be found in design guides. Otherwise, the structural hot spot stress approach can be used. In the latter case, several recommendations for the placement of sensors to measure the structural stress can be found in literature. For instance, Niemi (1995) proposes to perform linear extrapolation of the stresses measured at distances $0.4t_p$

and $1.0t_p$ from the weld toe, where t_p is the plate thickness. Other classification societies, such as the Lloyd's register approach, herein adopted, uses the stress measured at $0.5t_p$ as the structural stress (Ye & Moan 2008).

Ship structures are naturally subjected to variable amplitude stress cycles. If the distribution of the stress cycle amplitudes is known, Miner's damage accumulation rule (Miner 1945) given by Equation (2.12) can be used to find a representative equivalent constant amplitude stress range.

Based on Miner's damage accumulation rule, an equivalent constant amplitude stress range can be defined by Equations (2.13) and (2.14). For the case study discussed in this chapter, it was found that the Weibull distribution provides a very good fit for the stress range data of the analyzed aluminum detail. The three-parameter PDF of this distribution is given by Equation (2.17).

4.3.2 Fatigue life

For an equivalent constant amplitude stress range, fatigue life can be measured as the number of cycles to failure as follows

$$N = \frac{A}{S^m} \tag{4.1}$$

where A = fatigue coefficient dependent on the type of the detail, m = slope of the S-N lines in logarithmic scale, and S = stress acting on the detail. This number of cycles N, in conjunction with the average annual number of cycles N_{avg} obtained by the SHM data, returns an estimation of the fatigue life t_f in years, using the following equation

$$t_f = \frac{N}{N_{avg}} \tag{4.2}$$

and, therefore, the remaining fatigue life T_{rem} as

$$T_{rem} = t_f - t_s \tag{4.3}$$

where t_s is the already spent service life.

4.3.3 Fatigue reliability

The reliability index β has been used herein as the structural performance indicator. It is directly linked to the probability of failure P_f (i.e. the probability of violating a certain limit state), through the following relationship (Kwon and Frangopol 2010)

$$\beta = \Phi^{-1}\left(1 - P_f\right) \tag{4.4}$$

in which $\Phi^{-1}(\cdot)$ is the inverse of the standard normal cumulative distribution function.

For the probabilistic assessment of the remaining fatigue life, the reliability is quantified based on the following performance function

$$g(t) = \Delta - D(t) \tag{4.5}$$

where Δ = Miner's critical damage accumulation index, indicating the allowable accumulated damage and assumed lognormal distributed with mean 1.0 and coefficient of variation (COV) 0.48 (Collette & Incecik 2006); $D(t)$ = Miner's damage accumulation index, which can be expressed as

$$D(t) = \frac{N(t)}{A} \cdot S_{re}^{m} = \frac{t \cdot N_{avg}}{A} \cdot S_{re}^{m} \tag{4.6}$$

where A and m = S-N relationship parameters (see Equation 4.1), S_{re} = equivalent constant amplitude stress range (see Equations 2.13 and 2.14), and N_{avg} = average annual number of cycles.

Based on Equations (4.4) and (4.5) and assuming that all the random variables (i.e. S_{re}, A, and Δ) follow the lognormal distribution (Ayyub *et al.* 2002; Kwon & Frangopol 2010), the fatigue reliability index β can be found as follows:

$$\beta(t) = \frac{\lambda_{\Delta} + \lambda_{A} - m \cdot \lambda_{S_{re}} - \ln N(t)}{\sqrt{\zeta_{\Delta}^2 + \zeta_{A}^2 + (m \cdot \zeta_{S_{re}})^2}} \tag{4.7}$$

where λ and ζ are the lognormal parameters associated with different random variables.

By setting a fatigue reliability threshold β_{target} and considering Equation (4.7), the fatigue life t_f can be determined as follows

$$t_f = \frac{e^{k - m \cdot \lambda_{S_{re}}}}{N_{avg}} \tag{4.8}$$

where

$$k = \lambda_{\Delta} + \lambda_{A} - \beta_{target} \cdot \sqrt{\zeta^2} \tag{4.9}$$

and

$$\zeta^2 = \zeta_{\Delta}^2 + \zeta_{A}^2 + \left(m \cdot \zeta_{S_{re}}\right)^2 \tag{4.10}$$

Equation (4.8) represents an immediate way to estimate the reliability-based fatigue life for a selected operational condition, once the associated stress range distribution is known.

4.4 Fatigue Reliability under Multiple Operational Conditions

Investigating the long-term fatigue reliability of a ship detail requires analyzing all operating conditions that the vessel is expected to encounter. The main factors that have to be taken into account are ship speed, wave height and period, and heading angle. Long-term fatigue assessment of high-speed vessels can be performed using the lifetime weighted sea method (Hughes 1988). This method predicts the ship long-term response as a combination of short term structural responses evaluated for various operational conditions. In this type of analysis, the response is usually obtained by structural analysis. Stress transfer functions, determined at the studied location for the specified ranges of wave heights and periods and heading angles, are used to calculate the stress energy spectrum and the spectral moments. The short-term responses are combined into a long-term one, for a prescribed operational profile, through the probabilities of the different short-term operational conditions. Moreover, under the assumption of Gaussian distributed loads and narrow-band load response, closed form solutions are available for the determination of the cumulative damage accumulation (Jensen 2001; ABS 2010). As mentioned previously, this process consists of significant assumptions that are not always realistic for high-speed naval vessels and may be avoided by using the SHM data.

When SHM information is available, the short-term response of the ship detail, for a selected operational condition, can be directly found using strain measurements recorded during seakeeping trials, performed on the vessel at the beginning of its service life. Subsequently, for a prescribed operational profile with assigned probabilities of occurrence p_j of different sea states, speeds, and heading angles, the total damage

accumulation index D_T can be found, under the assumption of linear damage accumulation, as

$$D_T = T_r \cdot \sum_{j=1}^{n_o} p_j \cdot D_j \tag{4.11}$$

where n_o = number of operational conditions encountered by the ship during the reference time T_r (years), and D_j = annual damage accumulation index for the detail associated with the jth operational condition. An alternative approach to compute D_T is to find an equivalent stress range by using Equation (2.13) and calculating the total damage accumulation under this equivalent condition. Finally, the fatigue life T_f can be found as

$$T_f = \frac{T_r}{D_T} = \frac{1}{\sum_{j=1}^{n_o} p_j \cdot D_j} \tag{4.12}$$

Similarly, the fatigue reliability under multiple operational conditions can be evaluated using the performance function

$$g(t) = \Delta - D_T \tag{4.13}$$

which can be expressed as

$$g(t) = \Delta - T_r \cdot \sum_{j=1}^{n_o} p_j \cdot D_j \tag{4.14}$$

By substituting Equation (4.6) into Equation (4.14), the performance function can be rewritten as

$$g(t) = \Delta - T_r \cdot \sum_{j=1}^{n_o} p_j \cdot N_{avg_j} \cdot \frac{S_{re_j}^m}{A} \tag{4.15}$$

where N_{avg_j} = average number of cycles acting on the detail during one year of exposure to the jth operational condition, and S_{re_j} = constant equivalent stress range acting on the

detail at the *j*th operational condition. The stress range and the number of cycles can be found using the SHM data collected during the water trials. Equation (4.15) can be used to find the time-variant fatigue reliability, and the fatigue life can be determined by comparison with a prescribed target reliability threshold.

For the case where the random variables follow the lognormal distribution, it has not been possible to determine the analytical solution of Equation (4.15) in terms of the reliability index due to the presence of the sum over the different operational conditions constituting the complete operational profile. Accordingly, an approximate reliability-based fatigue life is herein proposed, based on the individual fatigue lives associated with different operational conditions. Denoting t_{f_j} as the reliability-based fatigue life under the *j*th operational profile, an approximate damage accumulation index D^* can be defined for the detail after exposure to n_o operational states, as

$$D^* = T_r \cdot \sum_{j=1}^{n_o} \frac{p_j}{t_{f_j}} \tag{4.16}$$

where t_{f_j} can be calculated using Equations (4.8) – (4.10) as

$$t_{f_j} = \frac{e^{k_j - m \cdot \lambda_{S_{re,j}}}}{N_{avg,j}} \tag{4.17}$$

Thus, the reliability-based fatigue life T_f is obtained as

$$T_f = \frac{T_r}{D^*} = \frac{1}{\sum_{j=1}^{n_o} \frac{p_j}{t_{f_j}}} \tag{4.18}$$

This approach, in which short-term monitoring data are used to predict the long-term response, offers several advantages compared to adopting either a single long-term load response or a long-term monitoring program. A unified long-term load response has

the main drawback of being strongly dependent on the anticipated long-term operational profile for the ship. For high speed naval vessels, usually, a safe operational envelope can be defined to establish ship use limitations to specific sea conditions in order to reduce the likelihood of damage to the ship structure. In fact, the reaction of the crew towards the operational envelope has a significant effect on the actual long-term loading profile (Collette 2005). A change in the operational profile will alter the predicted long-term response and, as a result, the estimated fatigue life has to be re-calculated. If the fatigue life estimation is required for a different operational profile, the analysis has to be entirely redone since the combination of the short-term responses constitutes the first step in the fatigue assessment. In this regards, the approximate approach proposed herein only requires to update the probabilities of occurrence p_j for the new long-term operational profile and evaluate the reliability-based fatigue life by Equation (4.18). Therefore, the assessed fatigue life can be easily updated whenever new information on the actual operational profiles of the ship is available. It is worth noting that the reliability threshold should be selected a priori by the vessel manager, and that the proposed procedure allows determining the fatigue life with respect to the selected threshold.

On the other hand, long-term monitoring programs are expensive due to the high cost associated with the monitoring systems, as they require regular maintenance activities and regular data processing, which may add a significant burden to the operational cost of the ship. In general, the cost of long-term monitoring program consists of the (a) general access and preparation cost, (b) monitoring system cost, (c) maintenance cost, and (d) continuous analysis and report preparation cost. The latter

often constitutes the largest part of the monitoring program cost (Frangopol *et al.* 2008a,b).

4.5 Case Study

4.5.1 General

The fatigue assessment and reliability analysis presented in this chapter are applied to the HSV-2 swift, an aluminum wave piercing catamaran, with an overall length of 98 meters, designed and built in Tasmania, Australia (Incat 2012). The HSV-2 is capable of reaching speeds of 38-47 knots while maintaining an average speed of 35 knots (Incat 2012). The ship is also equipped with a T-foil that is used by the ride control system to stabilize the ship motions at high speeds. A general view of the ship is shown in Figure 4.3 (a) based on Brady (2004b,c), Salvino and Brady (2008), and Incat (2012). The ship was completed in December 2003 and it was instrumented with various types of sensors, during the period 2003-2004, to measure the (a) primary load response, (b) stress concentrations, (c) secondary slam loads, (d) ramp, crane, vehicle deck, and helicopter deck strains. Moreover, the ship was instrumented with accelerometers at various locations and an over-the-bow wave height system supplemented by Tsurumi Seiki Co. Ltd. (T.S.K) (T.S.K. 2013). Foil strain gauges as well as piezoelectric accelerometers were wired and connected to remote junction boxes and an instrumentation trailer (Brady 2004b). The instrumentation required the use of remote junction boxes to provide a cabling scheme in which small sensor wires from multiple locations were combined and routed in larger cables for termination at the instrumentation trailer; a two-pair signal cable connecting the sensor to the remote junction boxes was installed by the monitoring personnel (Brady

2004b). The main objectives of the monitoring plan were to (a) develop safe operating limits for the HSV-2 swift based on structural responses measured during calm water powering trials and rough water seakeeping trials, (b) comparing these limits to the safe operational envelope established by the American Bureau of Shipping, and (c) quantify the adequacy of the structure against global loads, as well as, slam events (Brady 2004b).

As indicated in (Brady 2004b), a total of 16 sensors were placed for measuring the structural response due to global loading. These sensors, denoted as T1-1 to T1-16, recorded the global bending stresses, pitch connecting moments, and split responses. Another group of sensors, T2-1 to T2-9 and T2-12 to T2-21, was installed to measure the stress concentration at various locations. Positions of the structural response sensors (i.e., T1 and T2 sensors) were selected based on detailed finite element analysis and previous experience with similar vessels (Brady 2004b). Data recorded by these sensors have a sample rate of 100 Hz. Seakeeping trials were set up to expose the ship to different operational conditions covering multiple speeds, wave headings, and sea states. Thus, the trials were performed by executing octagon patterns where wave headings of 0°, 45°, 90°, 135°, 180°, 225°, 270°, 315°, and 360° were encountered. However, considering the symmetry of the vessel, most of the runs were executed to cover only 5 heading angles. A total of 22 trial octagons have been performed at different speeds ranging between 2 and 35 knots at sea states 4 and 5. To study the effect of the ride control system on the structural response, a portion of those trial octagons was performed with the T-foil deployed while the rest was performed with the T-foil retracted. Slam load analysis performed by (Brady 2004a) showed that deploying the T-foil may slightly increase the slam pressure; however, it reduces the rate of slams. The study by Brady (2004a) was

based on a comparison at speed 20 knots with no assessment with respect to fatigue, which is sensitive to both the pressures and the number of cycles. In this chapter, a comparison of the fatigue response with respect to the T-foil deployment is performed at different operational conditions.

4.5.2 Fatigue analysis

For fatigue analysis, the global response (i.e., T1) or stress concentration sensors (i.e., T2) can be used. Since many of the construction details have no direct match in the design guides, the nominal stress approach was not used in this study. Thus, the T2 strain gauges are used with the hot spot structural stress *S-N* approach. Among those sensors, the sensor T2-4, placed to measure the bending response on keel frame 26 on the port side, is analyzed herein. This sensor and its mirrored sensor T2-5, installed on the same frame but on the starboard side, show the highest strain response among all the T2 sensors. The location of frame 26 and the sensor T2-4 are shown in Figure 4.3 (b) and 4.3 (c), respectively.

The strain gauge measurements provide the loading effects for the fatigue assessment process. Since strains at the studied T2 sensor are well below the yield limit, Hooke's law is used to convert strains to stress values. For the resistance, the *S-N* relationship based on the hot spot approach proposed in (Collette & Incecik 2006) is used herein. This approach provides the mean *S-N* line based on regression analysis of 21 tests reported in (Tveiten 1999). In this chapter, both deterministic and probabilistic fatigue assessment are performed. For the deterministic case, the design curve is obtained by shifting the mean *S-N* line by two standard deviations of $log(A)$ to the left (Fisher *et al.* 1998). On the other hand, for reliability analysis, the mean *S-N* line is used. Both the

design and the mean *S-N* line are plotted in Figure 4.4. The intercepts of the adopted design and mean *S-N* lines are reported in Table 4.1.

4.5.3 Analysis of SHM data

Ship structures are normally subjected to various simultaneous loading actions, such as low frequency (i.e., wave induced), high frequency, still water, and thermal loadings. The still water and thermal loadings have, usually, very low frequency and they affect only the mean stresses. Therefore, they have minimal effect on fatigue damage accumulation (Munse *et al*. 1982). The response due to wave induced and dynamic loadings can be captured using strain measurements recorded by monitoring systems showing, typically, the overall response to both loading conditions. Since the effect of this combined load on the fatigue damage accumulation is herein analyzed, it has not been necessary to identify low and high frequency load components. This is in contrast with ultimate load capacity analyses in which the decomposition into low and high frequency loads is essential (Okasha *et al.* 2011). However, digital filters have been used herein to remove low amplitude stress cycles associated with very high frequencies induced by external noise and having negligible effect on the fatigue accumulation. After analyzing the Fourier transforms of signals recorded during various operational conditions, it has been chosen to process all signals with a low-pass Butterworth filter (Giovanni & Sorrentino 2007) with 7.0 Hz cut-off frequency. A sensitivity analysis has been performed to investigate the effect of the cut-off frequency on the annual fatigue damage accumulation, showing only marginal increase in the annual fatigue damage accumulation for cut-off frequencies above 7 Hz. In Figures 4.5 (a) and 4.5 (b), the amplitudes of the Fourier transform of two strain signals recorded at speeds 20 and 35 knots, respectively, are plotted. The raw

signal, in the time domain, is shown in Figure 4.6 (a) for run 133, and a close-up look is shown in Figure 4.6 (b) to demonstrate the effect of the filtering process. The MATLAB® signal processing toolbox in version 2012a (Mathworks Inc. 2012) has been used.

After filtering the signal, the rainflow algorithm (Downing & Socie 1982) is used to construct the stress range bin histograms and obtain the average number of cycles for each operational condition. The resulting stress range histograms are used to find the equivalent constant amplitude stress range using Equation (2.14). A distribution fitting process is performed, using the maximum likelihood method, to find the best fit for the stress range data among multiple candidate distributions, namely, lognormal, Rayleigh, Weibull, and exponential. Goodness of fit is judged using the Kolmogorov-Smirnov test (Ang & Tang 2007) as well as probability plots. Analyses of the fitting data showed that the Weibull distribution provides the best fit for the short term stress range records. The fitting results are illustrated in Figure 4.7 for the Run 70 with speed 20 knots for head sea conditions; in particular, Figures 4.7 (a), (b), and (c) show the probability plot of the stress range data for the Weibull, lognormal, and exponential distributions, respectively. Additionally, Figure 4.7 (d) shows the stress range bin histogram along with the best distribution fit.

4.5.4 Fatigue damage accumulation

Fatigue damage assessment is performed for the detail equipped with the sensor T2-4 using the strain measurements for the range of available operational conditions. Equation (2.12) is used for this task considering an annual ship operation rate o_r = 2/3 (i.e., it is considered that the ship is operated 2/3 of the time). The results of such analysis provide indications on the effect of different operational conditions on the fatigue damage. Figure

4.8 (a) shows the annual damage accumulation with respect to the speed for sea states 4 and 5. It should be noted that the strain records of the operational condition at sea state 5 with speed 20 knots and heading angle 0° were not included in the monitoring data. As expected, the damage accumulation increases with the speed. Higher sea states have significant effect on the damage accumulation especially at speeds higher than 30 knots. At 35 knots, an increase of 250% in the damage accumulation is found when the sea state changes from 4 to 5. Additionally, the study is performed with respect to the significant wave height and the encountered wave period, which is dependent on the ship speed. Results reported in Figure 4.8 (b) illustrate the variation of the annual fatigue damage accumulation of the detail with respect to the encountered wave period for different values of the significant wave height *H*. As shown, the damage accumulation decreases with the increase in the encountered wave period. Additionally, the accumulation increases with the increase in the significant wave height *H*; this effect is amplified for low values of the encountered wave period (i.e., at higher navigation speeds). It is also observed that the difference in the damage accumulation occurring at sea state 4 for speeds 20 and 30 knots is very small. This can be attributed to the difference in the wave period between the two operational conditions.

The effect of the T-foil deployment on the fatigue damage accumulation at various operational conditions has been also investigated. Results are depicted in Figure 4.9 for sea state 5 and head sea condition, considering various speeds, and T-Foil deployed or retracted. At low speeds (15 knots and below) the effect of the T-foil on the damage accumulation seems negligible. However, with the increase in speed, a different behavior is observed; at 30 knots, the damage accumulation is lower with the T-foil

retracted, with a reduction of 30% in the damage accumulation when compared to the case with the T-foil deployed; whereas, at 35 knots, the T-foil deployment reduces the damage accumulation by about 30%. Therefore, with respect to the fatigue damage accumulation, the T-foil seems to be not effective at speeds 30, 15, and 2 knots.

The effect of the heading angle is next analyzed; the annual damage accumulation with respect to the heading angle at speed 15 knots is reported in Figure 4.10 for different sea states. The same trend in the results is observed for the two considered sea states with respect to the heading angle; however, an upwards shift in the damage accumulation occurs with the higher sea state. The damage accumulation is maximum for head sea condition and minimum for beam (i.e., heading angle = 90°) and following seas (i.e., heading angle = 180°). For heading angles 45° and 135°, the damage accumulation level is almost equal, residing at around 75% of that occurring at head sea conditions. Similar results were found for the case of T-foil deployed, shown in Figure 4.11 (a). The damage accumulation has similar values to the case of T-foil retracted at most heading angles, except for the head sea (i.e., heading angle = 0°) and the following sea in which the T-foil deployment causes a slight increase in the damage accumulation. This observation is in line with the results shown in Figure 4.9. The effect of heading angle on the fatigue damage accumulation trend changes with higher speed. Figure 4.11 (b) shows the annual damage accumulation at speed 35 knots, for different heading angles and T-foil deployed or retracted. As expected, the T-foil reduces significantly the damage accumulation for most heading angles except 135° and 180°. In these cases, the damage accumulation shows no sensitivity with respect to the T-foil condition. Figures 4.12 (a) and (b) provide, in polar plot representation, the annual damage accumulation at speeds 15 and 30 knots

for sea states 4 and 5, respectively. As shown, the speed of the ship has a significant effect on the damage accumulation at different heading angles and sea states.

4.5.5 Fatigue reliability

Fatigue reliability for the individual operational conditions is found by means of Equations (4.5) and (4.6) using the software CalREL (Liu *et al.* 1989) that implements second order reliability method (SORM). Figure 4.13 plots the time-variant reliability index for different operational conditions, assuming that the ship is subjected to the same operational condition throughout its service life, with an annual operational rate $o_r = 2/3$. Figure 4.13 (a) shows the reliability profiles at speed 30 knots for different sea states whereas Figure 4.13 (b) highlights the effect of the speed on the fatigue reliability by showing the fatigue reliability profile for speeds 15, 20, 30, and 35 knots, at sea state 5. Figure 4.13 (c) shows a comparison between the reliability profiles obtained with the T-foil deployed and retracted at speed 35 knots. As expected from previous results, using the T-foil improves the reliability at high speeds, increasing the predicted fatigue life by more than 100%, specifically, 28.1 years and 13.4 years for target reliability indices of 2.0 and 3.0, respectively. The effect of the heading angle is shown in Figure 4.13 (d) in which the reliability is plotted for 0°, 45° and 90° heading angles. For other heading angles, since the damage accumulation is significantly low, the resulting reliability profiles are extremely high compared to those associated with the considered angles; thus, these profiles have been excluded from the plot.

When the real operational profile recorded in the ship log files is considered, a different reliability profile has to be expected. If the time spent in each operational condition or the probability of being in each operational condition is known, the overall

fatigue reliability, as a result of being exposed to multiple operational states, can be found using Equation (4.15). Additional information on obtaining these probabilities and the overall operational profile of a ship can be found in (Glen *et al.* 1999a). This information, in conjunction with the SHM data recorded during the sea keeping trials at an early stage of the ship service life, can be used to project the long-term reliability profile of the ship. As an example, a simple operational profile is provided in Table 4.2 where the probabilities of being in each sea state, heading angle, and speed are given for three different operational conditions (i.e., C1, C2 and C3). In this case, the reliability analysis is performed using the software CalREL. Figure 4.14 (a) shows the reliability profiles of each operational condition, assuming complete operability of the ship in this condition, and the overall reliability profile arising from the real operability in the mixed operational states. The target service life can be easily estimated by establishing a reliability index threshold β_{target}. Setting β_{target} = 2.0 returns a fatigue life of 13.30 years at the detail, whereas, β_{target} = 3.0 gives 6.38 years of fatigue life. This fatigue life seems to be relatively short, especially when compared to other types of structures such as steel ships and bridges. However, as previously mentioned, the analyzed detail shows significantly higher strain response compared to other monitored locations. This suggests the need for more frequent inspections at the analyzed detail to detect and repair any cracks before they reach their critical sizes.

The simplified approach provided by Equations (4.16)-(4.18) is also used to find the fatigue life at each operational state and the overall fatigue life at the detail. The time to failure for each operational state and given by Equation (4.17), is listed in Table 4.2 for target reliability indices 2.0 and 3.0. Using Equation (4.18) for the listed operational

states returns a fatigue life of 13.27 years and 6.34 years for target reliability index of 2.0 and 3.0, respectively. Results obtained by Equations (4.16)-(4.18) are within 5% of those calculated using SORM. However, this simplified method can be used to immediately update the fatigue life, if any future changes should affect the ship operational profile. For example, the updated operational profile given in Table 4.3 is analyzed. This profile provides the same operational states reported in Table 4.2 with modified probabilities; in addition, more operational states characterized by having the T-foil retracted for speeds lower than 35 knots are considered. The fatigue reliability profiles for the individual operational conditions and the overall updated profile are given in Figure 4.14 (b). The fatigue life can be easily updated to account for the modified operational profile. Using Equations (4.16)-(4.18), a fatigue life of 15.83 and 7.56 years is obtained for β_{target} = 2.0 and 3.0, respectively, compared to 15.92 and 7.65, given by the SORM. As shown, both methods yield similar fatigue life estimates for different target reliability indices.

4.6 Conclusions

In this chapter, fatigue assessment of aluminum high speed naval vessels with respect to individual operational conditions has been performed. In addition, an approach for the reliability-based fatigue assessment and life estimation has been proposed. Operational data of the ship, in terms of the time spent at each operational condition (i.e., sea state, heading angle, and speed), were used, in conjunction with the sea trial SHM data, to project the long-term fatigue reliability of a ship detail. The hot spot structural stress approach was used for the fatigue assessment; however, the proposed methodology can be applied to any stress analysis method. The proposed approach allows to (a) evaluate the reliability-based fatigue life in a straightforward manner; (b) analyze the effect of

different operational conditions on the fatigue damage accumulation to adjust the ship safe operational profile and minimize the probability of fatigue failures; (c) plan the ship route in order to minimize the fatigue damage accumulation; and (d) promote the real-world application of reliability-based methods using SHM information. The proposed fatigue life estimation method is applied to strain data of the HSV-2 obtained during the seakeeping trials of the vessel. The following conclusions can be drawn:

1. Operational conditions have different effects on the fatigue damage accumulation. Some combinations of speeds, sea states, and wave headings have a significant effect on fatigue damage accumulation. These operational conditions should be identified and they should be avoided to prevent the accelerated damage to the ship structure.
2. The effect of the T-foil on the damage accumulation has to be investigated carefully for different operational conditions. For the analyzed vessel, it was found that at speeds 30 and 15 knots, the damage accumulation is larger when the T-foil is deployed. However, for speed 35 knots, the T-foil deployment significantly reduces the damage accumulation.
3. Although fatigue is a major aspect affecting the ship safety, other aspects, such as the serviceability and ultimate strength should also be studied.
4. The proposed approach enables the active integration of fatigue aspects in the LCM framework in which inspection and maintenance optimization can be performed, as well as the active route planning to minimize the fatigue damage accumulation at critical details during voyages.

Table 4.1 Deterministic parameters and random variables for fatigue assessment

Parameter	Notation	Distribution type	Mean value	COV[†]
Slope of *S-N* lines[††]	m	-	3.0	-
Miner's critical damage accumulation index[††]	Δ	Lognormal	1.0	0.48
Equivalent constant amplitude stress range	S_{re}	Lognormal	Eq. (4)	0.1
Intercept, mean value[*††]	$E(\log A)$	Lognormal	11.47	0.53
Intercept, lower bound[*]	$E(\log A) - 2 \times \sigma (\log A)$	-	11.07	-

[†] Coefficient of variation
[††] Based on (Collette & Incecik 2006)
[*] Based on regression analysis of test results for aluminum details reported in (Tveiten 1999)

Table 4.2 Parameters of the first operational profile and the corresponding fatigue life

Operational Condition Parameters						Fatigue life (years)	
Operational state	Probability	Sea State	Heading Angle	Speed (knots)	T-Foil	β_{target} = 2.0	β_{target} = 3.0
C1	0.30	5	45°	15	Deployed	90.2	43.1
C2	0.45	5	0°	30	Deployed	6.55	3.13
C3	0.25	4	315°	35	Deployed	75.2	35.9

Table 4.3 Parameters of the updated operational profile and the corresponding fatigue life

Operational Condition Parameters						Fatigue life (years)	
Operational state	Probability	Sea State	Heading Angle	Speed (knots)	T-Foil	β_{target} = 2.0	β_{target} = 3.0
C1	0.20	5	45°	15	Deployed	90.2	43.1
C2	0.25	5	0°	30	Deployed	6.55	3.13
C3	0.20	4	315°	35	Deployed	75.2	35.9
C4	0.15	5	45°	15	Retracted	97.55	46.6
C5	0.20	5	0°	30	Retracted	10.76	5.15

(a)

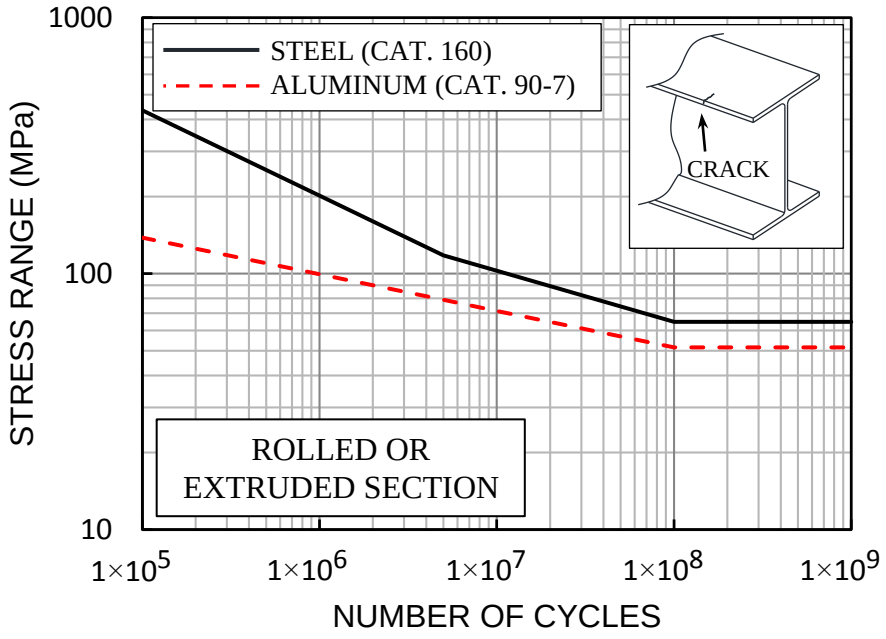

(b)

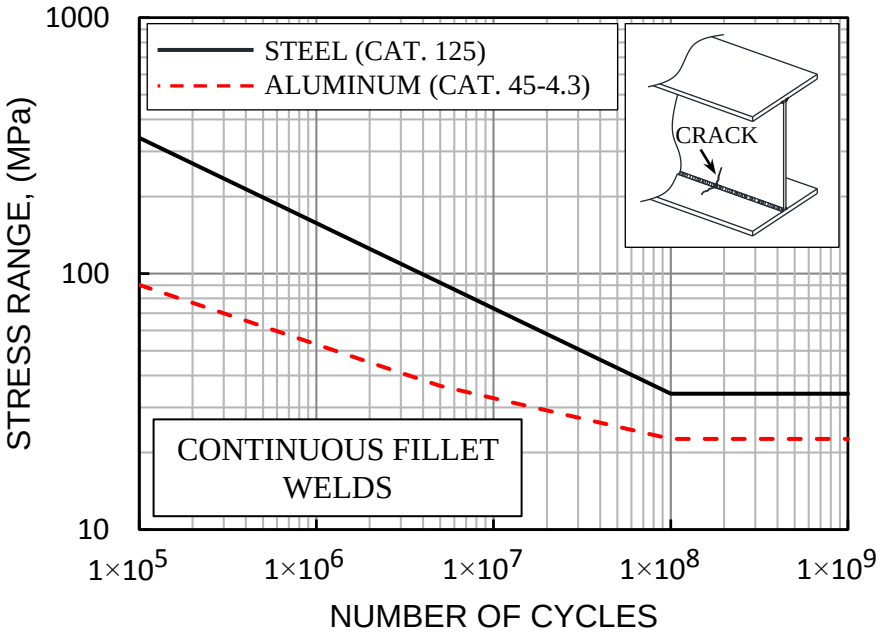

Figure 4.1 Comparison between Eurocode *S-N* lines for steel (Eurocode 2010) and aluminum (Eurocode 2009) details; (a) rolled or extruded sections, and (b) members with longitudinal fillet weld

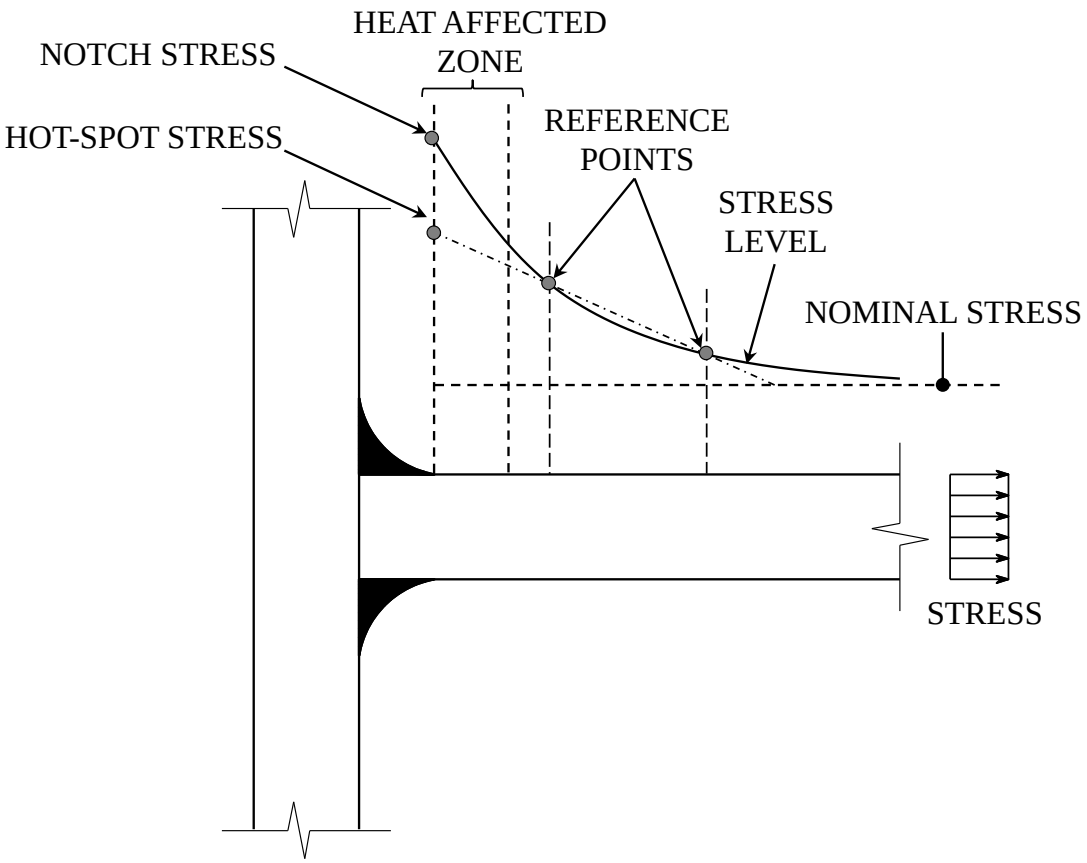

Figure 4.2 Schematic showing different stress types for fatigue analysis

(a)

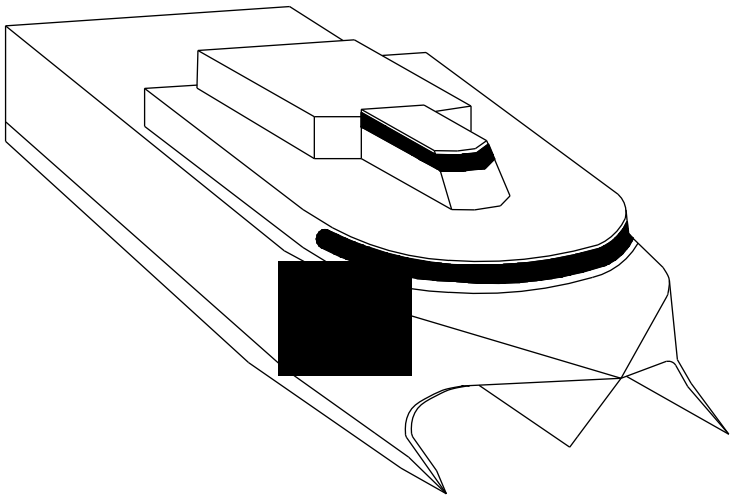

(b)

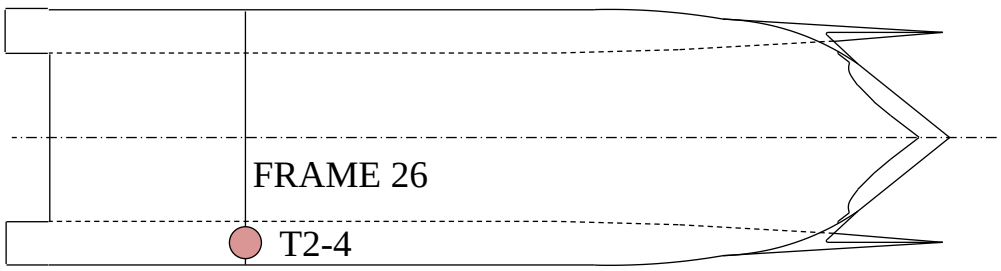

(c)

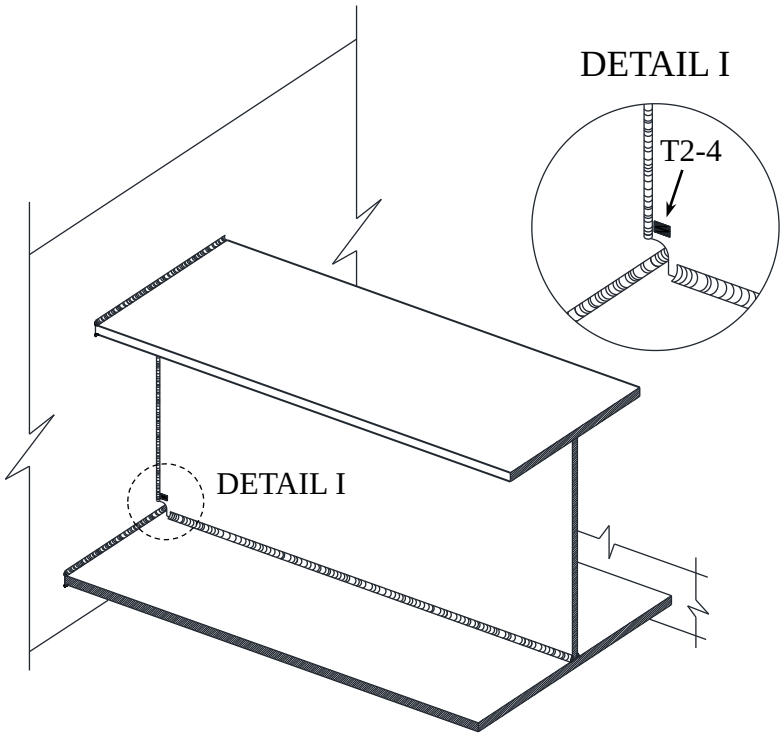

Figure 4.3 The vessel under investigation (based on Brady (2004b,c), Salvino and Brady (2008), and Incat (2012)); (a) general overview of the ship, (b) sketch of the plan view showing the location of the detail on Frame 26, and (c) the analyzed detail

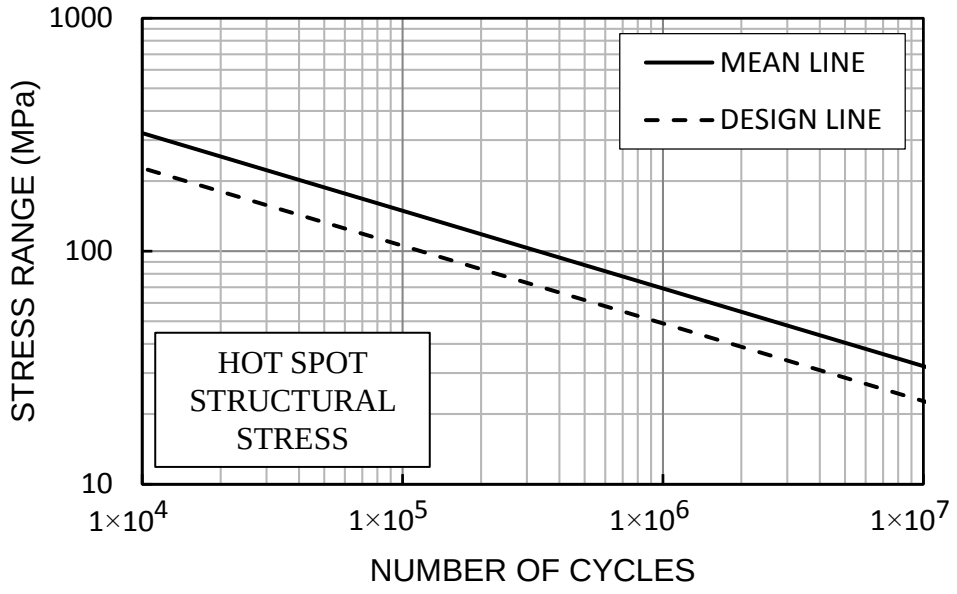

Figure 4.4 The adopted hot spot structural stress *S-N* lines

(a)

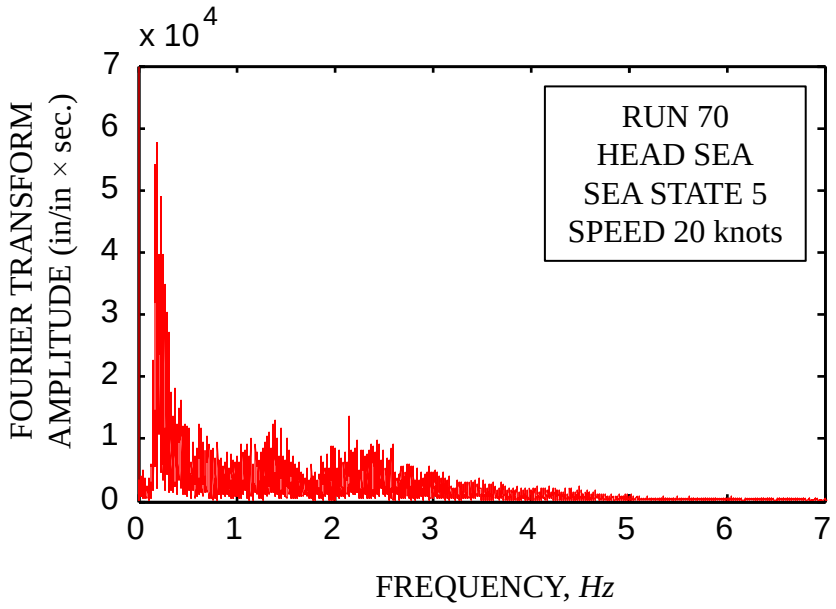

(b)

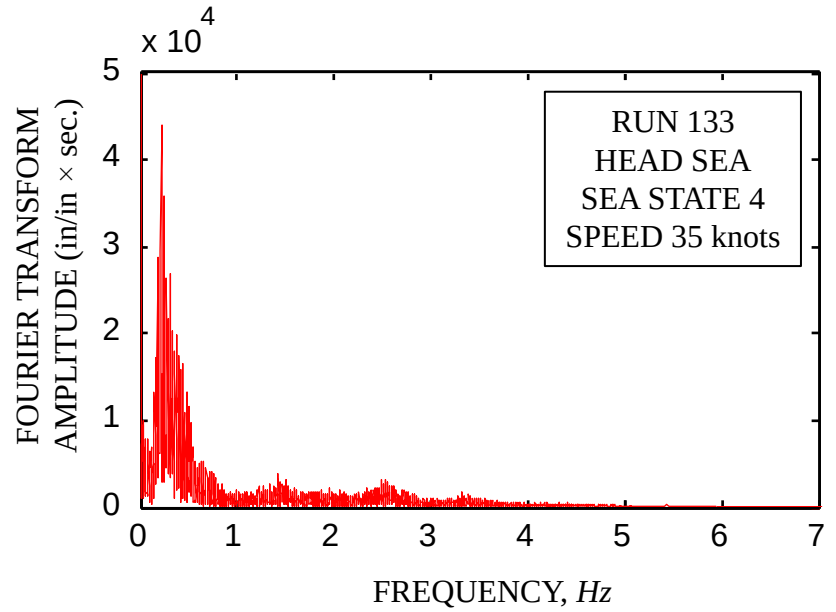

Figure 4.5 Amplitudes of the Fourier transform of strain signals; (a) for speed 20 knots at head sea condition and sea state 5, and (b) for speed 35 knots at head sea condition and sea state 4

(a)

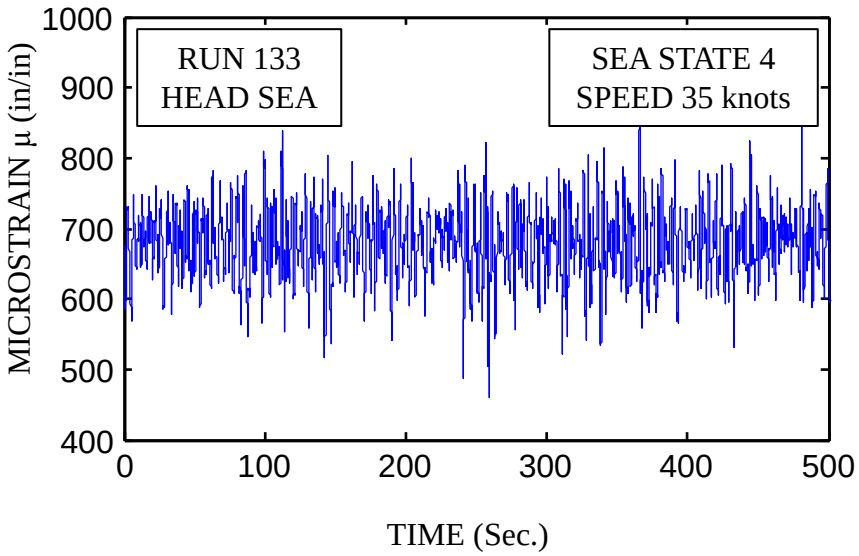

(b)

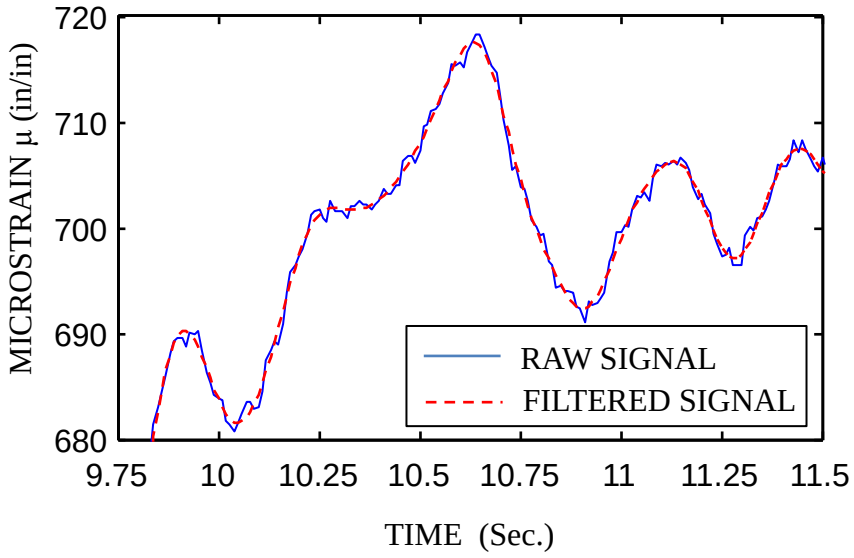

Figure 4.6 A sample of SHM data; (a) raw signal without filtering, and (b) comparison of the response before and after the filtering process

(a)

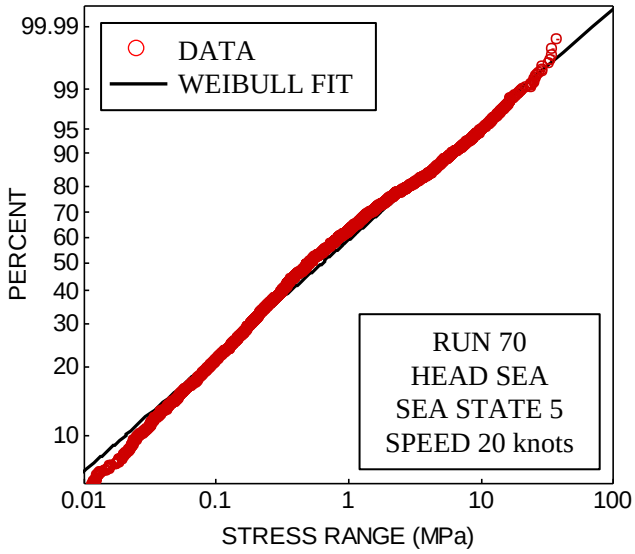
DATA
WEIBULL FIT
RUN 70
HEAD SEA
SEA STATE 5
SPEED 20 knots
PERCENT
99.99
99
95
90
80
70
60
50
40
30
20
10
0.01
0.1
1
10
100
STRESS RANGE (MPa)

(b)

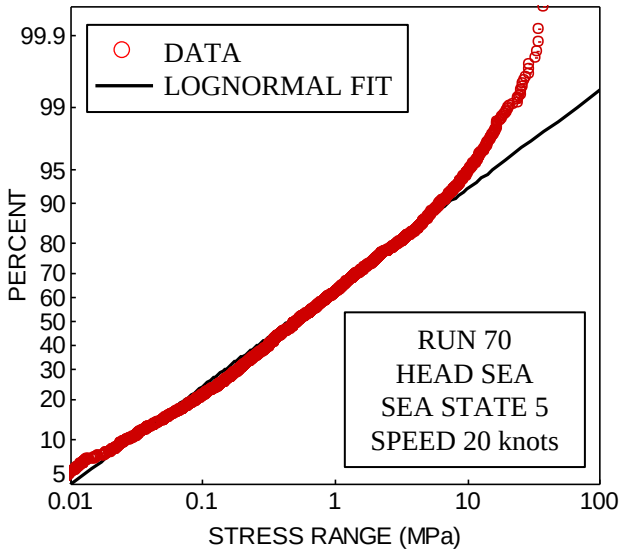
DATA
LOGNORMAL FIT
RUN 70
HEAD SEA
SEA STATE 5
SPEED 20 knots
PERCENT
99.9
99
95
90
80
70
60
50
40
30
20
10
5
0.01
0.1
1
10
100
STRESS RANGE (MPa)

(c)

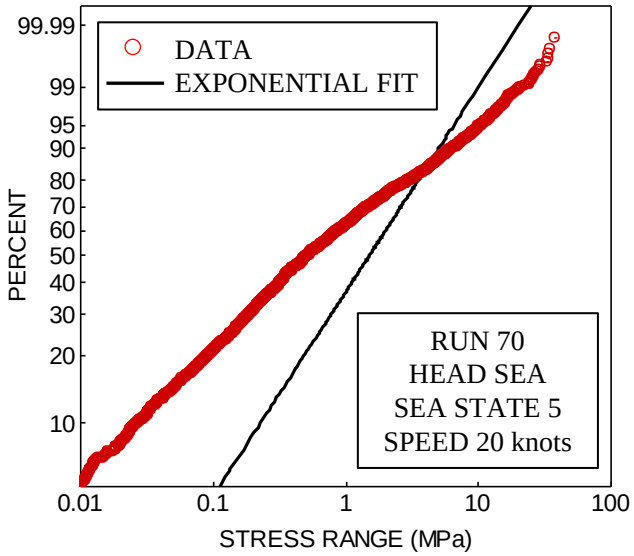

(d)

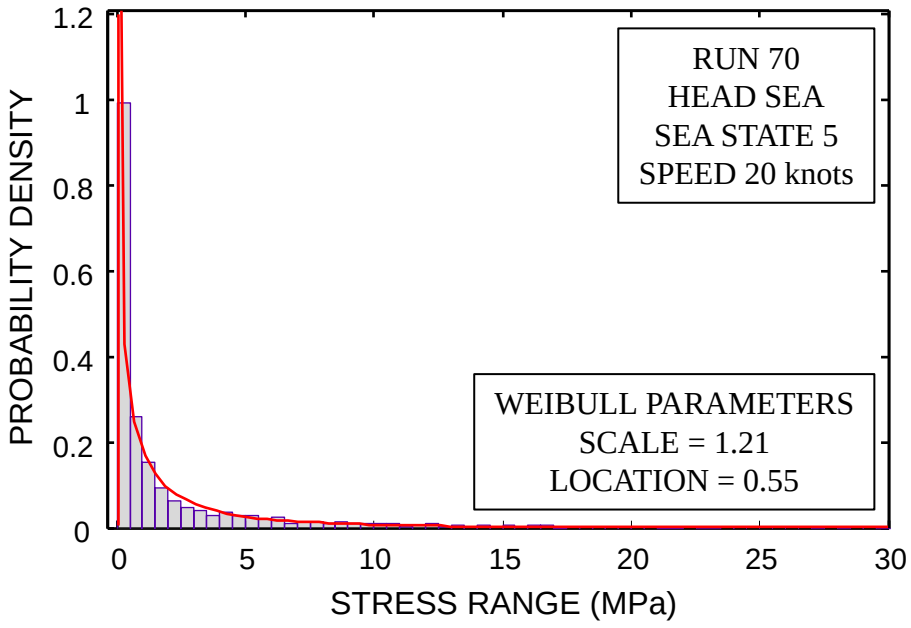

Figure 4.7 Distribution fitting process; probability plot of the stress range for multiple distribution types (a) Weibull, (b) lognormal, and (c) exponential; (d) histogram and Weibull PDF of the stress range

(a)

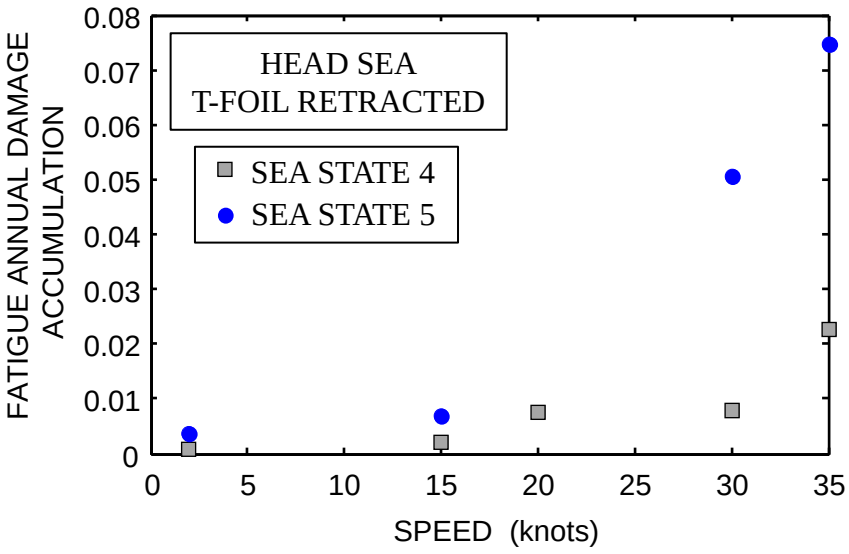

(b)

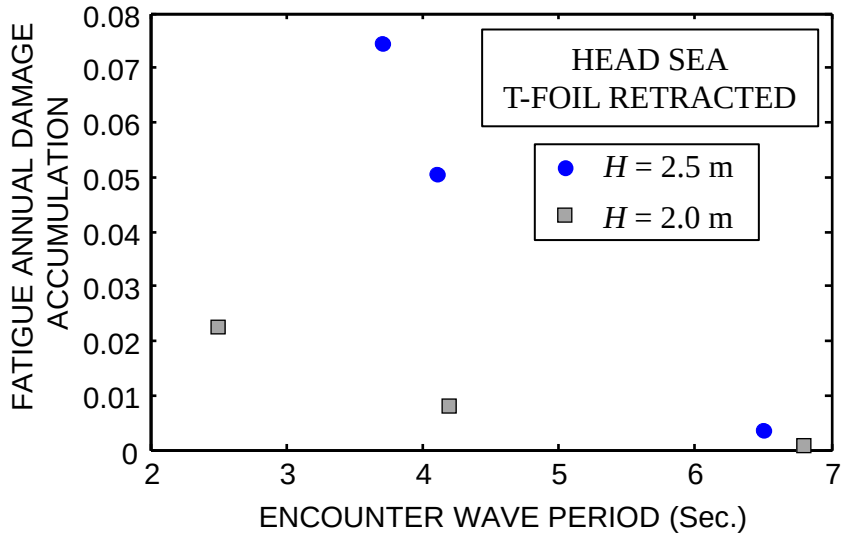

Figure 4.8 Variation of the annual fatigue damage accumulation of the detail with respect to (a) speed of the ship for different sea states, and (b) encountered wave period for different values of the significant wave height H

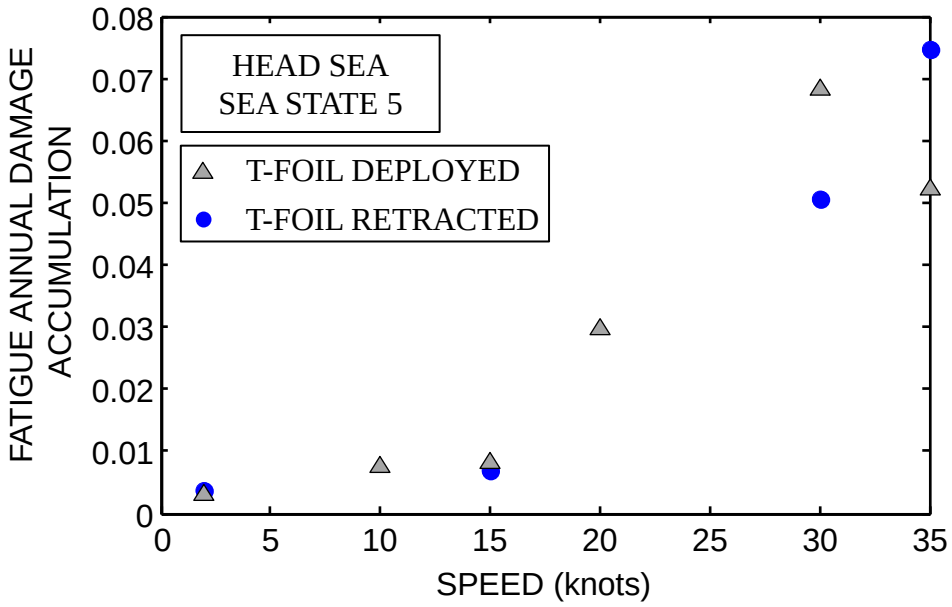

Figure 4.9 Variation of the annual fatigue damage accumulation of the detail with respect to the speed of the ship showing the effect of the T-foil deployment on the fatigue damage accumulation

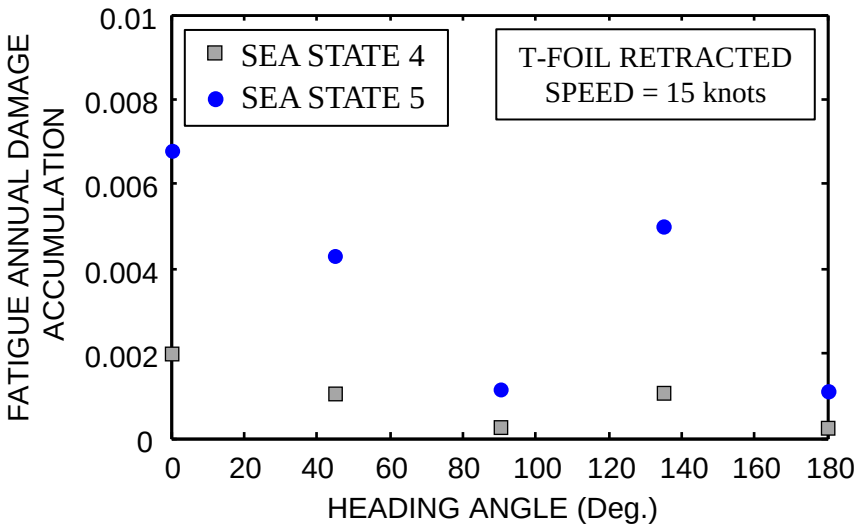

Figure 4.10 Variation of the annual fatigue damage accumulation of the detail with respect to the heading angle for different sea states

(a)

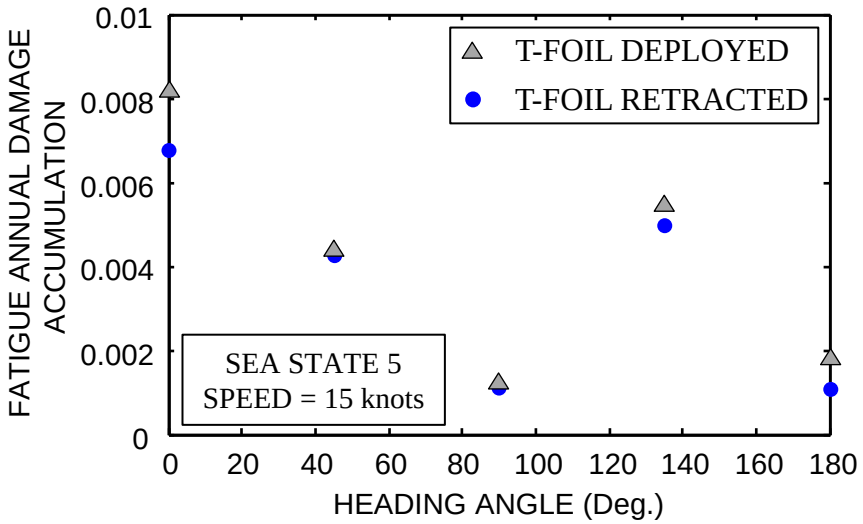

(b)

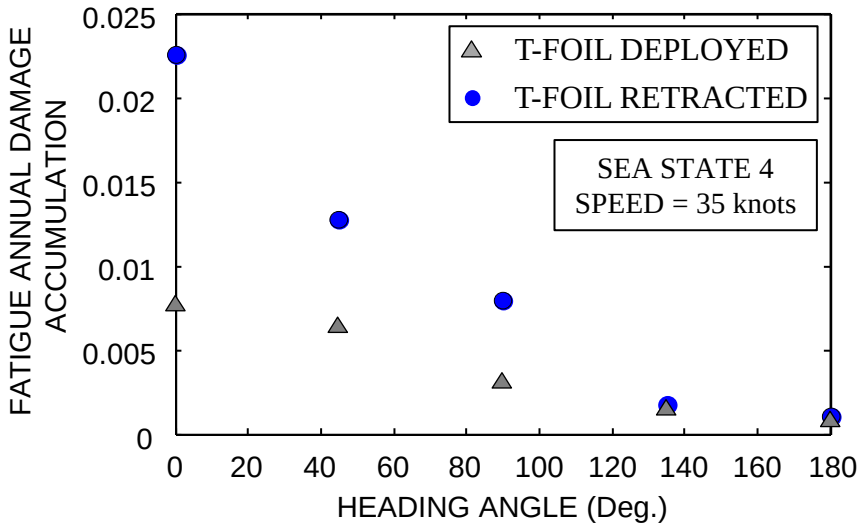

Figure 4.11 Variation of the annual fatigue damage accumulation of the detail with respect to the heading angle showing the effect of T-foil deployment at (a) sea state 5 and speed 15 knots, and (b) sea state 4 and speed 35 knots

(a)

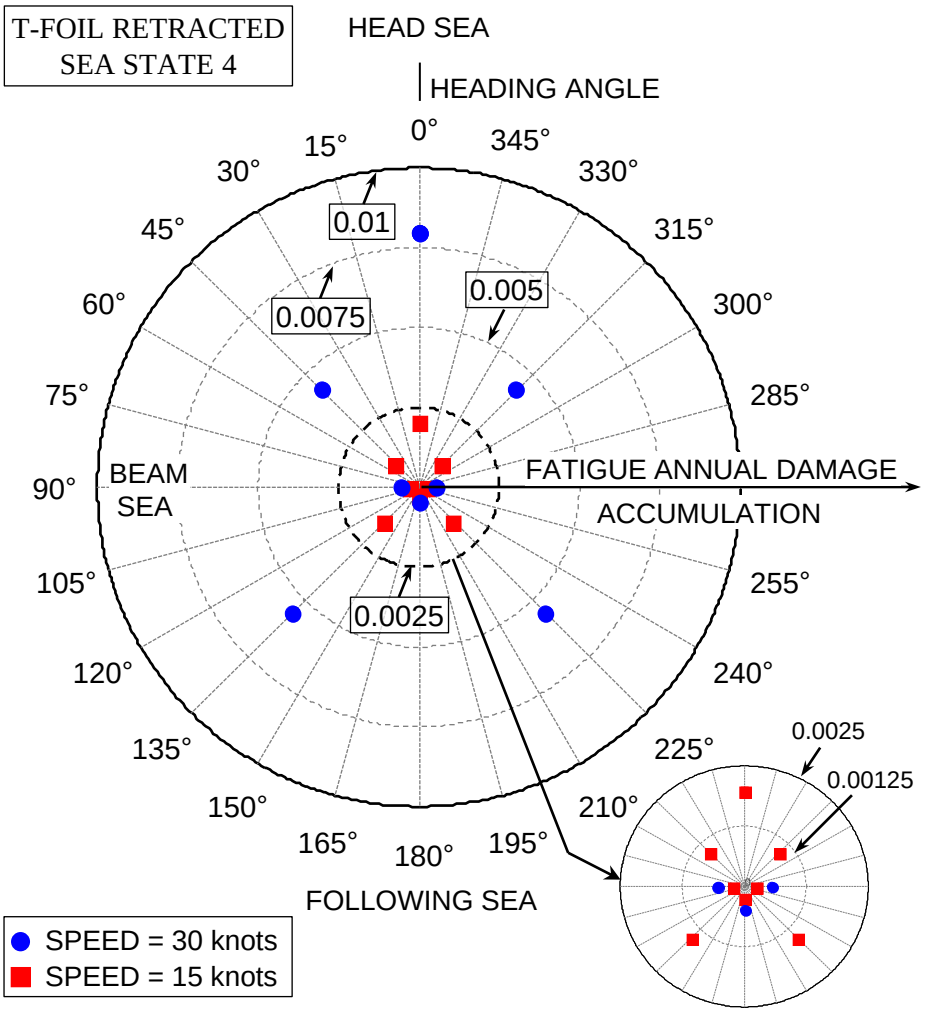
T-FOIL RETRACTED
SEA STATE 4
HEAD SEA
HEADING ANGLE
0°
15°
30°
345°
330°
45°
315°
60°
300°
75°
285°
90°
BEAM
SEA
105°
255°
120°
240°
135°
225°
150°
210°
165°
195°
180°
FOLLOWING SEA
0.01
0.0075
0.005
0.0025
FATIGUE ANNUAL DAMAGE
ACCUMULATION
0.0025
0.00125
SPEED = 30 knots
SPEED = 15 knots

(b)

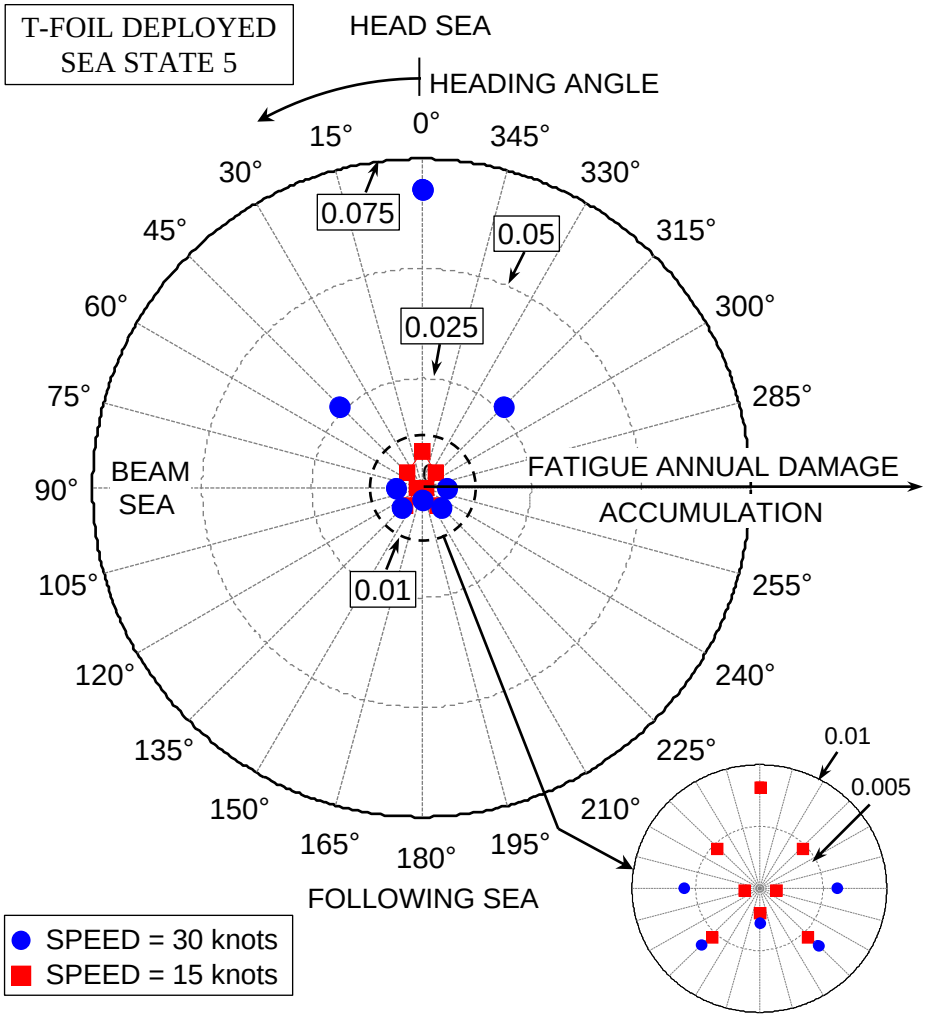

Figure 4.12 Comparison between the annual fatigue damage accumulation at speed 15 and 35 knots with respect to the heading angle for (a) sea state 4 with the T-foil retracted, and (b) sea state 5 with the T-foil deployed

(a)

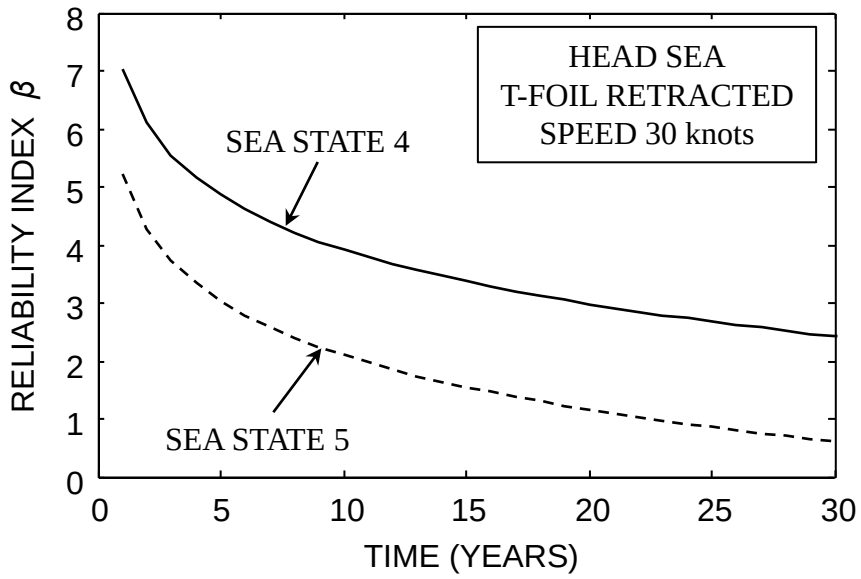
HEAD SEA
T-FOIL RETRACTED
SPEED 30 knots
SEA STATE 4
SEA STATE 5
RELIABILITY INDEX β
TIME (YEARS)
0
1
2
3
4
5
6
7
8
0
5
10
15
20
25
30

(b)

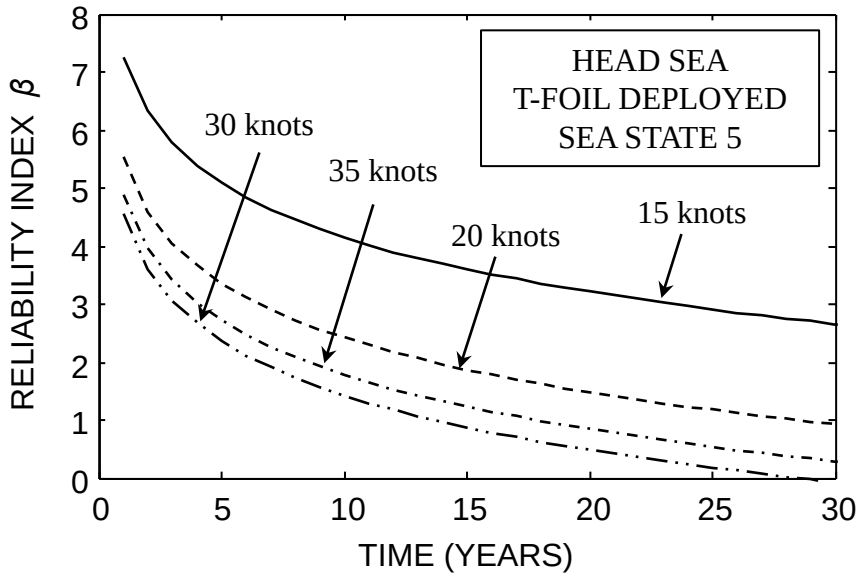
HEAD SEA
T-FOIL DEPLOYED
SEA STATE 5
30 knots
35 knots
20 knots
15 knots
RELIABILITY INDEX β
TIME (YEARS)
0
1
2
3
4
5
6
7
8
0
5
10
15
20
25
30

(c)

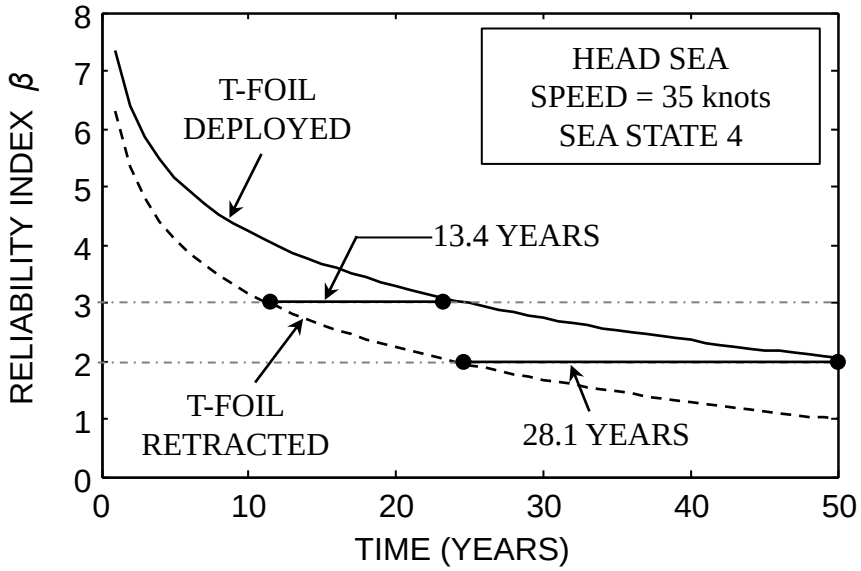

(d)

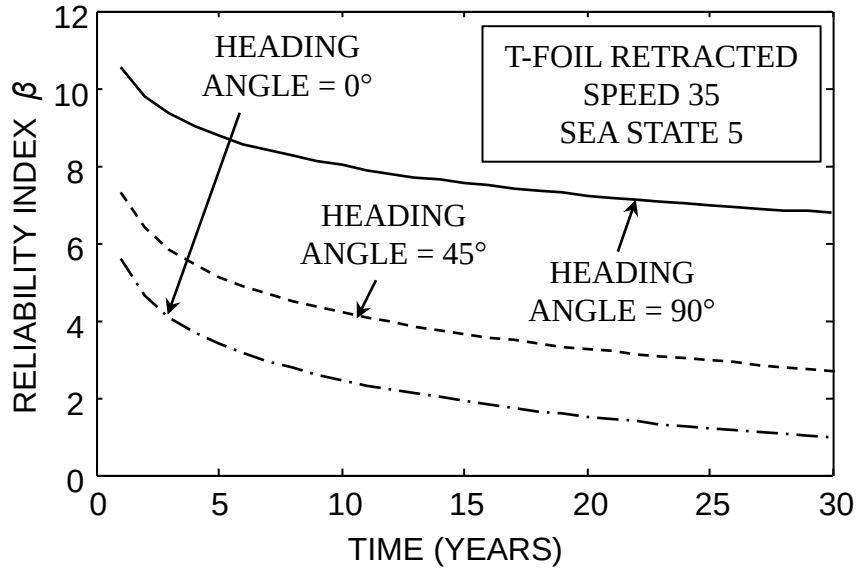

Figure 4.13 Time-variant fatigue reliability index and its sensitivity with respect to the effect of (a) sea states, (b) speeds, (c) T-foil deployment, and (d) heading angle

(a)

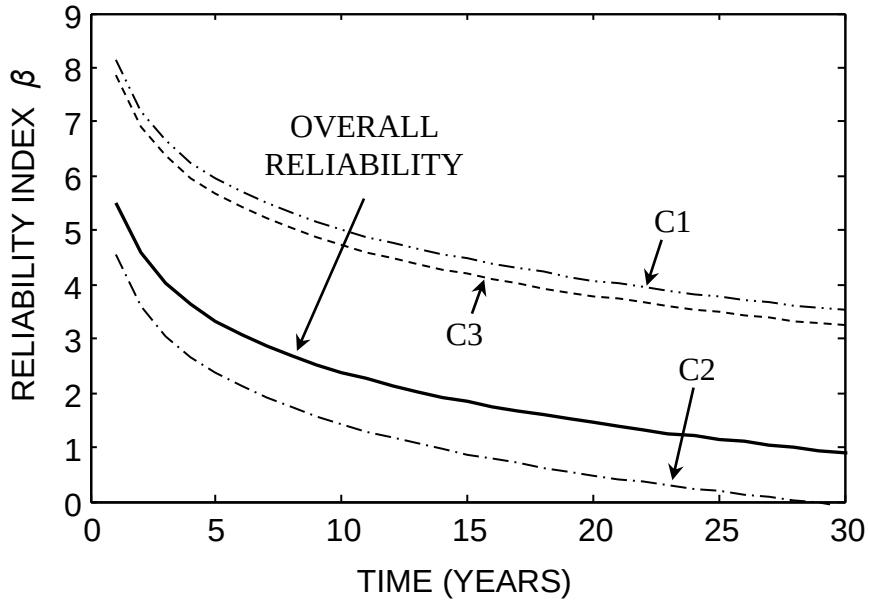

(b)

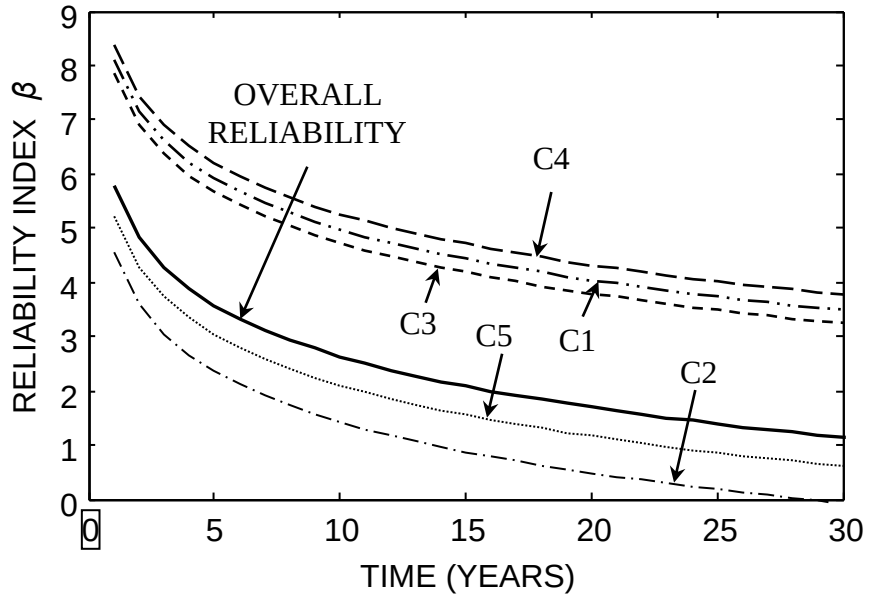

Figure 4.14 Time-variant fatigue reliability index for (a) original individual operational states and the overall reliability index profile, and (b) updated individual operational states and the overall reliability profile

CHAPTER 5 A FRAMEWORK FOR INSPECTION, MONITORING, AND MAINTENANCE OPTIMIZATION

5.1 Overview

This chapter proposes a comprehensive probabilistic framework for optimum inspection, monitoring, and maintenance planning for deteriorating structures. The proposed framework covers the following aspects of the LCM (a) the service life prediction under uncertainty accounting for damage occurrence and propagation, (b) the relation between the degree of damage and the probability of damage detection of an inspection or monitoring method, and (c) the effects of maintenance and repair on the service life, life-cycle cost, and maintenance delay. The optimum inspection, monitoring, and maintenance types and times, in addition to monitoring durations, are obtained through an optimization formulation which simultaneously minimizes the life-cycle cost, maximizes the expected service life, and minimizes the expected maintenance delay over the life-cycle. The life-cycle cost includes the cost of inspection, monitoring, and maintenance actions, as well as the cost of failure of the investigated componenet/system. The service life, life-cycle cost, and maintenance delay along with inspection and maintenance actions are formulated using a decision tree model. The selection of the appropriate maintenance type depends on the degree of damage. Based on the investigated structure and the available inspection, monitoring, and maintenance methods, the proposed approach can be used to schedule only inspection and maintenance actions, monitoring and maintenance actions, or inspection, monitoring, and maintenance actions. Several examples of the proposed framework are included. These examples cover RC bridges

subjected to corrosion damage, in addition to steel bridges and ships under fatigue deterioration.

The work in this chapter is based on the published and submitted papers Kim *et al.* (2013), Soliman *et al.* (2013b), and Soliman *et al.* (2014b).

5.2 Background

In the previous chapters, reliability and service life prediction of bridges and naval vessels under fatigue deterioration have been performed. The optimization of inspection and maintenance actions was not included. However, if the acceptable reliability levels (i.e., threshold) are specified, reliability profiles resulting from these approaches can be used for threshold-based maintenance optimization (see Example 2.1). If it is required to schedule inspections and monitoring actions, in addition to maintenance, the problem becomes more complex and a more comprehensive framework is needed. This is especially true if the optimization should also provide the optimum inspection and maintenance types (Okasha & Frangopol 2010a). Regardless of the optimization goals, the first step is the accurate prediction of the deteriorating structural performance under uncertainty. A significant amount of effort has been made to predict the service life of deteriorating structures. Fatigue and corrosion have been considered as predominant deterioration mechanisms (Fisher 1984; Chaker 1992; Zayed *et al.* 2002; Schijve 2003; Chung *et al*. 2006; Sohanghpurwala 2006). The propagation of fatigue cracks and corrosion over time have been modeled using experimental and theoretical studies. However, a single representative prediction model that can be applied to multiple deterioration mechanisms does not exist. This is due to the fact that the damage

propagation is a complex process that is highly dependent on the uncertain parameters which govern the deterioration process (Ahmad 2003; Fatemi & Yang 1998).

In the last decades, several probabilistic approaches for the optimum maintenance planning of deteriorating structures have been provided. Lifetime optimization methodologies for planning repair strategies of corroded RC structures were developed by Enright & Frangopol (1999), Estes & Frangopol (1999), Miyamoto *et al.* (2000), Stewart (2006), and Orcesi & Cremona (2009), among others. Furthermore, several probabilistic approaches for obtaining optimum maintenance strategies have been developed and applied to steel and aluminum structures including ships and bridges subject to fatigue and corrosion (Garbatov & Guedes Soares 2001; Luki & Cremona 2001; Zayed *et al.* 2002; Kwon & Frangopol 2011, 2012a,b).

Inspection and Monitoring results are generally used to determine if the damage exists, what degree of damage is, and furthermore, the types of maintenance. For this reason, integrated inspection, monitoring, and maintenance planning should be considered. Although these interventions significantly improve the structural performance, they impact the total life-cycle cost of a structure, especially if their application requires putting the structure out of service for a certain period of time. Moreover, if the deterioration can lead to catastrophic failures, delayed maintenance can endanger the serviceability and survival of a structure. Therefore, minimizing the maintenance delay, defined as the average time lags between the damage occurrence and the application of maintenance actions and between damage occurrence after the maintenance and the end of the service life, may require additional inspections and maintenance actions to be performed yielding a higher life-cycle cost. Thus, interventions

must be rationally planned along the service life of a structure to maintain an optimal balance between the service life, life-cycle cost, and maintenance delay.

Several approaches for the probabilistic inspection and/or maintenance planning for deteriorating structures have been proposed (Chung *et al.* 2006; Garbatov & Guedes Soares 2001; Kim & Frangopol 2011a; Kwon & Frangopol 2012a). In these studies, probabilistic performance indicators such as the probabilistic damage level (i.e., crack size or degree of corrosion) or reliability index have been used. The main outcomes of such studies include the optimum NDI times and types, as well as, the ideal maintenance times.

The use of monitoring systems with automated ability to detect fatigue and corrosion damage propagation has emerged as an alternative to traditional NDI methods. These systems rely on installing sensors that continuously monitor and record the structural response or emissions and attempt to identify and localize the damage based on the recorded data. Thus, they can detect the damage with minimal disturbance to the operational schedule of the structure, which is especially beneficial for the case of ships. An example of such systems is the acoustic emission (AE) monitoring for steel and aluminum structures (Wang *et al.* 2010; Maslouhi 2011; Yu *et al.* 2011). However, the use of long-term monitoring may impose a high life-cycle cost associated with the continuous need to transfer and process acquired data, in addition to the maintenance of the monitoring system itself. As a result, several studies focused on optimizing the inspection and monitoring activities along the service life of a structure. Kim & Frangopol (2011a) proposed an approach for the inspection and monitoring optimization of structures under fatigue effects. The approach was focused on minimizing the expected

damage detection delay and the inspection and monitoring cost. Orcesi & Frangopol (2013) proposed another approach in which the optimization problem was formulated to find the best monitoring plan to minimize the error in the collected data that arises from interrupting the monitoring activities throughout the service life. Minimizing the monitoring cost was also included as an objective. Although these studies performed the scheduling for inspection and monitoring actions, maintenance and repair planning was not included; this limits their applicability and precludes them from being integrated into a method to extend service life.

This chapter proposes a comprehensive probabilistic framework for optimizing the inspection, monitoring, and maintenance activities during the service life of deteriorating structures with emphasis on bridges and ships. A multi-objective optimization problem is formulated and solved to simultaneously minimize the total life-cycle cost, maximize the expected service life, and minimize the expected maintenance delay. The life-cycle cost includes the costs associated with inspection, monitoring, and maintenance activities, as well as the expected failure cost. This last cost is computed by combining the monetary loss resulting from structural failure and the time-based probability of failure defined in terms of the required service life and the PDF of the service life extended through the application of maintenance actions. The proposed approach contributes to the LCM problem by (a) being able to simultaneously schedule inspection, monitoring, and maintenance activities, (b) integrating the probability of failure and the failure cost into the life-cycle cost formulation, and (c) providing the ability to minimize the delay associated with the application of maintenance actions along the service life. The outputs of this approach are the optimum inspection times, monitoring times and durations, and

critical damage level for applying maintenance. The types of maintenance actions are determined based on the degree of damage. This approach provides the ability to use the measured damage level during inspection and monitoring actions to identify the need for maintenance. Accordingly, the resulting management plans allow for an effective and reliable decision making process. The proposed approach is applied to several case studies including a general example, naval ship details under fatigue, and an RC bridge under corrosion.

5.3 Time-based Performance and Probability of Failure

In this framework, the structural performance is evaluated in terms of the time-dependent damage level (i.e., crack size or degree of corrosion) and lifetime functions. For fatigue damage, the approach based on the LEFM is used to predict the crack growth (see Section 2.2.3.2). For corrosion damage, although the approach can be used or structures under general and pitting corrosion, the latter has been primarily addressed by the examples in this chapter. The model proposed by Val & Melchers (1997) is used to predict the damage (see Equations (2.28) and (2.29)) caused by pitting corrosion of steel reinforcement in RC bridge members.

Due to uncertainties associated with damage initiation and propagation, Monte Carlo simulation is used to draw samples from the time to failure T of the component under investigation. The PDF of T, $f_T(t)$, can be then obtained through an appropriate distribution fitting process such as the maximum likelihood method (Ang & Tang 2007). For small time interval Δt and a given time t, this PDF provides the probability that the

failure will occur between the time t and $(t+\Delta t)$. Therefore, it has the following probabilistic interpretation (Leemis 1995)

$$f_T(t) = \frac{P\left(t \le T \le (t+\Delta t)\right)}{\Delta t} \tag{5.1}$$

where $P(\cdot)$ represents the probability of occurrence of the event between parentheses. Based on the simulated PDF, $f_T(t)$, the cumulative probability of failure, $F_T(t)$, representing the probability that the time to failure T (i.e., service life) of a component is less than t, can be computer (see Equation (2.9)). The simulation process and the resulting PDF and CDF of the time to failure are show schematically in Figure 5.1.

In order to compute the probability of failure and the expected cost of failure, a failure event must be defined. Several definitions for failure can be found in literature. For instance, reliability theory states that the failure occurs when the demand on the structure exceeds its capacity (Melchers 1999). Chung *et al.* (2006), Kim & Frangopol (2011a), and Soliman & Frangopol (2014) defined the probability of failure as the probability that the crack will reach its critical size without being detected by the inspection plan. In this chapter, the time-based probability of failure is computed based on the CDF, $F_T(t)$, of the service life T, which can be extended through the application of maintenance actions. If a specific service life t^* is required, the probability of failure P_f, given as the probability that the critical damage level will be reached before t^*, is computed as $P_f = P(T \le t^*) = F_T(t^*)$. The application of maintenance actions will change the PDF and CDF of the service life in the manner shown in Figure 5.1 and,

consequently, will change the probability of failure. P_f is later incorporated into the optimization scheme presented in this chapter.

5.4 Non-destructive Inspection and Monitoring

Among the available NDI techniques used in civil and marine structures, the liquid penetrant, ultrasonic, and magnetic particle inspection methods are widely used for fatigue crack detection. The choice of the appropriate inspection methods depends on the crack type. For example, the liquid penetrant method is more appropriate for surface cracks whereas the ultrasonic inspection (UI) can detect small and embedded cracks. However, UI requires considerable experience for interpreting the results and is generally more expensive (Fisher *et al*. 1998). Although these methodologies provide sufficient detection capabilities, they generally require the location of the crack to be known a priori, which may not always be true. Additionally, given the large scale of a ship structure and the number of locations that should be inspected, these NDI methodologies may require a long time to be applied to all the critical locations. Moreover, a detailed inspection may require the dry docking of the ship thus incurring large economic consequences.

As a result, scientific communities and inspection agencies shifted their focus towards developing monitoring methodologies which can provide automated damage detection, quantification, and localization with minimal interruption to the service schedule of the structure. This is especially important for ships. Examples of these methodologies are the AE method (Wang *et al.* 2010) and the ultrasonic guided waves (Cho & Lissenden 2012) technique. Although these methodologies may have a lower

ability in detecting and quantifying the crack size when compared to other methodologies, their use can significantly reduce the inspection time and provide the ability to monitor the damage propagation in real-time. Therefore, the choice of the most appropriate inspection and/or monitoring method depends on multiple variables including the cost, detection ability of the used method with respect to the growing defect, and the need for dry docking, among others. Accordingly, as proposed in this chapter, this choice can be made by solving an optimization problem with the inspection and monitoring times and types as its design variables.

5.5 Probability of Damage Detection

The *PoD* has been widely used to assess the capacity of the inspection method to detect cracks. This probability is defined as the probability that an existing crack with a specific size will be detected using a given inspection method (Chung *et al.* 2006). Additionally, the *PoD* has been used as an indicator of the quality of inspection methods which can be given by the probability of detecting a specific crack size or the minimum detectable crack size for the inspection method (Kim & Frangopol 2011a). The *PoD* has been successfully used for the probabilistic inspection optimization for civil, marine, and aerospace structures (Righiniotis 2004;Chung *et al.* 2006; Kale & Haftka 2008; Kim & Frangopol 2011b). Several NDI methods also exist for corrosion damage detection including half-cell potential, radiographic, and ultrasonic tests.

Several forms for the *PoD* function exist such as the shifted exponential, logistic curve, and the lognormal CDF; the latter is adopted in this chapter. The lognormal *PoD* function is given as (Crawshaw & Chambers 1984)

$$PoD = 0 \qquad \text{for} \quad 0 \le a \le a_{\min}$$
$$PoD = 1 - \Phi\left[\frac{\ln(a) - \alpha}{\beta}\right] \qquad \text{for} \quad a > a_{\min} \tag{5.2}$$

where $\Phi[\cdot]$ denotes the standard normal CDF, a is the crack size, a_{min} is the minimum detectable crack size, and α and β are the *PoD* function parameters and they depend on the quality of inspection methods.

For scheduling monitoring activities, recent studies have also shown that the *PoD* functions can be used with monitoring methods such as the AE technique. Although the typical procedure when using AE is to determine the flaw size by other NDI method such as the ultrasonic inspection, Pollock (2007, 2010) shows that it is possible to obtain the crack size by using the AE monitoring and that the probability of detecting a certain crack size increases with the increase in the monitoring duration. Hence, in this chapter, a time-dependent *PoD* model for monitoring is considered as shown in Figure 5.2 and is expressed as

$$PoD = 0 \qquad \text{for} \quad 0 \le a \le a_{\min}$$
$$PoD = 1 - \Phi\left[\frac{\ln(a) - \alpha}{\beta}\right] \cdot R_{t_{md}} \qquad \text{for} \quad a > a_{\min} \tag{5.3}$$

where $R_{t_{md}}$ is a reduction factor depending on the monitoring duration t_{md}.

For *PoD* of corrosion damage, another form of the *PoD* function is used, as will be discussed later in the examples of this chapter.

5.6 Framework for Optimum Inspection and Maintenance Planning

The general framework proposed in this chapter provides an optimum intervention (i.e.,

inspection, monitoring, and maintenance) schedule. This framework includes the following main subjects (a) prediction of damage occurrence and propagation; (b) service life prediction; (c) relation between degree of damage and probability of damage detection; (d) effect of maintenance on service life and cost under uncertainty; and (e) an optimization process associated with maximizing the service life, minimizing the life-cycle cost, and minimizing the maintenance delay based on (a) to (d). The results from this framework are the optimum inspection qualities and times, optimum monitoring times and durations, and types of maintenance actions. The framework is general and can be applied to a wide range of structures such as naval ships, airplanes, bridges, and buildings under various deterioration mechanisms.

In order to evaluate the expected service life, life-cycle cost, and the maintenance delay associated with a given management plan, the event tree model, shown in Figure 5.3 for one intervention, is adopted. In this model, the set of possible events that may occur at a certain inspection or monitoring action can be represented by the different branches of the event tree. Each of these branches has a probability of occurrence $P(B_k)$ where *k* is the branch number. As shown in Figure 5.3, if the inspection or monitoring is performed after the initial service life (i.e., $t_1 > T^o$, where t_1 is the first intervention time and T^o is the initial service life with no maintenance), no further maintenance actions are performed. After an inspection or monitoring, if damage is detected, an in-depth inspection is performed to assess the degree of damage. This two-step inspection plan is adopted to minimize the probability of repairing a damage that does not exist.

Through an appropriate maintenance action after damage detection, damage propagation can be stopped or the degree of damage can be reduced, and as a result, the

service life of a deteriorating structure can be extended. These effects of maintenance on damage propagation and service life are illustrated in Figure 5.4. As shown, maintenance A results in a damage propagation delay causing service life extension of T^A. Maintenance B represents the replacement of the deteriorating element in the structure. The service life extension associated with maintenance B is T^B.

In this study, the selection of the maintenance type is performed according to the degree of damage d as follows: (a) no maintenance for $0 \le d < d_A$; (b) maintenance A for $d_A \le d < d_B$; and (c) maintenance B for $d \ge d_B$. d_A and d_B are the damage criteria for determining a maintenance type. Based on this model, the probability of occurrence of each branch can be found as shown in Figure 5.3 for one inspection. The probabilities $P_{t_i}(X)$ and $P_{t_i}(Y)$ in Figure 5.3 represent the probability that the intervention performed at t_i is executed before and after the initial service life, respectively. $P_{t_i}(D)$ and $P_{t_i}(ND)$ are the probabilities of detecting and not detecting the damage at t_i, and $P_{t_i}(NM)$ is the probability of not performing maintenance at the same time (i.e., $P(0 \le d < d_A)$), and $P_{t_i}(M_A)$ and $P_{t_i}(M_B)$, are the respective probabilities of performing maintenance A (i.e., $P(d_A \le d < d_B)$) and maintenance B (i.e., $P(d \ge d_B)$) at t_i.

5.6.1 Expected service life

The computed service life will depend on the probabilities of occurrence of the branches in the event tree model. For branches B_1, B_4, B_5, no maintenance is performed and the service life associated with these branches will be equal to the initial service life T^o. For branch B_2, since maintenance A is performed, the service life will be extended by an amount T^A. Therefore, the service life associated with branch B_2 is

$$T_2 = t_1 + T^A \tag{5.4}$$

where t_1 is the time of application of the first inspection or monitoring action, and T^A is the service life extension after maintenance A. Similarly, the service life associated with Branch B_3 is

$$T_3 = t_1 + T^B \tag{5.5}$$

Where T^B is the service life extension after maintenance B. Accordingly, the expected service life is

$$E[T] = \sum_{k=1}^{N_b} P(\mathrm{B}_k) \cdot T_k \tag{5.6}$$

where N_b is the total number of branches and T_k is the service life associated with the *k*-th branch. Similarly, when more than one inspection or monitoring action is performed, the probability of branch occurrences can be found and the expected service life can be computed.

5.6.2 Expected total life-cycle cost

For inspection and maintenance scheduling, it is crucial to consider the cumulative cost of interventions along the service life. The expected life-cycle cost can be found as

$$E[C_{tot}] = \sum_{k=1}^{N_b} P(\mathrm{B}_k) \cdot C_k + P_f \cdot C_f \tag{5.7}$$

where P_f is the probability of failure computed as shown in Figure 5.1, C_f is the monetary loss associated with the failure of the damaged location. C_k is the total cost associated with branch k, obtained by summing inspection and monitoring costs (i.e., C_{insp} and

C_{mon}, respectively), as well as in-depth inspection and repair costs (i.e., $C_{insp,d}$ and C_{main}, respectively), for the considered branch

$$C_k = C_{insp} + C_{mon} + C_{insp,d} + C_{main} \tag{5.8}$$

in which

$$C_{insp} = \begin{cases} 0 & \text{for } N_{insp} = 0 \\ \sum_{l=1}^{N_{insp}} \dfrac{C^{(insp)}}{\left(1+r_d\right)^{t_{insp}^{(l)}}} & \text{for } N_{insp} \geq 1.0 \end{cases} \tag{5.9}$$

$$C_{mon} = \begin{cases} 0 & \text{for } N_{mon} = 0 \\ \sum_{m=1}^{N_{mon}} \dfrac{C^{(mon)}}{\left(1+r_d\right)^{t_{mon}^{(m)}}} & \text{for } N_{mon} \geq 1.0 \end{cases} \tag{5.10}$$

$$C_{insp,d} = \begin{cases} 0 & \text{for } N_{insp,d} = 0 \\ \sum_{j=1}^{N_{insp,d}} \dfrac{C^{(insp,d)}}{\left(1+r_d\right)^{t_{insp,d}^{(j)}}} & \text{for } N_{insp,d} \geq 1.0 \end{cases} \tag{5.11}$$

$$C_{main} = C_{m_A} + C_{m_B} \tag{5.12}$$

where

$$C_{m_A} = \begin{cases} 0 & \text{for } N_A = 0 \\ \sum_{n=1}^{N_A} \dfrac{C^{(m_A)}}{\left(1+r_d\right)^{t_A^{(n)}}} & \text{for } N_A \geq 1.0 \end{cases} \tag{5.13}$$

$$C_{m_B} = \begin{cases} 0 & \text{for } N_B = 0 \\ \sum_{y=1}^{N_B} \dfrac{C^{(m_B)}}{\left(1+r_d\right)^{t_B^{(y)}}} & \text{for } N_B \geq 1.0 \end{cases} \tag{5.14}$$

in which $C^{(insp)}$, $C^{(mon)}$, $C^{(insp,d)}$, $C^{(m_A)}$, and $C^{(m_B)}$ are the costs of a single inspection, monitoring, in-depth inspection, maintenance A action, and maintenance B action, respectively. $t_{insp}^{(l)}$ is the *l*-th inspection time, $t_{mon}^{(m)}$ is the *m*-th monitoring time, $t_{insp,d}^{(j)}$ is the *j*-th in-depth inspection time, $t_A^{(n)}$ is the *n*-th maintenance A time, and $t_B^{(y)}$ is the *y*-th maintenance B time. N_{insp}, N_{mon}, $N_{insp,d}$, N_A, and N_B are, respectively, the number of inspections, monitoring, in-depth inspection, and maintenance A, and maintenance B actions associated with the *k*-th branch, and r_d is the annual discount rate of money, introduced to convert the future monetary value of inspections and repairs, performed at different times, to the present one.

In general, the cost of inspection consists of direct and indirect components. The direct cost consists of the access, equipment, and operator costs. The access cost covers the expenses for accessing and preparing the different locations that need to be inspected. It depends on the structure and also on the inspection method since several NDI methods require surface preparation. Equipment cost depends mainly on the type of the NDI used in the inspection. For instance, the ultrasonic inspection would require special, expensive equipment to be performed when compared to the liquid penetrant inspection. The operator cost includes the fees of the inspector, interpretation of the results, and writing the inspection report. The indirect cost covers the economic losses associated with the non-operation status of the structure during the time required for performing the inspection. Therefore, this cost will significantly increase if the inspection requires long time to be performed or if it is necessary to remove the ship from service to perform the inspection.

Monitoring the crack size by using acoustic emission devices could be characterized by lower indirect cost since the operator is only required to set up the equipment. However, it will have additional running costs as it involves long-term data acquisition, transfer and interpretation, and maintenance of the monitoring hardware.

5.6.3 Expected maintenance delay

Maintenance delay, as previously indicated, is defined as the average time lags between the damage occurrence and the application of the maintenance actions and between damage occurrence after the repair and the end of the service life. Reducing this delay is crucial for structures subjected to highly random loading (e.g., naval vessels); especially if sudden failures are possible. In the proposed framework, this expected delay is computed as

$$E[D] = \sum_{k=1}^{N_b} P(\mathrm{B}_k) \cdot D_k \tag{5.15}$$

where D_k is the maintenance delay associated with the *k*-th branch. If no maintenance is performed (i.e., branches B_1, B_4, and B_5 in Figure 5.3), maintenance delay is computed as

$$D_{1,4,5} = T^o - t_{occ} \tag{5.16}$$

where t_{occ} is the damage occurrence time. For branch B_1, in which maintenance is performed, the maintenance delay is computed assuming that the maintenance will directly follow the inspection action, and takes the form

$$D_2 = \frac{(t_1 - t_{occ}) + (T^o - t_{occ})}{2} \tag{5.17}$$

where t_1 is the time of the first maintenance. This accounts for both the time lags between the first damage occurrence and the repair action and between the damage occurrence after the repair and the end of the service life. When more than one maintenance action is performed, the average maintenance delay arising from the application of the first maintenance and the subsequent ones is considered.

The formulated event tree model for obtaining the expected service life, life-cycle cost, and maintenance delay associated with each intervention plan is integrated into an optimization process to find the optimum inspection, monitoring and maintenance. A flowchart describing the details of the optimum intervention planning is shown in Figure 5.5.

5.7 Illustrative Examples

For the purpose of illustration, several examples are provided. The first is a general example which demonstrates the features of the approach by performing inspection and maintenance optimization. The next two examples perform inspection and maintenance optimization on a steel ship detail subjected to fatigue and an RC structure subject to corrosion. The last example performs inspection, monitoring, and maintenance optimization on a steel ship detail under fatigue deterioration.

5.7.1 Example 5.1

Suppose that a structure is deteriorating in which the damage occurrence time t_{occ} follows a lognormal distribution with mean and standard deviation of 5 years and 1 year, respectively (denoted as LN(5 *years*; 1 *year*)). The time-dependent damage intensity δ of this structure is expressed as

$$\delta(t) = 0 \qquad \text{for } t < t_{occ} \tag{5.18a}$$

$$\delta(t) = exp\left[\left(t - t_{occ}\right) / \lambda\right] - 1 \qquad \text{for } t \geq t_{occ} \tag{5.18b}$$

where λ = scale parameter considered as a random variable following a lognormal distribution with mean 50 and standard deviation 10. The damage occurrence time t_{occ} and scale parameter λ are assumed to be statistically independent. Damage intensity δ ranges from zero (*i.e.*, no damage) to one (*i.e.*, full damage. In this example, the initial service life T^o is assumed to be the time when the damage intensity δ reaches 0.5 (*i.e.*, the threshold of damage intensity δ_{thres} = 0.5). The PDF of T^o is shown in Figure 5.6. The mean and standard deviation of T^o are 25.27 years and 4.18 years, respectively. The PDF in this figure is based on the histograms of time obtained from the Monte Carlo simulation. The vertical fluctuation in the PDFs of Figure 5.6 is affected by both the number of simulations (100,000 samples herein) and the bin values of the histogram of time (0.001 years herein).

In this illustrative example, two types of maintenance actions are applied to delay the damage intensity propagation (i.e., both can be classified as maintenance A type). There will be no increase in the damage intensity for the effective duration t_{eff}. The uncertainty associated with t_{eff} of these maintenance actions is accounted for by considering t_{eff} as a random variable following lognormal distribution. The effective duration $t_{eff,I}$ of the first maintenance has a lognormal PDF as follows LN(10 *years*; 2 *years*). $t_{eff,II}$ of the second maintenance is associated with LN(20 *years*; 4 *years*). The selection of maintenance type depends on the damage intensity through the in-depth inspection after damage detection as indicated in Figure 5.3. When the damage intensity δ

is less than δ_I ($0 \le \delta < \delta_I$), there is no maintenance. The first and second maintenances are applied where $\delta_I \le \delta < \delta_{II}$, and $\delta \ge \delta_{II}$, respectively. The *PoD* function in terms of the damage intensity δ is based on Equation 5.2 as

$$PoD = 0 \qquad \text{for } 0 \le \delta \le \delta_{min} \qquad (5.19a)$$

$$PoD = 1 - \Phi\left[\frac{\ln(\delta) - \ln(\alpha_\delta)}{\beta_\delta}\right] \qquad \text{for } \delta > \delta_{min} \qquad (5.19b)$$

The relation between parameter α_δ and β_δ in Equation (5.19) is assumed as $\beta_\delta = -0.1ln(\alpha_\delta)$. When the damage intensity δ is equal to α_δ, the *PoD* is 0.5. Smaller value of the parameter α_δ is associated with higher quality of inspection, and α_δ represents the inspection quality in this illustrative example. Furthermore, the minimum detectable damage intensity δ_{min} is defined as the damage intensity associated with *PoD* = 0.001. The inspection planning for a single scheduled inspection is formulated as an optimization problem to maximize the mean of the service life $E[T]$ as

Find	t_i	(5.20)
to maximize	$E[T]$	(5.21)
given	PDF of T^o, α_δ, δ_I and δ_{II}	(5.22)

where t_i = scheduled inspection time (*years*) (*i.e.*, design variable); α_δ = damage intensity at which the given inspection method has 50% *PoD*. δ_I and δ_{II} are the damage intensity criteria to determine the maintenance types. Using the decision tree model (see Figure 5.3), the service lifetime T for a single scheduled inspections is formulated as indicated in Equation (5.6). As mentioned previously, considering uncertainties associated with damage initiation time and propagation, T is treated as a random variable. The objective

is to maximize the expected T (see Equation (5.21)). The PDF of T^o (see Figure 5.6), α_δ, δ_I , δ_{II} are given as indicated in Equation (5.22). This problem is solved by the optimization toolbox (*i.e.*, constrained nonlinear minimization including active-set and interior-point optimization algorithms) provided in MATLAB® version R2011a (MathWorks Inc. 2011b).

The results of the optimization are summarized in Table 5.1. This table shows the effects of the inspection quality and damage intensity criteria for selecting a maintenance type on the optimum inspection time and the expected service life. When an inspection method associated with α_δ = 0.1 is used, and damage intensity criteria for selecting a maintenance type are δ_I = 0.3 and δ_{II} = 0.5, the optimum inspection time t_i = 21.08 years, the expected service life $E[T]$ = 32.33 years, and the corresponding CDF of T is shown in Figure 5.7 (a). The CDF of the service life describes the probability that the service life T is at most a specific value of lifetime t (*i.e.*, $P(T \leq t)$). For example, the probability that T is less than 33.65 years is 0.5 (*i.e.*, $P(T \leq 33.65 \text{ years}) = 0.5$), and, therefore, 33.65 years is the median of T as shown in Figure 5.7 (a). If the inspection method with α_δ = 0.5 is used instead of α_δ = 0.1, $E[T]$ will be reduced from 32.33 years to 25.72 years (see Figure 5.7 (a) and Table 5.1). Figure 5.7 (b) shows the CDFs of service lives associated with δ_I = 0.0 and δ_{II} = 0.0 (*i.e.*, only the second type of maintenance is available when damage is detected), and δ_I = 0.0 and δ_{II} = 1.0 (*i.e.*, only the first type of maintenance is available when damage is detected) for given inspection quality (*i.e.*, α_δ = 0.1). Since the second type of maintenance has larger effective duration t_{eff} for which there is no increase of damage intensity, E(T) associated with δ_I = 0.0 and δ_{II} = 0.0 is larger than that associated with δ_I = 0.0 and δ_{II} = 1.0 (see Figure 5.7 (b) and Table 5.1).

5.7.2 Example 5.2

The approach proposed in this chapter is next applied to a naval ship hull structure described in Kim & Frangopol (2011c). In Kim & Frangopol (2011c), the purpose was to establish the optimum inspection planning based on minimization of the expected damage detection delay without considering maintenance effect. The application in this chapter considers maintenance effects and a real inspection method (*i.e.*, ultrasonic inspection). The joint between the longitudinal stiffener and bottom plate is assumed to be the fatigue critical location. The detailed schematic representation of this location is provided in Kim & Frangopol (2011c). Under repeated loading due to sea water waves, the fatigue crack in the bottom plate can initiate and propagate on the edge connected to the stiffener in the transverse direction. In order to predict the crack length size, Equation (2.22) is used with the variables defined in Table 5.2. It is assumed that the geometry function $Y(a)$ in Equation (2.22) is one (Madsen *et al.* 1991, and Akpan *et al.*, 2002).

In this example, the ultrasonic inspection method is applied to detect the fatigue crack. The *PoD* function defined in Equation (5.2) is used, and the associated parameters are α = 0.122 and β = –0.305 (Forsyth & Fahr 1998). The scheduled inspection cost $C^{(insp)}$ and in-depth inspection cost $C^{(insp,d)}$ are assumed to be \$5,000 and \$10,000, respectively. Furthermore, it is assumed that one maintenance option is available and the structure returns to its initial state after the maintenance action is applied (*i.e.*, the service life is extended by the initial service life T^o). The maintenance cost is assumed \$100,000. The initial service life T^o , in this example, refers to the time when the crack size reaches 50 *mm*. Using Monte Carlo simulation for Equation (2.22) the mean and

standard deviation of T^o is computed as 13.97 years and 7.12 years, respectively. The effect of correlation between the material parameters *C* and *m* (see Equation 2.22) was also studied. A correlation coefficient of -0.89 (Cramer & Friis-Hansen 1994) between ln*C* and *m* produces a reduction 1% and 6% in the mean and standard deviation of T^o, respectively. The results presented next are for the uncorrelated case.

Maximization of the service life and minimization of total life-cycle cost (consisting only of inspection and maintenance costs) conflict each other since the service life extension requires additional financial resources. In order to find a well-balanced solution, a bi-objective optimization consisting in maximizing the expected service life and minimizing total life-cycle cost simultaneously has to be solved. When the available number of scheduled inspections is two (*i.e.*, N_I = 2), the bi-objective optimization problem is

Find t_1, t_2, and a_r (5.23)

to maximize $E[T]$ and minimize $E[C_{tot}]$ (5.24)

such that $t_2 - t_1 \geq 1$ year (5.25)

given PDF of T^o, N_I = 2, α and β (5.26)

The design variables are the inspection times (*i.e.*, t_1 and t_2), and the critical crack size a_r for maintenance. Maintenance is applied only when the detected crack size *a* is larger than the critical crack size a_r. The objective functions of expected service life $E[T]$ and expected total life-cycle cost $E(C_{total})$ for two scheduled inspections, *n* = 2, can be formulated using the decision tree shown in Figure 5.3. The time interval between inspections should be at least one year. The PDF of T^o, and the parameters α and β

associated with an ultrasonic inspection method are given. The optimization toolbox (*i.e.*, genetic algorithm for multi-objective optimization) provided in MATLAB® version R2011a (MathWorks Inc. 2011a) is used to find the Pareto optimal solution set of the bi-objective optimization formulations in Equations (5.23)-(5.26).

GAs with 500 generations and 100 populations provides the Pareto solution set as shown in Figure 5.8. The design variables and objective function values of three representative solutions (A_I, A_{II} and A_{III}) in Figure 5.8 are provided in Table 5.3. When solution A_I is used as an optimum inspection and maintenance plan, the ultrasonic inspection should be applied at time 19.54 years and 39.72 years, and the critical crack size a_r is 2.30 *mm*. The corresponding expected service life E[T] and total life-cycle cost $E(C_{total})$ are 19.89 years and \$37,849, respectively. If solution A_{III} is selected instead of solution A_I, $E[T]$ is extended from 19.89 years to 26.80 years, and $E[T]$ increases from \$37,849 to \$124,281. This is because critical crack size a_r of solution A_{III} is smaller than that of solution A_I as shown in Table 5.3. The smaller value of a_r is related to the case where maintenance is more probable.

5.7.3 Example 5.3

The proposed approach is applied to the RC slab of the Colorado highway bridge E-16-Q. The RC slab is 12.19 *m* (4 *ft*) wide and 18.29 *cm* (7.2 *inch*) thick, and is supported by seven stringers. A detailed description of this bridge can be found in Akgül (2002). This example focuses on corrosion of the top transverse reinforcement bars of the slab. The diameter of the reinforcement d_o is treated as a random variable associated with LN(12.7 *mm*; 0.25 *mm*).

Corrosion initiation time t_{occ} of the slab is estimated as a lognormally distributed random variable with mean and standard deviation of 6.41 years and 2.89 years, respectively (Akgül 2002). Corrosion damage propagation is based on the pitting corrosion model of Equations (2.27)-(2.29). The ratio between maximum and average corrosion penetrations R_c in Equation (2.27) is assumed to be normally distributed with mean value of 5.0 and standard deviation of 1.0. The corrosion rate r_{corr} is considered as LN(0.05 *mm*/*year*; 0.01 *mm*/*year*).

The service life of RC structures can be predicted based on the ratio of the average corrosion penetration depth to the initial radius of reinforcement. The allowable ratio for service life estimation ranges from 0.035 to 0.08 (Torres-Acosta & Martinez-Madrid 2003). In this chapter, the allowable ratio for service life estimation is assumed to be 0.06, and the associated maximum pit depth *PT* is calculated as 3.25 *mm* using Equations (2.28) and (2.29). Finally, the initial service life T^o when the *PT* reaches 3.35 *mm* is obtained with mean and standard deviation of 20.54 years and 5.28 years, respectively.

In this example, *PoD* function defined in Equation (5.19) is used. Damage intensity $\delta(t)$ for localized (or pitting) corrosion at time *t* is defined as (Kim *et al.* 2011)

$$\delta(t) = \frac{PT(t)}{d_o} \tag{5.27}$$

where d_o = initial diameter of the reinforcement. As mentioned previously, the damage intensity is used to determine the type of maintenance. In this example, corrosion protection using sealer and deck repair are considered as the two available maintenances. It is assumed that the sealer leads to preventing increase of corrosion damage intensity

within the effective time interval (i.e., maintenance A) which is treated as a random variable LN(6 *years*; 0.5 *year*). When deck repair is used, the top layer of reinforcement steel and concrete are replaced, and the RC deck is restored to its original structural performance (i.e., maintenance B) (Sohanghpurwala 2006). The scheduled inspection cost $C^{(insp)}$ considering the quality of inspection represented by α_δ is estimated by (Mori & Ellingwood 1994)

$$C^{(insp)} = C_s \left(1 - 0.7\alpha_\delta\right)^{r_{ins}} \tag{5.28}$$

where C_s = \$30,000 and r_{ins} = 10 herein. In this example, it is assumed that the in-depth inspection cost $C^{(insp,d)}$ is \$20,000, and maintenance costs associated with corrosion protection and deck repair are \$60,000 and \$300,000, respectively.

The formulation of bi-objective optimization problem to maximize the expected service life $E[T]$ and minimize the expected total life-cycle cost $E[C_{tot}]$, including only the inspection and maintenance costs, is

Find $\mathbf{t_{insp}} = \{t_1, \ldots, t_n\}$, $\boldsymbol{\alpha_\delta} = \{\alpha_{\delta,1}, \ldots, \alpha_{\delta,,n,}\}$, (5.29)

and $\boldsymbol{\delta} = \{(\delta_{I,1}; \delta_{II,1}), \ldots, (\delta_{I,n}; \delta_{II,n})\}$

to maximize $E[T]$ and minimize $E[C_{tot}]$ (5.30)

such that $t_i - t_{i-1} \geq 1$ year (5.31)

$0.01 \leq \boldsymbol{\alpha_\delta} \leq 0.5$ (5.32)

$\delta_I \leq \delta_{II}$ (5.33)

given PDF of T^o, and N_I (5.34)

The design variables of this problem are the inspection times $\mathbf{t_{insp}}$, parameter $\boldsymbol{\alpha_\delta}$ representing inspection quality, and damage intensity criterion vector $\boldsymbol{\delta}$ for selecting the maintenance type. The time interval between inspections should be at least 1 year, and the parameter $\boldsymbol{\alpha_\delta}$ has to range from 0.01 to 0.5. If the identified damage intensity δ from an in-depth inspection is less than δ_I, there is no maintenance. For $\delta_I \leq \delta < \delta_{II}$, corrosion protection using sealer is applied to extend the service life. Furthermore, deck repair is used for $\delta \geq \delta_{II}$. The PDF of initial service life T^o, and number of inspections N_i are given (see Equation (5.34)). The optimization toolbox (*i.e.*, genetic algorithm for multi-objective optimization) in MATLAB® version R2011a (MathWorks Inc. 2011a) is used to find the Pareto optimal solution set. The maximum number of generations is fixed at 500 with population of 100.

Figures 5.9 (a), (b) and (c) show the Pareto solution sets for n = 1, 2 and 3 inspections, respectively. Table 5.4 provides the values of design variables and objective functions associated with the six representative solutions selected in Figure 5.9 (*i.e.*, $B_{I,1}$ and $B_{II,1}$ in Figure 5.9 (a); $B_{I,2}$ and $B_{II,2}$ in Figure 5.9 (b); and $B_{I,3}$ and $B_{II,3}$ in Figure 5.9 (c)). If solution $B_{II,1}$ in Figure 5.9 (a) is selected, the inspection method with $\alpha_{\delta,1}$ = 0.09 has to be applied at 19.68 years. The corresponding damage intensity criteria for maintenance type are $\delta_{I,1}$ = 0.01 and $\delta_{II,1}$ = 0.05 as indicated in Table 5.4. This means that if the damage intensity δ was found to be less than 0.01 from the in-depth inspection performed after the scheduled inspection at 19.68 years, no maintenance is required, and furthermore, if δ was found to be between 0.01 and 0.05, or larger than 0.05, corrosion protection with sealer or deck repair should be applied, respectively. This strategy will extend the service life to be 29.99 years with the cost of $168,680. The expected service

life $E[T]$ of solution $B_{II,2}$ is larger than that of solution $B_{I,2}$ (see Figure 5.9 (b)). However, solution $B_{II,2}$ is more expensive than solution $B_{I,2}$. This is because solution $B_{II,2}$ is associated with higher quality inspection (*i.e.*, smaller value of $\alpha_{\delta,1}$) and, as shown in Table 5.4, it has a less damage intensity criterion $\delta_{II,1}$ than solution $B_{I,2}$.

5.7.4 Example 5.4

The proposed intervention optimization routine is next illustrated on a steel ship side shell detail subjected to fatigue. In this example, the inspection, monitoring, and maintenance optimization will be performed on the critical location shown in Figure 5.10. The stress fluctuations at this detail are mainly caused by hydrodynamic and wave induced pressures. Equation (2.22) is used to predict the time-variant crack size assuming the crack growth exponent m = 3.0. The crack growth coefficient C, is considered to follow a lognormal distribution with a mean of 2.3×10^{-12} (British Standards Institute 2005), using units of mm/cycle for crack growth rate and $\mathrm{N/mm}^{3/2}$ for the stress intensity factor range, and a coefficient of variation (COV) of 0.3. The initial crack size a_o is assumed to follow a lognormal distribution with mean of 0.5mm (Chung *et al.* 2006) and a COV of 0.1. The stress range S_{re} is considered as a random variable following a Weibull distribution (Kim & Frangopol 2012) with a mean of 20 MPa and COV of 0.1, and the function $Y(a)$ is considered to be constant, $Y(a)$ = 1.12 (Guedes Soares & Garbatov 1999b). The average annual number of cycles N_{avg} is also considered to follow a lognormal distribution (Kim & Frangopol 2011b) with a mean value of 1.0×10^{6} and a COV of 0.1. The critical crack size is assumed herein to be 50 mm and the required service life t^* is considered 20 years. Monte Carlo simulation with 100,000 samples is next performed to draw samples from the time to failure of the detail which is also

considered as the initial service life. Figure 5.11 (a) shows the histogram of the initial service life T^o. As shown, the mean value of T^o (i.e., time to reach the critical crack size) is 21.1 years with a standard deviation of 11.1 years. Figure 5.11 (b) shows the PDF, $f_{T^o}(t)$, and the CDF, $F_{T^o}(t)$, of the initial service life. These functions are used next to find the optimum intervention schedule for the investigated detail. It is assumed herein that the damage occurs when the crack size reaches 1.0 mm.

In this section, the optimum interventions schedules, including the optimum inspection and/or monitoring times, monitoring durations, and crack size threshold for performing maintenance are obtained. As in Example, 5.2, the maintenance action is assumed to restore the performance to the initial level. Minimizing the expected life-cycle cost, minimizing expected maintenance delay, and maximizing the service life are considered as optimization objectives. In order to analyze the effect of the different objectives on the optimal solutions, bi-objective optimization problems are first constructed and solved to find the optimum trade-offs between each of the two objectives, and then investigated in a tri-objective problem. In this example, the ultrasonic technique is considered as the inspection method for fatigue crack detection, while the AE technique is considered as the crack monitoring methodology. The *PoD* parameters α and β associated with ultrasonic inspection are considered 0.122 and -0.305, respectively (Forsyth & Fahr 1998). In this example, three options for the monitoring duration are considered, namely, one day, one week, and six weeks. Based on Pollock (2007, 2010), the parameters α and β associated with AE monitoring for six weeks are 0.801 and -0.491, while for monitoring periods of one week and one day, a reduction

factor $R_{t_{md}}$ of 0.65 and 0.5, respectively, is applied to the *PoD* function as shown in Equation (5.3).

Optimum interventions to maximize expected life and minimize expected total cost

At this stage, the optimum intervention schedule is obtained as the solution of an optimization problem with the objective of maximizing the expected service life and minimizing the expected total cost of interventions. The problem is formulated as follows

$$\text{given} \quad N_I, \underline{\mathbf{C}}, \mathbf{PoD}, \text{ and } f_{T^o}(t) \tag{5.35}$$

$$\text{Find } \mathbf{t}_i = \{t_1, t_2, t_3, ..., t_{N_I}\},\ \mathbf{t}_{md,i} = \{t_{md,1}, t_{md,2}, t_{md,3}, ..., t_{md,N_I}\}, a_r \tag{5.36}$$

$$\text{such that} \quad t_i - t_{i-1} \geq 1.0\ year \tag{5.37}$$

$$\text{to maximize } E[T] \text{ and minimize } E[C_{tot}] \tag{5.38}$$

where $\mathbf{t}_i$ is a vector consisting of the design variables of intervention times, $\mathbf{t}_{md,i}$ is a vector consisting of the monitoring durations, $t_{md,i}$ is the monitoring time associated with the *i*-th intervention and it is equal to zero for the case of inspection, a_r is the critical crack size for repair, N_I is the number of interventions, $\underline{\mathbf{C}}$ is a vector consisting of the cost of inspection $C^{(insp)}$, monitoring $C^{(mon)}$, in-depth inspection $C^{(insp,d)}$, repair $C^{(rep)}$, and failure cost C_f. **PoD** is a matrix containing the *PoD* parameters α and β associated with the inspection and monitoring. As indicated by Equation (5.37), a constraint has been imposed requiring that the time between successive interventions should be at least one year. Additionally, based on the problem formulation, maintenance is applied when the

detected crack size is at least a_r. The cost of inspection $C^{(insp)}$ is considered to be \$5,000. The monitoring cost is expressed as

$$C^{(mon)} = C_1^{mon} + C_2^{mon} \cdot t_{md} \tag{5.39}$$

in which C_1^{mon} is the initial monitoring cost which covers the hardware and installation expenses and $C_2^{mon} \cdot t_{md}$ is the running monitoring cost which increases with the increase in the monitoring duration. In this example, C_1^{mon} is considered \$15,000 and C_2^{mon} is zero for monitoring activities lasting for one day and \$1,000/week for monitoring of one and six weeks. The in-depth inspection cost and maintenance cost are assumed to be \$15,000 and \$50,000, respectively. The discount rate of money r_d is assumed to be zero.

With all the input parameters defined and using the formulation for the expected service life and total cost given by Equations (5.8)-(5.14), the bi-objective optimization problem is constructed and solved by using the Global Optimization Toolbox provided in version R2013b of MATLAB® (MathWorks Inc. 2013). A Generic Algorithm (GA) with 400 as the population size and 300 as the maximum number of generations is adopted to develop the Pareto-optimal solution set provided in Figure 5.12. It should be noted that convergence occurred before the maximum number of generations were met in all the problems. GAs are used in this chapter due to the stochastic nature of their search algorithm and the subsequent avoidance of converging to local minima for this type of problem. The provided Pareto-optimal set of solutions represents the optimum trade-offs between the two conflicting objectives. The Pareto-optimal solutions in Figure 5.12 consist of three Pareto fronts associated with one, two, and three interventions. Each of the optimal solution shown in the front has an associated set of information for the

optimal intervention times and types and the critical crack size for maintenance. Four representative solutions are highlighted in Figure 5.12 and described in detail in Table 5.5. For instance, Solution A1 specifies ultrasonic inspection to be performed at the year 19.72 with a critical crack size for maintenance of 5.96 mm. This yields an expected service life of 28.99 years and a total cost of $28,630. Solution A2, characterized by a higher life-cycle cost and expected service life, specifies inspection to be performed at 15.13 years with a critical crack size for maintenance of 4.23 mm. Therefore, with respect to a given number of interventions, solutions with higher expected cost and service life are associated with a small crack size for maintenance and earlier intervention times. As shown, the four optimal plans (i.e., A1, A2, A3, and A4) presented in Table 5.5 and Figure 5.12 specify only inspections using ultrasonic to be performed at all interventions. This is due to the high cost considered and low probability of detection associated with the AE monitoring compared to those of the ultrasonic inspection.

However, if changes occur to the cost structure of the problem, different trends can be obtained. That is, the Pareto-optimal solutions for the expected service life versus the life-cycle cost optimization problem are altered if the cost for ultrasonic inspection is changed to $15,000. This may occur if the inspection requires a long time to be performed or if it is necessary to remove the ship from service to perform the inspection. The cost of ultrasonic and AE are now comparable resulting in an implementation of AE amongst the optimal management plans. Figure 5.13 (a) compares the Pareto-optimal solution fronts of the optimization problem with different cost values of the ultrasonic inspection. Three representative solutions B1, B2, and B3 are selected on Figure 5.13 (a) and shown in details in Figure 5.13 (b) and Table 5.5. AE monitoring tends to appear

later in the intervention plans as the size of fatigue cracks increase and AE is more likely to detect them. It should be noted that, when incorporating a large cost of failure into the cost formulation, the Pareto-optimal solution may be affected. Expected failure cost is, therefore, included in the subsequent optimization problems in the formulation of mean life-cycle cost.

Optimum interventions to minimize expected maintenance delay and minimize expected total cost

Understanding the joint effect of minimizing the maintenance delay and the life-cycle cost on the optimum intervention plans requires solving a bi-objective optimization problem. Therefore, a second optimization problem is constructed and solved using the same formulation given by Equations (5.35)-(5.37) with the objectives of minimizing the expected maintenance delay $E[D]$ and minimizing the total life-cycle cost $E[C_{tot}]$. Using \$15,000 for the cost of inspection, and the same GA setup as in the previous bi-objective problem, the optimal solution fronts for $N_I = 3$ are shown in Figure 5.14 for failure costs C_f = \$0 and C_f = \$500,000. Two representative solutions, C1 and C2, are chosen from the front associated with C_f = \$0 and shown in Table 5.6. The management plan associated with C1 has a low probability of repair (i.e., $P(\mathrm{B}_2)$ = probability of occurrence of branch B_2 in Figure 5.3) indicated by the large crack size a_r, and thus a low repair cost which yields a low life-cycle cost. The solution C2 has a lower crack size a_r which yields a higher probability of repair and a higher cost.

The optimal front with failure cost of \$500,000 presented in Figure 5.14 shows the effect of probability of failure on the optimal solutions. Solutions C3 and C4 are

highlighted and presented in Table 5.6. With the inclusion of the failure cost, it is observed that the repair crack size a_r is generally smaller than the case with C_f = \$0. This indicates a higher probability of performing repairs during an intervention. Comparison among solutions on the front associated with C_f = \$500,000 shows that the low life-cycle cost indicates interventions performed later in the service life with lower probability of failure (i.e., Solution C3). While C4 represents a solution which minimizes the maintenance delay by scheduling closely spaced interventions with a high probability of repair. However, these solutions yield a higher life-cycle cost due to the high probability of failure since these repairs are performed early in the service life.

Optimum interventions to minimize expected maintenance delay and maximize expected service life

A third optimization problem is constructed and solved using the same formulation given by Equations (5.35)-(5.37) with the objectives of minimizing the maintenance delay $E[D]$ and maximizing the expected service life $E[T]$. Figure 5.15 shows the solution fronts for N_I =1 and 3. As shown, minimizing the maintenance delay conflicts with maximizing the expected service life requiring a bi-objective optimization to find the optimal trade-offs. Solutions D1, D2, and D3 are highlighted in Figure 5.15 and also shown in Table 5.6. The formulation of maintenance delay allows the solutions associated with three interventions (i.e., D2), to have lower maintenance delay values than those specifying only a single intervention to be performed (i.e., D1). The minimal maintenance delay objective drives management plans towards more frequent and closely spaced interventions; this reduces the expected service life. This effect is demonstrated by comparing the management plans associated with D2 and D3. Additionally, as the initial

intervention time is delayed, the maintenance delay increases while the extended life also increases.

Optimum interventions to minimize expected maintenance delay, minimize expected total cost, and maximize expected service life

It can be seen from the solution of the previous optimization problems that the three objectives conflict. In order to find the optimal trade-offs among the three objectives, a tri-objective optimization problem is formulated and solved using the same formulation given by Equations (5.35)-(5.37) to maximize $E[T]$, minimize $E[D]$, and minimize $E[C_{tot}]$. The Pareto-optimal solution sets of the problem using 400 as the population size and 300 as the number of generations are shown in Figure 5.16 for three interventions and cost of failure of \$0 and \$500,000. Details of representative solutions from both fronts are shown in Table 5.7. In both fronts, solutions with minimal maintenance delay correspond to solutions where the inspection and repair actions are performed early in life and are closely spaced. This reduces the mean expected life of the structure and precludes optimal solutions with high service life and low maintenance delay. Moreover, in the front associated with the C_f = \$500,000, these solutions have high life-cycle cost due to the high probability of failure resulting from the application of early maintenance actions. Based on the results of this tri-objective optimization problem, decision makers can choose the solution which fits the available budgets and the operational constraints. For instance, considering the front associated with \$500,000 failure cost, for a maximum allowable life-cycle cost of \$250,000, the optimization problem provides solutions with expected service life ranging from 31.17 to 51.26 years with a corresponding range of

7.68 to 23.5 years in the expected maintenance delay. Next, based on the expected service life and maintenance delay requirements, an optimum management solution can be selected.

In this tri-objective optimization problem, solutions for the case with no failure cost generally have higher crack size for repair which is translated to a lower probability of repair (i.e., the application of maintenance actions). In order to investigate the effect of the cost of failure on the optimal solutions, the optimization problem is solved again with C_f = \$100,000. Figure 5.17 shows the progression of the probability of failure averaged over the solutions in the Pareto front, as well as the average total probability of repair, P_{rep}^{total}, for C_f = \$0, C_f = \$100,000, and C_f = \$500,000. The probability of repair is computed from the event tree model as the sum of the probabilities of performing one, two, and three repairs in the management plan. As shown, as the cost of failure increases, the total probability of repair among the optimum solutions increases while the probability of failure decreases.

5.8 Conclusions

This chapter incorporates probabilistic performance prediction methodologies into an optimization routine to find the optimal intervention plan which simultaneously minimizes the expected maintenance delay, minimizes the expected life-cycle cost, and maximizes the expected service life. The proposed intervention planning methodology provides the optimum inspection and/or monitoring times, monitoring durations, and the optimum damage level to perform maintenance. The proposed framework consists of several parts: (a) prediction of damage occurrence and propagation and service life of a

deteriorating structure under uncertainty, (b) determining the relation between the degree of damage and the probability of damage detection of an inspection method, and (c) formulation of the service life considering effects of interventions on the service life, life-cycle cost, and maintenance delay under uncertainty. Ultrasonic inspections and acoustic emission crack size monitoring are used as the inspection and monitoring techniques, respectively. However, any inspection or monitoring methodology, with a well characterized probability of damage detection, can be included in the proposed approach. The expected life-cycle cost includes the cost of inspection, monitoring, and maintenance actions performed along the service life, as well as the expected cost of failure. The proposed framework was applied to several examples including a naval vessel and a bridge under fatigue and corrosion. The following conclusions can be drawn:

1. The formulation of service life, total life-cycle cost, and maintenance delay is based on decision tree model. Considering the uncertainties associated with damage propagation, inspection quality, and effect of maintenance on the service life, the PDFs and the associated probability descriptors (*e.g.*, mean, standard deviation) of service life, total life-cycle cost and maintenance delay can be obtained. In this chapter, the mean values of service life and total life-cycle cost are used to define the objective functions of the optimization problem.
2. The service life extension requires additional financial resources. Therefore, maximizing the service life and minimizing the total life-cycle cost conflict. In order to find a well-balanced solution, bi-objective optimization with maximizing the expected service life and minimizing the total life-cycle cost simultaneously has to be solved. Through comparison among the Pareto solutions obtained from

this bi-objective optimization, the effects of inspection quality, number of inspections, damage criteria for determining maintenance types on the expected service life and total life-cycle cost are revealed.

3. Minimizing the maintenance delay, maximizing the service life, and minimizing the life-cycle cost are conflicting objectives. Minimizing the maintenance delay tends to increase the life-cycle cost of the structure.
4. Establishing the optimal LCM plans which fulfill the three conflicting objectives can be achieved by using the proposed tri-objective optimization approach.
5. For low values of ultrasonic inspection cost compared to that of acoustic emission monitoring, the optimization scheme suggest that only management plans where ultrasonic inspections are performed are optimal. This is also due to the lower probability of damage detection associated with the acoustic emission crack monitoring, However, if the cost of ultrasonic inspection increases due to the additional time required to perform the inspection, solutions with acoustic emission monitoring appear in the optimal solution front.
6. The monetary value associated with the structural failure has a significant effect on the optimum solutions. A higher value yields solutions which have higher overall probability of performing repairs and lower probability of failure.
7. The results of the proposed approach are affected by the changes in the values of the inspection and monitoring costs, as well as by the ability of inspection and monitoring to detect the damage. Therefore, the accurate estimation of these quantities is required to establish the proper LCM plans.

8. This approach can be extended to cover structures with multiple critical fatigue locations. Additionally, it can include other deteriorating mechanisms such as corrosion and corrosion-induced fatigue and applied to other marine and civil structures.
9. The results of the proposed framework depend on the accuracy of damage propagation and service life prediction models. Information from each inspection can be used to update the damage propagation and service life, and efficient use of this information can lead to more accurate and reliable inspection and maintenance scheduling. The topic of updating the LCM plans based on inspection outcomes is addressed in the next chapter of this study.
10. The proposed approach in its current format can be only applied to structures under time-dependent deterioration. However, the approach can be extended to a risk-based inspection and maintenance optimization methodology where the damage induced by extreme events, such as earthquakes and hurricanes, can be assessed and the risk-based decision making process can be included.

Table 5.1 Optimum Inspection Time t_i, and Expected Service $E[T]$.

	Damage intensity criteria		Inspection quality		
	δ_I	δ_{II}	$\alpha_\delta = 0.1$	$\alpha_\delta = 0.3$	$\alpha_\delta = 0.5$
t_i (years)	0.0	0.0	16.05	21.07	24.26
$E[T]$ (years)			45.15	38.82	26.17
t_i (years)	0.3	0.5	21.08	21.30	24.26
$E[T]$ (years)			32.33	31.76	25.72
t_i (years)	0.0	1.0	16.05	21.07	24.24
$E[T]$ (years)			35.22	32.06	25.72

Table 5.2 Variables for crack growth model

Deterministic and random variables	Notation (Units)	Mean	COV †	Type of distribution
Stress range***	S_{re} (ksi)	5.8	0.1	Weibull
Annual number of cycles***	N_{avg} (cycles/year)	1.0×10^{6}	0.2	Lognormal
Initial crack size*	a_o (inch)	0.0197	0.2	Lognormal
Material crack growth parameter**	C	1.77×10^{-9}	0.3	Lognormal
Material crack growth parameter**	m	2.54	-	Deterministic

† Coefficient of variation; * Chung *et al*. (2006); ** based on Dobson *et al*. (1983);

*** based on engineering judgment
1 ksi = 6.895 MPa; 1 inch = 25.4 mm

Table 5.3 Design variable and objective function values associated with Pareto optimum solutions in Figure 5.8.

Pareto optimum solution	Number of inspections N_I	Objective values		Design variables		
		$E[T]$ (years)	$E[C_{tot}]$ (×\$1,000)	Inspection time (years)		Critical crack size for maintenance (*mm*)
				t_1	t_2	a_r
A_1	2	19.89	37.85	19.54	39.72	2.30
A_{II}	2	24.07	79.85	14.04	29.70	1.86
A_{III}	2	26.80	124.28	11.12	23.22	1.81

[redacted]

Pareto optimum solution	Number of inspections [redacted]	Objective values		Design variables											
		[redacted] (years)	[redacted] (×$1,000)	Inspection time (years)			Inspection quality			Damage intensity criteria for maintenance type					
				$t_{insp,1}$	$t_{insp,2}$	$t_{insp,3}$	$\alpha_{\delta,1}$	$\alpha_{\delta,2}$	$\alpha_{\delta,3}$	$\delta_{I,1}$	$\delta_{II,1}$	$\delta_{I,2}$	$\delta_{II,2}$	$\delta_{I,3}$	$\delta_{II,3}$
$B_{I,1}$	1	25.02	69.94	23.37	-	-	0.17	-	-	0.01	0.08	-		-	-
$B_{II,1}$	1	29.99	168.68	19.68	-	-	0.09		-	0.01	0.05	-		-	-
$B_{I,2}$	2	33.24	219.03	20.70	38.72	-	0.11	0.11	-	0.09	0.14	0.07	0.16	-	-
$B_{II,2}$	2	40.01	348.12	18.77	38.01	-	0.07	0.10	-	0.07	0.13	0.05	0.12	-	-
$B_{I,3}$	3	40.42	311.49	21.90	43.80	65.82	0.10	0.11	0.12	0.07	0.13	0.08	0.13	0.08	0.15
$B_{II,3}$	3	47.89	473.47	19.33	38.93	59.01	0.07	0.10	0.11	0.07	0.12	0.08	0.12	0.07	0.10

[redacted]

Optimum Solution	Number of Interventions	Intervention times (years)			Intervention type			Critical Crack size for Maintenance (mm)	Objective Values	
		t_1	t_2	t_3	Action 1	Action 2	Action 3		$E[T]$ (years)	$E[C_{tot}]$ ($1000)
A1	1	19.72	-	-	Ins	-	-	5.96	28.99	28.63
A2	1	15.13	-	-	Ins	-	-	4.23	30.77	45.57
A3	2	16.98	34.18	-	Ins	Ins	-	4.80	39.77	77.21
A4	3	16.53	33.72	52.41	Ins	Ins	Ins	4.52	48.50	111.02
B1	1	15.05	-	-	Mon[3]	-	-	5.58	30.46	55.06
B2	2	17.25	36.72	-	Ins	Mon[2]	-	7.29	38.46	77.04
B3	3	13.36	26.94	41.68	Ins	Ins	Mon[1]	4.10	51.58	174.00

Ins = Inspection; Mon = Monitoring
Mon[1] refers to t_{md} = one day; Mon[2] refers to t_{md} = one week; Mon[3] refers to t_{md} = six weeks

Optimum Solution	Number of Interventions	Intervention times (years)			Intervention type			Critical crack size for maintenance (mm)	Objective Values		
		t_1	t_2	t_3	Action 1	Action 2	Action 3		$E[T]$ (years)	$E[C_{tot}]$ ($1000)	$E[D]$ (years)
C1	3	19.70	20.73	25.12	Ins	Ins	Mon[1]	9.86	-	112.19	18.07
C2	3	1.02	2.08	8.27	Ins	Ins	Mon[1]	6.96	-	239.44	7.69
C3	3	9.92	30.87	33.87	Ins	Mon[1]	Mon[1]	3.51	-	173.44	16.12
C4	3	1.26	2.27	6.39	Ins	Ins	Ins	1.86		356.50	7.44
D1	1	6.53	-	-	Mon[3]	-	-	6.20	27.34	-	13.39
D2	3	1.39	3.42	7.47	Ins	Ins	Mon[3]	7.57	28.29	-	7.96
D3	3	10.94	23.75	38.22	Ins	Mon[1]	Mon[1]	3.17	51.17	-	17.25

Ins = Inspection; Mon = Monitoring

Mon[1] refers to t_{md} = one day; Mon[3] refers to t_{md} = six weeks

[redacted]

Optimum Solution	Number of Interventions	Intervention times (years)			Intervention type			Critical Crack size for Maintenance (*mm*)	Objective Values		
		t_1	t_2	t_3	Action 1	Action 2	Action 3		$E[T]$ (years)	$E[C_{tot}]$ ($1000)	$E[D]$ (years)
E1	3	18.98	21.72	26.53	Ins	Ins	Mon[1]	7.60	33.05	111.12	17.75
E2	3	1.06	2.08	8.36	Ins	Ins	Mon[1]	7.10	29.09	239.60	7.47
F1	3	12.07	25.44	39.59	Ins	Mon[1]	Ins	6.40	51.81	265.96	21.03
F2	3	1.04	2.23	4.10	Ins	Ins	Ins	4.26	24.86	433.50	6.47

Ins = Inspection; Mon = Monitoring
Mon[1] refers to t_{md} = one day

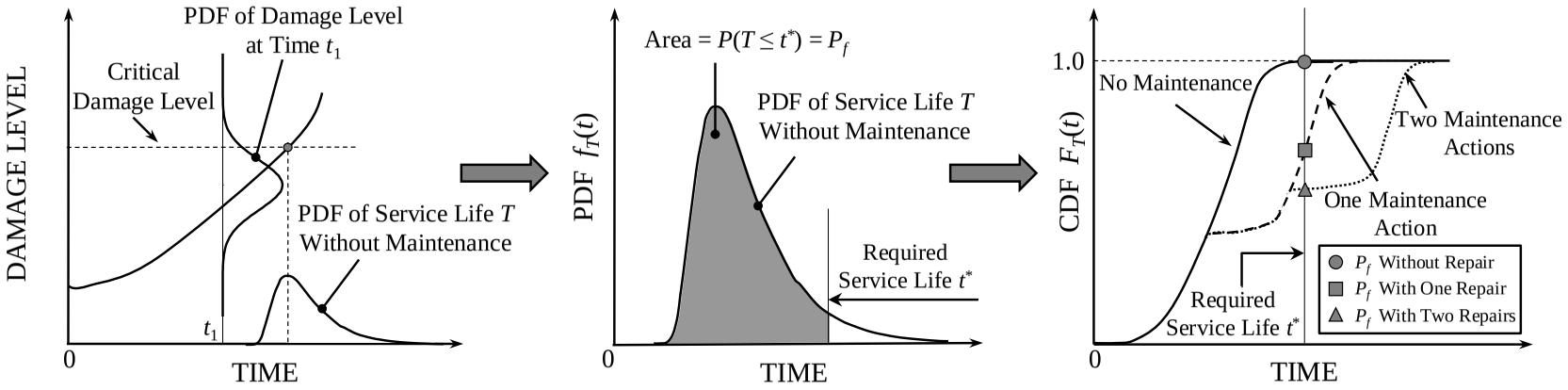
DAMAGE LEVEL
PDF of Damage Level
at Time t_1
Critical
Damage Level
PDF of Service Life T
Without Maintenance
t_1
0
TIME
Area = $P(T \le t^*) = P_f$
PDF $f_T(t)$
PDF of Service Life T
Without Maintenance
Required
Service Life t^*
0
TIME
1.0
CDF $F_T(t)$
No Maintenance
Two Maintenance
Actions
One Maintenance
Action
Required
Service Life t^*
P_f Without Repair
P_f With One Repair
P_f With Two Repairs
0
TIME

[redacted]

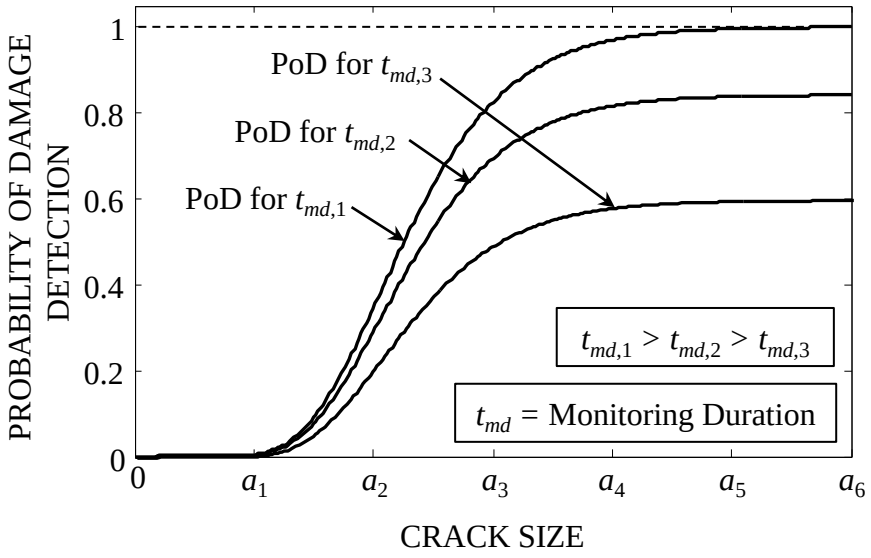

Figure 5.2 Probability of damage detection with respect to monitoring duration

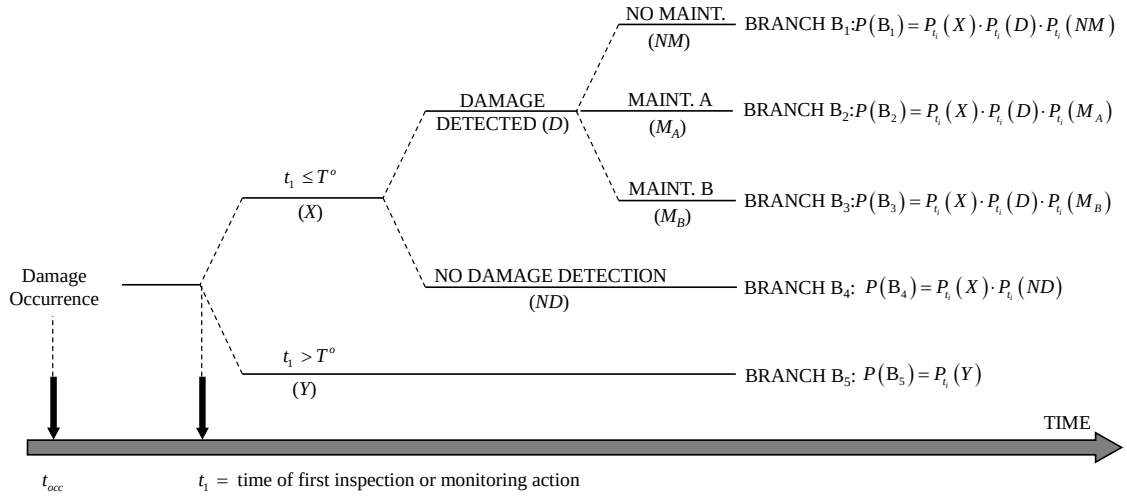

Figure 5.3 Event tree model for damage detection and repair, later incorporated in formulating the life-cycle cost, expected service life, and maintenance delay, considering one intervention

(a)

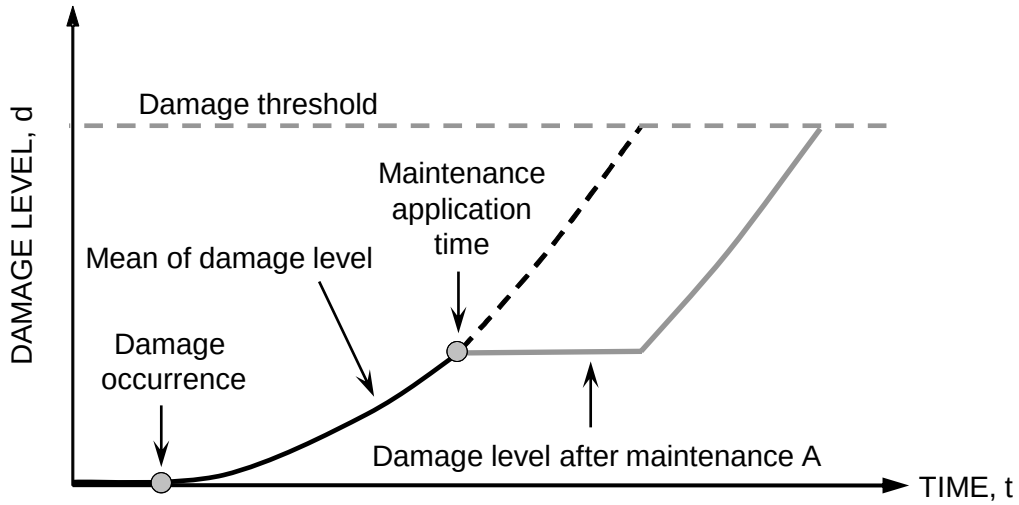

(b)

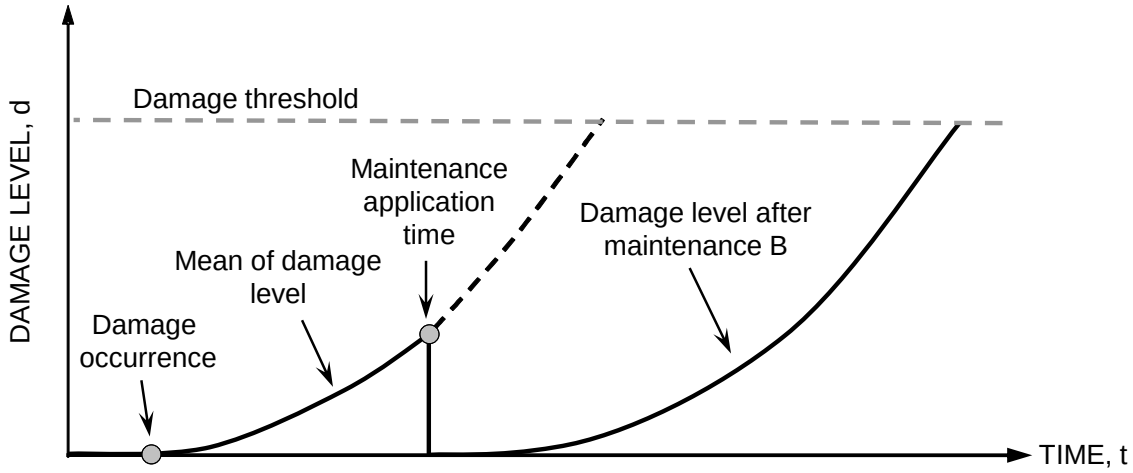

Figure 5.4 Effect of both maintenance types on the damage level; (a) maintenance A, and (b) maintenance B

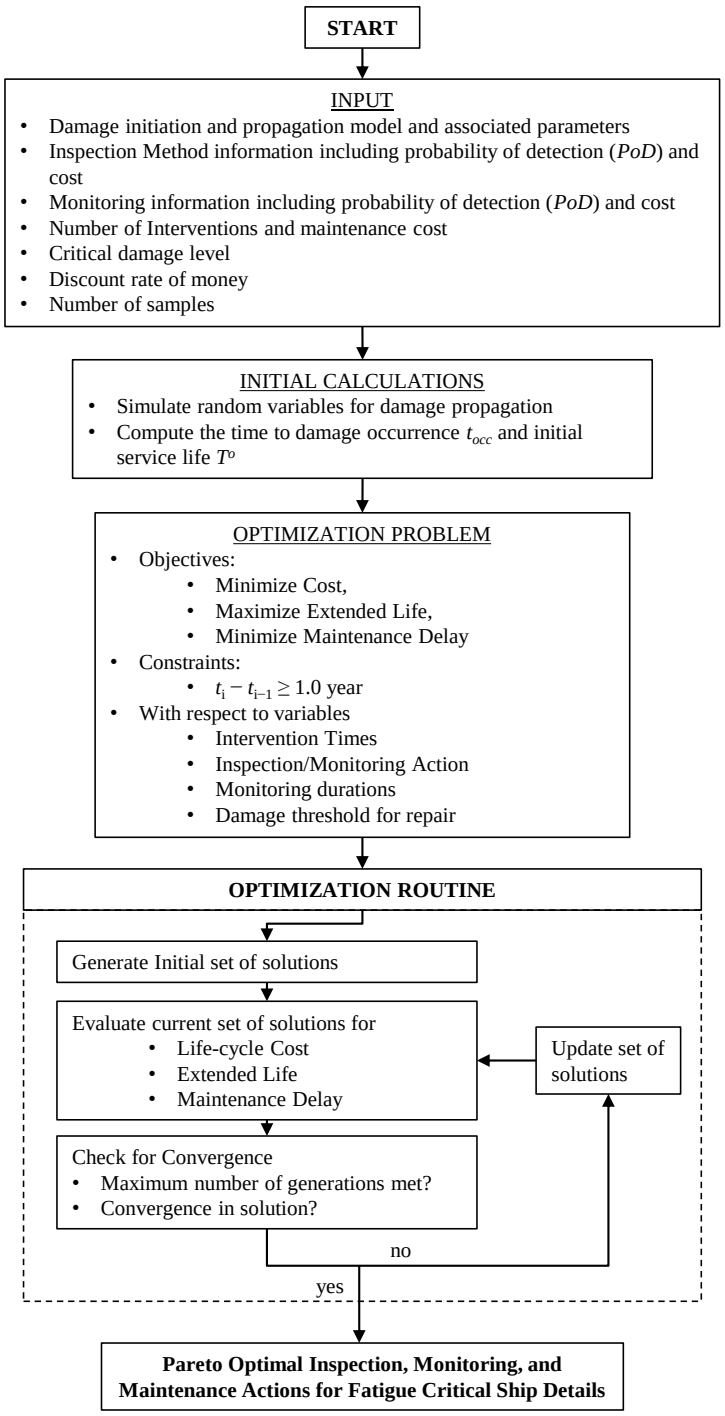

Figure 4

Figure 5.5 Flowchart of the proposed intervention optimization approach

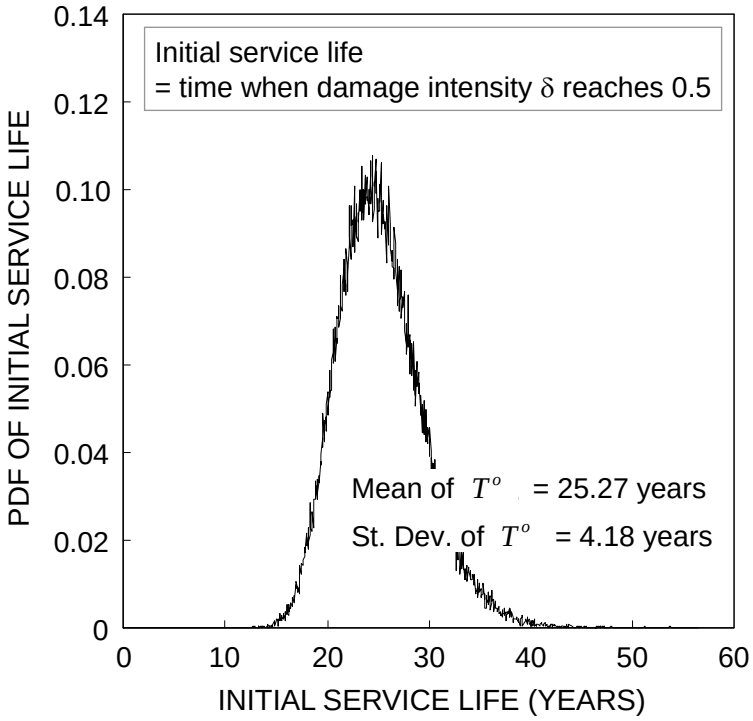

Figure 5.6 PDF of initial service life for Example 5.1

(a)

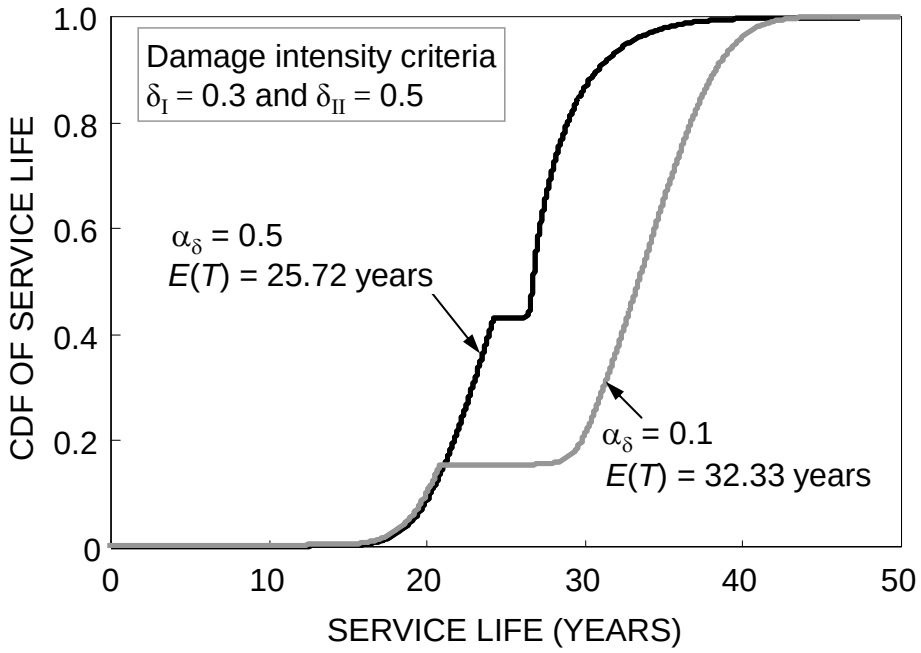

(b)

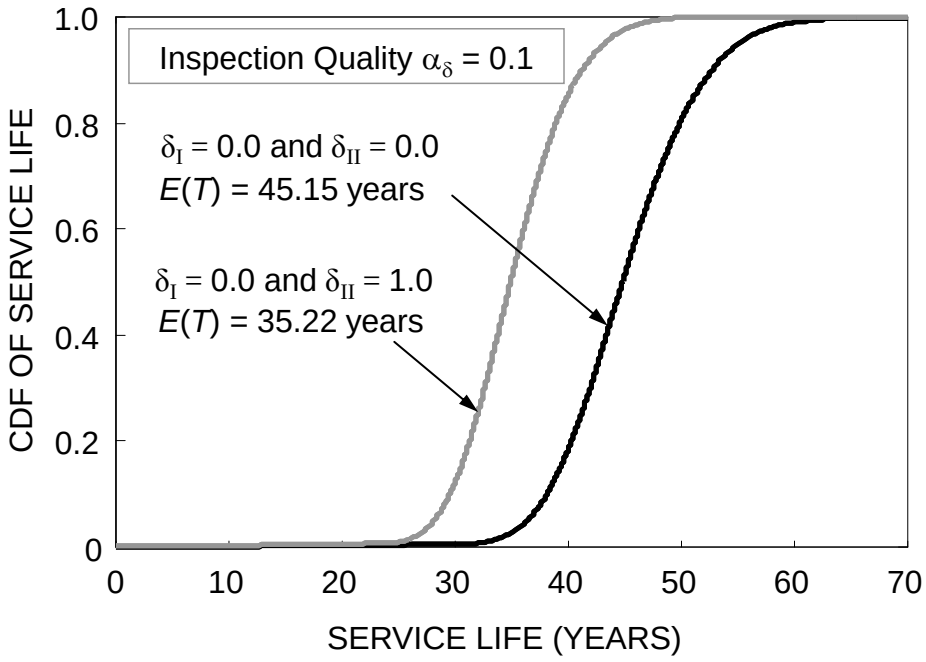

Figure 5.7 CDF of service life: (a) effect of inspection quality; (b) effect of damage intensity criteria on service life

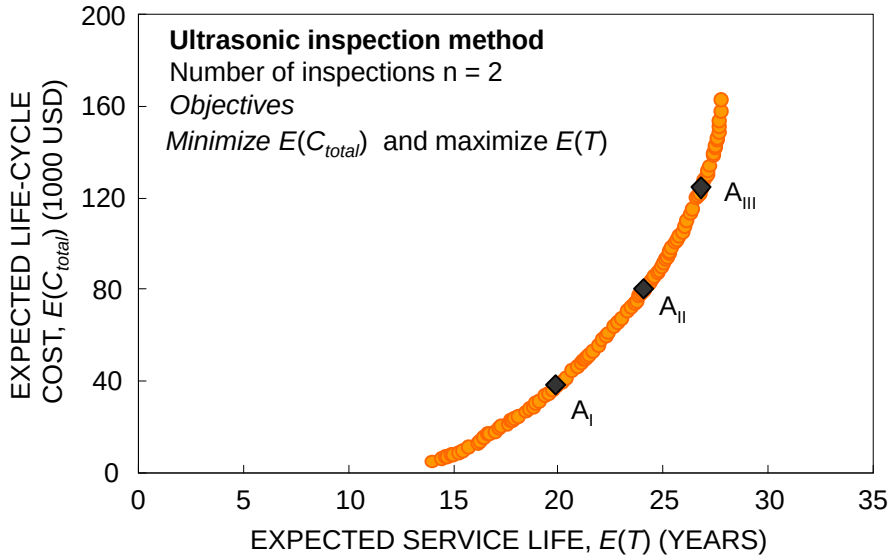

Figure 5.8 Pareto solution set for inspection and maintenance planning for Example 5.2

(a)

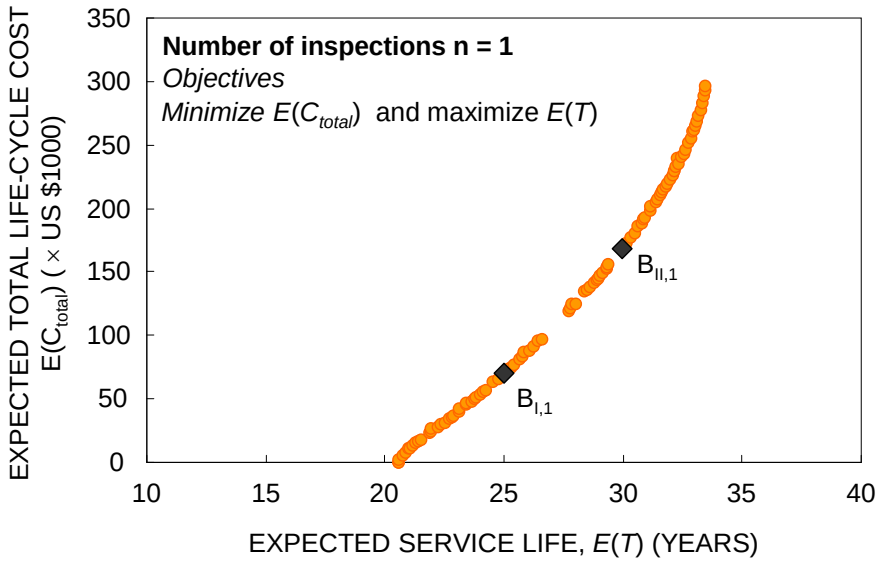
Number of inspections n = 1
Objectives
Minimize E(C_total) and maximize E(T)
EXPECTED TOTAL LIFE-CYCLE COST
E(C_total) (× US $1000)
EXPECTED SERVICE LIFE, E(T) (YEARS)
B_I,1
B_II,1
0
50
100
150
200
250
300
350
10
15
20
25
30
35
40

(b)

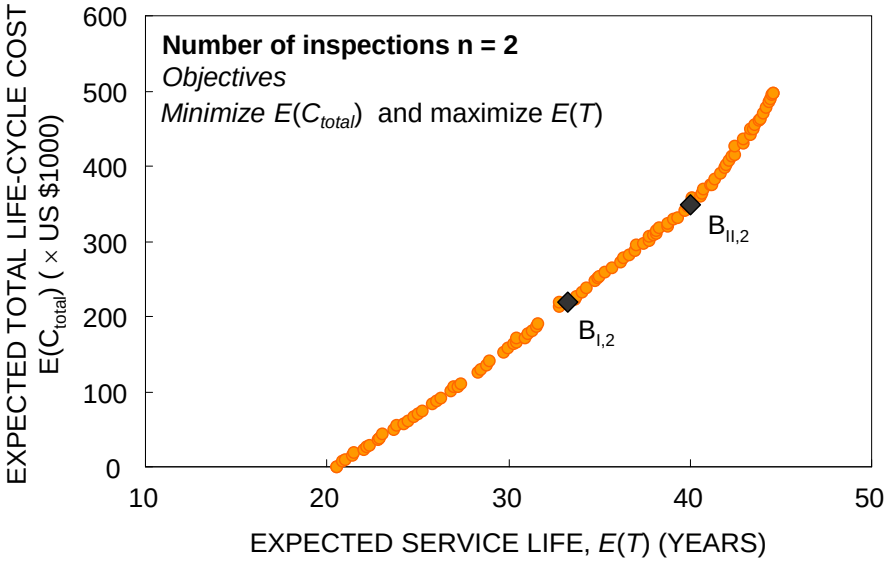
Number of inspections n = 2
Objectives
Minimize E(C_total) and maximize E(T)
EXPECTED TOTAL LIFE-CYCLE COST
E(C_total) (× US $1000)
EXPECTED SERVICE LIFE, E(T) (YEARS)
B_I,2
B_II,2
0
100
200
300
400
500
600
10
20
30
40
50

(c)

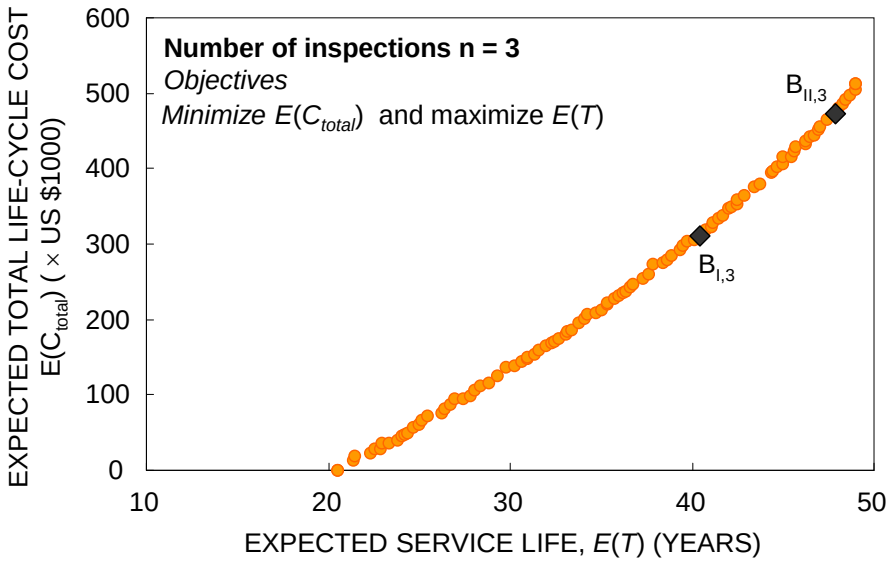

Figure 5.9 Pareto solution sets for number of inspections: (a) n =1; (b) n = 2; and (c) n = 3

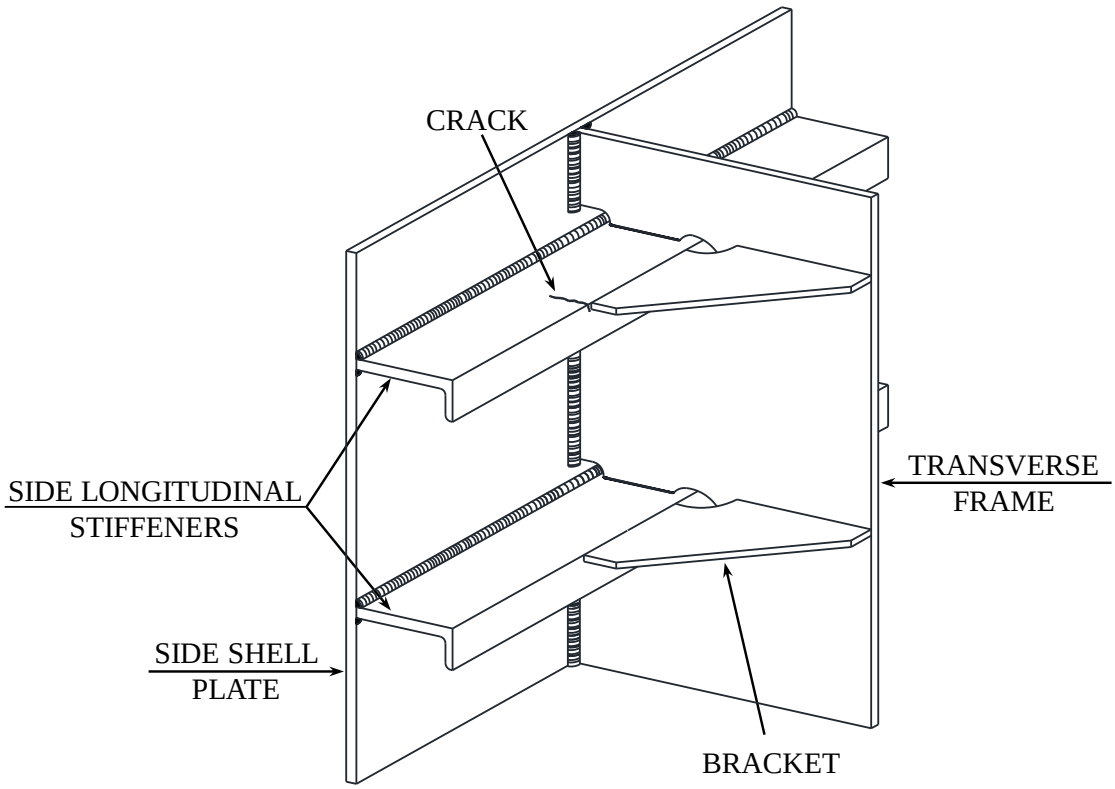

Figure 5.10 The studied critical location in Example 5.4

(a)

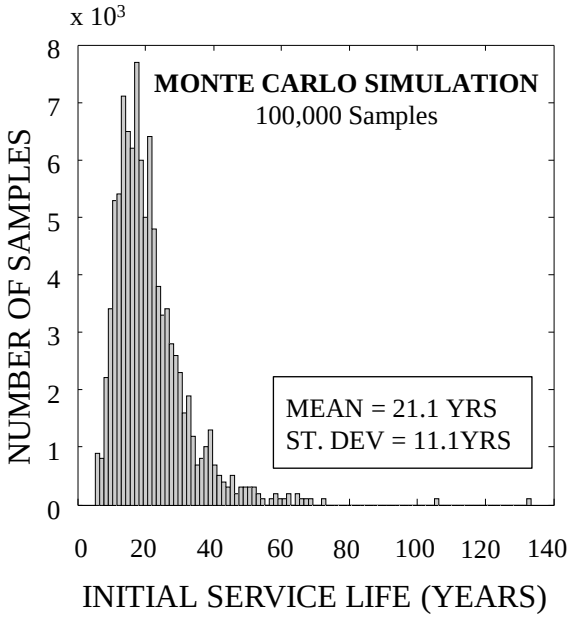

(b)

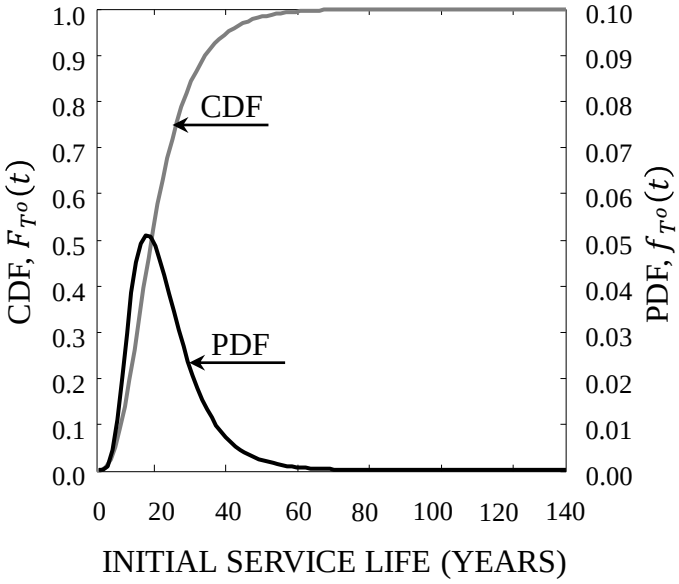

Figure 5.11 Results of the Monte Carlo simulation: (a) histogram of the initial service life, and (b) PDF and CDF of the initial service life of the studied detail

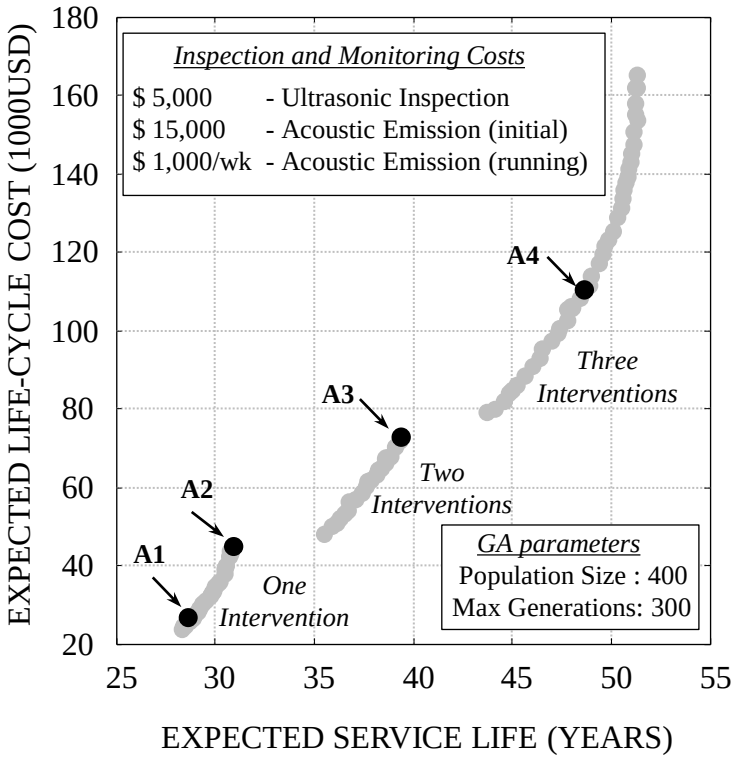

Figure 5.12 Pareto-optimal solutions for minimizing the expected total life-cycle cost, and maximizing the expected service life for one, two, and three scheduled interventions

(a)

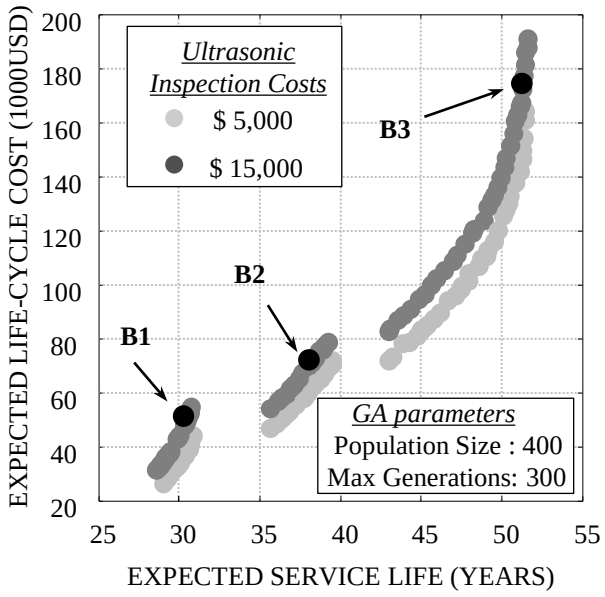

(b)

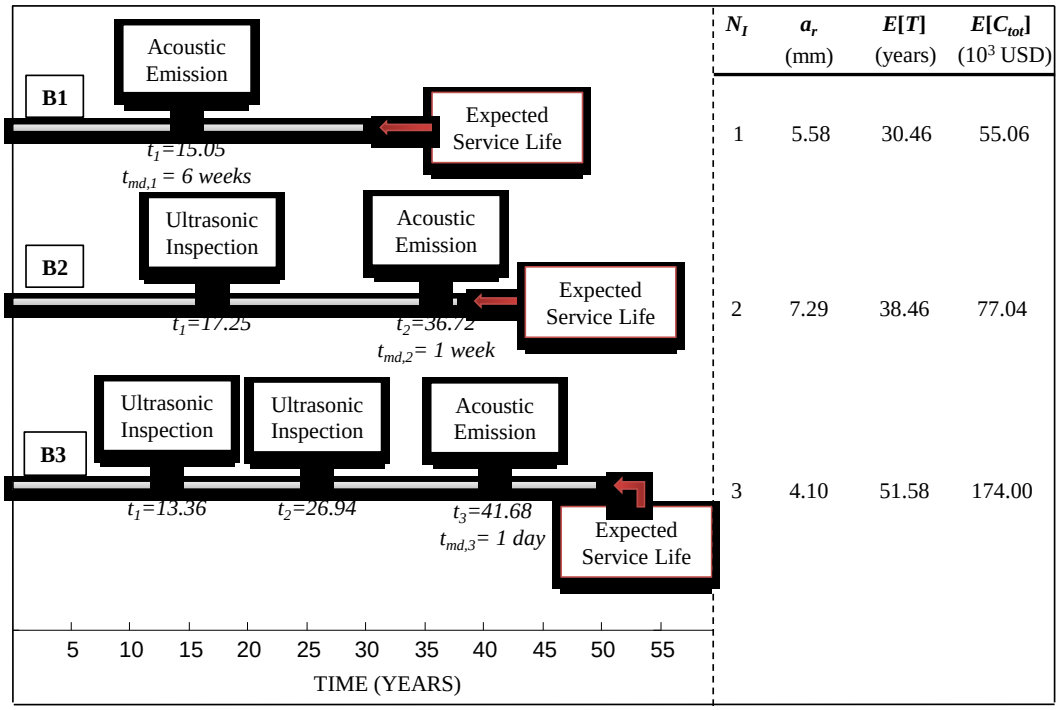

N_I	a_r (mm)	$E[T]$ (years)	$E[C_{tot}]$ (10^3 USD)
1	5.58	30.46	55.06
2	7.29	38.46	77.04
3	4.10	51.58	174.00

Figure 5.13 Optimization solution for minimizing the expected total life-cycle cost, and maximizing the expected service life; (a) Pareto-optimal solutions for different inspection costs, and (b) details of three representative solutions B1, B2, and B3

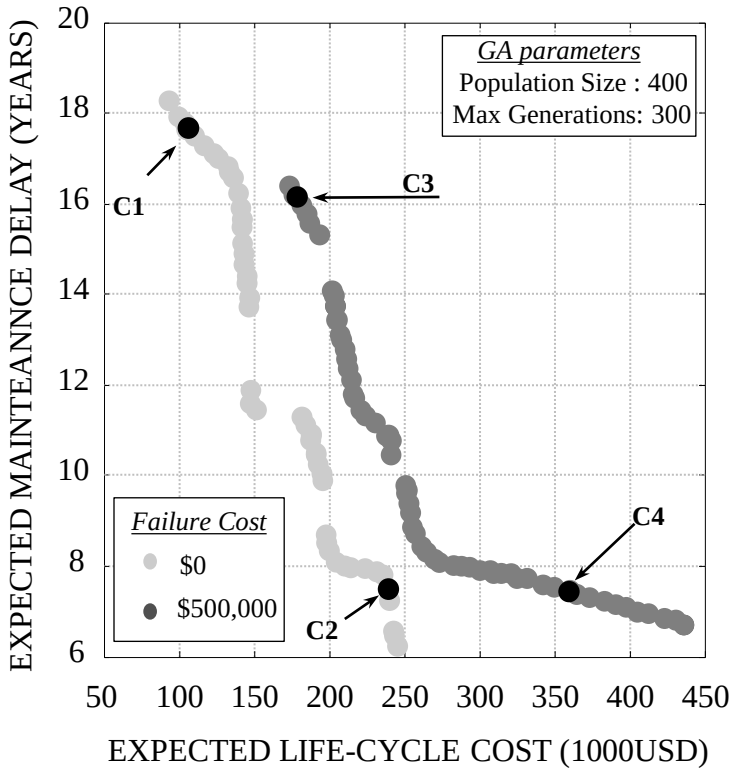

Figure 5.14 Pareto-optimal solutions for minimizing the expected maintenance delay, and minimizing the life-cycle cost for three scheduled interventions and different failure costs

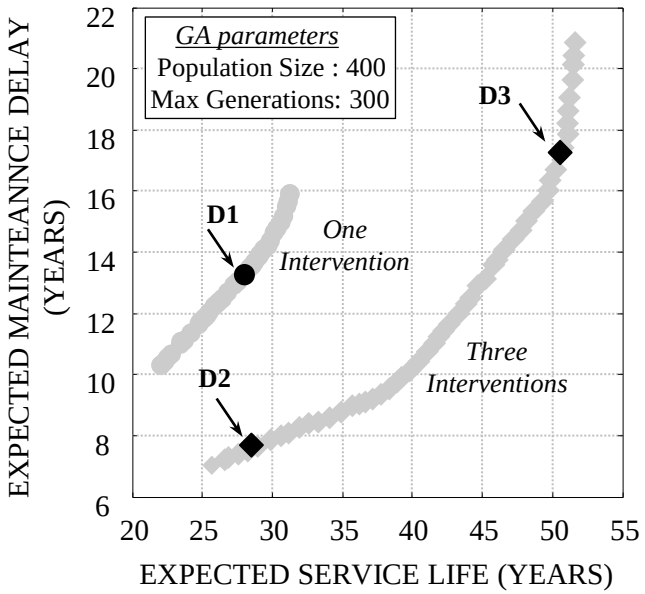

Figure 5.15 Pareto-optimal solutions for minimizing the expected maintenance delay, and maximizing the expected service life for one and three scheduled interventions

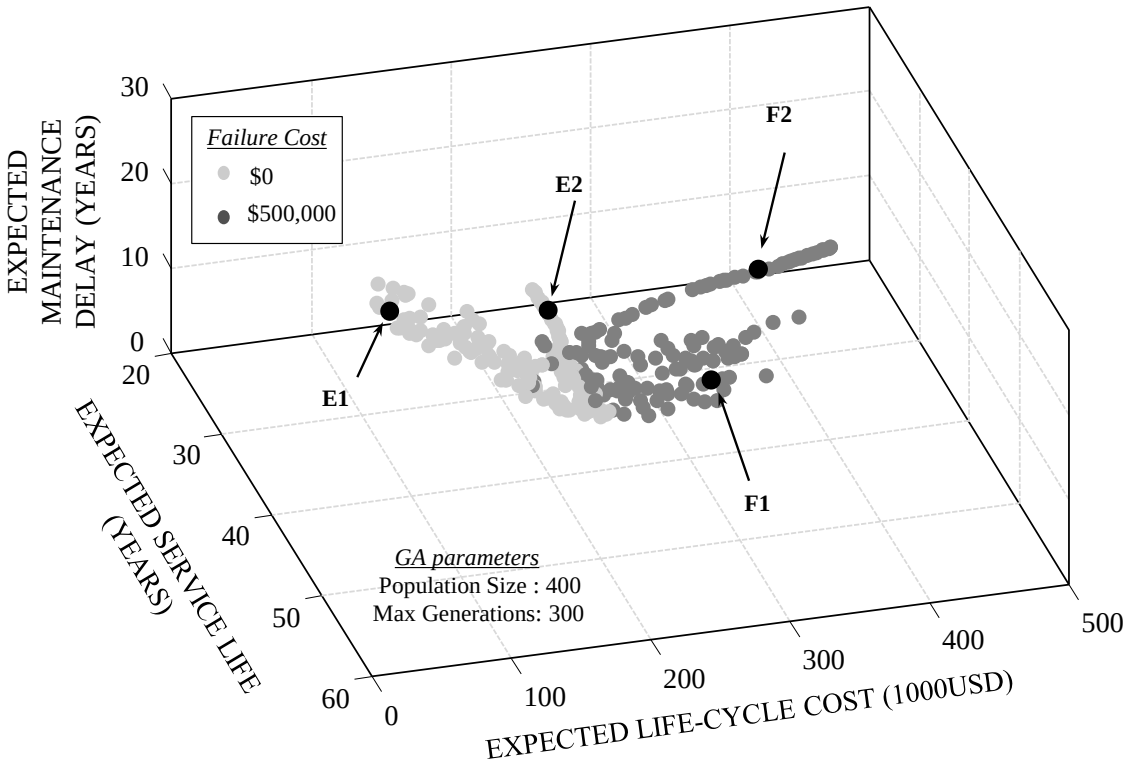

Figure 5.16 Pareto-optimal solutions of the tri-objective optimization problem with different failure costs C_f

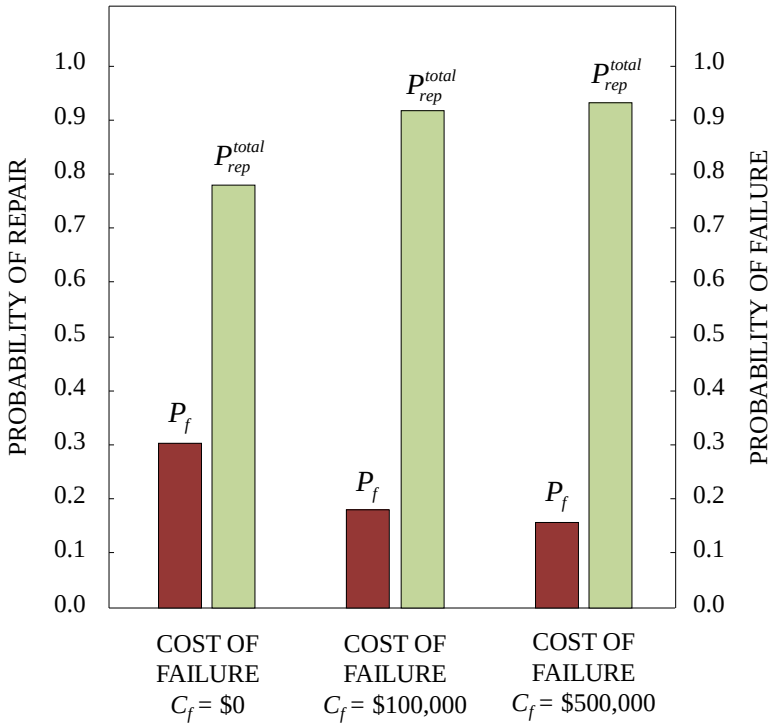

Figure 5.17 Effect of the failure cost C_f on the average probability of repair and the average probability of failure of optimum solutions

CHAPTER 6 INTEGRATION OF INSPECTION INFORMATION IN UPDATING LIFE-CYCLE MANAGEMENT PLANS

6.1 Overview

Successful management of deteriorating structures requires the reliable prediction of damage occurrence as well as the time-dependent damage propagation under uncertainty. Reliability of the performance prediction process can be significantly improved by integrating information gained from inspection and monitoring actions. This integration leads to more accurate prediction of the time-dependent damage level and, eventually, to a better decision making process.

In this chapter, a probabilistic approach is proposed to find an optimum management plan for fatigue sensitive structures integrating the available information from inspection actions. The proposed approach utilizes a probabilistic time-dependent damage criterion, inspection cost and failure cost to find the optimum inspection times under uncertainty. New information resulting from inspection actions performed during the lifetime of the structure is used to update the damage propagation parameters as well as the optimization procedure. This process results in an enhanced management plan which can provide the manager the ability to make real-time decisions based on inspection results. The integration of this new information and its impact on the LCM process is thoroughly investigated. In addition, a realistic fatigue critical detail is used to illustrate the proposed probabilistic approach.

This chapter is based in the papers Soliman and Frangopol (2013b, 2014a) and Frangopol & Soliman (2013,2014a,b,c).

6.2 Background

Effective inspection and monitoring actions are crucial aspects in the LCM framework. They provide the useful means to: (a) reduce uncertainties in loading and resistance of the structure, (b) indicate the current condition of the structure, and (c) detect the possible damaged locations within the structure. Since the results of these actions allow decision making, inspection and monitoring times should be optimized to ensure that damage will be detected before causing significant effect on the structural performance. For this reason, in recent years, the optimum planning for inspection and monitoring actions in a life-cycle context has gained a higher importance. On the other hand, results of inspection and monitoring actions may not give a clear indication on the future propagation of a detected damage. Accordingly, maintenance and repair actions should be planned based on inspection/monitoring outcomes along with the results of the prediction models under uncertainty (Zheng & Ellingwood 1998).

The intervention planning approaches, such as the one presented in Chapter 5 of this study, handled well the scheduling process by providing inspection, monitoring, and repair schedules that optimize the management goals. However, these approaches for repair scheduling, despite their effectiveness, does not allow the integration of new information collected through future inspection or monitoring actions into the existing management plans. In general, detecting a damage level that is significantly different from the predicted one would indicate that the prediction model may not be suitable for addressing the problem.

In an attempt to address this issue, other inspection and repair scheduling procedures were proposed. These procedures consider updating the structural

performance indicators of the inspected location based on the inspection results. This can be performed by defining time-based safety margins and updating time-variant probability of failure according to inspection outcomes. Madsen *et al.* (1987, 1991) proposed an approach which uses the LEFM to perform the inspection and repair scheduling. Based on the inspection outcomes, the failure probabilities and probabilities of repair are updated by conditioning them upon the inspection outcomes. Cramer & Bea (1991) used an *S-N* approach combined with formulae relating the crack size to the remaining service life of through thickness cracks for calculating the time-variant probability of failure for the studied detail. Moan & Song (2000) proposed a reliability-based model that can find the reliability of a series of inspected and uninspected fatigue details. In their approach, the reliability of the system can be updated based on the results of inspection of several components in the system. The discussed reliability-based inspection scheduling methods plan the inspection based on the predicted reliability profile and the target reliability index; i.e., an inspection is performed when the reliability index reaches the threshold value. If updating is performed, yielding an updated reliability profile, the next inspection is scheduled when the updated profile reaches the threshold. However, the updating process in this manner does not modify the model parameters based on the inspection outcomes and, therefore, the updated reliability profile may not be representative for the actual damage propagation. Therefore, the results of the updated inspection scheme may be questionable, especially considering the fact that the detected damage level, in most of the cases, will be different than the predicted one at the inspection time (Zheng & Ellingwood 1998).

An alternative approach is to use Bayesian updating of the damage propagation model parameters. In this approach, the information from inspection actions is used to represent the likelihood function which can be combined with the prior knowledge of the model parameters to yield an updated posterior distribution of the model parameters. Hence, the performance prediction is performed using the posterior parameters to achieve more reliable results. This approach was investigated by Heredia-Zavoni & Montes Iturrizaga (2004). They used the probability of detection in an updating procedure to predict the posterior distribution of the initial crack size at a certain point in time, and the measurement was used as the new data to update the probability density function of the initial crack size. However, inspection optimization and scheduling was not considered as a goal of the study. Perrin *et al.* (2007) used Bayesian techniques and Markov chain Monte Carlo (MCMC) for fatigue crack growth analysis based on data collected during experimental investigations. Their results showed the feasibility of updating the model parameters based on crack size measurements. Li *et al.* (2013) used Bayesian updating to study the effect of the sensor degradation on the estimation of the remaining useful life of structures. None of these performance updating studies was aimed to provide the optimal inspection schedule under uncertainty. Additionally, they don't directly support the decision making process since the management actions based on inspection outcomes are not provided. Thus, there still exists the need for integrated management plans that provide optimal intervention times and types while making use of the available inspection and monitoring information to improve the performance prediction process, and hence, better and effective decisions can be made.

In this chapter, a LCM framework for fatigue critical structures integrating inspection outcomes is proposed. A cost-based optimization approach is formulated to find the optimal inspection times while considering uncertainties associated with the damage propagation model and the damage detection technique. The optimization approach finds the optimal inspection time, which minimizes the life-cycle cost consisting of inspection and failure costs, for each of the considered inspection methods. Bayesian updating is used to find the posterior distributions of fatigue crack growth model parameters based on inspection results. The updated models are subsequently used to find the next inspection times based on the measured crack size. By analyzing the space of possible inspection outcomes, effective inspection plans can be achieved and rational real-time decisions regarding future inspection and/or rehabilitation actions can be made. The proposed framework is shown in Figure 6.1. Each of the modules in Figure 6.1 will be discussed in detail in the next sections of this chapter.

6.3 Fatigue Damage in Steel Structures (A brief Review)

In this chapter, the Paris equation (Paris & Erdogan 1963) will be used herein to predict the time-variant crack size. As previously indicated in Chapter 2 of this study, the time (years) associated with the crack growth from a size a_o to a_N can be calculated considering an annual average number of cycles N_{avg} as

$$t_a = \frac{1}{N_{avg} \cdot C \cdot S_{re}^m} \cdot \int_{a_o}^{a_N} \frac{da}{\left[Y(a)\sqrt{\pi \cdot a}\right]^m} \tag{6.1}$$

where a = crack size; N = number of cycles; and C and m = material parameters, S_{re} = stress range, and $Y(a)$ = geometry function.

The expected service life of a detail is calculated using Equation (6.1) by considering the crack size a_N to be equal to the critical crack size. The calculated service life using this model will be subsequently used to find the optimum inspection times for a detail.

6.4 Non-Destructive Fatigue Damage Inspection of Steel Bridges

Fatigue critical structures such as steel bridges, offshore structures and ships are inspected at regular or irregular time periods to spot any damage in the structure and apply the required maintenance actions. Recent research work shows that irregular inspection schedules are more cost-effective than regular inspection plans (Kwon & Frangopol 2011). These inspections are crucial to maintain the structural integrity. The probability of detection, which is defined as the probability of detecting an existing crack with a specific size using an inspection method (Chung *et al.* 2006), is generally used to represent the quality of the inspection method (Frangopol *et al.* 1997a,b; Zheng and Ellingwood 1998).

The first step in assessing a fatigue critical structure is to identify the most critical details to be inspected. Next, the most appropriate inspection type for each location should be selected. The selection of the inspection type depends on the defect type and geometry. Among the available nondestructive inspection techniques, the liquid penetrant inspection, ultrasonic inspection, eddy current inspection, magnetic particle inspection, and acoustic emission inspection are widely used for fatigue crack detection. Each of these methods has its advantages and disadvantages. For instance, the ultrasonic inspection type has a higher probability of detection for embedded cracks; however, it requires a high experienced inspector (Fisher *et al.* 1998).

6.5 Probability of Damage Detection

The quality of an inspection type can be generally expressed by the probability of detection of a given crack size. The relationship between the probability of detection and the crack size was investigated by Berens & Hovey (1981), Berens, (1989), and Frangopol *et al.* (1997b). In this chapter, the lognormal CDF is used to represent the probability of detection for different inspection types as a function of the crack size a. The probability of detection PoD is (Crawshaw & Chambers 1984)

$$PoD = 1 - \Phi\left(\frac{\ln(a) - \lambda}{\beta}\right) \tag{6.2}$$

where $\Phi(\cdot)$ = standard normal CDF, λ and β are, respectively, the location and scale parameters of the cumulative lognormal PoD curve. The parameters λ and β in Equation (6.2) are dependent on the quality of the inspection type.

6.6 Probability of Failure at a Critical Detail

In this chapter, the probability of failure is considered as the probability that the adopted inspection plan fails to detect an existing crack before reaching its critical size. This probability can be formulated using the event tree analyses, in which the probabilities of possible inspection outcomes can be evaluated. For a given number of inspections n, the probability of detecting the crack before failure PD can be formulated considering both the PoD and the probability that the inspection will be applied before the time to failure T. The formulation of PD is based on the event tree model shown in Figure 6.2 for a number of inspections n equal to one. PD is associated with Branch 2 in this event tree and is expressed as

$$PD = P\left(t_{insp_1} \le T\right) \cdot PoD(t_{insp_1}, \rho) \tag{6.3}$$

where T = time to failure of the detail, t_{insp_1} = time of application of the first inspection, $P\left(t_{insp_1} \le T\right)$ = probability that the first inspection is applied before the failure of the detail, and $PoD(t_{insp_1})$ = probability of crack detection at the first inspection. Similarly, the event tree model can be extended to find the probability of detecting the crack before failure for n inspections, which can be expressed as

$$PD = \sum_{j=1}^{n} \left(\prod_{i=1}^{j} \left[P(t_{insp,i} \le T) \cdot \overline{PoD}(t_{insp,i-1}) \right] \cdot PoD(t_{insp,i}) \right) \tag{6.4}$$

where $P(t_{insp,i} \le T)$ = probability that the ith inspection is performed before the time to failure of the detail T, $PoD(t_{insp,i})$ = probability of detecting the crack at the ith inspection, $\overline{PoD}(t_{insp,i-1})$ = probability of not detecting the crack at the $(i-1)$th inspection, and $\overline{PoD}(t_{insp,0}) = 1$ for the first inspection (i.e., i = 1). The probability of damage detection at a certain inspection is calculated as a function of the crack size using Equation (6.4). Accordingly, the probability of failure can be defined as

$$P_{fail} = 1 - PD \tag{6.5}$$

in which P_{fail} represents the probability that the inspection plan will fail to detect an existing crack before reaching its critical size. The probability P_{fail} is integrated in the proposed framework to find the optimum inspection times.

6.7 Expected Total Cost

The expected total cost includes the cost of inspection actions, expected maintenance cost and the expected failure cost (Mori & Ellingwood 1994). Since the proposed approach does not cover the selection of appropriate maintenance actions, the total cost will be considered as the inspection cost and the expected failure cost. The total inspection cost C_{insp}^{T} can be estimated as

$$C_{insp}^{T} = \sum_{i=1}^{n} \frac{C_{insp,i}}{(1+r)^{t_{insp,i}}} \tag{6.6}$$

in which n = number of inspections, $t_{insp,i}$ = application time of the ith inspection, r = annual discount rate of money, and $C_{insp,i}$ = the cost of performing the ith inspection. The cost $C_{insp,i}$ depends on many aspects such as the inspection quality, the location of the inspected detail within the structure, and the time required to perform the inspection, among others.

The failure cost is the cost associated with monetary losses arising from the failure of detecting the damage before reaching the critical state and the consequences of such failure. The expected failure cost is expressed as (Frangopol *et al.* 1997b)

$$E(C_{\text{fail}}) = P_{fail} \cdot C_{\text{fail}} \tag{6.7}$$

where P_{fail} = probability of failure calculated using Equation (6.5) and C_{fail} = monetary losses as a result of the crack reaching it critical size. Accordingly, the total expected cost can be found as

$$E(C_{total}) = C_{insp}^{T} + E(C_{fail}) \tag{6.8}$$

6.8 Integrated Life-cycle Management Framework

Inspection outcomes provide new information which can be effectively integrated into the management framework to update damage evolution prediction models. In this chapter, the new information is considered as the crack size measured during an inspection action. Based on the inspection outcome, a likelihood function is built and combined with the prior knowledge of the model parameters to provide the posterior distributions of the crack growth model parameters. These posterior distributions are used to find an updated crack growth profile. These steps can be performed many times during the lifetime of the structure, where the previous knowledge, as well as the current inspection outcomes, can be incorporated to find the future crack growth. However, in this chapter, this process will be performed before implementing the inspection plan. Possible inspection outcomes will be evaluated and integrated into the management plan such that effective actions can be taken. Having the results of this framework ready beforehand allows for immediate decision making based on the inspection results. The detailed flowchart of the proposed framework is given in Figure 6.3. As shown, the LCM framework starts with an input of the deterioration model parameters. These parameters include material properties and loading conditions. Needless to say, available SHM data can improve the quality of management process, especially for evaluating the loading conditions at the studied location (Frangopol 2011). Inputs also include the damage thresholds, inspection type parameters, and the cost data.

Next, the damage evolution profile with time is constructed. In this chapter, Monte Carlo simulation is used to find the crack growth profiles. Based on these profiles, the optimum inspection times which yield the minimum total cost are found. The PDF of the predicted crack size at the time of inspection is then evaluated using the simulation

results and a set of inspection outcome possibilities are defined. The updating process is performed based on the defined inspection outcomes and posterior distributions of model parameters are used to find the updated damage propagation profiles. Crack size thresholds are defined for selecting the appropriate management actions based on inspection outcomes. In this chapter, management actions are built upon crack size thresholds as follows: (a) perform future inspection for $a_I \leq a_{insp,i} \leq a_{II}$, (b) perform immediate repair and re-assessment for $a_{insp,i} \geq a_{II}$, and (c) perform re-assessment for $a_{insp,i} \leq a_I$, where $a_{insp,i}$ is the crack size measured at the ith inspection, and a_I , a_{II} are the crack size thresholds for determining the appropriate management actions considering the difference between the crack size measured during inspection and the one predicted at the time of inspection. The allowable difference can be determined depending on the importance of the damaged detail within the structure. A detail with high importance would require an increased damage prediction accuracy and, in turn, a smaller allowable difference between the measured and the predicted crack sizes; thus, closer thresholds. In this chapter, these thresholds are determined in terms of the descriptors of the PDF of the predicted crack size at the time of inspection. The result of this process is an interactive management plan which gives the manager a deeper insight into the safety level and the remaining service life according to the crack size measured at a certain inspection.

6.9 Bayesian Updating of Model Parameters

The Bayesian approach is employed herein to update the crack growth model parameters. This process reduces the uncertainties in the model parameters and leads to a more accurate damage prediction process. The prior knowledge about the model parameters

can be combined with the new information resulting from inspection actions to yield the posterior distribution of model parameters as

$$P(\boldsymbol{\theta}\,|\,\mathbf{d}) = \frac{P(\boldsymbol{\theta})\cdot P(\mathbf{d}\,|\,\boldsymbol{\theta})}{\int P(\boldsymbol{\theta})\cdot P(\mathbf{d}\,|\,\boldsymbol{\theta})d\boldsymbol{\theta}} \tag{6.9}$$

where $P(\boldsymbol{\theta}\,|\,\mathbf{d})$ = posterior distribution of model parameters $\boldsymbol{\theta}$ given additional information $\mathbf{d}$; $P(\boldsymbol{\theta})$ = prior distribution of model parameters; $P(\mathbf{d}\,|\,\boldsymbol{\theta})$ = likelihood function of obtaining information $\mathbf{d}$ conditioned by $\boldsymbol{\theta}$; $\mathbf{d}$ and $\boldsymbol{\theta}$ are the vectors of observed data and model parameters, respectively. In this case, the vector of observed data contains crack sizes obtained during inspections as

$$\mathbf{d} = \{a_{insp,1}\ ,\ a_{insp,2}\ ,\ .....,\ a_{insp,n}\ \} \tag{6.10}$$

where $a_{insp,i}$ = measured crack size at the ith inspection and n = number of inspections. In Equation (6.9), $\int P(\boldsymbol{\theta})\cdot P(\mathbf{d}\,|\,\boldsymbol{\theta})d\boldsymbol{\theta}$ represents a normalizing constant which can be dropped (Martinez & Martinez 2002) leading to

$$P(\boldsymbol{\theta}\,|\,\mathbf{d}) \propto P(\boldsymbol{\theta})\cdot P(\mathbf{d}\,|\,\boldsymbol{\theta}) \tag{6.11}$$

The prior distributions of the crack growth model parameters can be found based on the material properties. In this study, the distributions of the material crack growth parameters m, C, and the initial crack size a_o are updated using the discussed approach. The likelihood function of obtaining field measurements d given the model parameters θ can be expressed as (Perrin *et al.* 2007)

$$P(\mathbf{d}\,|\,\boldsymbol{\theta}) = \prod_{i=1}^{n}\left[\frac{1}{\sqrt{2\pi}\cdot\sigma_e}\cdot\exp\left(-\frac{1}{2}\left(\frac{d_i - a_{p,i}}{\sigma_e}\right)^2\right)\right] \tag{6.12}$$

where d_i and $a_{p,i}$ are the observed and predicted data, respectively, at the ith inspection; σ_e represents a single error term combining the measurement and modeling errors which is

assumed to follow a normal distribution with zero mean and a standard deviation σ_e (i.e., $N(0, \sigma_e)$).

By knowing the likelihood function and the prior distribution of the model parameters, the posterior distribution of the model parameters can be found by using Markov chain Monte Carlo simulation. The Metropolis algorithm (Metropolis *et al.* 1953) is employed herein to draw samples from the posterior distribution when the chain has converged. Those samples can be used as an approximation to the target posterior distribution.

6.10 Metropolis Algorithm

The Metropolis method (Metropolis *et al*. 1953) used in this study is a special case of the Metropolis-Hasting algorithm (Hasting 1970). The algorithm obtains the state of a chain $\boldsymbol{\theta}_{t+1}$ by sampling a candidate vector $\boldsymbol{\theta}^*$ from a proposal distribution $q(\boldsymbol{\theta}^* \mid \boldsymbol{\theta}_t)$ depending only on the previous state of the chain $\boldsymbol{\theta}_t$. The proposal distribution for the Metropolis method is symmetric, in which the candidate vector is accepted as the next state of the chain with probability

$$\alpha(\boldsymbol{\theta}_t, \boldsymbol{\theta}^*) = \min\left\{1, \frac{P(\boldsymbol{\theta}^* \mid \mathbf{d})\ q(\boldsymbol{\theta}_t \mid \boldsymbol{\theta}^*)}{P(\boldsymbol{\theta}_t \mid \mathbf{d})\ q(\boldsymbol{\theta}^* \mid \boldsymbol{\theta}_t)}\right\} \tag{6.13}$$

where the proposal distribution cancel out due to symmetry (i.e., $q(\boldsymbol{\theta}_t \mid \boldsymbol{\theta}^*) = q(\boldsymbol{\theta}^* \mid \boldsymbol{\theta}_t)$). The random generation here adopts a random walk algorithm, in which $\boldsymbol{\theta}_{t+1} = \boldsymbol{\theta}_t + \zeta$, where ζ is a Gaussian noise parameter.

Thus the acceptance probability is

$$\alpha(\boldsymbol{\theta}_t, \boldsymbol{\theta}^*) = \min\left\{1, \frac{P(\boldsymbol{\theta}^*) \cdot P(\mathbf{d} \mid \boldsymbol{\theta}^*)}{P(\boldsymbol{\theta}_t) \cdot P(\mathbf{d} \mid \boldsymbol{\theta}_t)}\right\} \tag{6.14}$$

The flowchart of the adopted algorithm is shown in Figure 6.4. Since the first n_b sample may not represent the posterior distribution, the convergence of the chain has to be monitored (Gelman 1996). Convergence monitoring determines when the chain is considered safe to represent the target posterior distribution. In this chapter, a method proposed by Gelman (1996) is used, in which, multiple parallel chains are used with different starting points and the convergence to the target distribution is evaluated by calculating the estimated potential scale reduction factor $\hat{R}$. This factor, given by the ratio of the overall variance $\hat{\text{var}}(\nu)$ to the within-sequence variance W, is expressed as

$$\hat{R} = \frac{\hat{\text{var}}(\nu)}{W} \tag{6.15}$$

where υ is the scalar summary of interest (such as the mean value and standard deviation of the underlying random variables). It is sufficient to run the sequence until a value of 1.1 or 1.2 for $\hat{R}$ is reached (Gelman 1996). However, for multivariate chains, higher values of $\hat{R}$ can be used (Brooks & Gelman 1998). In this study, two parallel chains are used to sample from the posterior distribution and the convergence is considered to occur when the value of $\hat{R}$ for all the scalar summaries drops below 1.2. Hence, the first n_b samples generated before convergence, corresponding to the burn-in period, are discarded.

6.11 Example 6.1

The proposed management plan is illustrated on a steel ship side shell detail subjected to fatigue. The side shell structure is known to have multiple fatigue critical locations that

need to be inspected frequently (Ma *et al.* 1999). At these locations, the stress cycles are caused by the fluctuating hydrodynamic pressures as well as the pressure induced by waves. Another possible critical location is the intersection of bottom longitudinal stiffeners with transverse web frames (Glen *et al.* 1999b). At this location, the fluctuating stresses are mainly caused by the hull girder bending. The critical location considered in this example and shown in Figure 6.5 is the joint between the side shell plating and the longitudinal stiffener. In this example, the initial crack size a_o is assumed to follow a normal distribution with mean of 0.5 mm and a COV = 0.1. The material crack growth coefficient C is considered to follow a lognormal distribution with mean = 2.3×10^{-12} (British Standards Institution 2005), using units of mm/cycle for crack growth rate and $\mathrm{N/mm^{3/2}}$ for the stress intensity factor range, and a COV = 0.3 while the parameter m is assumed to follow a normal distribution with mean = 3.0 and a COV = 0.1. The correlation coefficient between the natural logarithm of the parameter C (i.e., $ln(C)$) and m is considered to be -0.9 (Cremona 1996). The stress range S_{re} is considered as a random variable following a Weibull distribution and the geometry function $Y(a)$ is considered to be constant = 1.12 (Guedes Soares & Garbatov 1999b). The critical crack size is assumed herein to be 50 mm. Descriptors of different parameters adopted for the crack size prediction are given in Table 6.1.

Based on Equations (6.1), Monte Carlo simulation is performed with 100,000 samples to find the time required to reach the critical crack size. Figure 6.6 shows the results of the Monte Carlo simulation, in which the mean and the standard deviation of the time required to reach different crack sizes are provided with the PDF of the time to reach a crack size of 10, 20, 30, 40 mm, and the critical crack size of 50 mm. As shown

in Figure 6.6, the mean value of the time to failure T (i.e., time to reach the critical crack size) is 22.7 years and the standard deviation is 10.81 years. The number of samples for the Monte Carlo simulation is selected based on the extensive convergence analyses where the simulation results were found to stabilize before the selected number of simulations. A sample of the convergence analyses is shown in Figure 6.7.

6.11.1 Optimum inspection times

The scheduling to find optimum inspection times is formulated as an optimization problem with the objective of minimizing the expected total cost $E(C_{total})$ as follows

$$\text{Find } t_{insp,1},\ t_{insp,2},\ t_{insp,3},\ldots,\ t_{insp,n} \tag{6.16}$$

$$\text{To minimize } E(C_{total}) \tag{6.17}$$

$$\text{Such that } t_{insp,i} - t_{insp,i-1} \geq 1.0 \text{ year} \tag{6.18}$$

$$\text{Given } n,\ \boldsymbol{\Psi},\ C_{fail},\ \mathbf{C}_{insp},\ r \text{ and the PDF of } T \tag{6.19}$$

where $t_{insp,i}$ = ith inspection time; $E(C_{total})$ = expected total cost as given by Equation (6.8); n = number of inspections; $\boldsymbol{\Psi}$ = matrix consisting of the *PoD* parameters λ and β for different available inspection types; $\mathbf{C}_{insp}$ = vector consisting of the cost of performing a single inspection using each of the available inspection types; C_{fail} = expected monetary losses as a result of the crack reaching it critical size without being detected by inspection; r = annual discount rate of money assumed to be 2%. The PDF of the time to failure T is obtained from the results of the Monte Carlo simulation process. As shown by Equation (6.18), the minimum time interval between consecutive inspection actions is set to be 1.0 year.

For this example, three inspection types are considered, namely, the eddy current inspection (ECI), the ultrasonic inspection (UI), and the liquid penetrant inspection (LPI).

Relative inspection costs for the three respective inspection types and the cost of failure, $C_{insp,ECI}$:$C_{insp,UI}$:$C_{insp,LPI}$:C_{fail}, are considered to be $5.0{:}4.0{:}3.0{:}1\times10^{3}$. The *PoD* parameters λ and β for each of the inspection types are shown in Table 6.2. These adopted *PoD* parameters are deduced based on inspection practices of the aerospace industry (Forsyth & Fahr 1998) and are used here for illustrative purposes. This optimization problem is solved using the optimization toolbox provided in MATLAB® version R2011a (MathWorks Inc. 2011b). In this manner, the optimum inspection times for a given inspection type are found.

Figure 6.8 shows the optimum inspection schedule for one (i.e., Schedules A, B, and C) and two scheduled inspections (i.e., Schedules D, E, and F) with inspection types of different qualities defined by the factors λ and β. For the case of two inspections, the shown times of the second scheduled inspections are independent of the results of the previous inspection (i.e., updating process is not utilized). As shown in Figure 6.8, the one scheduled inspection should be performed after 9.09, 12.38, and 14.95 years of service for ECI, UI, and LPI, respectively. For the case of two scheduled inspections, the first inspection is planned to be performed at 6.92, 10.3, and 12.72 years for the three respective inspection types. At the first inspection associated with Schedules D, E, and F, the mean predicted crack sizes are found by the Monte Carlo simulation to be 1.04 mm, 1.92 mm, and 2.95 mm, respectively. Optimum inspection schedules and their associated objective function values are given in Table 6.2.

6.11.2 Updated inspection schedules and damage evolution profiles

Based on the outcomes of the first scheduled inspection, the model parameters, and accordingly, the crack growth profiles are updated. Considering inspection Schedule D,

which has the highest quality of inspection, the first inspection is scheduled after 6.92 years in service. At this time, the mean of the predicted crack size $E(a_p(t_{insp,1}))$ is found to be 1.04 mm. Accordingly, the crack size threshold for re-assessment a_I is considered $0.5 \cdot E(a_p(t_{insp,1}))$, while the threshold a_{II} for repair and re-assessment of the inspected location is taken as $1.5 \cdot E(a_p(t_{insp,1}))$, yielding approximately 0.5 mm and 1.5 mm for a_I and a_{II}, respectively. For a measured crack size significantly smaller than the predicted one, a re-assessment is recommended to find the reason behind the large difference between the results. This re-assessment may result in finding different loading conditions in terms of the stress ranges or the number of loading cycles acting on the detail. Moreover, it may indicate different crack conditions (e.g., crack geometry or orientation) than those used in the prediction process. On the other hand, for crack sizes larger than a_{II}, repair and re-assessment would be recommended to maintain the safety of the structure against sudden failures that may occur due to the unstable growth of the existing crack.

The updating process for the studied range is performed using Equation (6.9) and the Metropolis algorithm discussed earlier in this chapter. The three crack growth parameters a_o, m, and C are updated in this procedure where the parameter σ_e is assumed 0.2mm (Perrin *et al*. 2007). Figure 6.9 shows the prior and posterior distributions of the three updated parameters for selected measured crack sizes at the time of the first scheduled inspection (i.e., 6.92 years). Two parallel chains are used simultaneously to monitor the convergence of the simulation process and the first n_b samples corresponding to the burn-in period are neglected. Figure 6.10 shows the evolution of the $\hat{R}$ values for different descriptors of the updated random variables. As a further check of the sampling

convergence, the slice sampling technique (Neal 2003) was also used and it was found to provide matching results to those obtained by the Metropolis algorithm. For the slice sampling, the MATLAB® R2011a statistical tool box (MathWorks Inc. 2011c) built-in sampling function was used to sample from the posterior distribution of the parameters. This algorithm, in its simplest form, draws the samples by selecting a horizontal slice at a vertical level drawn uniformly from the region under the function. The next sample which lies under the function is drawn uniformly from this horizontal slice (Neal 2003). The slice sampling technique does not require the definition of a proposal function which makes it favorable in many cases where the proposal function is difficult to obtain. Based on the posterior crack growth parameters resulting from the Metropolis algorithm, updated damage evolution profiles are obtained.

Figure 6.11 (a) shows the updated profiles of the mean time required to reach different crack sizes and Figure 6.11 (b) shows the updated PDFs of the time to failure for different crack sizes detected at the first inspection. The same updating approach is applied to inspection schedules E and F where the UI and LPI are respectively used. For the UI, the first inspection is scheduled after 10.3 years of service and the thresholds a_I and a_{II} are considered 1.0 mm and 3.0 mm, respectively. The mean of the updated crack growth profiles for this case are shown in Figure 6.12 (a) while the updated PDFs of the time to failure for different detected crack sizes are shown in Figure 6.12 (b). Similarly, Figures 6.13 (a) and 6.13 (b) shows updated crack growth profiles and the updated PDFs of the fatigue service life, respectively, for the LPI performed at 12.72 years of service life. Figures 6.14 (a)-(c) show, for the three inspection strategies, the descriptors (i.e., mean and standard deviation) of the remaining fatigue life for different measured crack

sizes at the first inspection along with the PDF of the remaining fatigue life for selected outcomes of the first inspection.

The next step is to find the optimum time of the second inspection based on the second inspection type and the outcomes of the first inspection. This is performed using the optimization approach given by Equations (6.16) – (6.19) for one scheduled inspection (i.e., n = 1). For the ECI performed at 6.92 years, optimum times for second inspection using the eddy current technique are given in Figure 6.15 (a) for different first inspection outcomes. Additionally, the inspection time resulting from the optimization process without updating (i.e., $t_{insp,2}$ = 9.9 years) is plotted. As shown in the figure, inspection times are significantly affected by the previous inspection outcomes. The approach can also consider scheduling the second inspection with different inspection type. Combining inspection types in a management plan where higher quality inspections are performed early in the life and lower quality inspections performed later can be effective since inspection types with lower quality will have acceptable ability to detect the damage when performed later in life (i.e., with higher damage levels). Accordingly, times for the second inspection using the ultrasonic and liquid penetrant techniques are calculated and shown in Figure 6.15 (a). Figures 6.15 (b) and 6.15 (c) show the times for performing UI and LPI, respectively, in both the first and second inspection. Updated second inspection times for different types of inspection are given in Table 6.3 along with the predicted parameters of the remaining fatigue life after the first inspection.

The procedure can also be used to find the remaining fatigue life after n inspections with specified outcomes. Figure 6.16 shows the remaining fatigue life after the second inspection based on the crack size measured during the first and second

inspection. For this process, the Metropolis algorithm uses the likelihood function with a number of inspections $n = 2$ where the second inspection outcome is chosen to cover a range of $a_{insp,1}$ + 0.5 mm up to 5.0 mm. Similar profiles covering different inspection types and outcomes after the second inspection can be plotted. This information about the remaining fatigue life along with the required safety levels and the available budgets can help the decision maker to effectively plan for the future repair actions.

6.12 Example 6.2

In this example, a fatigue critical bridge detail is analyzed. However, instead of using the crack size and the *PoD* for planning interventions, lifetime functions (see Section 2.2.2) are used to plan for threshold-based interventions. The approach is illustrated on a fatigue critical detail in the I-64 Bridge over the Kanawha River at Dunbar in West Virginia (currently carries westbound traffic). This study is only concerned with one of the plate girder spans crossing the Kanawha River; namely Span 9. The bridge was open for traffic in 1974 and was retrofitted in 1989 due to the presence of several fatigue cracks. The retrofitting included drilling holes at crack tips and installing retrofitting angles at various fatigue prone locations (Connor & Fisher 2001). In 2000, several locations of the bridge were monitored and analyzed by personnel from Lehigh University's Engineering Research Center for Advanced Technology for Large Structural Systems (ATLSS). The purposes of this monitoring program were (a) characterizing the potential for subsequent cracking; (b) evaluating the effectiveness of the existing retrofits; and (c) providing recommendations for any further retrofits. The monitoring of the bridge in 2000 revealed that the bridge has multiple types of fatigue critical details. It was found that some of the retrofitted locations experienced stresses high enough to cause crack propagation (Connor

& Fisher 2001). Recommendations were made for fixing the retrofitted details by adding heavier angles. However, some other critical details were found in which the monitoring shows a potential for fatigue cracking (Connor & Fisher 2001). Among those details, a bottom web gap detail located at the termination of the transverse connecting plate of the exterior girders is analyzed in this example. The detail is shown in Figure 6.17 along with a general plan view of the bridge.

At this detail, the bracing gusset plate is welded to both the transverse connecting plate and the girder web; however, the transverse connecting plate is not connected to the tension flange, leaving a small web gap above the tension flange which may be subjected to fatigue cracking due to the out-of-plane displacement. This detail is known for its poor fatigue behavior (Fisher *et al*. 1990).

The crack growth of the detail is assessed based on Monte Carlo simulation integrating Equation (6.1) and using 100,000 samples. This simulation process yields the PDF of the time to failure as an outcome. For this detail, the crack growth parameter C is assumed to follow a lognormal distribution with a mean 2.18×10^{-13} using units of *mm* for crack size a and *MPa* for stress range S_{re} (Barsom & Rolfe 1999). The COV of C is assumed to be 0.2. The parameter m is assumed to follow a normal distribution with mean 3.0 and COV = 0.1. The correlation coefficient between the natural logarithm of the parameter C (i.e., $ln(C)$) and m is considered -0.9 (Cremona 1996). The stress range and the average number of cycles are estimated based on the results of the long-term monitoring of the detail performed by ATLSS Center in 2000. As reported in Connor & Fisher (2001), the stress range acting on the detail is 34.45 *MPa*. This number is considered herein as the mean value of the stress range distribution with COV = 0.1

(Ayyub *et al*. 2002). The average number of cycles per day was found to be 7,500 (Connor & Fisher 2001). This number is considered herein as the mean value of the distribution of the number of cycles where the COV is considered 0.1 (Moses *et al*. 1987). The different parameters of the crack growth model are provided in Table 6.4. The cracking in this detail can be treated as a semi-elliptical edge crack of depth *a* (Fisher 1984). The range of the stress intensity factor ΔK (see Equation (2.21)) can be found in terms of the function *Y*(*a*), which is expresses as

$$Y(a) = F_e \cdot F_s \cdot F_w \cdot F_g \tag{6.20}$$

in which F_e, F_s, F_w and F_g are correction factors taking into account the effects of the elliptical crack shape, free surface, finite width (or thickness), and non-uniform stress acting on the crack, respectively. Therefore, ΔK is expressed as (Fisher 1984)

$$\Delta K = \left[\frac{0.923 + 0.199\left(1 - \sin\left(\frac{\pi a}{2t_w}\right)\right)^4}{\cos\left(\frac{\pi a}{2t_w}\right)} \right] \cdot F_e \cdot F_s \cdot F_w \cdot F_g \cdot S_{re} \cdot \sqrt{\pi a} \tag{6.21}$$

$$F_e = \frac{1}{E(k)} \tag{6.22}$$

$$E(k) = \frac{3\pi}{8} + \frac{\pi}{8}\left(\frac{a}{c}\right)^2 = \frac{\pi}{2} \quad for\ c \simeq a \tag{6.23}$$

$$F_s = 1.21 - 0.186\sqrt{\frac{a}{c}} = 1.025 \tag{6.24}$$

$$F_w = \left[\frac{2t_w}{\pi a} \tan\left(\frac{\pi a}{2t_w}\right) \right]^{\frac{1}{2}} \tag{6.25}$$

$$F_g = \frac{K_{tm}}{1 + 2.776\left(\frac{a}{t_w}\right)^{0.2487}} \tag{6.26}$$

$$K_{tm} = 1.621 \cdot \ln\left(\frac{Z}{t_w}\right) + 3.963 \tag{6.27}$$

where $E(k)$ is the complete elliptical integral of the second kind, c is the surface half-length of a surface crack, t_w is the web thickness, Z is the weld leg size, and K_{tm} is the maximum stress concentration factor at the weld toe. The free surface correction factor F_s, applied for this crack, is employed for a semicircular crack in a semi-infinite plate subjected to uniform stress. The factor F_w accounts for finite thickness of the web plate, while the shape correction factor F_e considers the three-dimensional elliptical crack shape. Finally, the correction factor F_g accounts for the stress gradient (i.e., non-uniform stress) acting on the crack (Fisher 1984).

Based on the parameters given in Table 6.4, and the Monte Carlo simulation process, the time-dependent crack size can be found as shown in Figure 6.18. Additionally, the mean and standard deviation of time t associated with crack length a_t, and PDFs of time for a_t = 2, 4, and 6*mm* are shown in Figure 6.18. Based on the Monte Carlo simulation process, the PDF of the time associated with reaching various crack sizes can be found. Setting the final crack size to the critical one provides the PDF of the time to failure of the detail. For this case, the PDF of the time to failure (i.e., time to reach a crack size of 10.16*mm*) is shown in Figure 6.19 (a). As shown, the mean time to failure of this detail is 16.81 years with a standard deviation of 8.43 years. Next, the cumulative probability of failure of the detail (i.e., $F_T(t)$) and its survivor function (i.e.,

$S_T(t)$) are obtained using Equations (2.9) and (2.10), respectively. Figure 6.19 (b) shows the survivor function of the detail and its associated cumulative probability of failure.

Inspection actions are next planned based on the established lifetime performance profile. These inspections are threshold-based, in which inspection actions are scheduled when the performance indicator reaches a predefined threshold. The inspections are scheduled to monitor the performance of the detail at certain points along its service life. Accordingly, maintenance decisions can be made if the inspection revealed that the performance is below the maintenance threshold for the detail. For this example, inspection thresholds are established such that the first inspection is performed when the cumulative probability of failure reaches 10^{-2}, whereas the second inspection is planned when the cumulative probability of failure reaches 0.15. This means that the second inspection is performed when there is 85% chance that the detail will have longer fatigue life. Needless to say, the selection of these thresholds depends mainly on the importance of the detail, its location within the bridge, and the structural redundancy. For the studied detail, and based on the original lifetime-performance profile, the first and second inspections should be applied, as shown in Figure 6.19 (b), at 6.7 years and 10.3 years, respectively.

Based on the crack size measurements collected during inspections, the fatigue crack growth model parameters can be updated. Accordingly, the crack growth profile and the PDF of the time to failure would be updated. Two cases are considered herein in which the inspection at 6.7 years is considered to reveal a crack size of 3.0*mm*, or a size of 1.5*mm*. Using Equation (6.12) as the likelihood function, the slice sampling technique is employed to draw samples from the posterior distributions of the model parameters

based on Equation (6.9). This process yields the updated distributions of the model parameters. Figure 6.20 (a) shows the prior distribution of the crack growth parameter C and its posterior distributions for the case of measured crack sizes of 3.0mm and 1.5mm. Similar plots can be generated for the PDF of the parameter m and the initial crack size a_o. Posterior crack growth model parameters are used again in the simulation process yielding an updated crack growth profile and PDF of time to failure. Figure 6.20 (b) shows the prior and updated profiles of the mean time to reach different crack sizes. Figure 6.21 shows the prior and posterior PDFs of the time to failure. As shown, for the first case, in which a crack of size 3.0mm is detected, the mean time to failure is reduced to 12.41 years with a standard deviation of 5.59 years. The second case, in which a crack of size 1.5mm is detected, results in a mean time to failure of 22.08 years with a standard deviation of 10.18 years.

The updated PDFs of time to failure are used next to find the lifetime reliability measures. Figure 6.22 shows the survivor function for both cases of crack size measured during first inspection (i.e., 3.0mm and 1.5mm). As shown, the updated profile may be significantly different from the prior one. Additionally, based on the updated profiles, the second inspection time may be influenced. For this example, the second inspection for the first and second cases should be performed at 8.6 and 14.5 years, respectively. These inspection times are different from the prior inspection time of 10.2 years. Based on the second inspection outcome, updated PDF of time to failure and survivor function can be also found. Thus, by updating the model parameters, an updated damage propagation profile is established. This profile gives more accurate information on the remaining

fatigue life as well as the reliability of the detail, allowing proper maintenance and management decisions to be made.

6.13 Conclusions

This chapter presents a probabilistic approach to find a comprehensive management plan for fatigue sensitive structures. This plan gives the time of the first inspection, and based on the inspection outcome and the predicted crack size, appropriate management actions are specified. These actions include re-assessment of the detail, propose a time for the second inspection action, or perform repair. The proposed approach uses Markov chain Monte Carlo method applied through the Metropolis algorithm to find the updated crack growth parameters after each inspection. Three parameters, namely, the initial crack size a_o, and material constants m and C are updated after each inspection. The posterior parameters are used next to find the updated time to failure and the next inspection times that fulfill the optimization goals. The approach is automated in a MATLAB environment and is found to be computationally feasible using parallel processing. The computational time is significantly affected by the sampling method adopted for updating the model parameters. Other factors such as the geometry and type of the fatigue crack and the optimization technique will also affect the computational effort. Convergence is monitored through the updating process by running multiple parallel chains and checking the variance within the chain and the overall variance. The result of this process is a comprehensive life-cycle inspection plan that can be directly implemented for the

structure and gives the manager the ability to make real-time decisions based on the inspection outcomes. The following conclusions are drawn:

1. The updating process significantly affects the performance estimation and it is crucial for the successful LCM process.
2. Using the proposed framework, management plans allowing for real-time decisions based on future inspection outcomes are possible to be developed. The outcomes of such plans are the next inspection times and the damage level-based thresholds for re-assessment and repair decisions.
3. The proposed LCM framework is general and can cover additional types of time-dependent deteriorating mechanisms such as corrosion and corrosion-induced fatigue.
4. Lifetime reliability measures such as the survivor function and the cumulative probability of failure can be effectively integrated into the LCM to assist the decision making process regarding future inspection and maintenance actions.
5. Different optimization techniques for inspection scheduling can be included in this framework according to the management needs. These goals may include extending the service life as an objective; however, care should be taken in selecting the optimization technique as it may significantly affect the computational effort.

Table 6.1 Random variables for crack-growth prediction associated with the detail analyzed in Example 6.1

Random variable	Notation (units)	Mean	Coefficient of variation	Distribution type
Initial Crack size	a_o (mm)	0.5	0.1	Normal
Material crack growth parameters	m	3.0	0.1	Normal
	C	2.3×10^{-12}	0.3	Lognormal
Stress range	S_{re} (MPa)	22.5	0.1	Weibull
Annual number of cycles	N_{av} (cycles/year)	1.0×10^{6}	0.1	Lognormal

[redacted]

Number of Inspections	Inspection schedule	Inspection method	PoD parameters (Forsyth and Fahr 1998)		Relative cost	Inspection times (years)		Objective value
			λ	β	$C_{insp} : C_{fail}$	$t_{insp,1}$	$t_{insp,2}$	$E(C_{total})$
$n = 1$	A	ECI	-0.968	-0.571	$5.0 : 1 \times 10^3$	9.09	-	35.16
	B	UI	0.122	-0.305	$4.0 : 1 \times 10^3$	12.38	-	195.19
	C	LPI	0.829	-0.423	$3.0 : 1 \times 10^3$	14.95	-	412.02
$n = 2$	D	ECI	-0.968	-0.571	$5.0 : 1 \times 10^3$	6.92	9.9	11.84
	E	UI	0.122	-0.305	$4.0 : 1 \times 10^3$	10.3	14.77	110.48
	F	LPI	0.829	-0.423	$3.0 : 1 \times 10^3$	12.72	17.9	310.45

[redacted]

Inspection type	First inspection time $t_{insp,1}$ (years)	Mean of predicted crack size at first inspection $a_p(t_{insp,1})$ (mm)	Measured crack size at first inspection $a_{insp,1}$ (mm)	Mean of remaining fatigue life (years)	St. dev. of remaining fatigue life (years)	Time interval between inspections $t_{insp,2}$ - $t_{insp,1}$ (years)	Second inspection time $t_{insp,2}$ (years)
Eddy current	6.92	1.04	0.5	26.48	12.63	10.66	17.58
			1.0	15.94	7.55	5.14	12.06
			1.5	10.19	4.95	3.05	9.97
Ultrasonic	10.30	1.92	1.0	18.98	8.73	8.15	18.45
			1.5	13.00	5.99	4.67	14.97
			2.0	9.38	4.31	3.30	13.3
			2.5	7.29	3.42	2.19	12.49
			3.0	5.89	2.76	1.89	12.19
Liquid penetrant	12.72	2.95	1.5	15.43	9.59	8.08	20.8
			2.0	11.24	5.09	5.32	18.04
			2.5	8.73	3.97	3.92	16.64
			3.0	7.35	3.34	3.11	15.83
			3.5	6.22	2.92	2.51	15.22
			4.0	5.37	2.60	2.09	14.81
			4.5	4.87	2.31	1.89	14.61

Table 6.4 Values of different random variables and deterministic parameters associated with the crack growth model for the detail in Example 6.2

Variable	Notation (Units)	Mean value	Coefficient of Variation	Type of distribution
Material crack growth parameter [a]	C	2.18×10^{-13}	0.2	Lognormal
Material crack growth exponent [a]	m	3.0	0.1	Normal
Initial crack size [b]	a_o (mm)	1.27	0.2	Lognormal
Daily number of cycles [c]	N_{avg} $(cycles/day)$	7500×365	0.1	Lognormal
Stress range [c]	S_{re} (MPa)	34.45	0.1	Weibull
Critical crack size	a_f (mm)	10.16	-	Deterministic

Data from: [a] Barsom & Rolfe (1999); [b] Fisher (1984); [c] Connor & Fisher (2001)

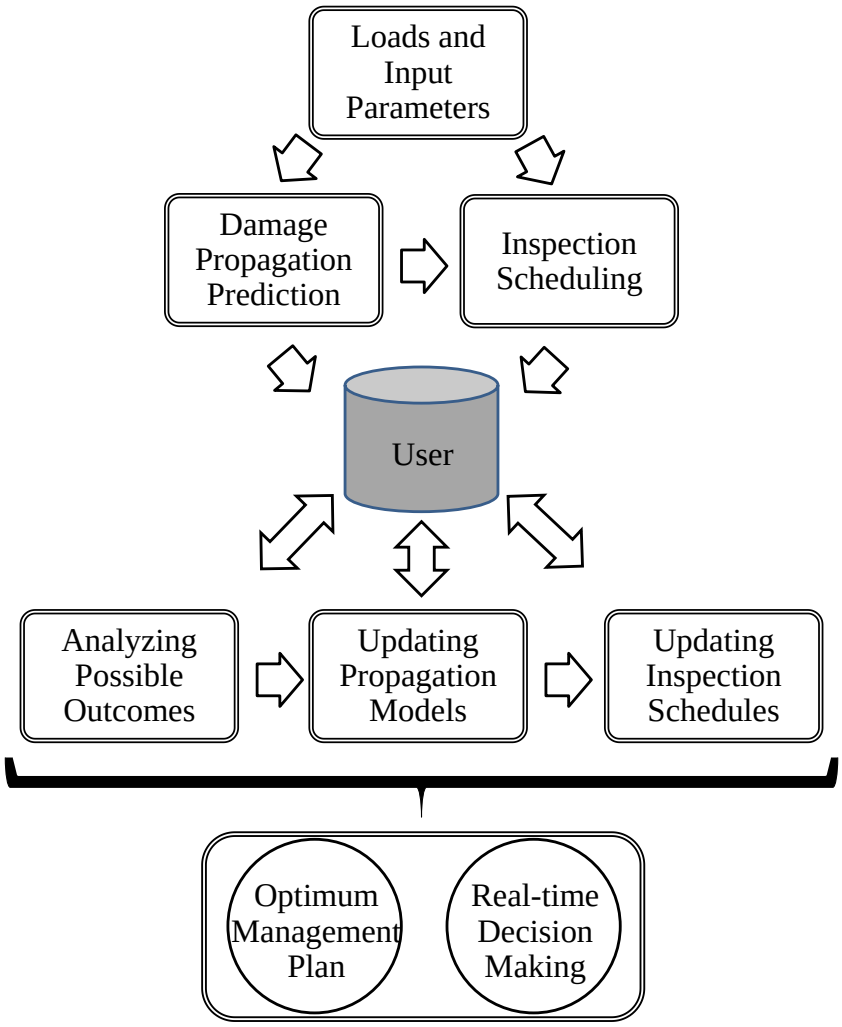

Figure 6.1 Schematic for the proposed management framework

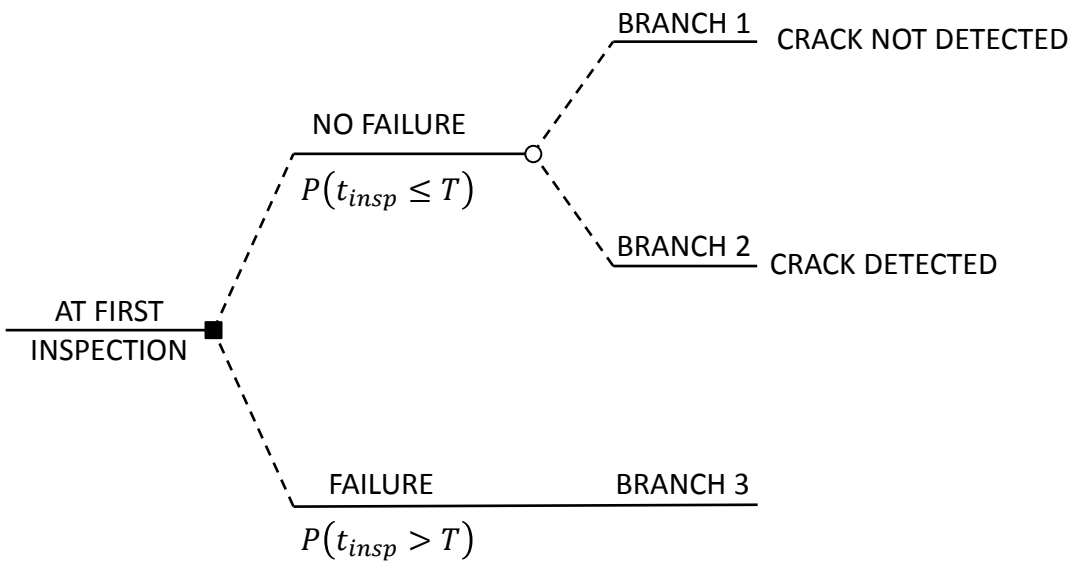

Figure 6.2 Event tree for one inspection at a given detail

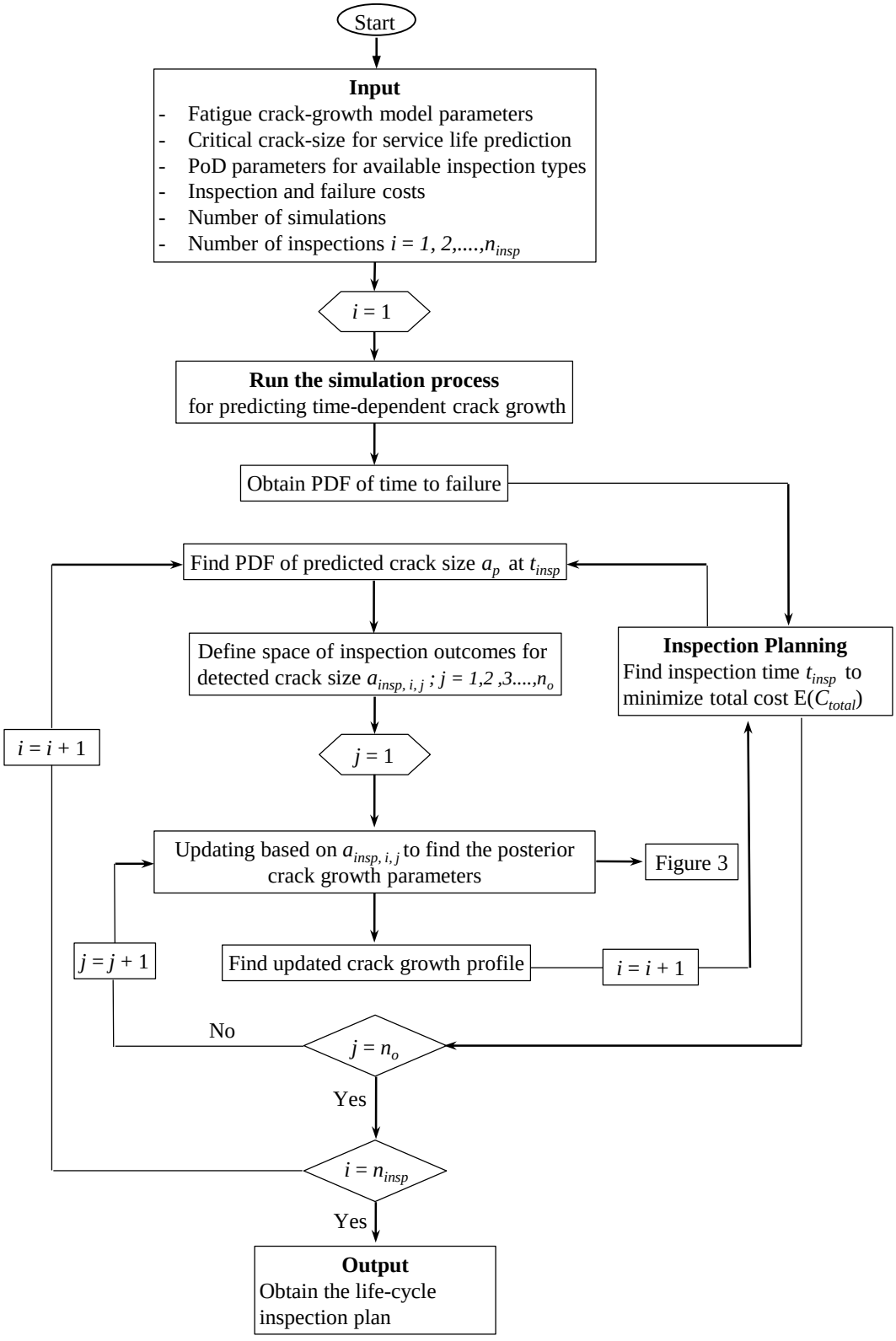

Figure 6.3 Flowchart for management framework

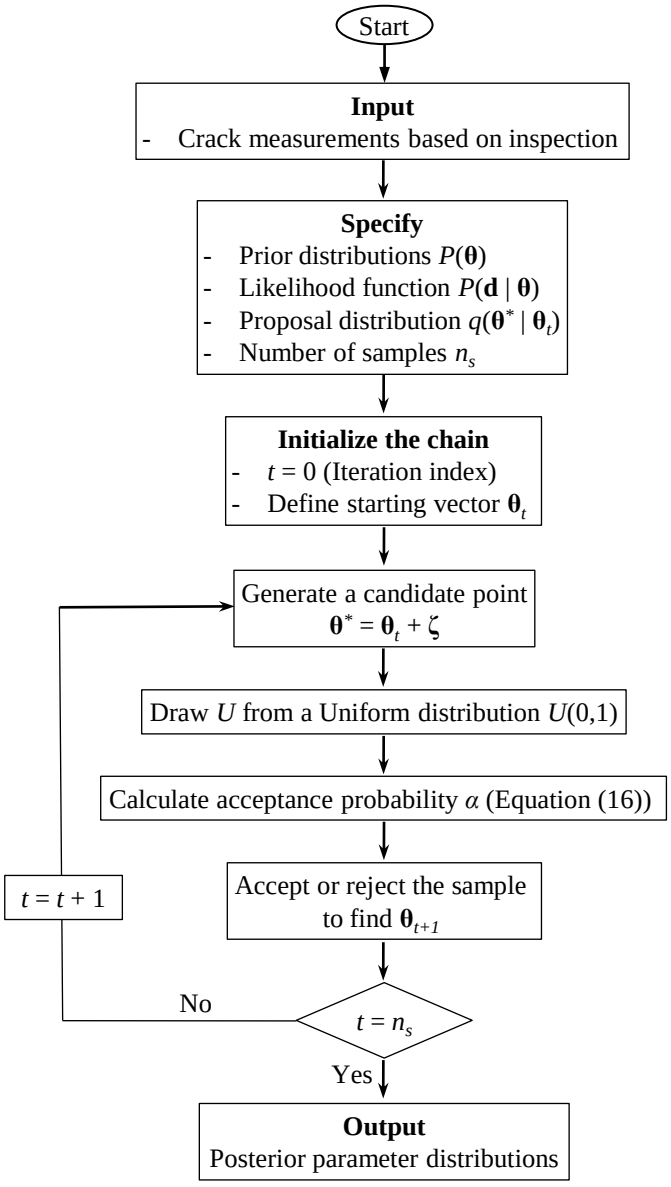

Figure 6.4 Flowchart for the updating Markov chain Monte Carlo simulation

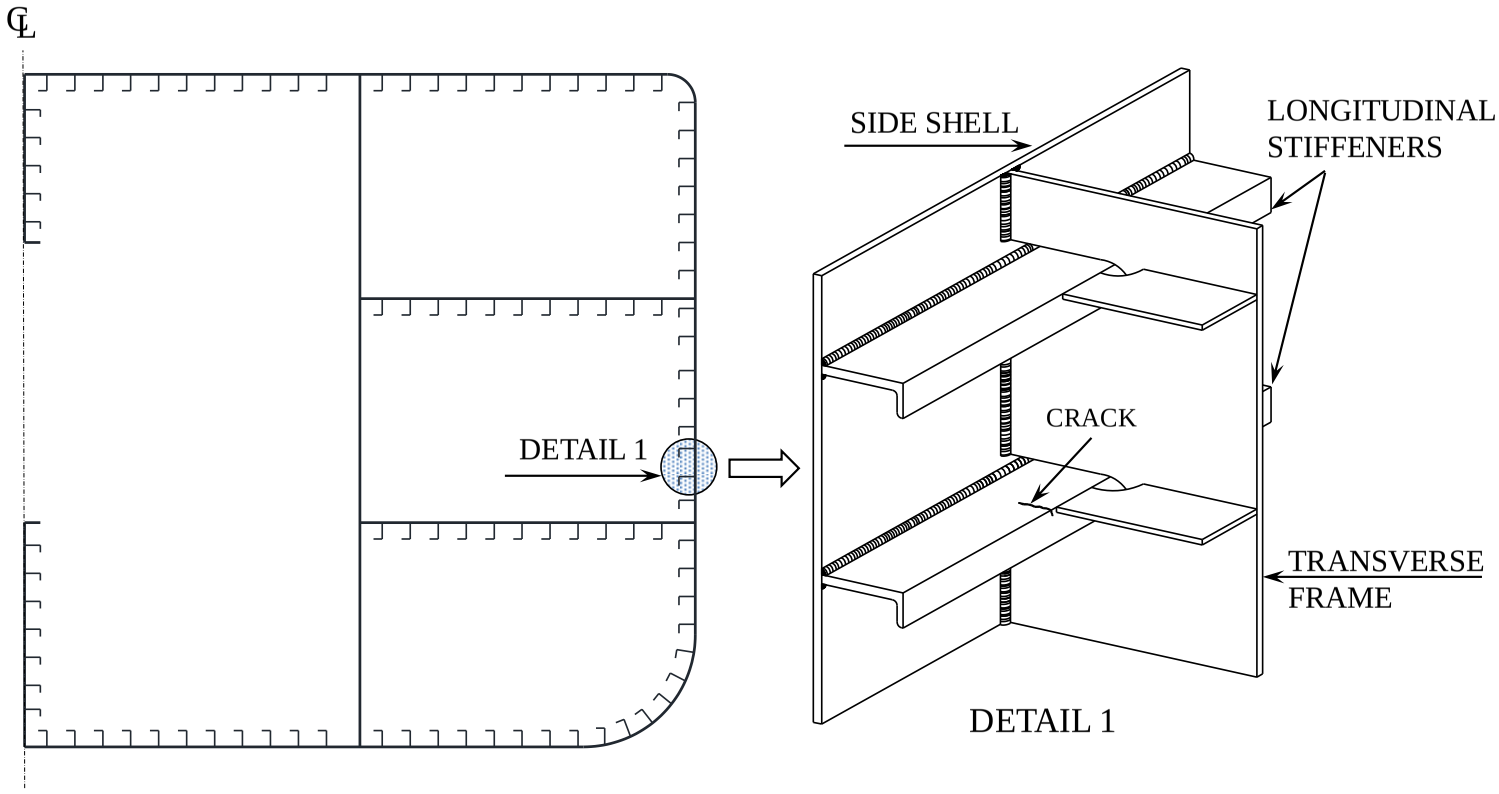
SIDE SHELL
LONGITUDINAL STIFFENERS
DETAIL 1
CRACK
TRANSVERSE FRAME
DETAIL 1
MID-SHIP CROSS-SECTION

[redacted]

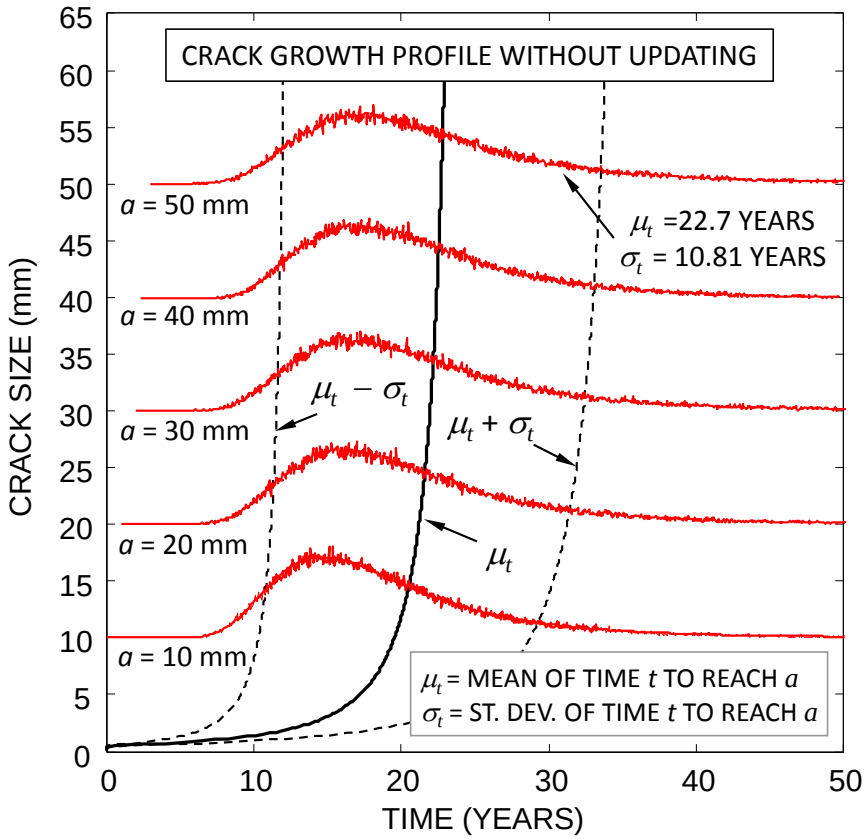

Figure 6.6 Time-variant crack size with the PDF of time to reach a size of 10, 20, 30, 40, and 50 mm

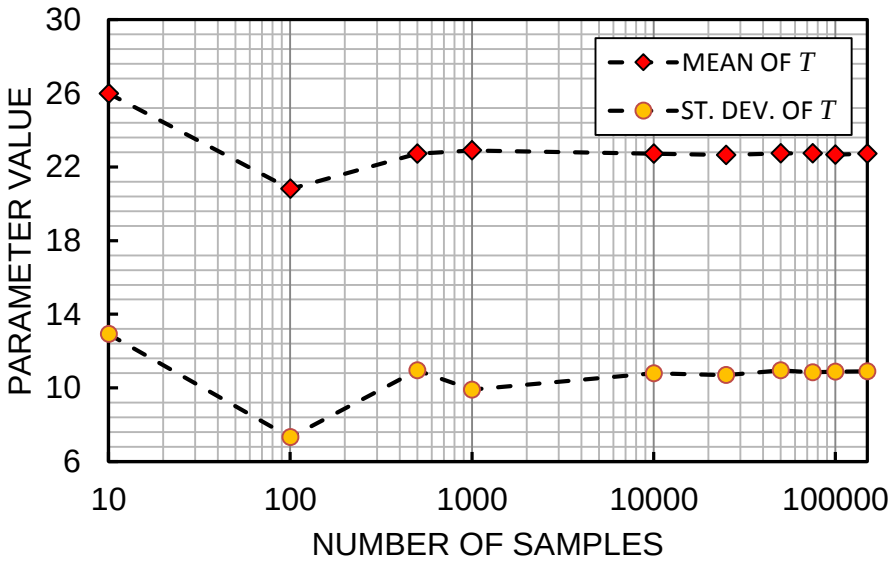

Figure 6.7 A sample of convergence analyses of the fatigue crack growth simulation process

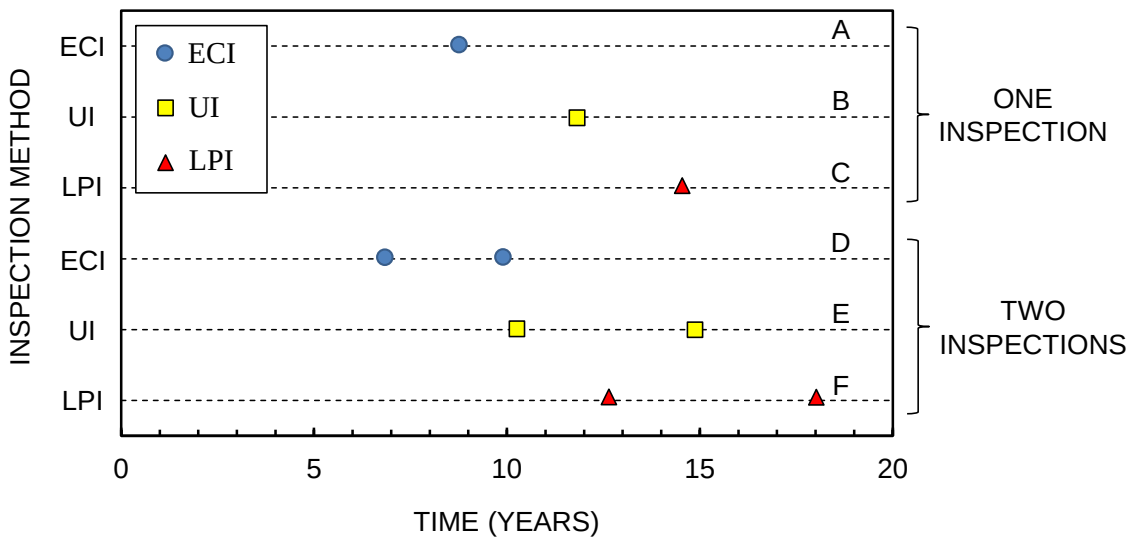

Figure 6.8 Optimum schedules for the adopted inspection types

(a)

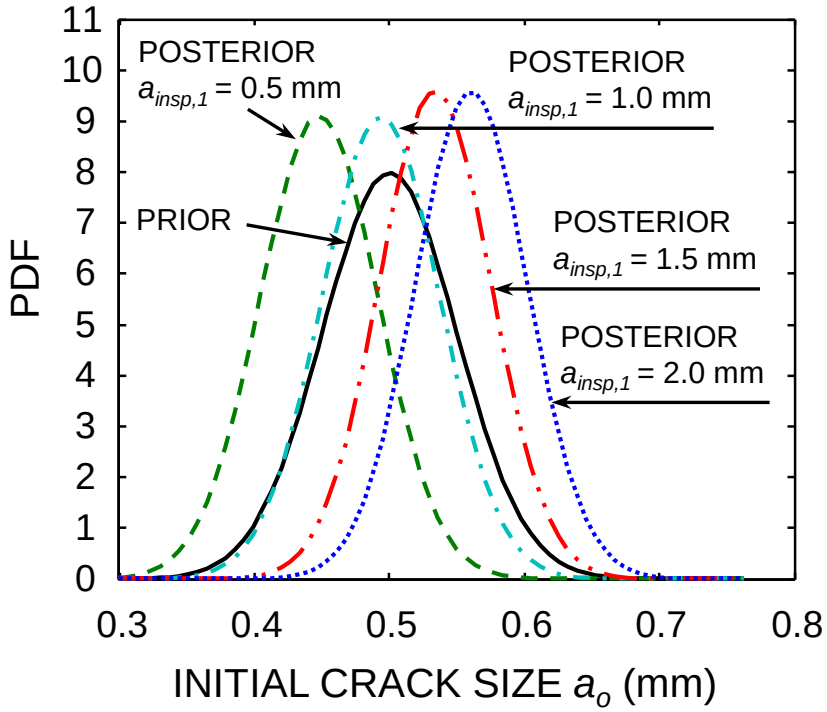
POSTERIOR
$a_{insp,1}$ = 0.5 mm
POSTERIOR
$a_{insp,1}$ = 1.0 mm
PRIOR
POSTERIOR
$a_{insp,1}$ = 1.5 mm
POSTERIOR
$a_{insp,1}$ = 2.0 mm
PDF
INITIAL CRACK SIZE a_o (mm)

(b)

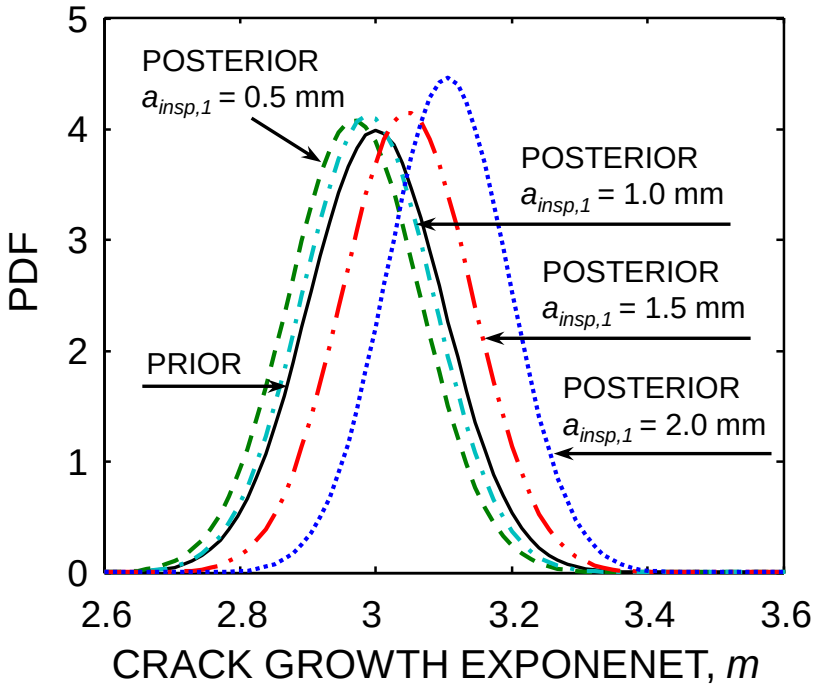
POSTERIOR
$a_{insp,1}$ = 0.5 mm
POSTERIOR
$a_{insp,1}$ = 1.0 mm
POSTERIOR
$a_{insp,1}$ = 1.5 mm
PRIOR
POSTERIOR
$a_{insp,1}$ = 2.0 mm
PDF
CRACK GROWTH EXPONENET, m

(c)

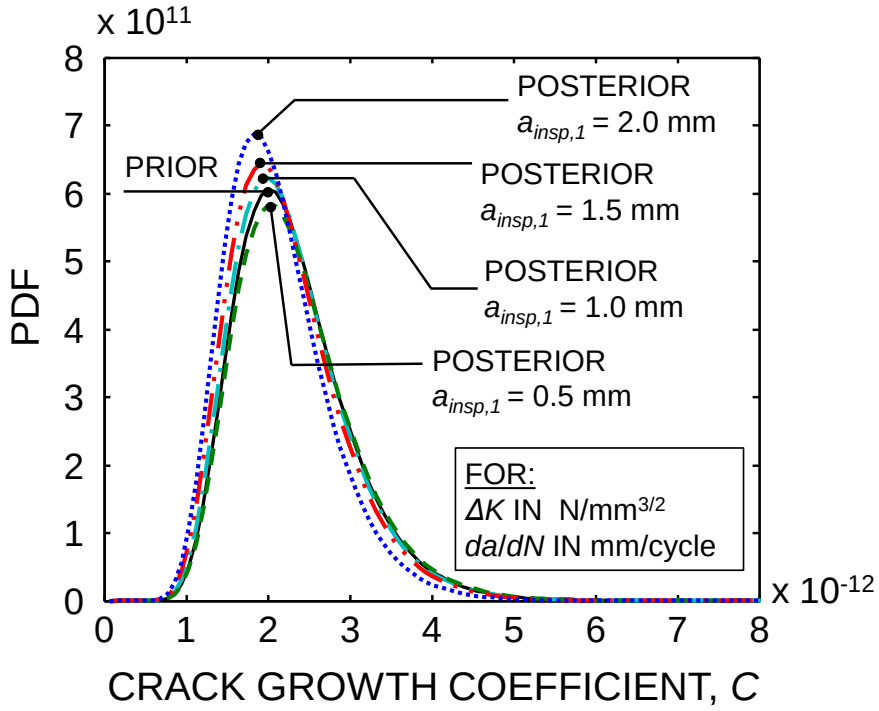

Figure 6.9 Prior and posterior distributions of model parameters based on detected crack sizes at the first inspection; (a) initial crack size, a_o, (b) crack growth exponenet m, and (c) crack growth coefficient C

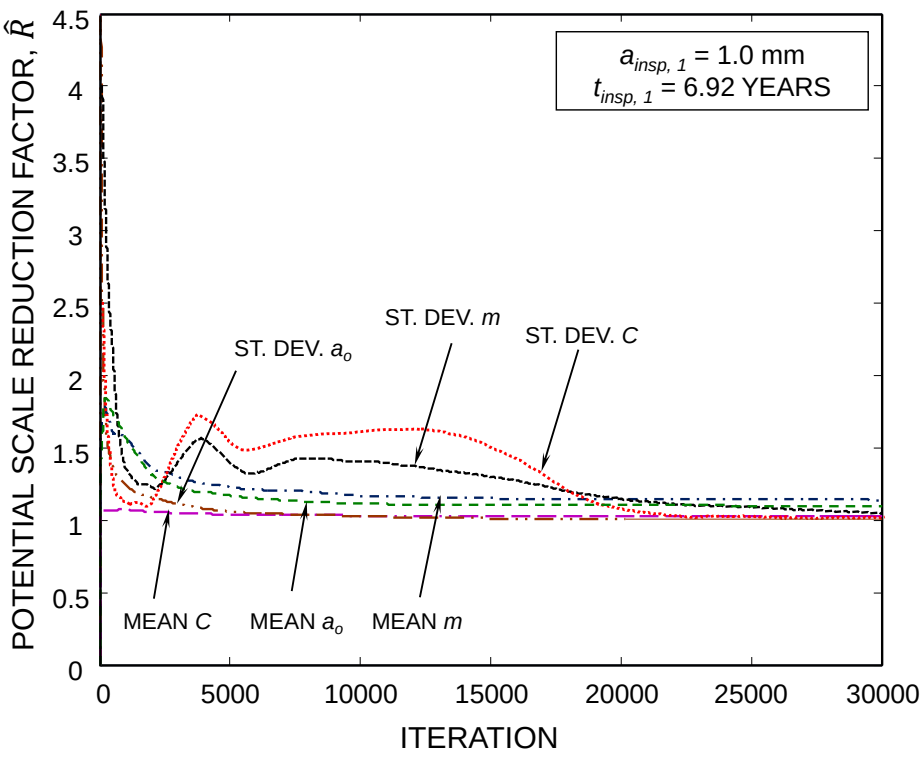

Figure 6.10 Evolution of $\hat{R}$ for the scalar summaries in the Markov chain Monte Carlo simulation process

(a)

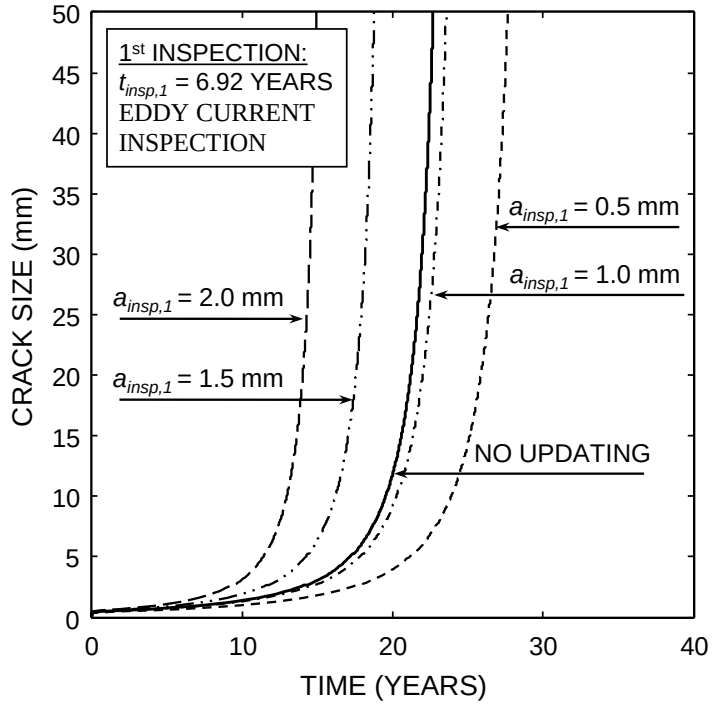

(b)

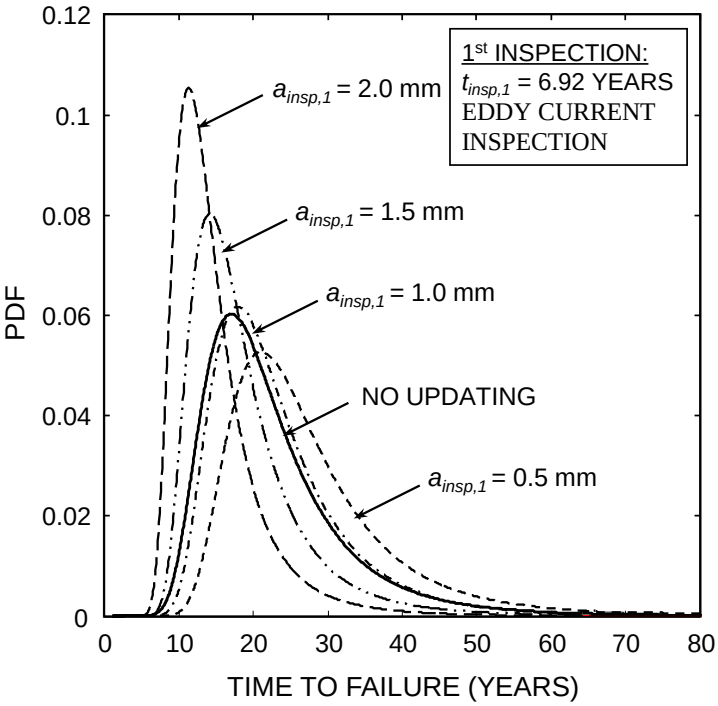

Figure 6.11 Updating results for different crack sizes measured at first inspection ($t_{insp,1}$ = 6.92 years); (a) updated mean of crack growth profiles, and (b) updated PDFs of the time to failure

(a)

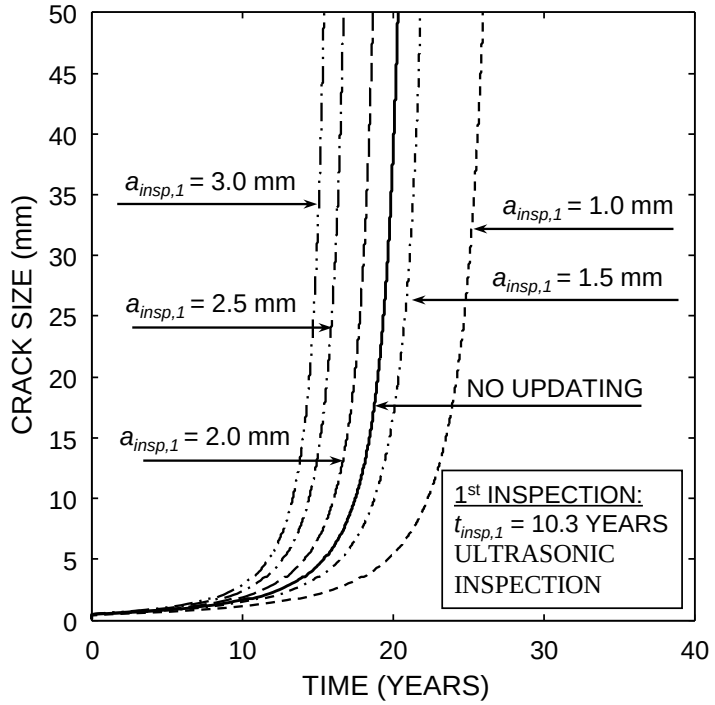

(b)

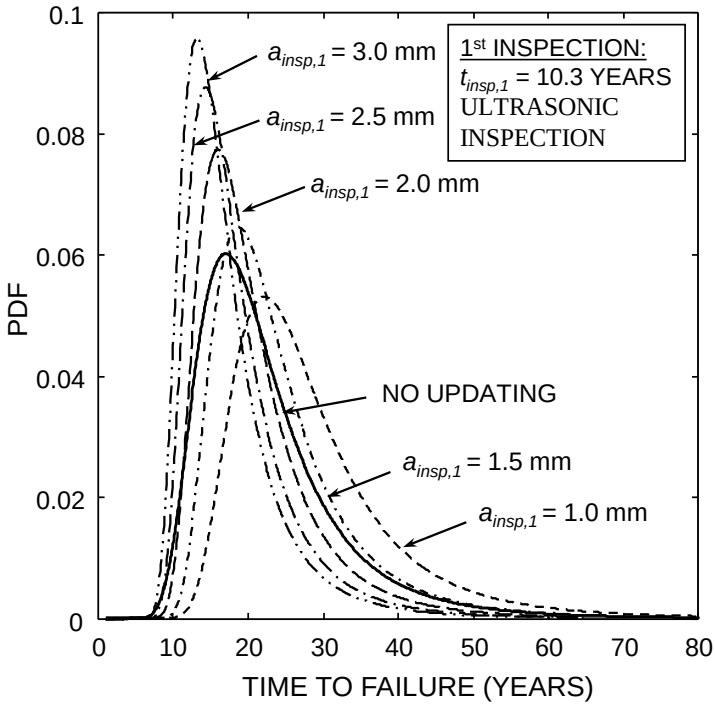

Figure 6.12 Updating results for different crack sizes measured at first inspection inspection ($t_{insp,1}$ = 10.3 years); (a) updated mean of crack growth profiles, and (b) updated PDFs of the time to failure

(a)

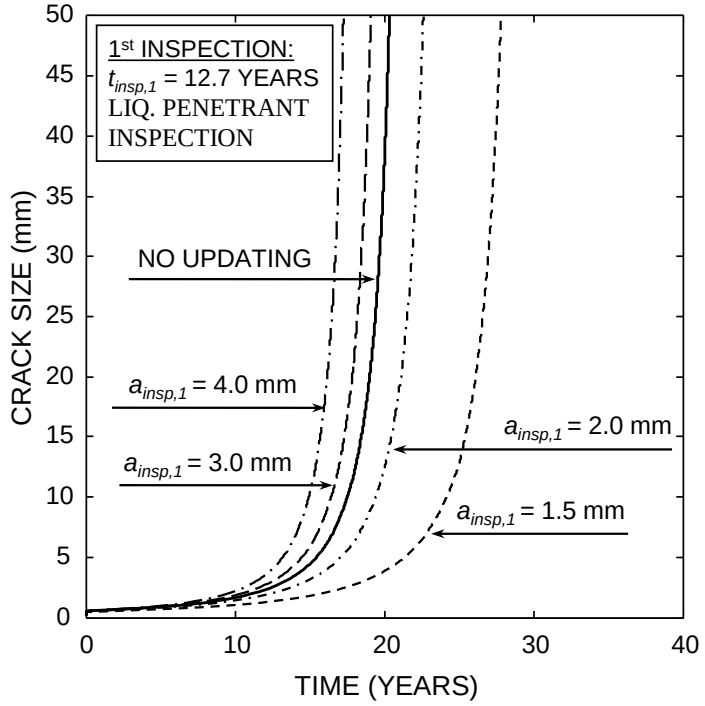

(b)

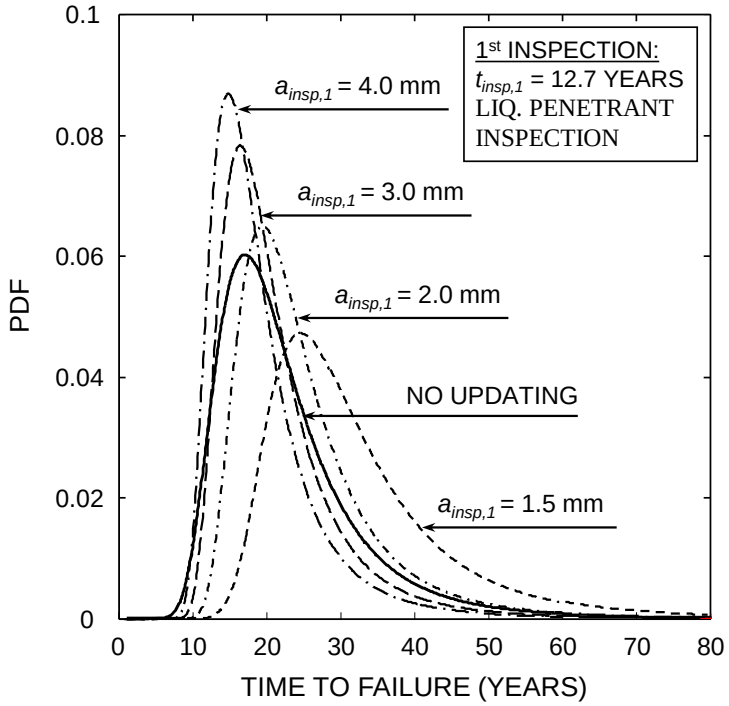

Figure 6.13 Updating results for different crack sizes measured at first inspection ($t_{insp,1}$ = 12.7years); (a) updated mean of crack growth profiles, and (b) updated PDFs of the time to failure

(a)

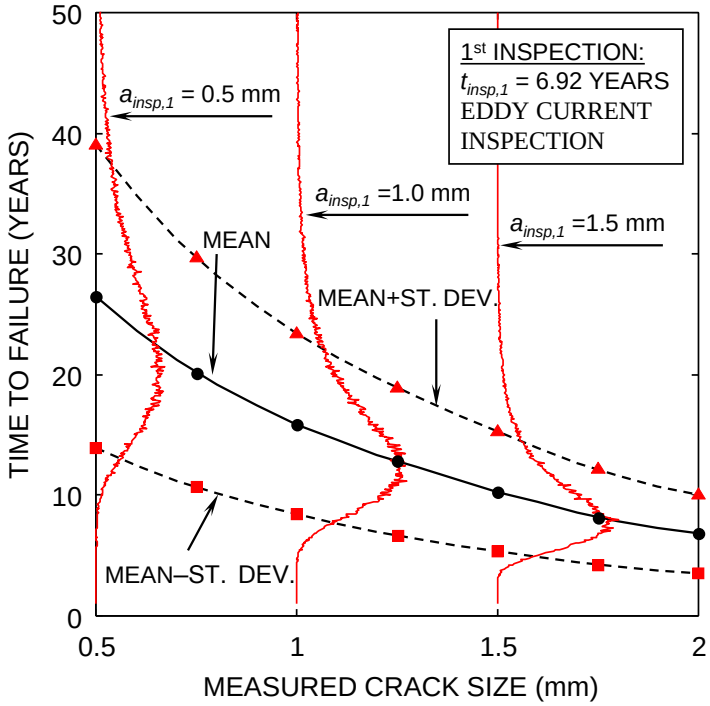
1st INSPECTION:
$t_{insp,1}$ = 6.92 YEARS
EDDY CURRENT
INSPECTION
$a_{insp,1}$ = 0.5 mm
$a_{insp,1}$ =1.0 mm
$a_{insp,1}$ =1.5 mm
MEAN
MEAN+ST. DEV.
MEAN–ST. DEV.
TIME TO FAILURE (YEARS)
MEASURED CRACK SIZE (mm)
0
10
20
30
40
50
0.5
1
1.5
2

(b)

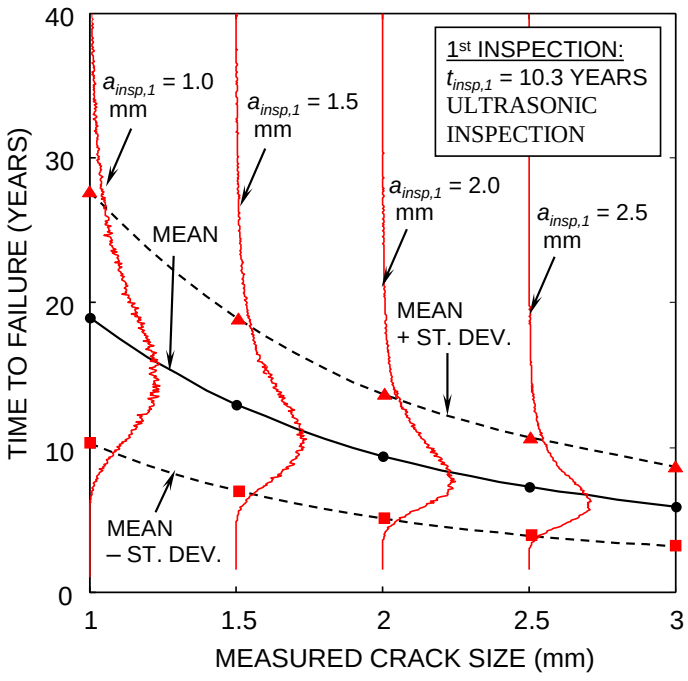
1st INSPECTION:
$t_{insp,1}$ = 10.3 YEARS
ULTRASONIC
INSPECTION
$a_{insp,1}$ = 1.0 mm
$a_{insp,1}$ = 1.5 mm
$a_{insp,1}$ = 2.0 mm
$a_{insp,1}$ = 2.5 mm
MEAN
MEAN + ST. DEV.
MEAN – ST. DEV.
TIME TO FAILURE (YEARS)
MEASURED CRACK SIZE (mm)
0
10
20
30
40
1
1.5
2
2.5
3

(c)

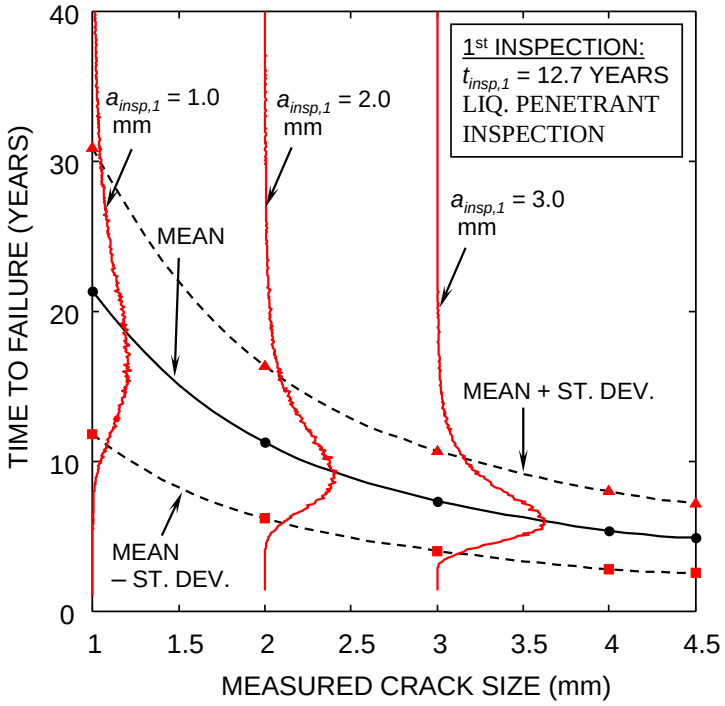

Figure 6.14 Remaining fatigue life with respect to the measured crack size at the first inspection; (a) first inspection performed at 6.92 years, (b) first inspection performed at 10.3 years, and (c) first inspection performed at 12.7 years

(a)

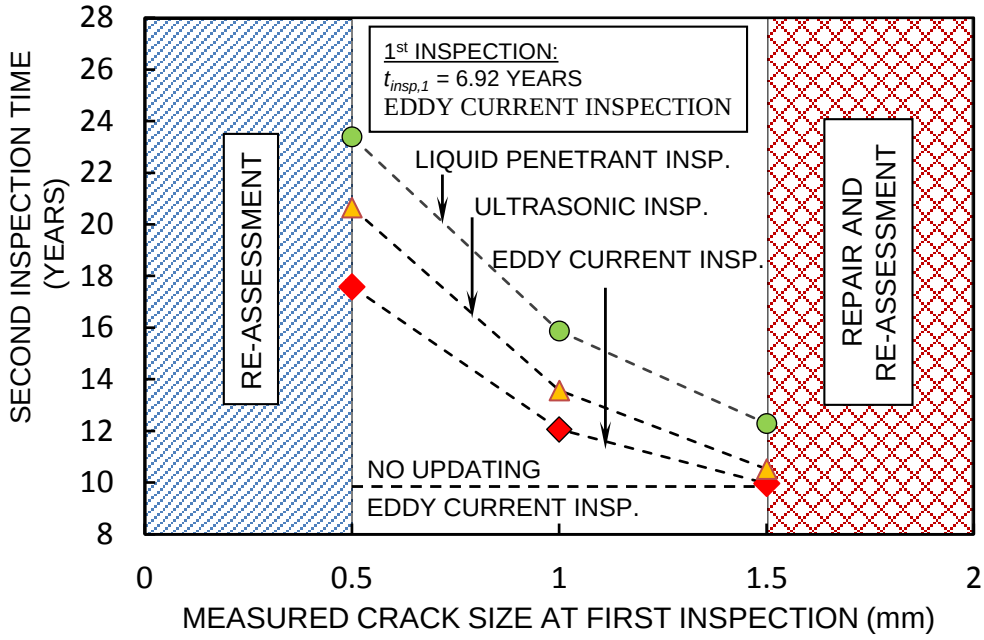
1st INSPECTION:
$t_{insp,1}$ = 6.92 YEARS
EDDY CURRENT INSPECTION
LIQUID PENETRANT INSP.
ULTRASONIC INSP.
EDDY CURRENT INSP.
NO UPDATING
EDDY CURRENT INSP.
RE-ASSESSMENT
REPAIR AND RE-ASSESSMENT
SECOND INSPECTION TIME (YEARS)
MEASURED CRACK SIZE AT FIRST INSPECTION (mm)
28
26
24
22
20
18
16
14
12
10
8
0
0.5
1
1.5
2

(b)

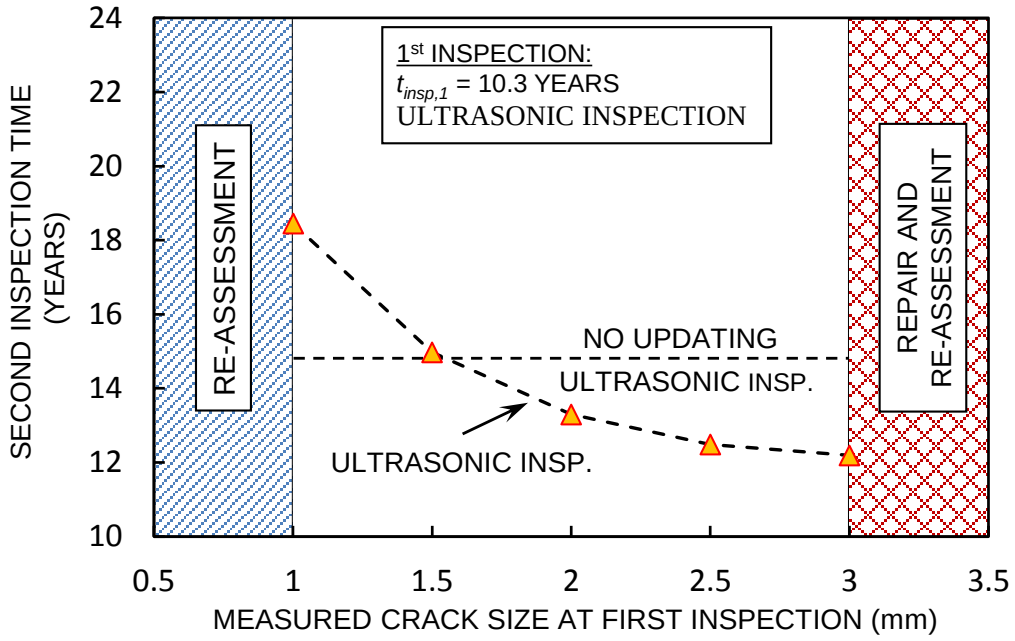
1st INSPECTION:
$t_{insp,1}$ = 10.3 YEARS
ULTRASONIC INSPECTION
NO UPDATING
ULTRASONIC INSP.
ULTRASONIC INSP.
RE-ASSESSMENT
REPAIR AND RE-ASSESSMENT
SECOND INSPECTION TIME (YEARS)
MEASURED CRACK SIZE AT FIRST INSPECTION (mm)
24
22
20
18
16
14
12
10
0.5
1
1.5
2
2.5
3
3.5

(c)

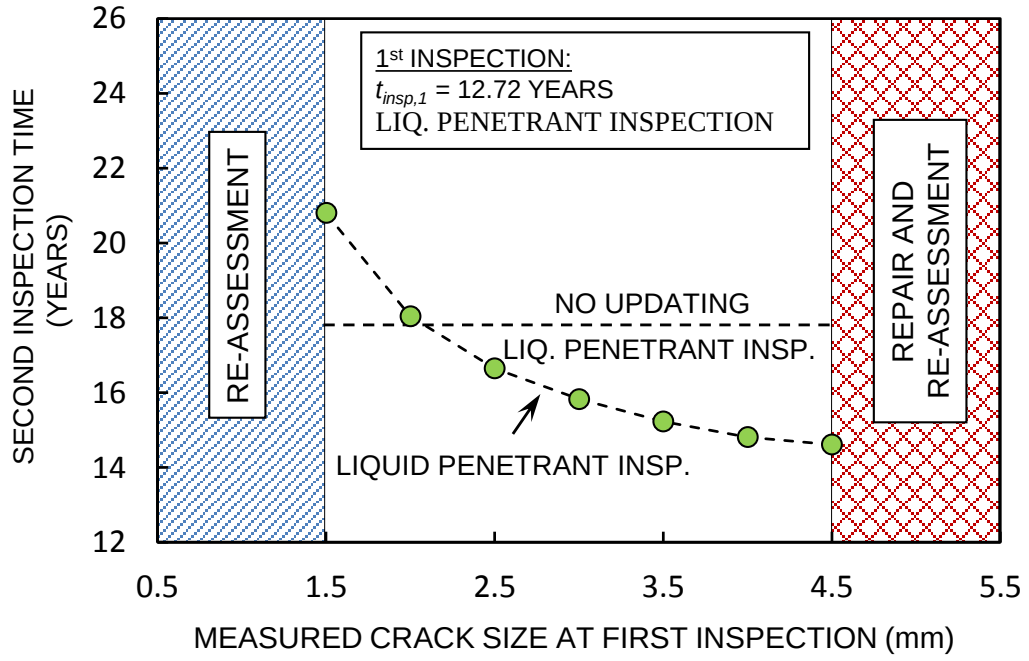

Figure 6.15 Second inspection times for different crack sizes measured at the first inspection; (a) ECI for first inspection and ECI, UI, and LPI for second inspection, (b) UI for first and second inspections, and (c) LPI for first and second inspections

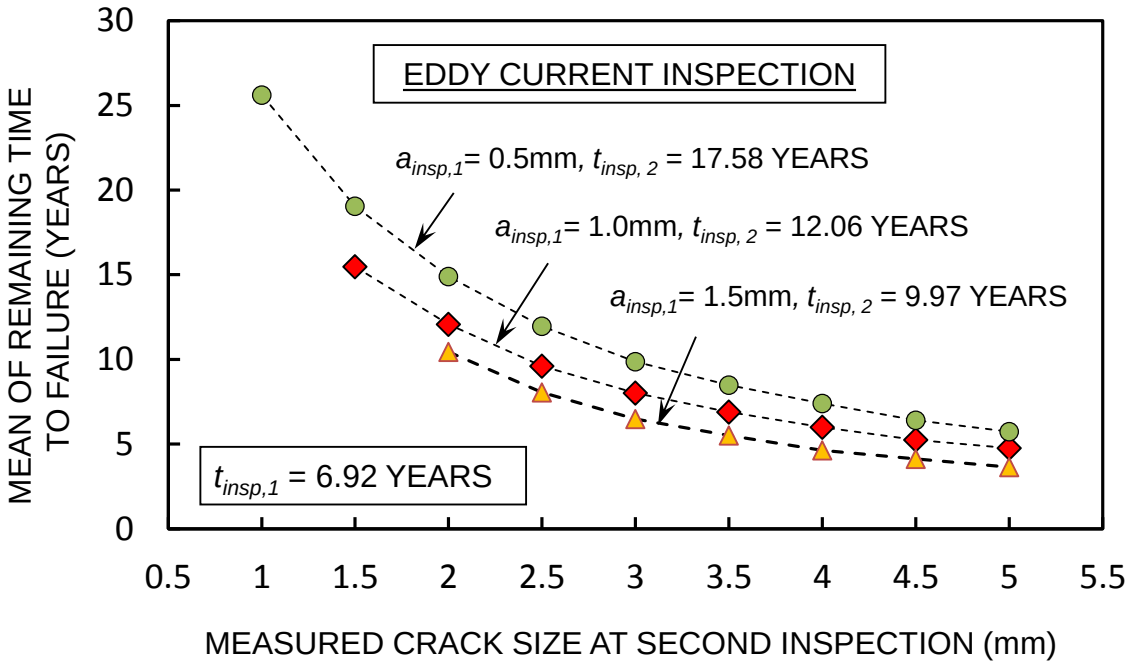

Figure 6.16 Mean of the remaining fatigue life based on the crack size measured at the second inspection for multiple outcomes of the first inspection

(a)

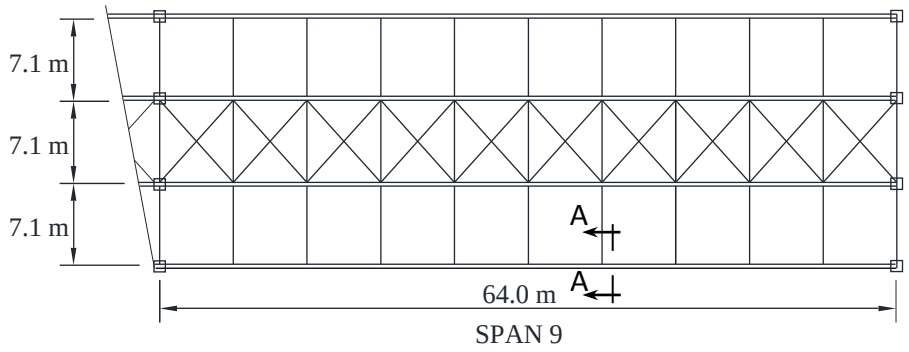

(b)

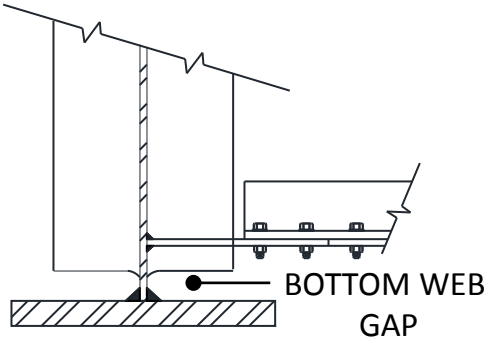

Figure 6.17 The studied bridge (a) Plan view of the bridge, and (b) lower part of cross-section A-A showing the analyzed detail (after Connor & Fisher (2001))

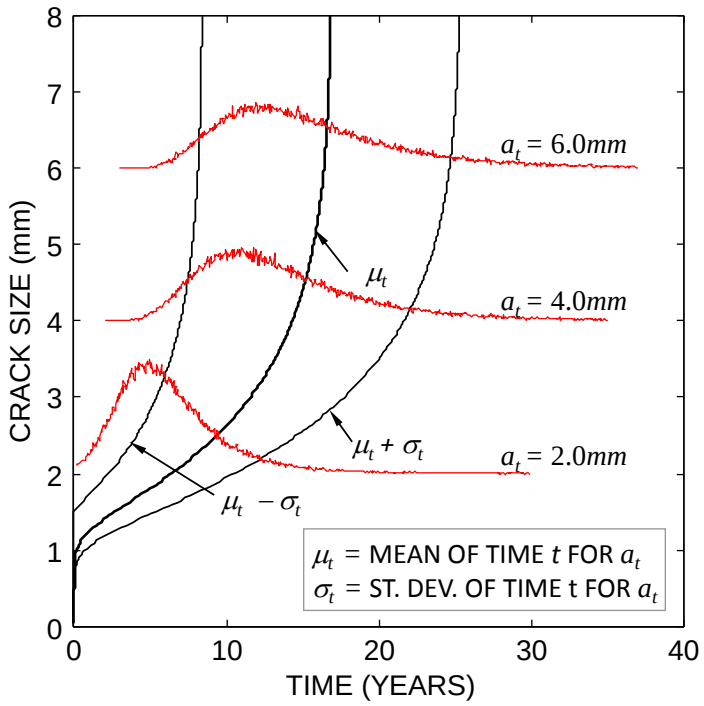

Figure 6.18 Time-dependent crack length with PDFs of times when at = 2.0mm, 4.0mm, and 6.0mm

(a)

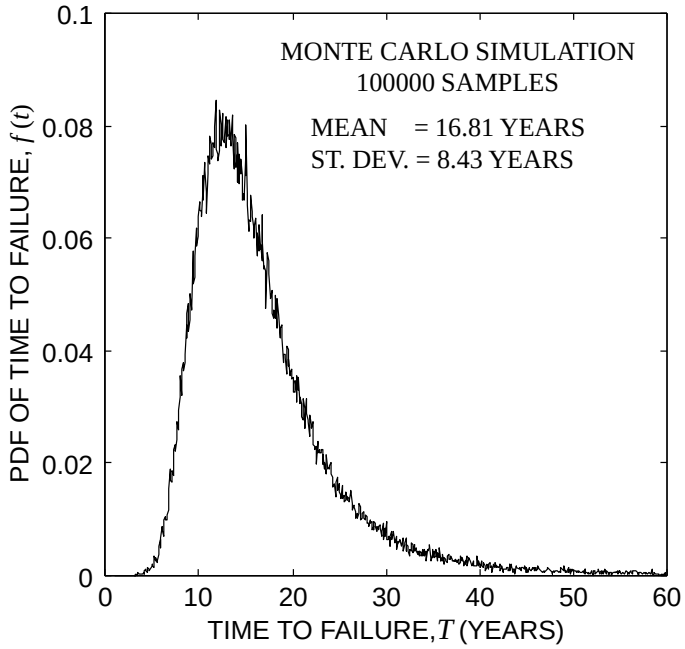

(b)

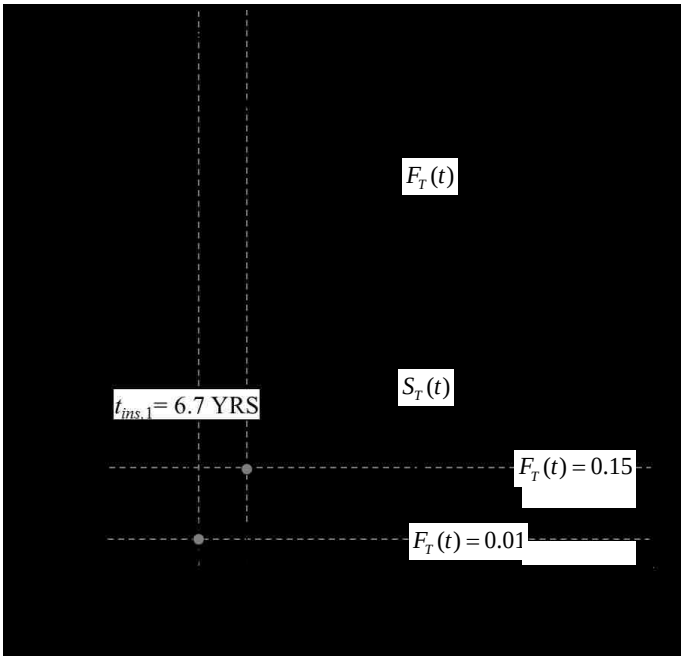

Figure 6.19 Lifetime measures of the analyzed detail (a) PDF of the time to failure, and (b) survivor function and cumulative probability of failure

(a)

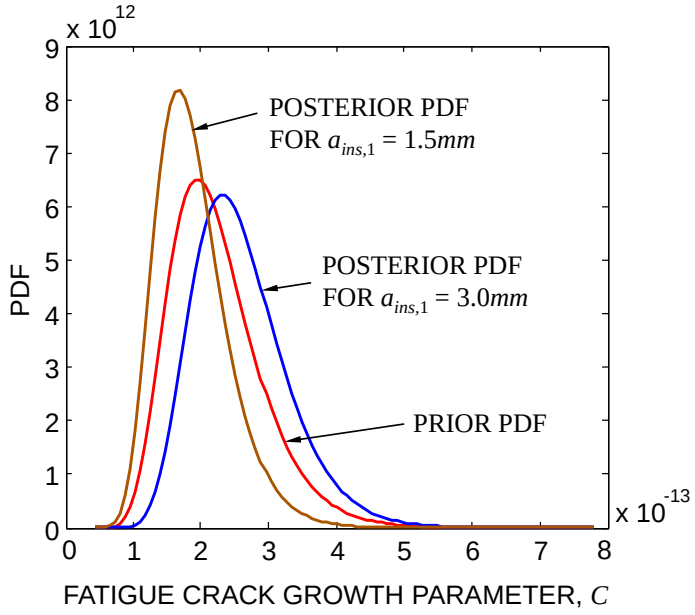

(b)

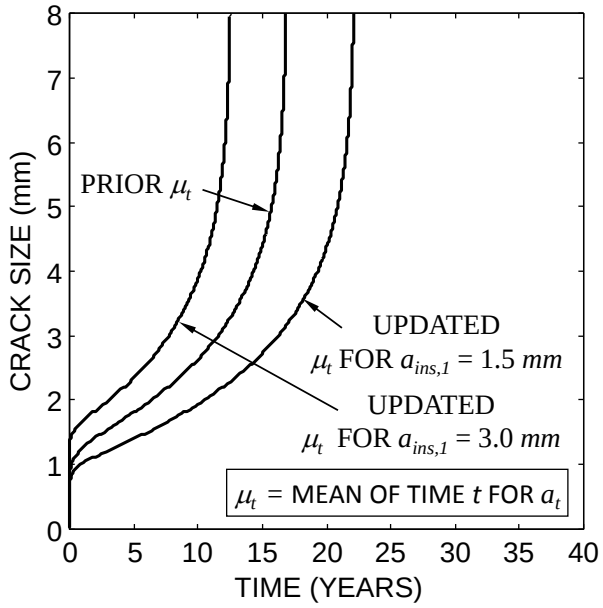

Figure 6.20 Updating results (a) crack growth parameter C prior and posterior distributions for different measured crack sizes, and (b) Time-dependent crack growth profiles before and after updating

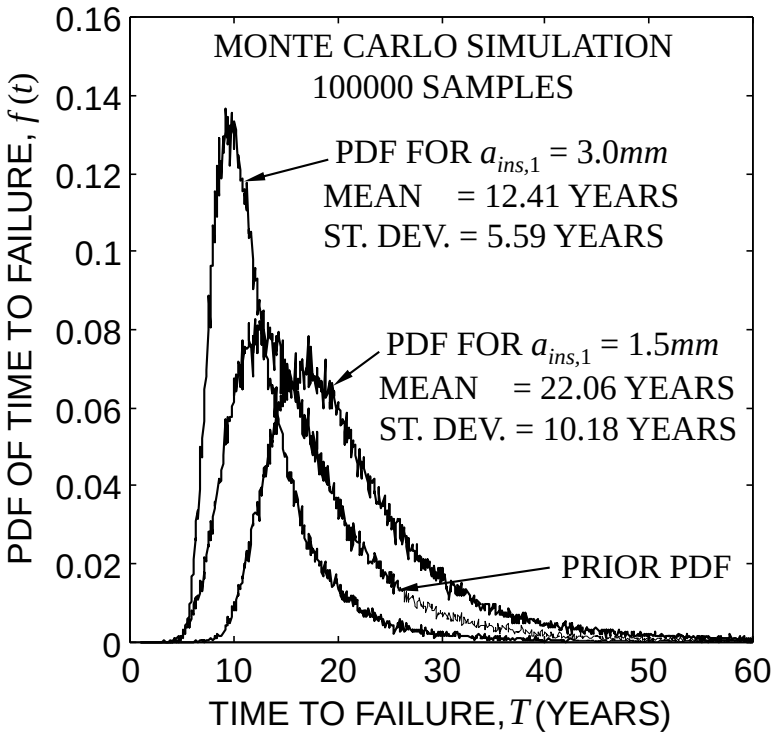

Figure 6.21 PDF of the time to failure before and after updating

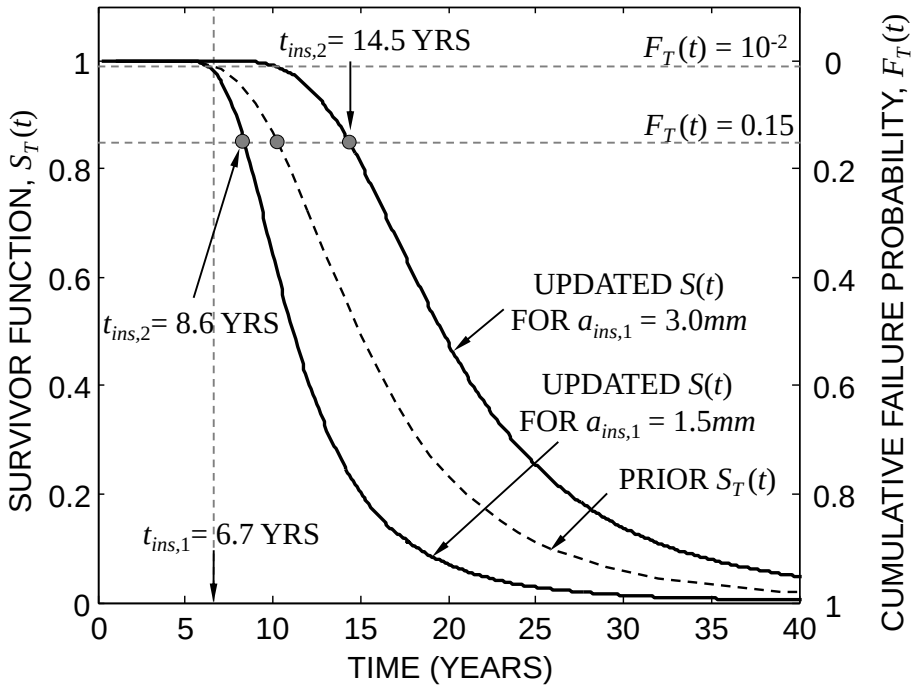

Figure 6.22 Lifetime survivor function before and after updating

CHAPTER 7 INSPECTION PLANNING FOR BRIDGES WITH MULTIPLE CRITICAL LOCATIONS

7.1 Overview

As can be seen from the previous chapters, inspection planning of aging structures is a complex process. This, in part, is due to the presence of various uncertainties associated with the performance prediction process and the damage detection capabilities of the inspection technique. The planning process becomes even more complex if the structure under investigation contains more than one critical location to be addressed in the LCM. In this case, the planning process starts with identifying the most critical locations of damage occurrence. These can be fatigue critical details or corrosion-prone locations. Nondestructive testing techniques, applied at different times along the service life, can be used to monitor the damage propagation and support the service life estimation. The next step is to establish an inspection plan which considers the available budget and the target performance level at all the critical locations of the investigated structure.

This chapter proposes a probabilistic approach for providing effective inspection plans for deteriorating bridges. The proposed approach can consider multiple fatigue and corrosion critical locations in the bridge and chooses the best inspection option among a set of predefined types of NDI methods for each location. Uncertainties in the damage initiation and propagation are considered, in addition to those associated with the damage detection process. A multi-objective optimization problem is formulated to find the optimum inspection times and the required NDT technique for each inspection. An existing steel bridge is used to illustrate the proposed probabilistic approach. Two

examples are provided, in the first one, inspection scheduling is performed in the presence of multiple critical fatigue details, while in the second one, fatigue deterioration in multiple locations and corrosion in the RC deck are considered.

The work in this chapter is based on the papers Soliman & Frangopol (2012) and Soliman *et al.* (2013a).

7.2 Background

As previously discussed, several approached for the inspection scheduling on bridges deteriorating under uncertainty are available in literature. In this context, Chung *et al.* (2006) formulated an optimization algorithm for inspection scheduling that minimizes the cost while considering the safety of fatigue critical bridges. The cost in their study included both the inspection cost and failure cost. Their approach was used to find the optimal time interval between inspections for different inspection methods. However, regular (i.e., routine) NDI may be only practical for a limited number of bridges that are known to be highly critical. Kim & Frangopol (2011b,c, 2012) established a procedure that can find the optimum inspection times while minimizing the expected damage detection delay. Their work was based on the fact that delayed damage detection would lead to a delayed maintenance which in turn may increase the risk of failure for a given structure. Their approach was applied to a fatigue critical detail (Kim & Frangopol 2011c, 2012) and a RC deck subjected to corrosion (Kim & Franopol 2011b). Orcesi & Frangopol (2011) introduced a probabilistic approach, based on lifetime functions, for optimizing the inspections and repairs of bridges. Kim & Frangopol (2011a) introduced a probabilistic approach for finding the optimal inspection and/or monitoring schedule for fatigue sensitive structures. Their approach included a

time-based failure criterion and safety margin with the target of minimizing the total cost. The cost included the monitoring/inspection cost in addition to the expected failure cost.

However, in the previously discussed studies dealing with inspection planning for deteriorating structures, only one detail has been considered for the inspection scheduling; neglecting the practical fact that a deteriorating bridge may contain more than one critical location. Each of these locations has its own deterioration rate and may require a different type of inspection than other locations. This points out to the importance of basing this scheduling on the *structural system level* rather than on the detail component level.

This chapter presents a probabilistic approach for the NDI scheduling of deteriorating bridges which considers multiple deteriorating locations. The proposed approach is able to handle the use of different inspection methods for each location at each inspection. The *PoD* function is used as an indicator of the inspection quality. Inspection scheduling is formulated as an optimization problem to find the inspection times which yield the highest probability of damage detection before failure in all the critical locations. Another case is studied in which the optimization problem is formulated to find the inspection schedule that minimizes the inspection cost and maximizes the probability of damage detection. Uncertainties in the damage imitation and propagation, as well as the damage detection models are considered. The proposed approach is applied to an existing fatigue critical bridge.

7.3 Fatigue and corrosion deterioration

In this chapter, LEFM based on Paris' equation (Paris & Erdogan 1963) is used for assessing fatigue behavior of steel details. As previously indicated, this equation is given by

$$\frac{da}{dN} = C \cdot (\Delta K)^m \tag{7.1}$$

where a = crack size, N = number of cycles, and ΔK = range of the stress intensity factor. C and m are material parameters. The range of the stress intensity factor can be expressed as

$$\Delta K = Y(a) \cdot S_{re} \cdot \sqrt{\pi a} \tag{7.2}$$

where S_{re} = the equivalent constant-amplitude stress range and $Y(a)$ = the generalized stress intensity factor which depends on the crack orientation and shape. This factor can be expressed as (Fisher 1984)

$$Y(a) = F_e \cdot F_s \cdot F_w \cdot F_g \tag{7.3}$$

in which F_e, F_s, F_w and F_g are correction factors taking into account the effects of the elliptical crack shape, free surface, finite width (or thickness), and non-uniform stress acting on the crack, respectively. The correction factors for several fatigue related cases were studied by (Albrecht & Yamada 1977; Fisher 1984; Yazdani and Albrecht 1990). More detailed empirical and exact solutions for these correction factors can be found in (Tada *et al.* 2000).

Considering the daily number of cycles N_{avg} to be constant over time, the time interval associated with a crack growth from a_o to a size of a_t can be calculated as

$$t = \frac{1}{365 \cdot N_{avg} \cdot C \cdot S_{re}^{m}} \cdot \int_{a_o}^{a_t} \frac{1}{\left(Y(a) \cdot \sqrt{\pi a}\right)^{m}} da \tag{7.4}$$

The time to failure of the detail is obtained by setting a_t in Equation (7.4) to be equal to the critical crack size a_f. Monte Carlo simulation technique can be used in this case, resulting in the PDF of the time to failure *T*. Additionally, data collected during structural health monitoring can be effectively used to find the stress range and the daily number of cycles affecting the detail, which will give more reliable fatigue life prediction (Ye *et al.* 2012).

Corrosion of steel reinforcement is one of the main factors causing the deterioration in RC members. Its effect is accelerated when the member is subjected to de-icing salt spray. Corrosion can damage the RC member in various ways such as cracking, spalling, and loss of steel section, among others. The corrosion of reinforcement mainly occurs due to concrete carbonation and chloride penetration. This chapter considers the chloride penetration as the main corrosion driving process. In this chapter, the corrosion initiation time is defined as the time for the chloride concentration at the rebar surface to exceed a predefined threshold limit. Fick's second law can be used to calculate the corrosion initiation time *T* as (Kim & Frangopol 2011b)

$$T_I = \frac{x^2}{4D\left[erfc^{-1}\left(C_{th}/C_o\right)\right]^2} \tag{7.5}$$

where x = depth of steel reinforcement from the concrete surface (*mm*), D = effective chloride diffusion coefficient (mm^2/year), C_o = surface chloride concentration (g/mm^3),

C_{th} = threshold limit of chloride concentration for reinforcement (g/mm^3), and $erfc(\cdot)$ = complementary error function.

Following the corrosion initiation, general (i.e., uniform) corrosion is considered, in which the corrosion process leads to a reduction in the cross-sectional area of the steel reinforcement. This reduction is assumed to be constant along the entire surface area of the reinforcing bars. The reinforcement area $A_s(t)$ at time t is found as

$$A_s(t) = \begin{cases} \dfrac{n_s \pi \, d_o^2}{4} & \text{for } 0 \le t \le T_I \\ \dfrac{n_s \pi \, (d_o - r_{corr}(t - T_I))^2}{4} & \text{for } t > T_I \end{cases} \tag{7.6}$$

where n_s = number of rebars subjected to corrosion effect; d_o = initial diameter of rebars (*mm*); and r_{corr} = rate of corrosion (*mm*/year).

7.4 Nondestructive inspection of steel bridges

Among the available NDI techniques for fatigue inspection, the liquid penetrant inspection (LPI), ultrasonic inspection (UI), eddy current inspection (ECI), and magnetic particle inspection (MPI) are mostly used for bridge inspection (Zheng & Ellingwood 1998). Each of these methods has its advantages and disadvantages. For instance, the UI can detect small cracks; however, it requires considerable experience for interpreting the results. MPI is simple but it requires considerable surface preparation. Eddy current technique is a useful technique that has been widely used for aerospace and ship applications. This technique requires no surface preparation and moderate experience for interpreting the results. Recently, eddy current technique has been used in some bridge applications (Lamtenzan *et al.* 2000).

7.5 Probability of Damage Detection

In general, two methods are mainly used in the analysis of NDI results to formulate the *PoD* functions: the hit and miss method and the signal response method (Chung *et al.* 2006). The *PoD* function can take multiple forms; however, among the most widely used are the log-logistic function and the cumulative lognormal distribution function. These two forms are, respectively, expressed as

$$PoD = \frac{\exp(\alpha + \beta \cdot \ln(a))}{1 + \exp(\alpha + \beta \cdot \ln(a))} \tag{7.7}$$

$$PoD = 1 - \Phi\left(\frac{\ln(a) - \lambda}{\zeta}\right) \tag{7.8}$$

where a is the crack size; α and β are the parameters which define the log-logistic *PoD* curve; $\Phi(\cdot)$ is the standard normal cumulative distribution function; and λ and ζ are, respectively, the location and scale parameters of the cumulative lognormal *PoD* curve. The parameters α, β, λ and ζ in Equations (7.7) and (7.8) depend mainly on the quality of inspection and are different for each inspection method. In this chapter, Equation (7.8) is used to represent the damage detection probability of NDI methods.

7.6 Inspection Planning

In this chapter, inspection planning is performed with the aim to find the optimum inspection schedule that satisfies a set of predefined goals such as minimizing the total inspection cost and/or maximizing the *PoD* before failure occurs. The process starts with predicting the time-dependent damage level (i.e., crack size or degree of corrosion) which, in turn, can be used along with the *PoD* function for the chosen inspection

method. However, this damage level is always an unknown quantity subjected to significant uncertainties. In this study, Monte Carlo simulation is used to predict the time-dependent crack size for each of the studied locations. Two outcomes can be drawn from this simulation process: the time-dependent damage level and the PDF of the time to failure *T*. In this chapter, *T* is defined as the time when the crack reaches a predefined critical crack size or the time when the loss in the area of reinforcement bars reaches 10% of the initial cross-sectional area due to corrosion. These outcomes will be used in next sections to find the probability of detection before failure (*PD*) at each inspection. Failure is considered to occur of the damage level reaches the critical level before being detected by the inspection plan. The proposed approach can handle different inspection methods for each location at a certain inspection time. This is considered herein due to the fact that some inspected locations might have surface flaws that can be easily detected using less expensive method such as the liquid penetrant or magnetic particle inspection. For this reason, a matrix consisting of the *PoD* function parameters for the considered inspections methods at each location is defined and used in an evaluation process to find the best inspection method for each detail, as will be shown later in this chapter.

7.6.1 Probability of Damage Detection before Failure for a Single Detail

The probability of damage detection PD_n after n inspection can be formulated considering both the *PoD* and the probability that the inspection will be applied before the time to failure *T*. The formulation of *PD* is based on the event tree model shown in Figure 6.2 for a number of inspections n equal to one. PD_1 (i.e., $n = 1$) is associated with Branch 2 in this event tree and is expressed as

$$PD_1 = P\left(t_{insp_1} \le T\right) \cdot PoD(t_{insp_1}, \rho) \tag{7.9}$$

where T = time to failure of the detail, t_{insp_1} = time of application of the first inspection, $P\left(t_{insp_1} \le T\right)$ = probability that the first inspection is applied before the failure of the detail, and $PoD(t_{insp_1}, \rho)$ = probability of crack detection at the first inspection using the inspection method ρ.

Similarly, the event tree model can be extended to find the probability of detecting the crack before failure for n inspections, which can be expressed as

$$PD_n = \sum_{j=1}^{n}\left(\prod_{i=1}^{j}\left[P\left(t_{insp_i} \le T\right)\cdot \overline{POD}\left(t_{insp_{i-1}}, \rho_{i-1}\right)\right]\cdot PoD\left(t_{insp_j}, \rho_j\right)\right) \quad (7.10)$$

where $P\left(t_{insp_i} \le T\right)$ = probability that the ith inspection is performed before the failure of the detail, $PoD\left(t_{insp_j}, \rho_j\right)$ = probability of crack detection at the jth inspection using the inspection method ρ_j, and $\overline{PoD}\left(t_{insp_{i-1}}, \rho_{i-1}\right)$ = probability of not detecting the crack at the $(i-1)$th inspection using the inspection method ρ_{i-1}, and $\overline{PoD}\left(t_{insp_0}, \rho_0\right) = 1$.

7.6.2 Probability of Damage Detection before Failure for Multiple Details

Using Equation (7.10), the probability of damage detection after n inspections can be found for a single detail. This approach can be extended to find the probability of damage detection at all the inspected locations after n inspections, which can be expressed, assuming the statistical independence between the events of detecting cracks at different details, as

$$PD_{n,L} = \prod_{k=1}^{L}\left(PD_{n,k}\right) \quad (7.11)$$

where L = total number of inspected details.

7.6.3 Inspection Cost

As previously indicated, the cost of inspection consists of the access cost, equipment cost and operator cost. For the case of bridge inspection, the access cost is the cost required to control the traffic and access the different locations that need to be inspected. This cost depends mainly on the location of the bridge, the volume of traffic that crosses the bridge, and the type of the bridge.

Equipment cost depends mainly on the type of the NDT used in the inspection. For instance, the ultrasonic inspection and eddy current inspection would require special equipment to be performed. The third item is the operator cost, which includes the fees of the inspector, interpretation of the results, and writing the inspection report. This cost depends on the type of the bridge, the number of inspected details and the type of inspection used for each detail.

The cost of a single inspection C_{insp} can be found by adding the access, equipment, and operator costs. Accordingly, this cost can be used to find the present cost of *n* inspections C_{insp}^{T} as follows

$$C_{insp}^{T} = \sum_{i=1}^{n} \frac{C_{insp}}{(1+r)^{t_{insp_i}}} \tag{7.12}$$

where r = annual discount rate of money.

7.7 Example 7.1

The proposed approach is applied to an existing fatigue critical bridge. The bridge is the I-64 Bridge over the Kanawha River at Dunbar in West Virginia (currently carries the westbound traffic), which was previously analyzed in Example 6.2. This bridge complex

spans over railroad tracks, local roads, and the Kanawha River. In this study, only two of the plate girder spans crossing the Kanawha River, namely, Spans 9 and 10 are investigated. A view of these spans is shown in Figure 7.1 (after Connor & Fisher 2001). In 2000, several locations of the spans over the Kanawha River were monitored and studied by personnel form the ATLSS Center of Lehigh University. As previously indicated, several details showing a potential for fatigue cracking were found (Connor & Fisher 2001).

With multiple fatigue critical locations in the bridge, difficult decisions have to be taken regarding the future interventions. For example, under the fact that these details have not yet shown signs of severe fatigue cracking, should these details be retrofitted or not ? In these situations, usually the manager chooses to postpone the retrofitting while proposing a plan for the future inspection of these details. In fact, this raises the next question on how can this bridge be inspected in the future to make sure that the cracks, if developed, can be effectively detected and repaired before failure. The answer to the last question is related to the optimum inspection planning proposed in this chapter, which should be able to handle the different critical details and ensure the highest probability of cracks detection before failure while maintaining the cost-effectiveness of the inspection.

For this bridge, three types of details were found to be fatigue critical (Connor & Fisher 2001). The first detail, shown in Figure 7.2, is a bottom web gap detail located at the termination of the transverse connecting plate of the exterior girders. This detail, referred to as Detail D1, is known for the bad fatigue behavior due to the distortion induced stresses and has been discussed in Example 6.2. The second detail (i.e., Detail D2), shown in Figure 7.3, is a longitudinal stiffener termination detail. D2 is subjected to

longitudinal in-plane stresses which are amplified at the weld termination. In some cases, due to the small web gap, it is also subjected to out-of-plane displacements inducing large longitudinal stresses that act in the same direction of the in-plane stresses. The last detail, Detail D3 (shown in Figure 7.4), is a weld termination at the connection of a bracing gusset plate and the transverse connecting plate. D3 was found to have small cracks at the regular inspection which were found to be growing out of the lack of fusion zone on the gusset plate (Connor & Fisher 2001).

7.7.1 Probabilistic time-dependent crack growth

In this section, the probabilistic time-dependent crack growth for each detail is estimated based on Equation (7.4) and a Monte Carlo simulation using 100,000 samples. The outcome of this simulation is the PDF of the time to failure of each detail. The descriptors for predicting time-dependent crack growth based on Equation (7.4) are provided in Table 7.1. The parameter C for crack growth in Equation (5) is assumed lognormally distributed with a mean of 2.18×10^{-13} using units of *mm* for crack size *a* and *MPa* for stress range S_{re} (Barsom & Rolfe 1999). This corresponds to a value of 3.6×10^{-10} using inches for *a* and *ksi* for S_{re}. The COV of C is assumed to be 0.2.

For the Detail D1, the cracking of this detail can be treated as a semi-elliptical edge crack of depth *a* (Fisher 1984). The range of the stress intensity factor can be found using Equations (6.31)-(6.27). For this detail, the average number of cycles was estimated as 7500 cycles per day (Connor & Fisher 2001) and is assumed herein to have a lognormal PDF with mean of 7500 and COV of 0.1 (Moses *et al.* 1987). The stress range was found to be 34.45 *MPa* (5.0 ksi) (Connor & Fisher 2001). This stress is considered here to be the mean value of the stress range distribution for this detail with a COV of 0.1

(Ayyub *et al.* 2002). Furthermore, the initial crack size a_o is assumed to be a lognormal random variable with mean of 1.27 mm (0.05 in) and COV of 0.2 (Kim & Frangopol 2011a). The final crack size a_f was assumed to be 10.16 mm (0.4 in). The PDF of time for the crack size to reach a_f (i.e., time to failure *T*) can be obtained as shown in Figure 7.5 (a).

The PDF of the time to failure for Detail D2 can be found using the same probabilistic model adopted for D1 (i.e., using Equation 7.4) with a stress concentration factor analogous to that of a welded cover plate detail (Connor & Fisher 2001). Data required for generating the PDF of the time to failure for Detail D2 are listed in Table 7.1. For the Detail D3, an estimate of the stress intensity factor range for the free edge crack can be made using the following relationship (Connor & Fisher 2001)

$$\Delta K = S_{re} \cdot \sqrt{\pi a} \tag{7.13}$$

where a = half the width of the lack of fusion zone at the root of the partial penetration groove weld and the reinforcing weld. Field observation performed by ATLSS personnel suggested that the lack of fusion zone is equal to 6.35 mm (0.25 in), giving the value of a_o = 3.175 mm (0.125 in). To account for uncertainty, this value is assumed to be a lognormal distributed random variable with mean of 3.175 mm (0.125 in) and a COV of 0.2. Using this information, the time to failure, which is the time required for the crack to propagate through the thickness of the gusset plate can be calculated. The final crack size is assumed to be 9.525 mm (0.375 in). The remaining data required for predicting the time to failure of this detail is listed in Table 7.1. Figures 7.5 (a), (b) and (c) show the PDF of time to failure for Details D1, D2 and D3, respectively.

7.7.2 Inspection quality

In this example, the inspection quality is modeled by using the lognormal *PoD* function given by Equation (7.8). Three types of NDI methods are utilized for this application, namely, the eddy current technique, ultrasonic inspection, and liquid penetrant inspection. Since the *PoD* function parameters depend on factors such as the crack geometry, the location of the crack, environmental conditions, the inspector training, the determination of these parameters requires extensive experimental investigation which is outside the scope of this study. Accordingly, these parameters are assumed as shown in Table 7.2. However, these parameters can be easily modified when more data regarding these types of details is available. It is assumed in this example that each inspection method will have the same *PoD* when applied to any of the studied details.

7.7.3 Inspection scheduling

Scheduling to maximize the probability of damage detection before failure

In this stage, the optimum inspection schedule is obtained as the solution of an optimization problem with the objective of maximizing the probability of detection before reaching the critical crack size for the three details. The problem is formulated as follows

$$\text{Find} \quad \mathbf{t}_{insp} = \left\{ t_{insp_1}, t_{insp_2}, t_{insp_3}, ..., t_{insp_n} \right\} \tag{7.14}$$

$$\text{to maximize} \quad PD_{n,L} \tag{7.15}$$

$$\text{such that} \quad t_{insp_i} - t_{insp_{i-1}} \geq 1.0 \; year \tag{7.16}$$

$$\text{given} \quad n, L, \boldsymbol{\Psi} \text{ and PDFs of } T \text{ for different details} \tag{7.17}$$

where $\mathbf{t}_{insp}$ = a vector consisting of the design variables of inspection times, t_{insp_i} = the *i*th inspection time in years, n = number of inspections, L = number of inspected details, and $\boldsymbol{\Psi}$ is a matrix containing the parameters of the inspection methods used for each inspection type for the three details (i.e., L = 3). Since the bridge consists of multiple fatigue critical details which may require inspections to be performed at a higher frequency than the biannual routine ones, a constraint has been imposed, as indicated by Equation (7.16), requiring that the time between successive NDI cycles should be at least one year.

The optimization algorithm can find the optimum inspection schedule using different inspection methods for each detail. For instance, the liquid penetrant inspection can be used for the third detail at each inspection while the first and second can be inspected using ultrasonic inspection. In this phase, the choice of the inspection method for each detail is applied by the user and the output is the inspection times. However, later in this application, the optimizer will be left to choose the most appropriate inspection method among a set of chosen methods for each detail. The optimization toolbox provided by version R2010a of MATLAB® (MathWorks Inc. 2010) is used to solve this single-objective optimization problem. The results of this optimization stage, provided in Table 7.3, show the optimum inspection times when using a single inspection method for the three details. Figure 7.6 shows the inspection schedule for the case of two inspections using different inspection methods. It can be seen from the results that as the quality of inspection decreases, the optimizer chooses the inspections to be performed later in life in order to maximize the probability of damage detection. It is also shown that for the selected *PoD* parameters, the eddy current technique can be used only three

times during the life giving almost 100% probability of crack detection before reaching the critical size (see Table 7.3).

Scheduling to find a tradeoff between the cost and the probability of damage detection before failure

For this optimization problem, the optimum inspection schedule is found as the solution of a bi-objective optimization problem where the first objective is to maximize the probability of detection before reaching the critical crack size $PD_{n,L}$ and the second objective consists of minimizing the expected inspection cost. The problem is formulated as follows

$$\text{Find } \mathbf{t}_{insp} = \left\{ t_{insp_1}, t_{insp_2}, t_{insp_3}, ..., t_{insp_n} \right\} \tag{7.18}$$

$$\text{to maximize } PD_{n,L} \text{ and minimize } C_{insp}^{T} \tag{7.19}$$

$$\text{such that } t_{insp_i} - t_{insp_{i-1}} \geq 1.0 \; year \tag{7.20}$$

$$\text{given } n, L, \boldsymbol{\Psi}, \mathbf{C}_{insp}, \text{ and PDFs of } T \text{ for different details} \tag{7.21}$$

where $\mathbf{C}_{insp}$ is a vector consisting of the cost of each inspection option. In this example, a fixed cost is applied at each inspection; this cost includes the access cost and a part of results interpretation and writing the report. The equipment cost is assumed to be different among different types of inspection. Moreover, for the cases where the optimizer chooses the ultrasonic and the eddy current methods at the same inspection, a penalty is added to the inspection cost to reflect the extra cost arising from providing the additional equipment and personnel to the bridge site. The cost of performing LPI for the three details is assumed to be 6000 USD, whereas, for using UI only or a combination of UI and LPI, the inspection cost is considered to be 8500 USD. In addition, a cost of 9500

USD is assumed for the case of performing ECI or ECI and LPI simultaneously. Finally, using both ECI and UI requires a cost of 10500 USD. It should be noted here that the cost of inspection methods depends heavily on the location of the detail within the bridge. For instance, if accessing the inspected detail requires traffic control, inspection methods which require surface preparation, such as the LPI and UI, would be very expensive. In these cases, the cost of LPI and UI may be higher than that of the ECI as the latter requires no surface preparation.

This optimization problem is solved using the genetic algorithms (GAs). This algorithm is based on the NSGA-II (Non-Dominated Sorting in Genetic Algorithms) algorithm developed by (Deb *et al.* 2002) and runs in the MATLAB environment. The GAs are used in this chapter due to their known robustness against convergence to local minima for this type of problems and due to the fact that they use the objective function and not its gradients (Frangopol 2011). The algorithm in this case provides a Pareto-optimal set of solutions which are optimum trade-offs between the two objectives. A solution is Pareto-optimal if there does not exist another solution that improves at least one objective without worsening another one (Arora 2012).

In this phase, the optimizer is left to choose the optimum time for each inspection in addition to the type of inspection for each detail. This is performed by using binary strings for describing the identifiers (ids) of the inspection options. The result of this process is a matrix in which each row represents an inspection plan and the binary codes in this row represent an inspection option. For simplicity, it is assumed that all the three methods of inspection are suitable for the three details. The Pareto-optimal solutions for the case of one inspection are provided in Figure 7.7. Figure 7.7 (a) shows the Pareto

front for the case of using an annual discount rate of money r = 0.0 % while Figure 7.7 (b) shows the optimization problem solution using r = 2.0 %. Each point on the Pareto-optimal solution set indicates a different inspection plan. This enables the decision maker to choose the inspection plan that suits the available budget and maintain the target probability of damage detection over a prescribed threshold. As shown by Figure 7.7, including the annual discount rate gives a more dispersed Pareto front. This is due to the fact that including the discount rate gives the opportunity of performing the same maintenance option at different times in the future where each one has different calculated present cost. Two selected inspection plans are identified on Figures 7.7 (a) and 7.7 (b) and the corresponding inspection schedules are shown in Table 7.4. Plan A1 corresponds to the solution with one inspection and a discount rate of 0% while plan A2 uses a discount rate of 2%. Both plans use the same inspection methods for each detail; however, when the discount rate is included, the optimization process provides multiple solutions using the same method but with different application times; each inspection plan has a unique cost and a corresponding $PD_{n,L}$. Thus, a solution that satisfies both the available budget and the required $PD_{n,L}$ can be easily selected.

Figure 7.8 (a) gives the Pareto-optimal inspection schedules for the case of two inspections considering an annual discount rate of money of 2%. Two inspection plans, B1 and B2, are selected on Figure 7.8 (a) and shown in details in Figure 7.8 (b) and Table 7.4. Each solution gives certain inspection times and types. It is observed from the results that solution B1 gives a *PD* of 0.995 while solution B2 gives 0.988 which is 0.7% decrease in the *PD*, However, solution B2 gives a cost reduction of almost 15.2%

compared to that of B1. This shows how valuable the results of the Pareto-optimization are; detailed examination of the results always yields highly efficient solutions.

Similar Pareto-optimal solutions are obtained for the case of three inspections and are shown in Figure 7.9 (a). Plans C1 and C2 are selected for evaluation and are shown in Table 7.4. Each plan yields a very high *PD* and they both assign the use of liquid penetrant to the three details at the last inspection. In fact, this was found in the majority of the Pareto-optimal solutions for the three inspections, where the optimizer chooses the low quality inspection to be performed later in the life of the structure since the probability of detecting larger cracks is high using the lower quality inspection method.

7.8 Example 7.2

This example applies the inspection scheduling methodology proposed in this chapter to same bridge analyzed in Example 7.1, where it is considered to be subjected to fatigue damage and corrosion in the steel reinforcement of the RC deck. The optimum inspection schedule is found as the solution of a bi-objective problem that minimizes the expected inspection cost and maximizes the probability of damage detection before failure. Two of the critical fatigue locations identified by the monitoring program are considered in this example. The first detail is the bottom web gap detail (i.e., Detail D1 in Example 7.1) while the second detail is the weld termination at the connection of a bracing gusset plate and the transverse connecting plate (i.e., Detail D3 in Example 7.1). These details are shown in Figures 7.2 and 7.4, respectively. In this example, Details D1 and D3 are considered in addition to the corrosion of the concrete deck for the inspection scheduling. The PDFs of the time to failure of the details D1 and D3 are shown in Figures 7.5 (a) and (c).

Since no data covering the concrete slab dimensions is given in the monitoring report, the corrosion initiation and propagation data are assumed and given in Table 7.5. In order to obtain the PDF of the time to failure for the corrosion damage, all the associated parameters are considered as lognormally distributed random variables. The failure for the corrosion location is considered to occur when the loss in the area of reinforcement bars reaches 10% of the initial cross-sectional area. Monte Carlo simulation is used for this purpose where the number of 10^5 simulations is found to be sufficient after extensive convergence analysis. The PDF of T for the corrosion damage is provided in Figure 7.10.

For inspection scheduling under corrosion damage, the *PoD* function is considered to be a function of the time-dependent damage intensity $\delta(t)$ which can be defined as (Kim & Frangopol 2011b)

$$\delta(t) = \begin{cases} 0 & \text{for } 0 \le t \le T_I \\ \dfrac{r_{corr}(t - T_I)}{d_o} & \text{for } t > T_I \end{cases} \tag{7.22}$$

Accordingly, the *PoD* function for corrosion detection can be defined as (Kim & Frangopol 2011b)

$$PoD(\delta) = \Phi\left(\frac{\delta - \delta_{0.5}}{\sigma_\delta}\right) \tag{7.23}$$

where $\delta_{0.5}$ = damage intensity at which the inspection method has 50% probability of detection; and σ_δ = standard deviation of the damage intensity $\delta_{0.5}$. The damage intensity $\delta_{0.5}$ reflects the quality of inspection; an inspection method with a lower $\delta_{0.5}$ will have a higher probability of damage detection.

The inspection scheduling is performed using the same formulation given by Equations (7.18)-(7.21). For fatigue inspection, three methods, namely the LPI, ECI, and UI are used. The *PoD* model given by Equation (7.8) is used with parameters of each inspection method given in Table 7.2. However, for corrosion inspection, the *PoD* model given by Equation (7.23) is used with $\delta_{0.5} = 0.05$. The same cost structure of LPI, ECI, and UI provided in Example 7.1 is also applied in this example. On the other hand, corrosion inspection is assumed to cost 9000 USD. The annual discount rate of money is considered to be 2%. This optimization problem is solved using GAs. The genetic algorithm for multi-objective optimization provided in MATLAB® version 2011a optimization toolbox (MathWorks Inc. 2011a) is used to find the Pareto-optimal solution set of the bi-objective optimization problem. The genetic algorithm is performed with 200 generations and a population of 150 for a given number of three inspections providing the Pareto-optimal solution set shown in Figure 7.11. The design variables and objective function values of two representative solutions are shown in Table 7.6. In this problem, the optimizer is left to choose the optimum time for each inspection in addition to the type of inspection for each detail. For simplicity, it is assumed that all the three methods of inspection are suitable for the two fatigue details. Tow representative solutions (i.e., F1 and F2) are selected and highlighted on Figure 7.11. The details of these solutions are provided in Table 7.6. As can be seen from the results, selecting solution F1 will yield a probability of detection of 0.88 while the inspection cost will be 25395, whereas solution F2 will give almost the same probability of detection but with significant decrease in the inspection cost.

7.9 Conclusions

This chapter presents a probabilistic inspection scheduling approach for deteriorating bridges using NDI techniques. The approach is capable of handling, simultaneously, multiple critical locations existing in the bridge. The method starts with predicting the time-dependent damage imitation and propagation of each location, which ultimately provides the PDF of the time to failure at each of the considered locations. The damage propagation information for different locations was used along with the *PoD* data of different inspection methods in a single-objective optimization process to select the optimum inspection times for different NDI methods. The objective of this optimization process is to maximize the probability of damage detection before failure of all inspected locations. Based on the provided inspection cost and damage propagation information, a bi-objective optimization process, aiming to maximize the probability of damage detection and minimize the total inspection cost, is formulated to find inspection times and select the best NDI technique for each location at different inspections. The following conclusions are drawn:

1- Establishing the inspection schedule that provides optimal inspection times and selects the best NDT technique for each location can be achieved using the proposed probabilistic optimization process.

2- Based on the studied examples, higher quality inspection methods do not have to be performed routinely throughout the lifetime of the structure. A limited number of optimally planned inspections can be enough to yield an acceptable *PD*. In fact, some inspection techniques can provide, compared to methods with lower quality, a significantly higher *PD* after a relatively small number

of inspections. The number of inspections, as well as their application times, can be provided by the solution of the optimization process.

3- Including a realistic discount rate of money improves the flexibility of the inspection planning by providing more dispersed Pareto-optimal solution fronts. Multiple solutions on this front may indicate the same type of NDI methods (with different application times); however, each solution corresponds to unique cost and *PD* pair allowing the bridge managers to select the best solution which fits the management constraints.

4- The proposed approach can be easily extended to consider additional types of time-dependent deteriorating mechanisms such as corrosion-induced fatigue affecting different locations of the bridge.

5- Due to the high uncertainty associated with the damage propagation, the results of the proposed method can be enhanced by including the ability to update the damage initiation and propagation model parameters information for different details after each inspection (as discussed in detail in Chapter 6 of this study).

Variable		Notation (Units)	Mean value	Coefficient of Variation	Type of distribution
Material crack growth parameter		C	2.18×10^{-13}	0.2	Lognormal
Material crack growth exponent		m	3	-	Deterministic
Detail D1	Initial crack size	a_o (mm)	1.27	0.2	Lognormal
	Daily number of cycles	N_{avg}	7500	0.1	Lognormal
	Stress range	S_{re} (MPa)	34.5	0.1	Weibull
	Critical crack size	a_f (mm)	10.16	-	Deterministic
Detail D2	Initial crack size	a_o (mm)	1.27	0.2	Lognormal
	Daily number of cycles	N_{avg}	1464	0.1	Lognormal
	Stress range	S_{re} (MPa)	17.25	0.1	Weibull
	Critical crack size	a_f (mm)	10.16	-	Deterministic
Detail D3	Initial crack size	a_o (mm)	3.175	0.2	Lognormal
	Daily number of cycles	N_{avg}	3329	0.1	Lognormal
	Stress range	S_{re} (MPa)	23.46	0.1	Weibull
	Critical crack size	a_f (mm)	9.525	-	Deterministic

Table 7.2 Adopted parameters of the *PoD* functions ($PoD = 1 - \Phi\left(\frac{\ln(a) - \lambda}{\zeta}\right)$) for eddy current, ultrasonic, liquid penetrant inspections (based on Fosyth & Fahr 1998)

Inspection Method	λ	ζ
Eddy current inspection (ECI)	-0.967584	-0.571075
Ultrasonic inspection (UI)	0.122218	-0.304791
Liquid penetrant inspection (LPI)	0.828552	-0.423416

Table 7.3 Inspection times and objective value for the single-objective optimization

Inspection method	n	Inspection times				$PD_{n,3}$
		t_{insp_1}	t_{insp_2}	t_{insp_3}	t_{insp_4}	
Eddy current inspection*	1	5.12	-	-	-	0.9824
	2	3.43	5.99	-	-	0.9996
	3	3.31	4.31	6.51	-	0.9999
Ultrasonic inspection	1	7.83	-	-	-	0.7838
	2	6.27	12.55	-	-	0.9416
	3	5.09	7.77	16.70	-	0.9802
	4	4.54	6.00	9.72	17.62	0.9908
Liquid penetrant inspection	1	11.75	-	-	-	0.2108
	2	9.08	16.32	-	-	0.4317
	3	7.82	10.91	18.46	-	0.5655
	4	7.21	9.11	13.42	19.67	0.6512

* For eddy current inspection, three inspections are sufficient to give the maximum probability of detection

[redacted]

Inspection plan	First inspection				Second inspection				Third inspection				Present Cost (USD)	[redacted]
	t_{insp_1} (years)	Inspection Method			t_{insp_2} (years)	Inspection Method			t_{insp_3} (years)	Inspection Method				
		D1	D2	D3		D1	D2	D3		D1	D2	D3		
A1*	5.12	ECI	ECI	ECI	-	-	-	-	-	-	-	-	9500	0.982
A2†	10.8	ECI	ECI	ECI	-	-	-	-	-	-	-	-	7665	0.786
B1†	4.33	ECI	ECI	ECI	14.35	UI	UI	LPI	-	-	-	-	15117	0.995
B2†	4.95	ECI	ECI	ECI	17.90	LPI	LPI	LPI	-	-	-	-	12822	0.988
C1†	3.48	ECI	ECI	ECI	6.13	ECI	ECI	ECI	14.38	LPI	LPI	LPI	21795	0.999
C2†	4.58	ECI	ECI	LPI	11.51	ECI	ECI	LPI	20.3	LPI	LPI	LPI	20253	0.997

[redacted]

Table 7.5 Descriptors of different random variables and deterministic parameters for Corrosion of RC slab

Variable	Mean	COV
do (mm)	15.88	0.02
x (mm)	30.2	0.02
C_o (g/mm^3)	0.15	0.1
C_{th} (g/mm^3)	109.68	0.1
D (mm^2/yr)	0.037	0.15
r_{corr} (mm/yr)	0.0582	0.3

Table 7.6 Design variables and objective values of selected optimum solutions of Example 7.2

Plan	First Inspection			Second Inspection			Third Inspection			Present Cost (USD)	$PD_{3,3}$
	t_{insp1} (years)	Inspection Method		t_{insp2} (year)	Inspection Method		t_{insp3} (years)	Inspection Method			
		D1	D3		D1	D3		D1	D3		
F1	3.55	ECI	ECI	5.55	ECI	ECI	8.5	ECI	ECI	25395	0.88
F2	4.95	UI	UI	8.4	UI	LPI	12.9	UI	LPI	22275	0.86

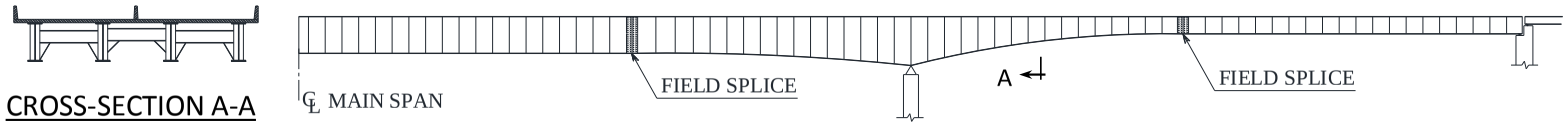

CROSS-SECTION A-A

ELEVATION

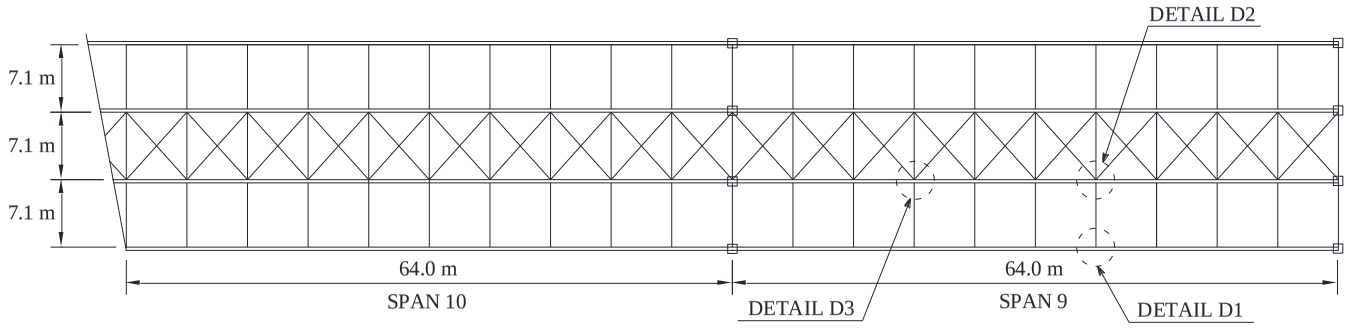

PLAN

[redacted]

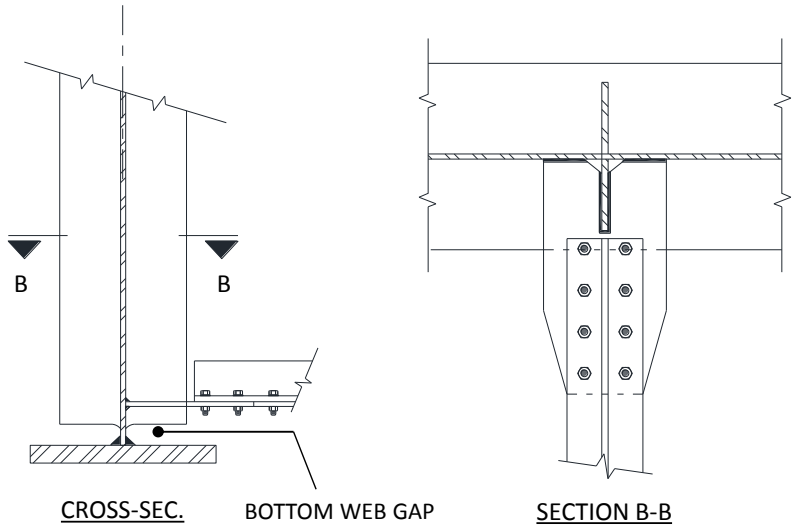

Figure 7.2 Detail D1 in Figure 7.1: bottom web gap (adapted from Connor and Fisher 2001)

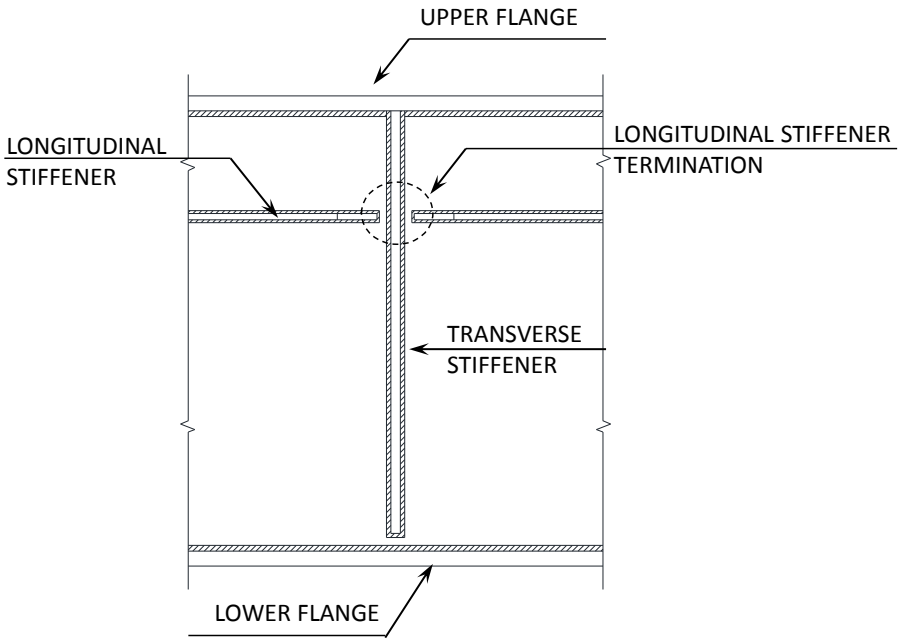

Figure 7.3 Detail D2 in Figure 7.1: longitudinal stiffener termination (adapted from Connor & Fisher 2001)

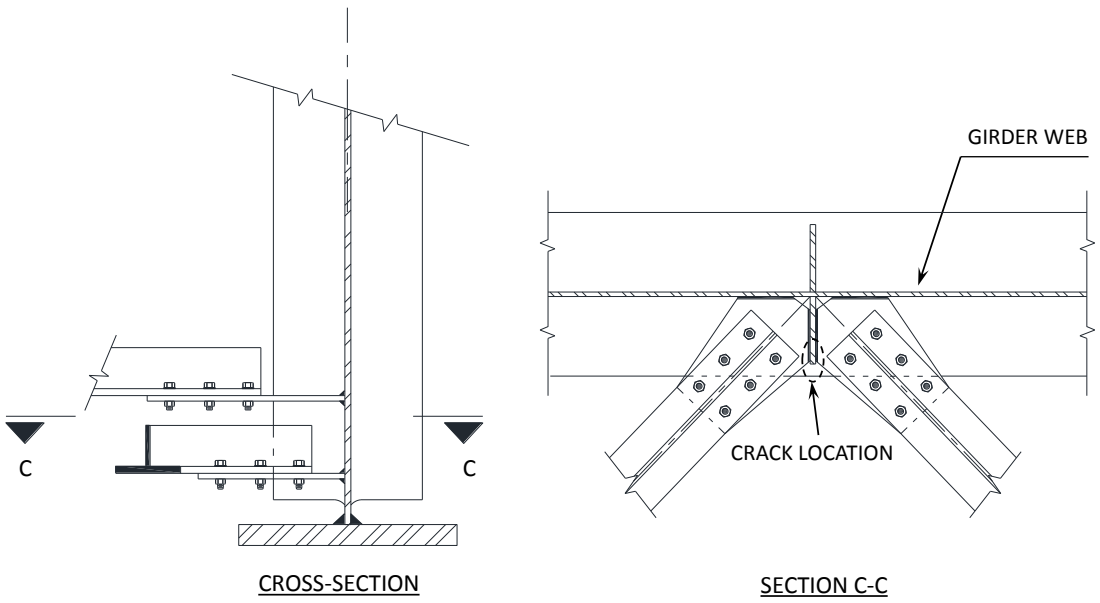

Figure 7.4 Detail D3 in Figure 7.1: gusset plate to transverse connecting plate welds (adapted from Connor & Fisher 2001)

(a)

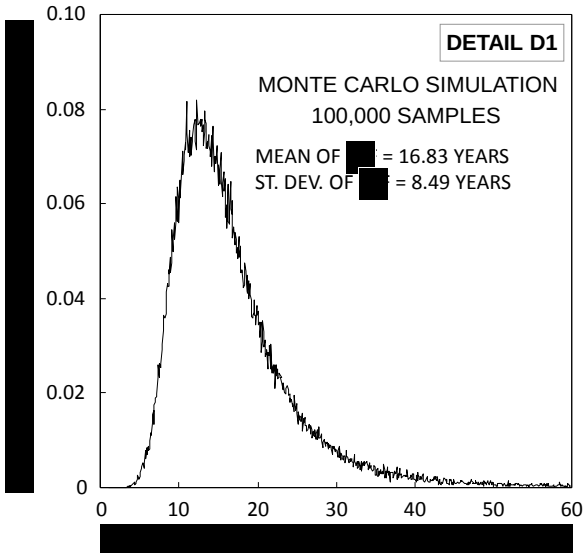
DETAIL D1
MONTE CARLO SIMULATION
100,000 SAMPLES
MEAN OF [redacted] = 16.83 YEARS
ST. DEV. OF [redacted] = 8.49 YEARS
0.10
0.08
0.06
0.04
0.02
0
0
10
20
30
40
50
60

(b)

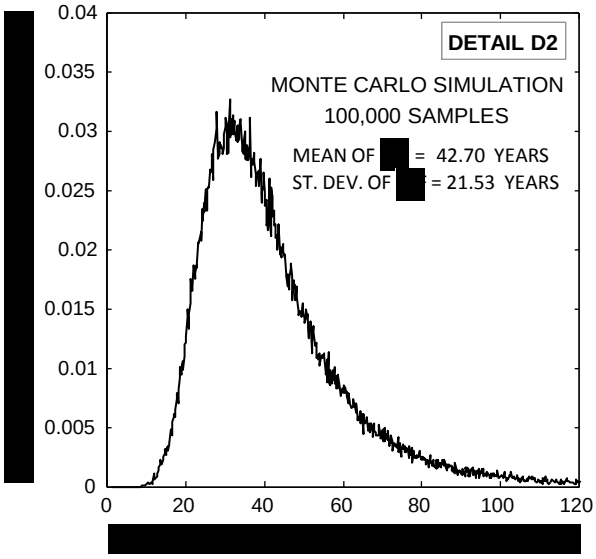
DETAIL D2
MONTE CARLO SIMULATION
100,000 SAMPLES
MEAN OF [redacted] = 42.70 YEARS
ST. DEV. OF [redacted] = 21.53 YEARS
0.04
0.035
0.03
0.025
0.02
0.015
0.01
0.005
0
0
20
40
60
80
100
120

(c)

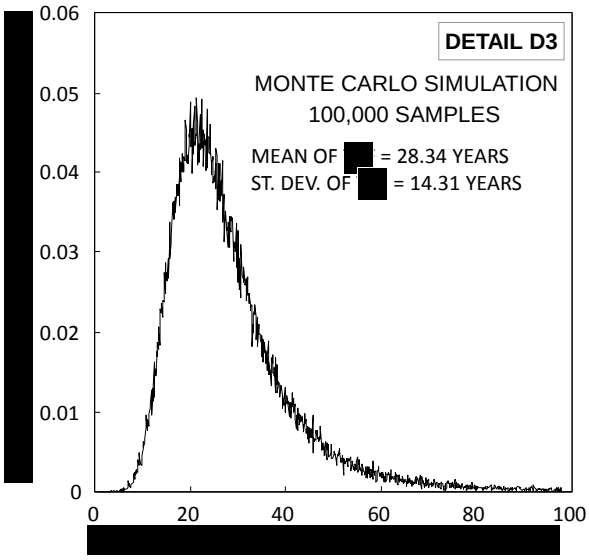

Figure 7.5 PDF for time to failure of (a) Detail D1; (b) Detail D2; and (c) Detail D3

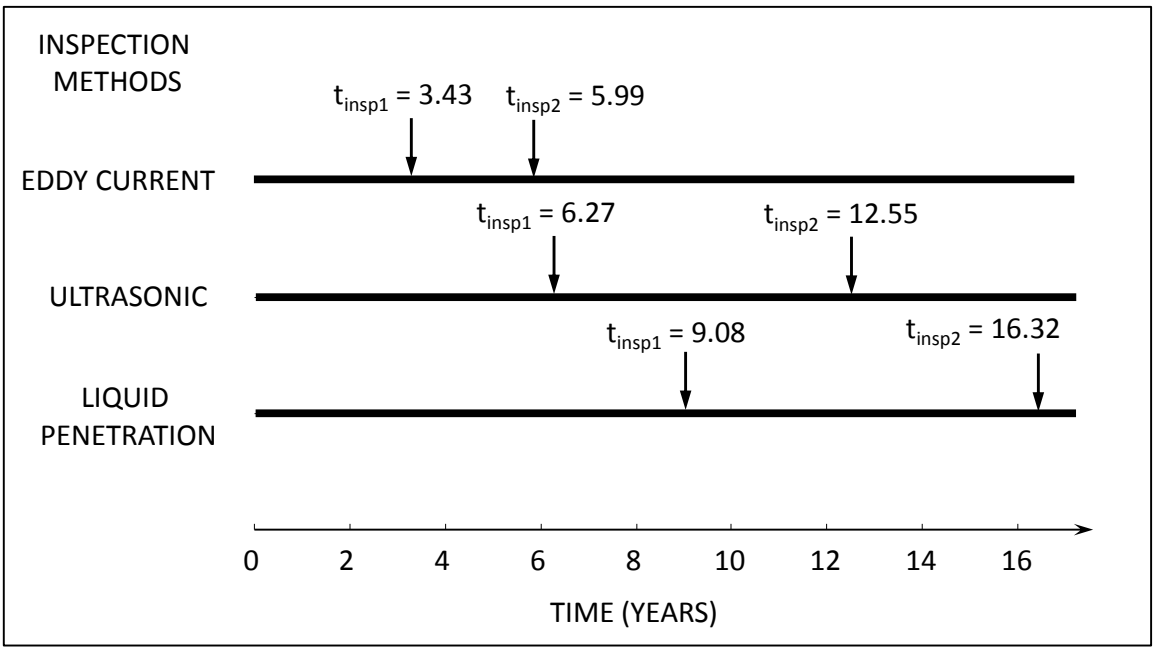

Figure 7.6 Optimum inspection schedules resulting from the single-optimization process of the case of two inspections

(a)

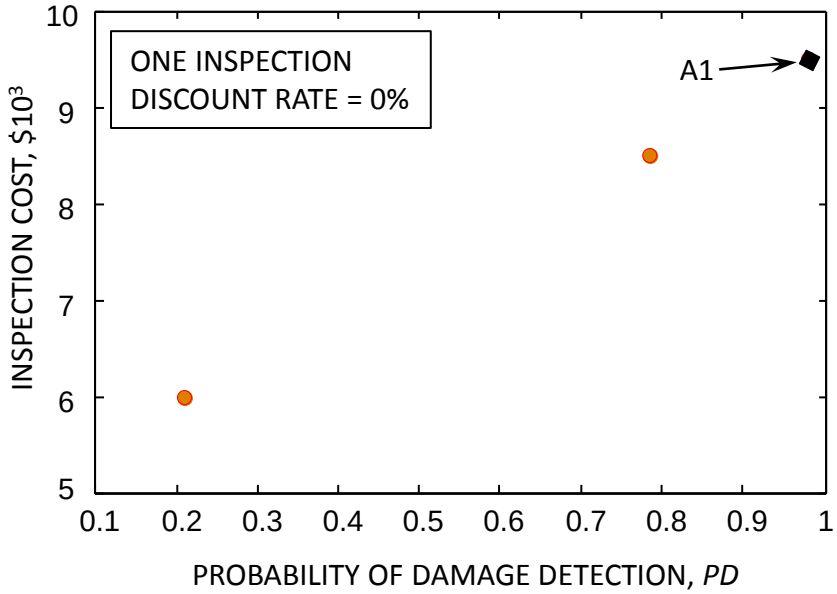

(b)

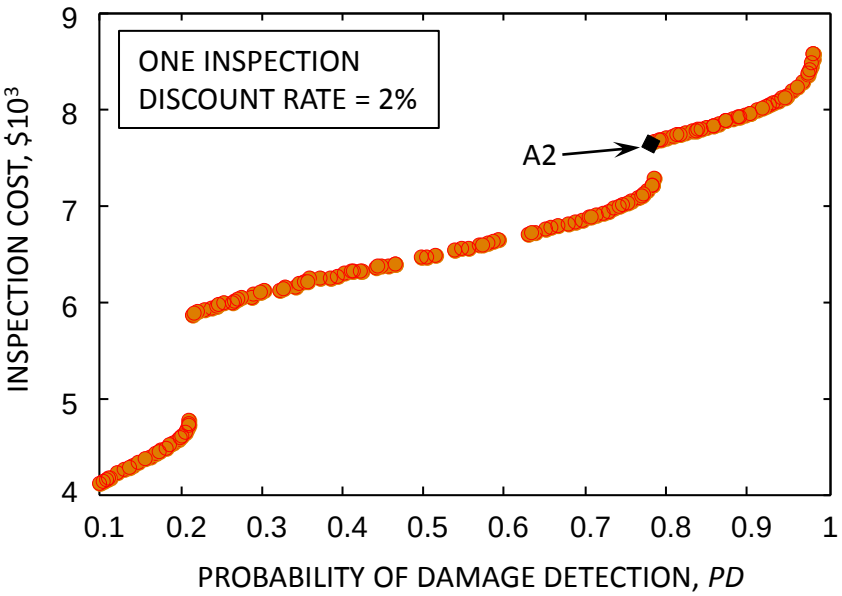

Figure 7.7 Pareto-optimal solutions for the case of one inspection with (a) discount rate = 0%; and (b) discount rate = 2%

(a)

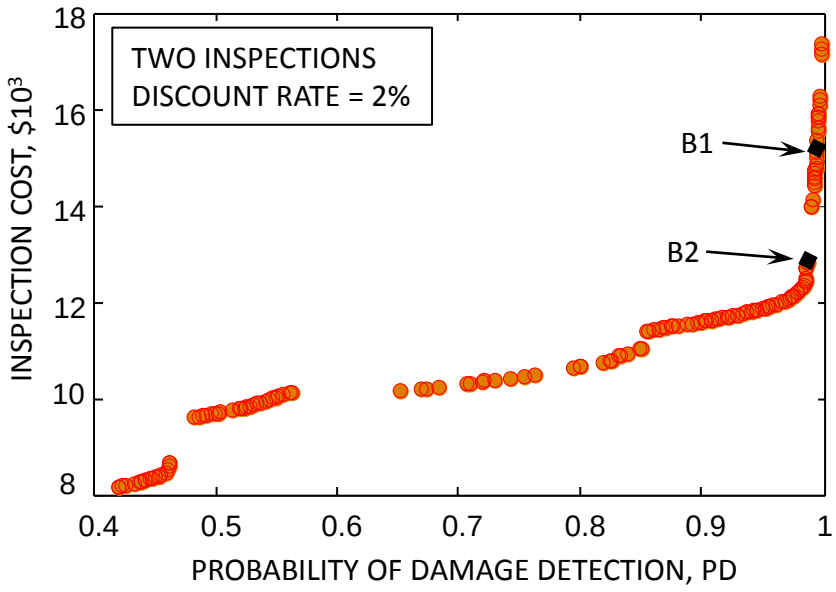

(b)

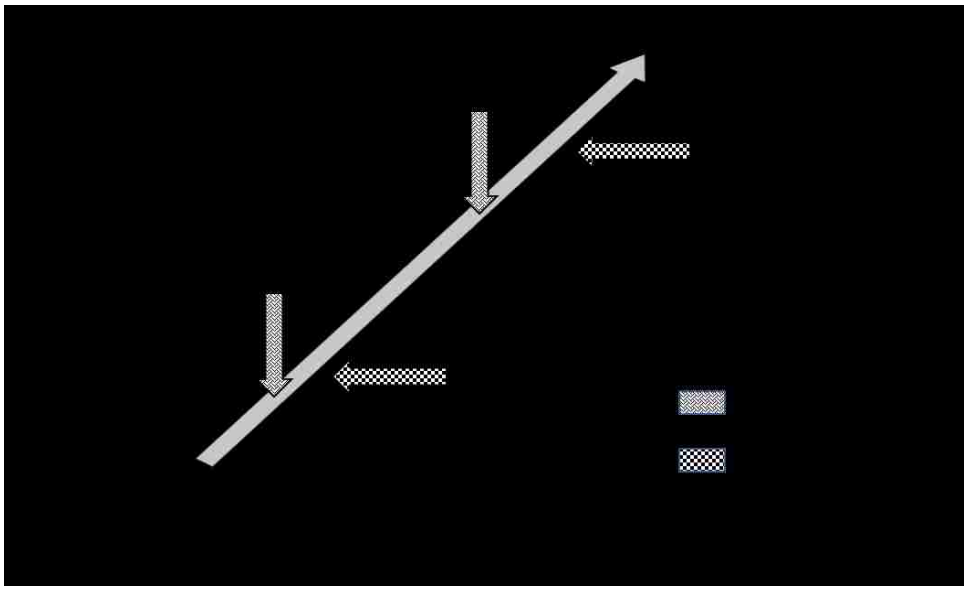

Figure 7.8 Optimal solutions for the case of two inspections (a) Pareto-optimal solution set, and (b) inspection schedules B1 and B2

(a)

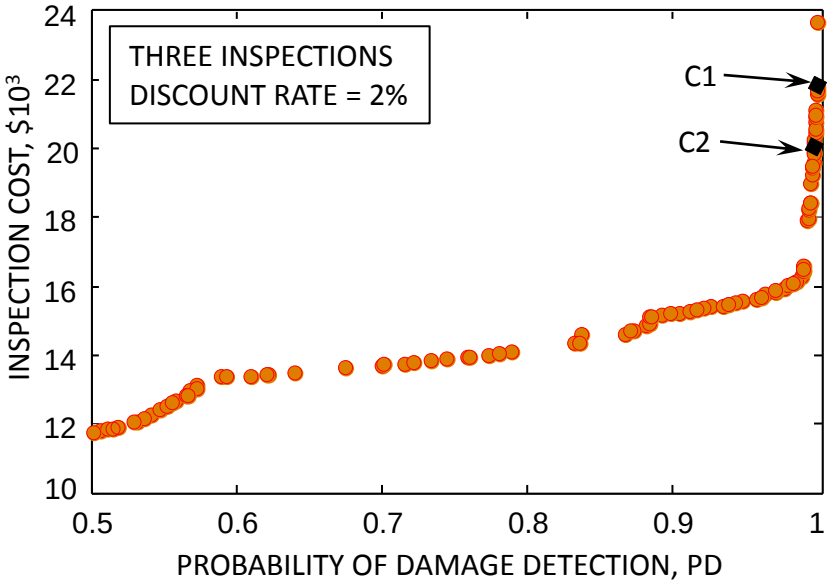

(b)

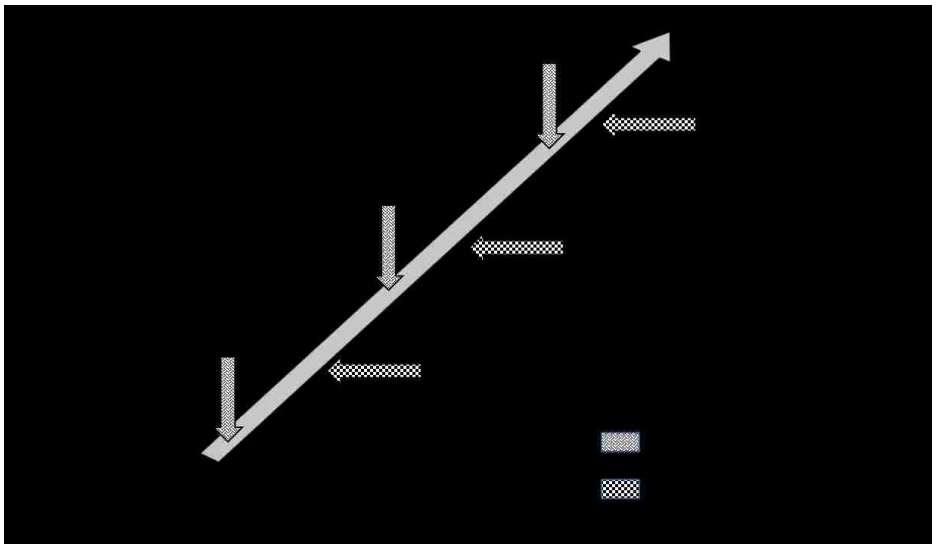

Figure 7.9 Optimal solutions for the case of three inspections (a) Pareto-optimal solution set, and (b) inspection schedules C1 and C2

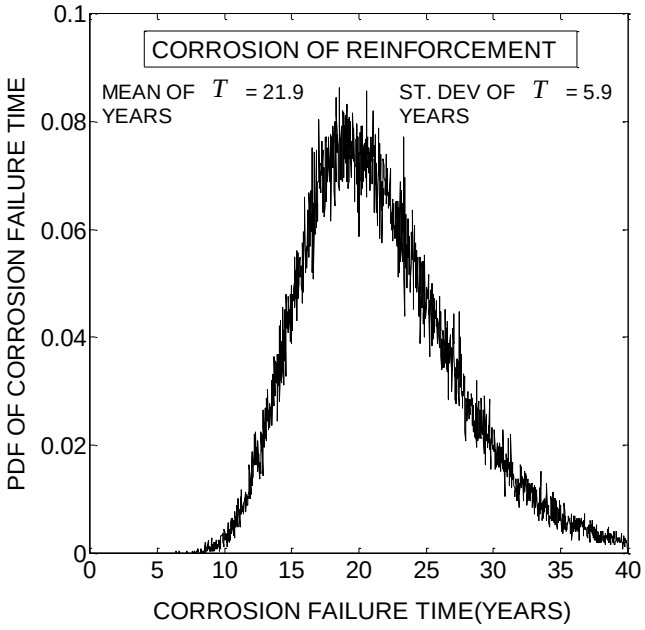

Figure 7.10 PDF of time to failure for corrosion of steel reinforcement

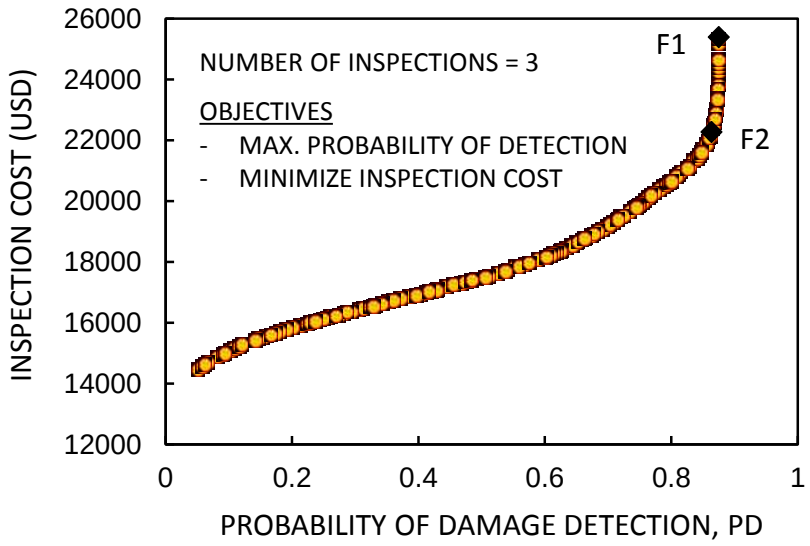

Figure 7.11 Pareto-optimal solution for three inspections

CHAPTER 8 SYSTEM-BASED INSPECTION AND MAINTENANCE OPTIMIZATION FOR BRIDGES UNDER CORROSION DETERIORATION

8.1 Overview

This chapter proposes a system-based optimization procedure for life-cycle inspection and maintenance planning for aging bridges. In this procedure, the structural system interactions and correlations are accounted for by modeling the structure as a series, parallel, or a series-parallel system whose components are subjected to time-dependent deterioration phenomena. Different possible repair options are considered depending on the damage state and the outcomes of each inspection. For each component, essential or preventive maintenance implemented to reduce the system failure rate, are performed when inspection results indicate that the prescribed threshold damage levels have been reached. Otherwise, no repair is performed. Optimum inspection and maintenance plans are achieved by solving an optimization problem with the objectives of minimizing both the expected system failure rate and expected cumulative inspection and maintenance cost over the life-cycle of the structure. The proposed approach is applied to an existing bridge. The work in this chapter is based on the published paper Barone *et al.* (2014).

8.2 Background

System-based life-cycle probabilistic concepts and methods for scheduling lifetime maintenance plans of deteriorating structural systems have been largely discussed in recent years and several approaches have been proposed. An extensive review of such

methods is reported in Frangopol & Liu (2007) and Frangopol (2011). Among these approaches, and to consider the system interactions, several methodologies are based on (a) structural reliability and probability of failure, (b) risk, or (c) lifetime distribution functions.

The reliability index has been implemented in several papers for maintenance planning of deteriorating structures, either using decision-tree analysis, single objective optimization, or multi-objective optimization (Mori & Ellingwood 1994; Estes & Frangopol 2003; Orcesi & Frangopol 2011a). Risk is also related to the annual probability of failure of the structure, but it considers economic losses due to failure. Risk-based decision making takes into account both the direct losses associated with failure (e.g. repair or rebuilding costs) (Ramirez *et al.* 2012) and the indirect losses caused by non-operational state of the system (Ang & Tang 1984; Ang & De Leon 2005).

In contrast to the reliability index and risk, defined in general as a function of the annual failure probability for a specific point-in-time, lifetime distributions keep memory of the events on the system during the structural life-cycle. Optimal maintenance planning using lifetime functions has been proposed considering multi-objective optimization based on system survivor function (Orcesi & Frangopol 2011b; Okasha & Frangopol 2010). Other performance indicators based on lifetime functions include the failure rate which has been considered for preventive maintenance of series systems in Caldeira Duarte *et al.* (2006). This indicator provides the probability of structural failure within a prescribed time interval conditioned on the structural survival up to this time interval. Additionally, it gives an indication on the rate of decrease in the structural

reliability, an attribute that makes it a valuable indicator in forecasting the structural performance for life-cycle planning purposes.

In this chapter, an approach for optimal inspection and maintenance planning for structural systems subjected to aging phenomena is proposed. The approach is system-based, in which the interaction of components in the system is considered by modeling the structural configuration as series, parallel, or series-parallel. Two different types of maintenance actions are considered (i.e., essential and preventive maintenance). The selection of the appropriate maintenance action is based on inspection outcomes and predefined damage level thresholds. For each structural component, when the damage level exceeds a certain threshold, essential maintenance (EM), which results in the total restoration of the initial component performance, is performed. For minor deterioration levels, preventive maintenance (PM), which stops the damage propagation for an effective period of time, is performed. Finally, when the inspection results report negligible damage levels, no repair is performed. Accuracy of inspection is taken into account as a function of the imperfections affecting inspection results. The optimum management plans are established by solving a bi-objective optimization problem which minimizes both the maximum expected system failure rate over the system life-cycle and the expected total cost of all inspection and maintenance actions. The proposed approach is applied to a general three-component system and an existing bridge subjected to deterioration due to corrosion of the steel girders and the reinforcement bars of the bridge deck.

8.3 Inspection and Maintenance Options

In most situations, the decision of repairing the structure and the extent of performed maintenance depends on the inspection outcome. Advanced degradation of the structural performance may require significant repairs to considerably improve the structural reliability. Preventive maintenance may be applied to reduce the failure rate of the structure if the structure has low deterioration and an acceptable service level. Moreover, for structures with minor degradation effects, it may be decided not to perform any maintenance actions. In this chapter, detailed in-depth inspections which implement non-destructive techniques are considered. Therefore, it can be assumed that these inspections can obtain detailed and accurate data about the deterioration state of inspected structural components. Several different techniques for corrosion damage detection in RC members have been developed in recent years, each one having its own advantages, costs and applicability (e.g., half-cell potential tests, infrared thermography, ground penetrating radar, among others) (Carino 1999, Clark *et al.* 2003, Wang *et al.* 2011).

In this chapter, the effect of the performance degradation is modeled as a continuous reduction of the structural capacity (resistance) $R_i(t)$ of the components over time. In-depth inspections are able to identify the damage level and to provide an estimation of the residual capacity of the components at the inspection time. On the other hand, inspection results are affected by uncertainties and imperfections. In order to consider these imperfections, a measurement error can be assumed to follow a normal distribution with zero mean. Taking into account both the imperfections associated with the structural resistance prediction and the inspection result, the estimated capacity $R_i^{(est)}$ for the component i immediately after inspection time t_{insp} can be considered as a

random variable having the mean of the predicted structural capacity at that time $\mu_{R_i}\left(t_{insp}\right)$ and standard deviation $\sigma_{insp} = k_{insp}\sigma_{R_i}\left(t_{insp}\right)$, where σ_{R_i} is the standard deviation of resistance accounting for the imperfections associated with the predictive model and $k_{insp} \geq 1$ is an index of the inspection accuracy with $k_{insp} = 1$ if no inspection imperfections are considered (i.e., perfect inspection).

Similar to the maintenance selection method proposed in Chapter 5, three possible maintenance options are considered for each component, in which the selection of the most appropriate method is based on the estimated capacity after the in-depth inspection $R_i^{(est)}$. Two different thresholds are defined for each component to determine the appropriate maintenance option based on its initial capacity. These thresholds are denoted $\delta_{EM,i}$ and $\delta_{PM,i}$ for EM and PM, respectively. However, in this approach $\delta_{EM,i}$ is smaller that $\delta_{PM,i}$ (i.e., $\delta_{EM,i} < \delta_{PM,i}$) since they are defined with respect to the structural resistance. This is in contrast to the thresholds d_A and d_B (i.e., $d_B > d_A$) defined in Chapter 5 with respect to the damage level. As shown in Figure 8.1 (a), EM results in total restoration of the component performance to its original value, and is performed when $R_i^{(est)} \leq \delta_{EM,i}$. Preventive maintenance, which blocks the deterioration for a certain period (as shown in Figure 8.1 (b)), is applied if the estimated component capacity is between the two thresholds, i.e. $\delta_{EM,i} < R_i^{(est)} \leq \delta_{PM,i}$. Finally, no repair is considered if $R_i^{(est)} > \delta_{PM,i}$. Therefore, for each component i, the probability of performing essential maintenance $P_{EM,i}$, preventive maintenance $P_{PM,i}$, or no repair $P_{NR,i}$ after one inspection

at a given instant of time can be evaluated by integration of the PDF of the estimated residual capacity $f_{R,i}(x,t)$, as:

$$\begin{aligned} P_{EM,i}(t) &= \int_0^{\delta_{EM,i}} f_{R,i}(x,t)\,dx \\ P_{PM,i}(t) &= \int_{R_{EM,i}}^{\delta_{PM,i}} f_{R,i}(x,t)\,dx \\ P_{NR,i}(t) &= 1-\left(P_{EM,i}(t)+P_{PM,i}(t)\right) \end{aligned} \tag{8.1}$$

These probabilities are graphically represented as the areas shown in Figure 8.2.

When several consecutive inspection/maintenance actions are considered, the set of possible events that may occur can be represented by an event tree model in which each branch is associated with a sequence of essential or preventive maintenance, or inspections with no maintenance. Each branch has a probability of occurrence $P(\mathrm{B}_k)$, where k is the branch number. Figure 8.3 shows the event tree associated with a single component subjected to two inspections. Possible repair options following each inspection are shown together with the probability associated with each branch. Therefore, for a system with N_C components and N_O possible repair options for each component, the total number of different branches after N_{insp} inspection is given by $N_b = (N_O)^{N_{insp}N_C}$.

8.4 Annual Failure Rate and Expected Total Maintenance Cost

In this chapter, the expected system failure rate $h_{sys}(t)$ is considered as the structural system performance indicator. The average system failure rate is defined as the probability of failure occurring between t and $t+\Delta t$, given that the system has survived up to time t, and averaged over the interval $[t,\ t+\Delta t]$ (Leemis 1995):

$$h_{sys}(t) = \frac{P\left[t \le T_F \le t + \Delta t \mid T_F \ge t\right]}{\Delta t} \tag{8.2}$$

The expected system failure rate may be expressed in terms of system survivor function $S_{sys}(t)$ (see Equation 2.10) as

$$h_{sys}(t) = \frac{S_{sys}(t) - S_{sys}(t + \Delta t)}{S_{sys}(t)\Delta t} \tag{8.3}$$

The use of the system failure rate takes advantage of the conditional failure time probability which provides additional information when compared to other performance indicators, such as the point-in-time reliability index which keeps no memory of the previous system events. As $\Delta t \to 0$, Equation (8.3) becomes the instantaneous failure rate, which is by definition the hazard function.

In order to compute the annual system failure rate in the examples of this chapter, the point-in-time annual probability of failure has been first evaluated by using the software RELSYS (Estes & Frangopol 1998). The point-in-time probability of system failure is defined as the probability of violating any of the limit state functions that define its failure modes (see Equation 2.6). For a series-parallel system, RELSYS computes the failure probability of the individual components. Then, each subsystem with parallel configuration is reduced to a single component having the same reliability of the initial subsystem. This reduces the entire structural system to an equivalent series-system whose reliability is equivalent to the initial system. Next, the software reduces this series system to a single component and evaluates its point-in-time probability of failure and reliability. Once the point-in-time annual failure probability $P_{sys}(t)$ for the system is known, the

time-dependent failure probability at the year t_n can be evaluated as (Decò & Frangopol 2011):

$$TDP_{sys}\left(t_n\right)=\sum_{i=1}^{n}P_{sys}\left(t_i\right)\prod_{j=1}^{i-1}\left(1-P_{sys}\left(t_{j-1}\right)\right) \tag{8.4}$$

where TDP_{sys} represents the cumulative distribution function of the system time-to-failure (i.e., $F_T(t)$). Hence, the system survivor function is:

$$S_{sys}\left(t\right)=1-TDP_{sys}\left(t\right) \tag{8.5}$$

Finally, by considering Equations (8.3) and (8.5), the annual system failure rate at the year t_n is:

$$h_{sys}\left(t_n\right)=\frac{TDP_{sys}\left(t_{n+1}\right)-TDP_{sys}\left(t_n\right)}{1-TDP_{sys}\left(t_n\right)} \tag{8.6}$$

The application of PM and EM reduces the annual system failure rate. The magnitude of this reduction depends on the maintenance application times, deterioration rate of the structural capacity, and loading conditions.

8.4.1 Life-cycle cost

The expected total cost of the maintenance plan is obtained herein as:

$$E\left[C_{tot}\right]=\sum_{k=1}^{N_b}P\left(\mathrm{B}_k\right)C_k \tag{8.7}$$

$P\left(\mathrm{B}_k\right)$ is the occurrence probability of branch *k*, C_k is the total cost associated with the *k*th branch, obtained by summing inspection cost, as well as preventive and essential maintenance costs, for the considered branch:

$$C_k = \sum_{i=1}^{N_{insp}} \frac{C^{(insp)}}{\left(1+r_d\right)^{t_{insp}^{(i)}}} + \sum_{j=1}^{N_{PM}} \frac{C_j^{(PM)}}{\left(1+r_d\right)^{t_{PM}^{(j)}}} + \sum_{j=1}^{N_{EM}} \frac{C_j^{(EM)}}{\left(1+r_d\right)^{t_{EM}^{(j)}}} \tag{8.8}$$

where $C^{(insp)}$ is the inspection cost, $C_j^{(PM)}$ and $C_j^{(EM)}$ are the costs of the *j*-th preventive and essential maintenance actions, respectively, $t_{insp}^{(i)}$ is the *i*-th inspection time, $t_j^{(PM)}$ and $t_j^{(EM)}$ are the *j*-th preventive and essential maintenance times, respectively, and r_d is the annual discount rate of money. In the following examples, r_d is assumed to be zero.

8.5 Example 8.1

Considering a single component subjected to a time-dependent increasing axial force and a cross-sectional area reduction over time, the structural failure probability can be assessed using the following performance function:

$$g(t) = A(t)\, f_y - L(t) \tag{8.9}$$

where $A(t)$ and $L(t)$ are the time-variant cross-sectional area and axial load, respectively, and f_y is the yield strength of the component material. The deterioration in the area is considered deterministically in the form of a continuous loss of cross-sectional area over time (Okasha & Frangopol 2009). The cross-sectional area $A(t)$ is considered a random variable with mean $\mu_A(t)$ and standard deviation $\sigma_A(t)$ given by:

$$\begin{aligned} \mu_A(t) &= \left(1-DR\right)^t A(0) \\ \sigma_A(t) &= 0.03\left(1+DR\right)^t A(0) \end{aligned} \tag{8.8}$$

where $A(0)$ is the initial cross-sectional area and DR is the deterioration rate. The load $L(t)$ is modeled as a random variable with mean:

$$\mu_L(t) = (1+l)^t L(0) \tag{8.10}$$

and coefficient of variation (COV) of 5%, where $L(0)$ is the initial load and l is the load increase parameter. The initial cross-sectional area $A(0)$ and the annual deterioration rate DR are considered to be 3.0 cm^2 and $2\text{x}10^{-3}$, respectively. The initial load and its annual increase rate are assumed 60 kN and $2\text{x}10^{-4}$, respectively. The yield stress is assumed to follow a lognormal distribution with parameters shown in Table 8.1, and $A(t)$ and $L(t)$ are assumed Gaussian. The annual failure rates resulting from performing two inspections after 15 and 25 years of service are presented in Figure 8.4 (a) for three possible branches of the event tree presented in Figure 8.3.

The annual failure rate profiles in Figure 8.4 (a) show the effect of the EM (i.e., restoring the structural resistance to the initial value) and PM (stopping the further reduction in the structural resistance for an effective period ΔT_{PM} of 5 years). As expected, the annual failure rate depends significantly on the maintenance activities performed after each inspection. In order to efficiently represent the effect of the maintenance plan on the structural resistance by means of a single function that takes into account all the possible events (i.e. preventive or essential maintenance or no repair at each inspection time), the expected annual failure rate, obtained as the summation of the annual failure rates associated with each branch and weighted by their occurrence probabilities $P(\mathrm{B}_k)$, is considered herein as

$$E\left[h_{sys}(t)\right] = \sum_{k=1}^{N_b} P(\mathrm{B}_k) h_{sys,k}(t) \tag{8.11}$$

where N_b is the total number of branches and $h_{sys,k}(t)$ is the annual failure rate associated with branch k.

Probabilities of occurrence of the branches $P(\mathrm{B}_k)$ for the single component, used to evaluate the expected annual failure rate and expected total cost, are next calculated considering the estimate residual cross-sectional area of the component $A^{(est)}$ after an in-depth inspection. The two thresholds δ_{EM} and δ_{PM} are defined with respect to the initial cross-sectional area of the component to determine the appropriate maintenance type. For this example, three different threshold sets are considered as follows:

threshold T1: $\delta_{EM,T1} = 0.95A(0)$; $\delta_{PM} = 0.98A(0)$

threshold T2: $\delta_{EM,T2} = 0.90A(0)$; $\delta_{PM} = 0.98A(0)$

threshold T3: $\delta_{EM,T3} = 0.85A(0)$; $\delta_{PM} = 0.98A(0)$

Accordingly, if $A^{(est)} \le \delta_{EM,T_i}$, essential maintenance is performed, whereas preventive maintenance is performed if $\delta_{EM,T_i} < A^{(est)} \le \delta_{PM}$. Otherwise, no repair is considered. Therefore, for the threshold set T1, if the inspection reveals that the residual area is less than $0.95A(0)$, essential maintenance has to be performed. Additionally, if the residual area obtained by inspection results is between $0.95A(0)$ and $0.98A(0)$, preventive maintenance is performed. Finally, if the residual area is more than $0.98A(0)$ no maintenance is performed after the inspection.

Figure 8.4(b) illustrates expected annual failure rates for the three threshold sets T1, T2 and T3, assuming inspections to be performed at 15 and 25 years. As shown, by increasing δ_{EM}, the probability of performing essential increases while that of performing preventive maintenance decreases. Therefore, the thresholds set T1 yields the lowest expected annual failure rate and the highest expected total cost.

8.6 Bi-objective Optimization for Establishing Optimal Intervention Plans

A bi-objective optimization procedure is next proposed to determine the optimal maintenance plan of deteriorating structural systems. The proposed approach simultaneously minimizes the lifetime maximum expected system failure rate and the expected total cost. The design variables are the optimum inspection times. To define the optimization problem several parameters have to be defined including (a) the observation time window t_{tot}, (b) the total number of inspections N_{insp} in the lifetime plan, (c) the performance functions $g_i(t)$ for the system components, (d) the in-depth inspection and repair costs, and (e) the in-depth inspection accuracy parameter.

Based on these assumptions, the Pareto-optimal solution front (Deb 2001) of maintenance plans can be obtained as the solution of the following optimization problem:

$$\text{Given: } t_{tot}, N_{insp}, g_i(t), C^{(insp)}, C_i^{(PM)}, C_i^{(EM)}, k_{insp} \tag{8.12}$$

$$\text{Find: } \mathbf{t}_{insp} = \left\{ t_{insp}^{(1)}, \ldots, t_{insp}^{(N_{insp})} \right\} \tag{8.13}$$

$$\text{To minimize: } \begin{cases} h_{\max} = \max\left(E\left[h_{sys}(t) \right] \right) \\ E\left[C_{tot} \right] \end{cases} \quad 0 \le t \le t_{tot} \tag{8.14}$$

$$\text{Such that: } t_{insp}^{(k+1)} - t_{insp}^{(k)} \geq \Delta T_{PM} \qquad k = 1, ..., N_{insp} \tag{8.15}$$

where $C^{(insp)}$, $C_i^{(PM)}$ and $C_i^{(EM)}$ are the inspection, preventive and essential maintenance costs, respectively, and k_{insp} is the constant associated with the inspection accuracy previously introduced. The constraints in Equation (8.15) have been added to guarantee that, on average, a new preventive maintenance is not performed before the effect of the previous one has ended.

8.7 Example 8.2

In this example, three different configurations of three-component systems, shown in Figure 8.5, have been analyzed. The system models cover the series, series-parallel, and parallel configurations. The performance function has been defined for each component, analogously to the single-component in Example 8.1, through Equations (8.9) – (8.11), taking into account the cross-sectional area loss of the components and increase of loads over time. Values of the parameters associated with the initial cross-sectional areas $A_i(0)$, deterioration rates DR_i, initial load $L(0)$ and coefficient l, as well as the components yield stresses $f_{y,i}$ are reported in Table 8.1. Cross-sectional areas of the components are considered uncorrelated, while perfect correlation is assumed between their yield stresses.

The annual probabilities of failure for the individual components and the three systems are plotted in Figure 8.6. These probability profiles are obtained by using RELSYS. As expected, the parallel system yields the lowest annual probability of failure among the three systems. Additionally, for the series-parallel system, the system performance is highly dependent on the behavior of the third component. Figures 8.7 (a),

(b), and (c) show the annual system failure rate of the three structural system models considering an in-depth inspection performed at 20 years of service. Each profile has 27 different repair options after the first inspection (i.e., no repair, preventive maintenance, and essential maintenance for each of the three components). As shown in Figure 8.7 (b) for the series-parallel system, among the 27 possible branches, it is possible to distinguish three groups related to the maintenance options (i.e., no repair, preventive, essential maintenance) of the critical component (i.e., component 3), whereas for the series or parallel systems, it is not easy to identify these distinctive groups. Therefore, when considering the series-parallel system, although the number of branches increases exponentially with the number of components, it is possible to reduce the number of analyzed scenarios focusing the attention exclusively on the most critical components.

The bi-objective optimization problem defined by Equations (8.12)-(8.15) is formulated and solved for the three systems considering two in-depth inspections during a time window of 40 years. The in-depth inspection accuracy parameter $k_{insp} = 1.3$ has been considered for the three systems. The two thresholds governing the probability of occurrence of the essential and preventive maintenance for each component have been selected as $\delta_{EM,i} = 0.90 A_i(0)$ and $\delta_{PM,i} = 0.98 A_i(0)$, respectively. These selected thresholds correspond to the previously defined threshold set T2. Nominal costs of 1, 10 and 100 have been considered for inspection, preventive and essential maintenance, respectively.

The defined optimization problem has been solved by means of GAs, using the optimization toolbox provided in MATLAB 7.12 (2011). Multi-objective GAs provide Pareto fronts of optimal solutions, representing a set of maintenance schedules

constituting dominant solutions with respect to the chosen objectives. MATLAB toolbox utilizes a controlled elitist GA, that is a variant of NSGA-II (Deb 2001). Single point crossover has been used, and the optimization has been performed considering an initial population size of 150 solutions and 200 maximum iterations. The objective function has been implemented to evaluate first the annual failure probability of the system for each branch of the event tree, by using RELSYS software. Average system failure rates are computed by Equations (8.4) and (8.6). Finally, maximum expected system failure rate and expected total cost are obtained by Equations (8.11) and (8.7), respectively. In order to increase the computational efficiency, branches with occurrence probability $P(\mathrm{B}_k) < 10^{-4}$ have been discarded, since they have negligible contribution towards the evaluation of the expected system failure rate. The bookkeeping technique described in Bocchini and Frangopol (2011) has been used to further improve the computational efficiency of the routine. In this technique, the objective function has been formulated such that when a new solution is evaluated, it is automatically stored into a table. For each set of design variables, the GA routine checks first if it is possible to retrieve immediately the solution from the table instead of evaluating the objective function itself.

Figure 8.8 (a) depicts the Pareto front obtained for the three systems considering two in-depth inspections ($N_{insp} = 2$). As the three Pareto fronts indicate, maximum expected system failure rate varies significantly with respect to the system configuration. Between the three considered systems, the parallel one has the lowest failure probability, and consequently the lowest maximum expected system failure rate. On the contrary, the highest values of the maximum expected system failure rate are associated with the series system. Three particular solutions X, X' and X'' of the Pareto fronts shown in Figure

8.8 (a) are reported in detail in Table 8.2. These solutions have been chosen so that they have the same expected total cost. The series and series-parallel systems optimal solutions require shorter time intervals between the two in-depth inspections, compared to the parallel system.

For each system configuration, the percentage of increase in total cost ΔC between the cheapest and the most expensive optimal solutions in the corresponding Pareto front is computed as:

$$\Delta C = \left| \frac{\min\left(E\left[C_{tot}\right]\right) - \max\left(E\left[C_{tot}\right]\right)}{\min\left(E\left[C_{tot}\right]\right)} \right| \tag{8.16}$$

and the corresponding percentage of reduction in the maximum expected annual system failure rate Δh as:

$$\Delta h = \left| \frac{\max\left(h_{\max}\right) - \min\left(h_{\max}\right)}{\max\left(h_{\max}\right)} \right| \tag{8.17}$$

where $h_{\max}$ is the maximum expected annual system failure rate. Figure 8.8 (b) presents the values of ΔC and Δh for the three different systems considered in this section. For this particular example, the series system shows the largest ΔC coupled with the smallest Δh, among the three systems. In contrast, the highest Δh is achieved for the series-parallel system. This occurs since the three high cost optimal solutions involve inspection times in the second half of the system life-cycle, maximizing the probability of performing maintenance on the component with highest deterioration rate (i.e., component 3 in Figure 8.5). This component has the most critical position in the series-parallel configuration.

8.8 Example 8.3

In this example, the proposed method is applied to the superstructure of the Colorado State Highway Bridge E-17-AH. The bridge RC deck is supported by nine steel girders and its cross-section is presented in Figure 8.9 (a). A detailed description of the bridge is provided in Estes (1997). Considering the symmetry of the symmetry and that the failure of the system is reached by either failure of the deck or any two adjacent girders, the bridge system can be analyzed as a series-parallel model composed of the deck and 5 girders as shown in Figure 8.9 (b). Neglecting the dead load due to the weight of the structure itself, limit state functions for deck and girders are defined as follows (Estes 1997):

$$g_{deck} = \left(0.563A(t)\, f_y - \frac{A^2(t)\, f_y^2}{244.8\, f_c} \right) \gamma_d - M_{deck}(t) = 0 \tag{8.18}$$

$$g_{gir,i} = Z_i(t) F_y \gamma_g - \eta_i I M_{gir,i}(t) = 0 \tag{8.19}$$

where $A(t)$ and f_y are the cross-sectional area and yield strength of the deck reinforcement bars, respectively; f_c is the 28-day compressive strength of deck concrete; $Z_i(t)$ is the plastic section modulus of the girder *i*; F_y is the yield strength of the steel girders; $M_{deck}(t)$ and $M_{gir,i}(t)$ are the moments acting on the deck and girder *i*, due to traffic loads; η_i and I are the traffic load distribution factor and impact factor of girders, respectively; γ_d and γ_g are modeling uncertainty factors of the resistance of deck and girders.

Load effects and corrosion of deck reinforcement bars and girders have been modeled following the data provided by Estes (1997). For the deck reinforcement bars, a uniform corrosion is assumed. The residual reinforcement bars area is:

$$A(t) = \frac{\pi}{4} n_{bar} d_{bar}(t)^2 \tag{8.20}$$

where n_{bar} is the number of reinforcement bars in the deck and $d_{bar}(t)$ is the bar diameter at time t:

$$d_{bar}(t) = \left(d_0 - 0.0203 i_{corr}(t - T_{ini})\right)^2 \tag{8.21}$$

where d_0 is the initial diameter, i_{corr} represents the rate of corrosion parameter, and T_{ini} is the initiation time of corrosion. For the steel girders, the corrosion propagation model proposed by Albrecht & Naeemi (1984) is assumed. Structural loads are evaluated as indicated in Estes (1997). Parameters for the traffic load moment distribution are obtained considering the average daily truck traffic on the bridge and are discussed in details in Estes (1997) and Akgül (2002). The random variables involved in the limit state functions in Equations (8.18) and (8.19) are reported in Table 8.3. The series-parallel system of the bridge represented in Figure 8.9 (b) has been analyzed by means of RELSYS software, and the annual failure probability $P_{sys}(t)$ of the system and its components is plotted in Figure 8.10 (a). As shown, after 50 years of service, the system failure probability is mostly controlled by the reliability of the reinforced concrete deck.

For the determination of the optimum maintenance plan, different possible actions have been considered for deck and girders. For the deck, it has been assumed that the in-depth inspections are able to identify the corrosion penetration in the deck and, therefore, to estimate the residual diameter of the reinforcement bars at the inspection time $d_{bar}^{(est)}$.

Thus, the estimated residual cross-sectional area of the bars $A^{(est)}(t)$ is obtained by Equation (8.20). Three possible actions have been considered for the deck: EM, PM, or no maintenance. As stated in the previous section, probability of occurrence of the different repair options is determined by the two predefined thresholds. In this example, these thresholds are defined in terms of initial mean of the reinforcement bars cross-sectional area at the initial time $\mu_A(0)$:

$$\delta_{EM,deck} = 0.90\mu_A(0);\ \delta_{PM,deck} = 0.98\mu_A(0) \tag{8.22}$$

Essential maintenance is performed when the estimated bar cross-sectional area is less then $\delta_{EM,deck}$, while PM is applied if $\delta_{EM,deck} < A^{(est)} \le \delta_{PM,deck}$. No repair is considered in the remaining cases. The EM is assumed to completely restore the initial performance of the deck, while the PM keeps the areas of reinforcement bars unchanged (i.e., corrosion is blocked) for the next five years.

In the case of the girders, resistance over time is dependent on the plastic section modulus $Z_i(t)$. Therefore, it has been considered that the in-depth inspection estimates the depth of corrosion in the girder and then, based on Estes (1997), the residual plastic section modulus $Z_i^{(est)}(t)$. Only the preventive maintenance option has been considered, to be performed when the estimated plastic section modulus is less than 98% of the mean initial one. Otherwise, no repair is performed. Essential maintenance of the girders does not significantly reduce the failure probability of the superstructure, as shown in Figure 8.10 (b) where the annual system failure probabilities of the structure without maintenance, with essential maintenance on the deck, and essential maintenance on the

girders at 30 years are compared. Therefore, such an expensive but not so effective option has not been included in the possible maintenance plans. The event tree associated with all possible repair options after one inspection is illustrated in Figure 8.11.

Cost of essential maintenance on the deck is $225,600 corresponding to the cost of deck replacement, based on data provided by Estes (1997). For preventive maintenance on the deck and girders, costs have been assumed as $40,000 and $75,000, respectively. In-depth inspection cost for the bridge superstructure is dependent on the accuracy of the inspection itself. High accuracy inspection will, necessarily, be more expensive. Therefore, in-depth cost inspection has been computed as:

$$C^{(insp)} = \left(C^*\right)^{\frac{1}{k_{insp}}} \tag{8.23}$$

where C^*=$50,000 has been assumed as cost of an *ideal* inspection (i.e., not subjected to any error), and $k_{insp} \geq 1$ is the index associated with the inspection accuracy.

The Pareto front of optimal maintenance plans for the bridge has been determined as the solution of the optimization problem described by Equations (8.12) – (8.15). The minimum interval between two successive inspections in this case is 5 years.

$$t_{insp}^{(k+1)} - t_{insp}^{(k)} \geq 5 \; years \qquad k = 1, ..., N_{insp} \tag{8.24}$$

As in the previous optimization problem, GAs and RELSYS have been used for determining the Pareto-optimal solutions for the bi-objective optimization problem. Figure 8.12 shows the Pareto front obtained considering two in-depth inspections ($N_{insp} = 2$), index of inspection accuracy $k_{insp} = 1.3$, and inspection cost $C^{(insp)} = \$4,200$. Three representative solutions, A, B and C, are selected in Figure 8.12 and reported in

details in Table 8.4 and Figures 8.13 – 8.15. The annual system failure rate associated with the three solutions is presented in Figures 8.13 (a), 8.14 (a), and 8.15 (a). In particular, the expected system failure rate is compared to the annual system failure rate of the two branches with the highest probability of occurrence. Additionally, the expected cumulative cost profiles of solutions A, B, and C are compared with cumulative cost profiles of the two branches having the highest probability of occurrence in Figures 8.13 (b), 8.14 (b), and 8.15 (b).

As shown in Figures 8.13 – 8.15, optimal solutions with low expected total cost are characterized by early maintenance times. These solutions are selected by the optimizer since the need for essential maintenance in the deck is avoided while attempting to minimize the expected total cost. More specifically, the algorithm selects the inspection times when the options of not repair and preventive maintenance for deck and girders have the highest probability of occurrence (i.e., earlier in service life). Conversely, high expected total cost involves high probability of occurrence of those branches in which essential maintenance for the deck is required at least once. For these cases, the optimal plans involve a first inspection/repair around half of the life-cycle of the structure, followed by the second one after a short term (around 10 years).

Finally, to analyze the effect of the inspection accuracy on the optimal maintenance plan, a comparison between two Pareto fronts has been performed, the first one obtained using the previous assumptions (i.e, $k_{insp} = 1.3$), and the second one obtained considering perfect inspection (i.e., $k_{insp} = 1.0$). The two resulting Pareto fronts, reported in Figure 8.16 (a), show that, when uncertainty in the inspection is taken into account, the expected total cost for a given maximum expected system failure rate decreases, with

respect to the perfect inspection case. This result is due to the higher cost associated with the perfect inspection. However, reducing the accuracy of the in-depth inspections involves an increasing probability of false alarms. This is shown in Figure 8.16(b), where a comparison is made between the probabilities of occurrence of the different branches for two solutions (A and A'), selected from the two Pareto fronts and having the same maximum expected system failure rate. The occurrence probabilities of branches vary significantly when changing the inspection accuracy. For the case with perfect inspection, the scatter in the probability of occurrence of branches is reduced, since it becomes dependent only on the imperfections associated with the prediction model. Probability of occurrence of dominant branches (namely 15, 17, 25 and 27), corresponding to the most appropriate management decision, is instead amplified. Consequently, the risk of occurrence of false alarms or wrong management decisions is reduced.

8.9 Conclusions

An efficient approach for optimal life-cycle maintenance schedule for deteriorating structural systems has been proposed. This approach is based on a bi-objective optimization procedure which simultaneously minimizes the maximum expected annual system failure rate and expected total cost of the inspection and maintenance plans. Effects of imperfections related to structural performance prediction and inspection accuracy have been considered. Different maintenance options have been taken into account for each component. Predefined thresholds, representative of the deterioration state of the system, were established to evaluate the probabilities of occurrence of the different repair options. The optimization problem has been introduced considering three-component systems with different configurations and then applied to an existing bridge

considering uncertainties related to material properties, corrosion, traffic loads and inspection outcomes. Based on the presented results, the following conclusions can be drawn:

1- For systems with different configurations of the same set of components, optimal inspection and maintenance plans for a configuration may not be optimal for a different one. This is due to the fact that only the expected total cost is component-dependent, while the expected system failure rate depends on both the system configuration and component failure rate.

2- Different maintenance strategies can be chosen from the Pareto set. Low cost maintenance plans are mainly associated with no repair or preventive maintenance, providing a small reduction of the expected system failure rate. In these cases, in-depth inspections should be concentrated in the early life of the structure. Maintenance plans with the highest impact on the structural performance are generally associated with in-depth inspections distributed along the last part of the life-cycle of the system. For these strategies, essential maintenance options on critical components are dominant.

3- The presence of constraints related to maximum allowable inspection and maintenance cost and system failure rate are crucial for deciding which strategy should be selected.

4- Improving the inspection accuracy reduces the risk of occurrence of false alarms. Therefore, the most appropriate management decisions are more likely to be selected.

Table 8.1 Parameters of random variables associated with the three-component system performance functions.

Variables	Component 1	Component 2	Component 3
$A_i(0)$ (cm^2)	3.0	2.9	3.1
DR_i (*per year*)	$2\text{x}10^{-3}$	$0.5\text{x}10^{-3}$	$3\text{x}10^{-3}$
$\mu_{f_y}(t)$ (*MPa*)	250	250	250
COV of $f_y(t)$	0.04	0.04	0.04
$L_i(0)$ (*kN*)	60	60	60
COV of $L_i(t)$	0.05	0.05	0.05
l_i (*per year*)	$0.2\text{x}10^{-3}$	$0.2\text{x}10^{-3}$	$0.2\text{x}10^{-3}$

Note: $\mu(t)$ = mean value, and COV = coefficient of variation.

Table 8.2 Optimal solutions for three-component systems in series, series-parallel and parallel configurations considering two in-depth inspections.

Solution	k_{insp}	$t_{insp}^{(1)}$ $(years)$	$t_{insp}^{(2)}$ $(years)$	$\max\left(E\left[h_{sys}(t)\right]\right)$ $\left(years^{-1}\right)$	$E[C_{tot}]$
X	1.3	21	27	$5.48\text{x}10^{-2}$	112
X′	1.3	19	28	$2.15\text{x}10^{-2}$	112
X″	1.3	10	30	$0.19\text{x}10^{-2}$	112

Note: Solutions X, X′, and X″ are shown in Figure 8.8.

Table 8.3 Mean μ and standard deviation σ of the random variables associated with the definition of the bridge limit state functions (Estes 1997).

Variables	Dimensions	μ	σ	Variables	Dimensions	μ	σ
f_y	*MPa*	386	42	F_y	*MPa*	252	29
f_c	*MPa*	19	3.4	d_0	*mm*	15.9	0.47
i_{corr}	*mm/year*	2.49	0.29	T_{ini}	*years*	19.6	7.51
η_1		0.982	0.122	η_2		1.14	0.142
η_3, η_4, η_5		1.309	0.163	I		1.14	0.114
γ_d		1.0	0.1	γ_g		1.0	0.1
Z_i	mm^3	Vary over time		$M_{deck}, M_{gir,i}$	*Nm*	Vary over time	

Table 8.4 Optimal solutions for Colorado State Highway Bridge E-17-AH considering two in-depth inspections.

Solution	k_{insp}	$t_{insp}^{(1)}$ $(years)$	$t_{insp}^{(2)}$ $(years)$	$\max\left(E\left[h_{sys}(t)\right]\right)$ $\left(years^{-1}\right)$	$E\left[C_{tot}\right]$ $(\$)$
A	1.3	41	50	0.64×10^{-3}	249,170
B	1.3	24	38	2.39×10^{-3}	160,010
C	1.3	12	21	4.92×10^{-3}	77,975
A′	1.1	40	49	0.63×10^{-3}	268,770

Note: Solutions A, B, C are shown in Figures 8.12 – 8.15, and A′ in Figure 8.16

(a)

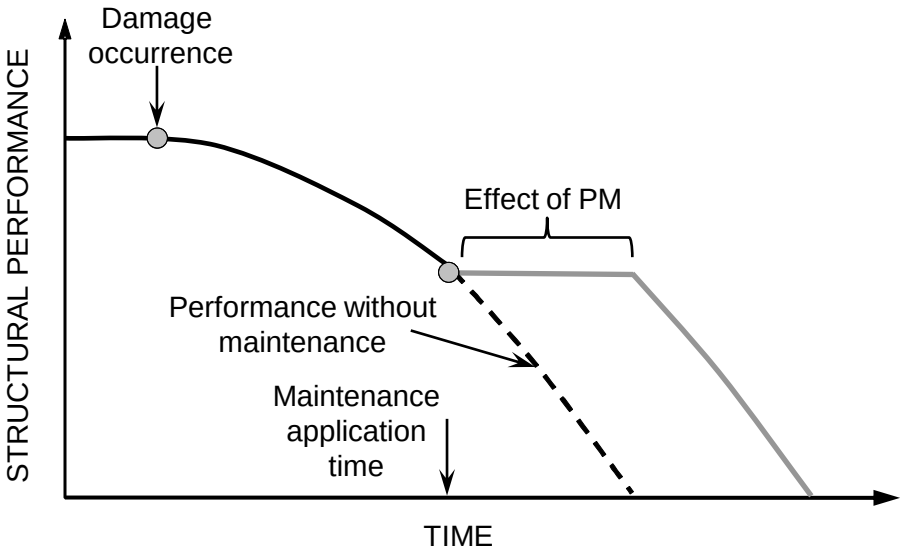

(b)

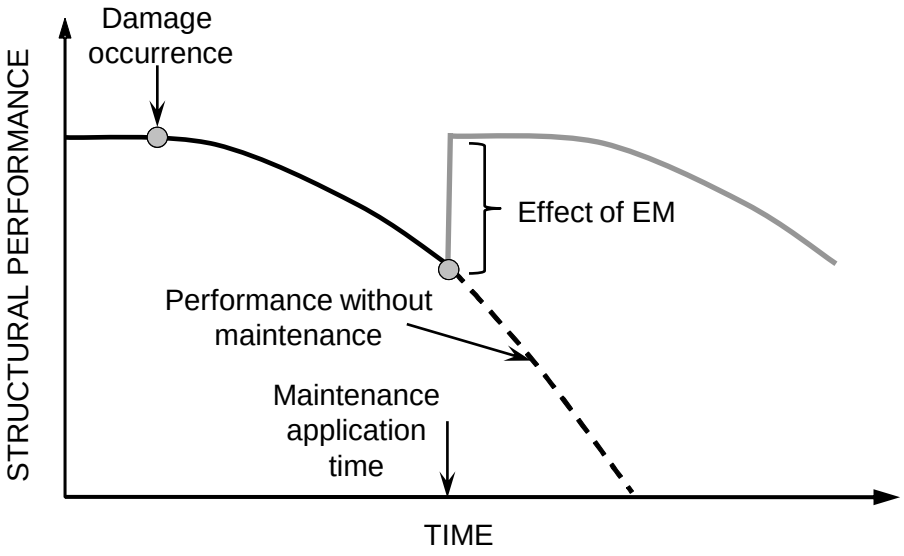

Figure 8.1 Effect of (a) preventive maintenance (PM) and (b) essential maintenance (EM) on structural performance

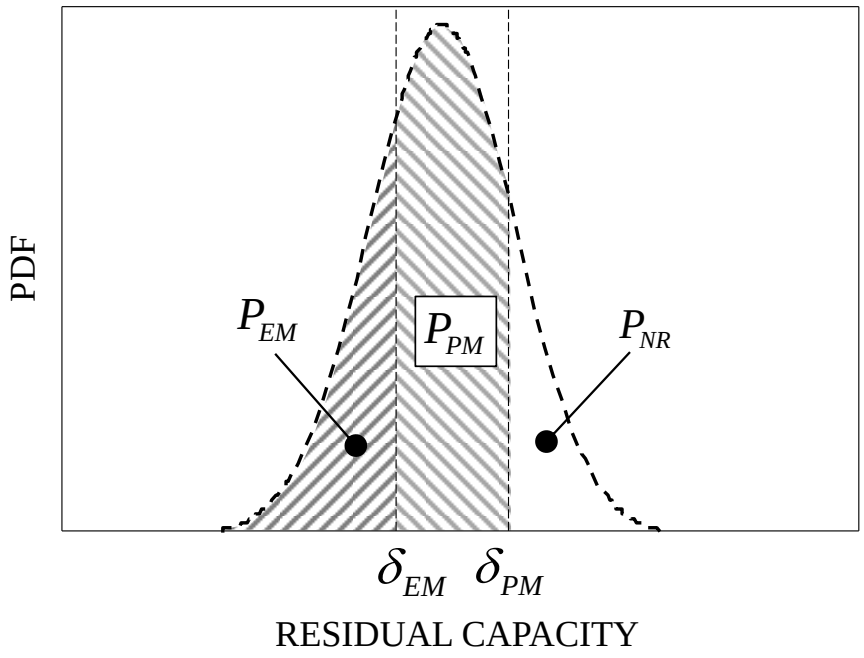

Figure 8.2 Probability of different intervention options based on estimated residual capacity

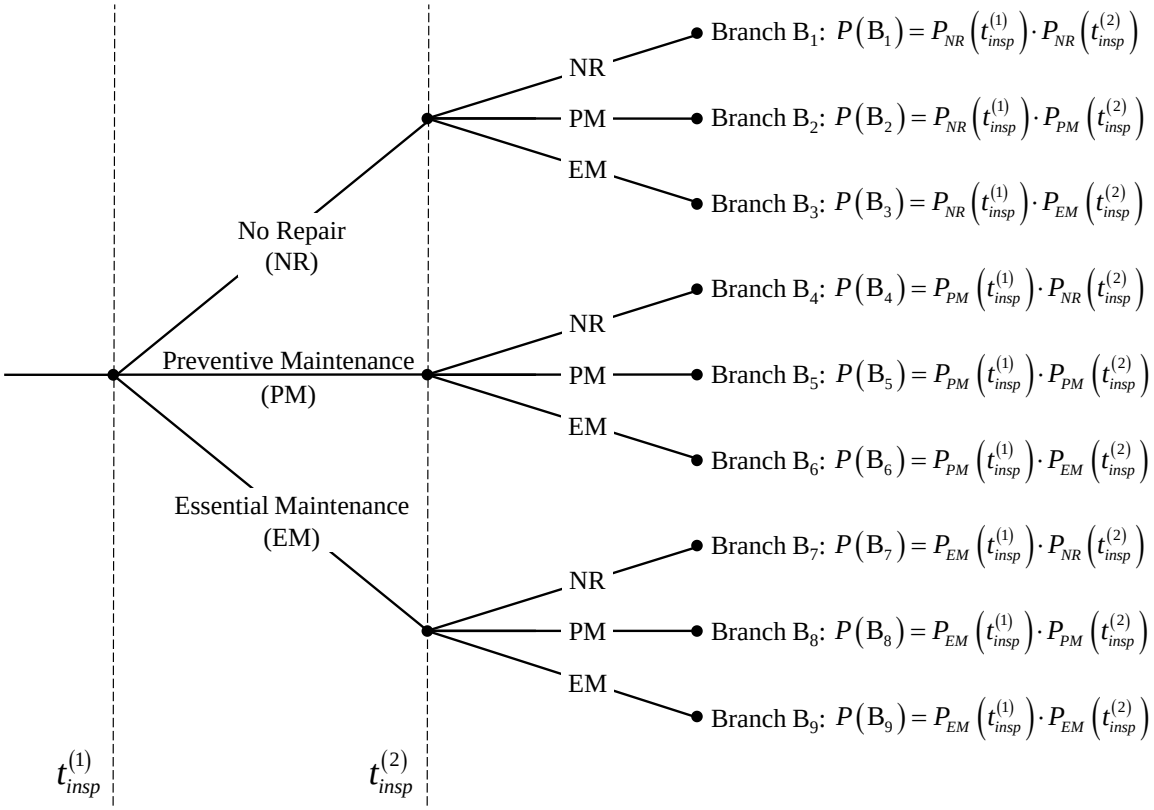

Figure 8.3 Event tree associated with a single component subjected to two inspections and considering three different intervention options

(a)

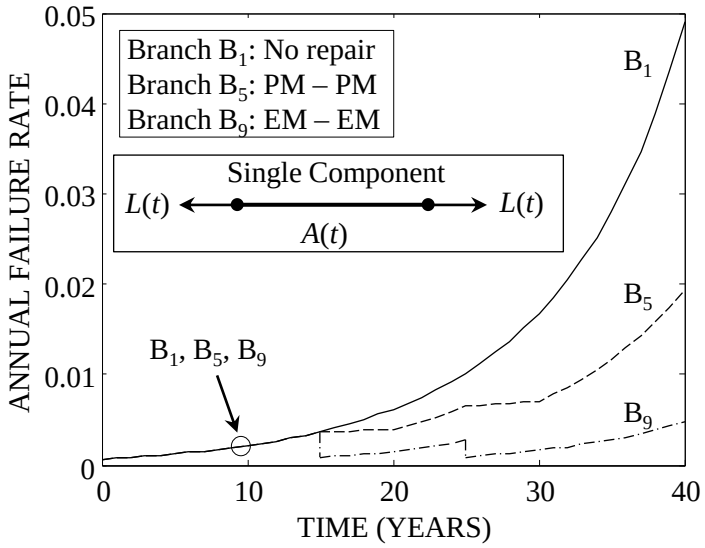

(b)

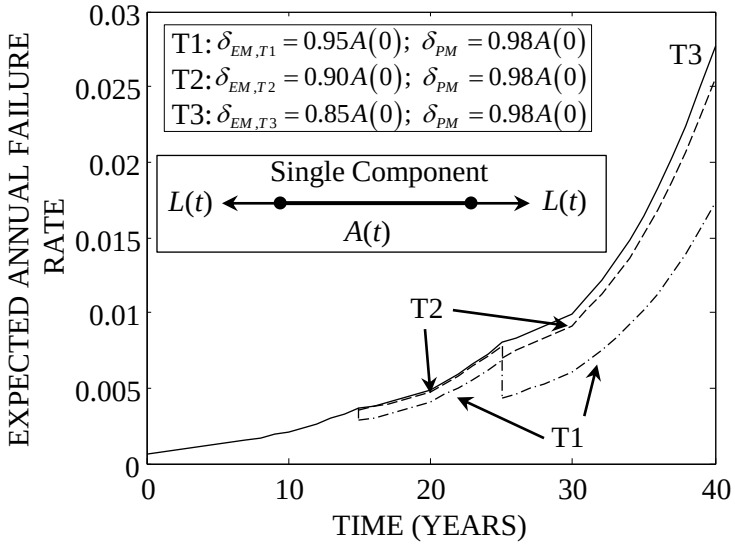

Figure 8.4 (a) Annual failure rate associated with branches B1, B5 and B9 in Figure 8.3 for a single component considering two in-depth inspections at 15 and 25 years, and (b) expected annual failure rate considering different threshold sets

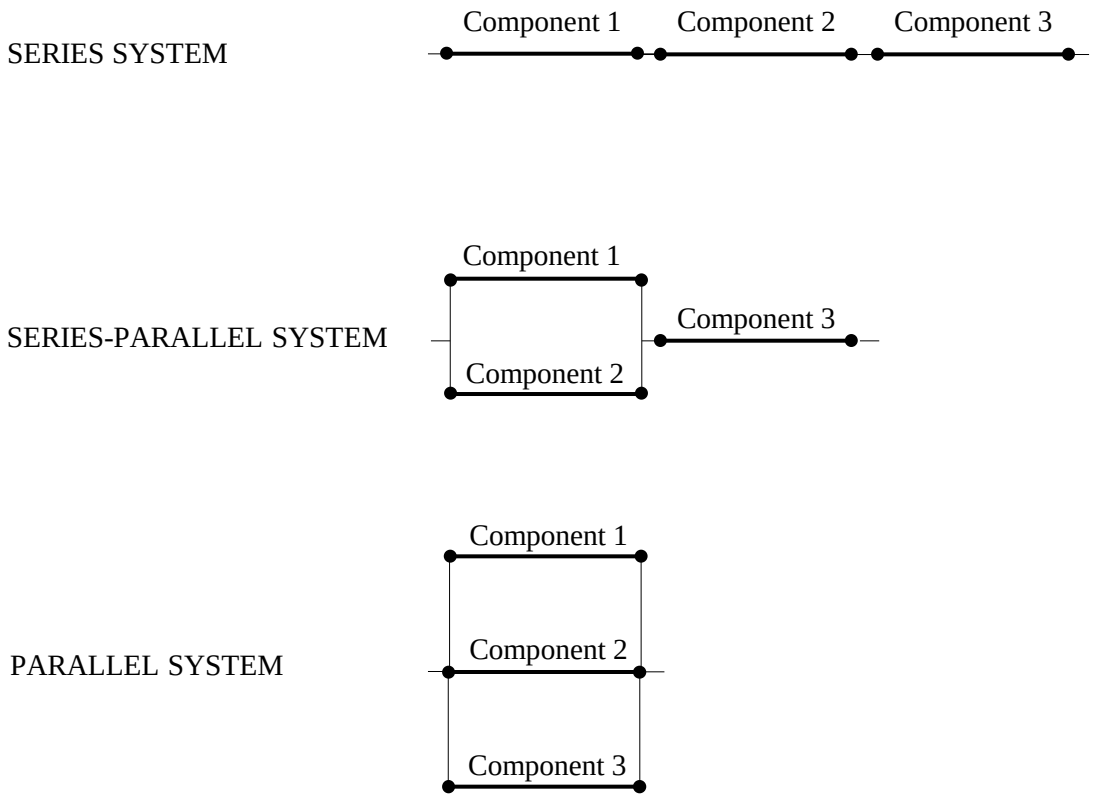

Figure 8.5 Series, series-parallel and parallel configurations of a three-component system

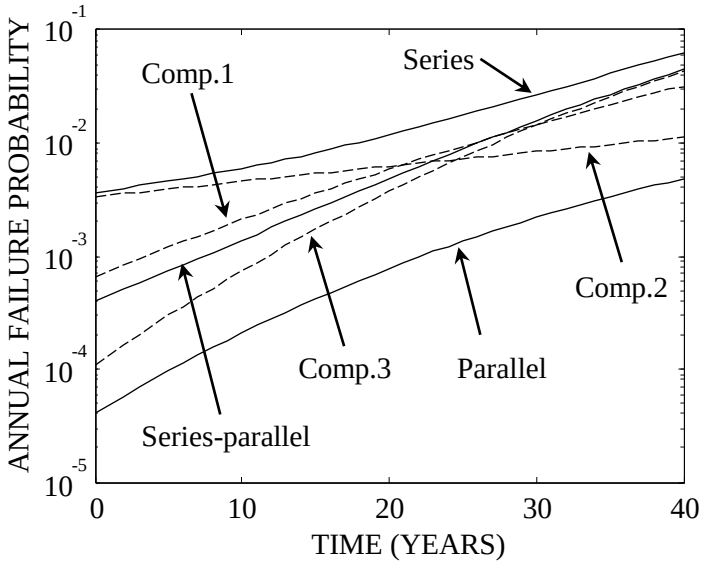

Figure 8.6 Annual failure probability of all components and systems

(a)

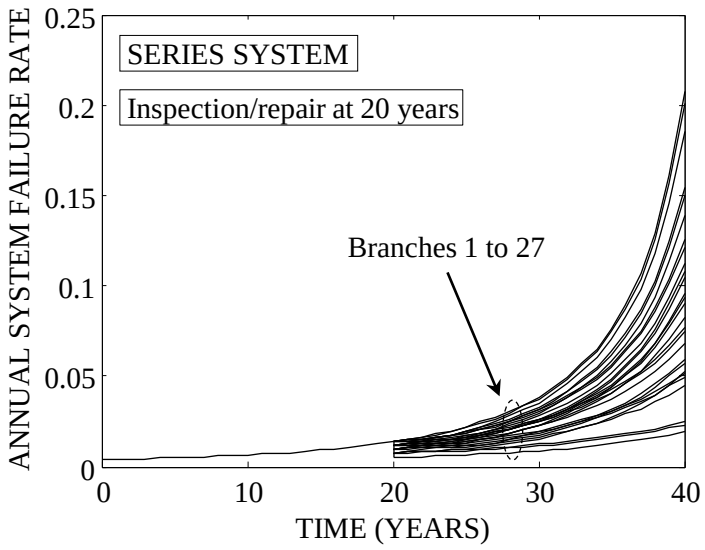
SERIES SYSTEM
Inspection/repair at 20 years
Branches 1 to 27
ANNUAL SYSTEM FAILURE RATE
TIME (YEARS)
0
0.05
0.1
0.15
0.2
0.25
0
10
20
30
40

(b)

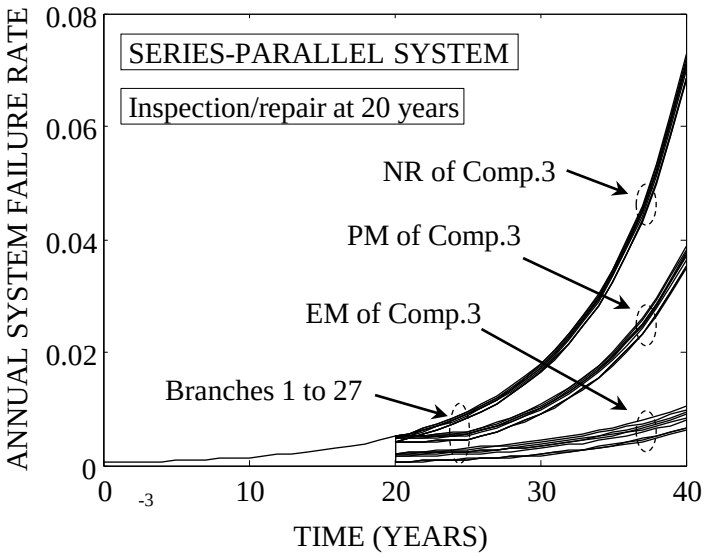
SERIES-PARALLEL SYSTEM
Inspection/repair at 20 years
NR of Comp.3
PM of Comp.3
EM of Comp.3
Branches 1 to 27
ANNUAL SYSTEM FAILURE RATE
TIME (YEARS)
0
0.02
0.04
0.06
0.08
-3
0
10
20
30
40

(c)

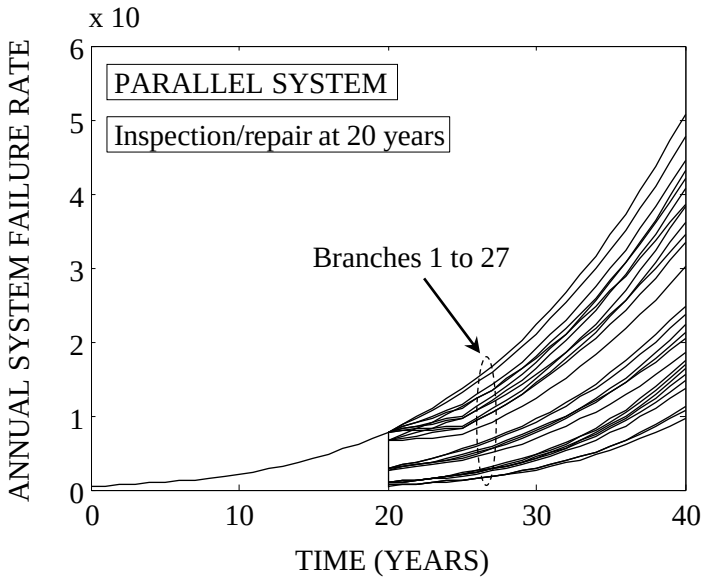

Figure 8.7 Annual system failure rates for three-component systems for the 27 branches associated with a single inspection/repair at 20 years: (a) series, (b) series-parallel, and (c) parallel system

(a)

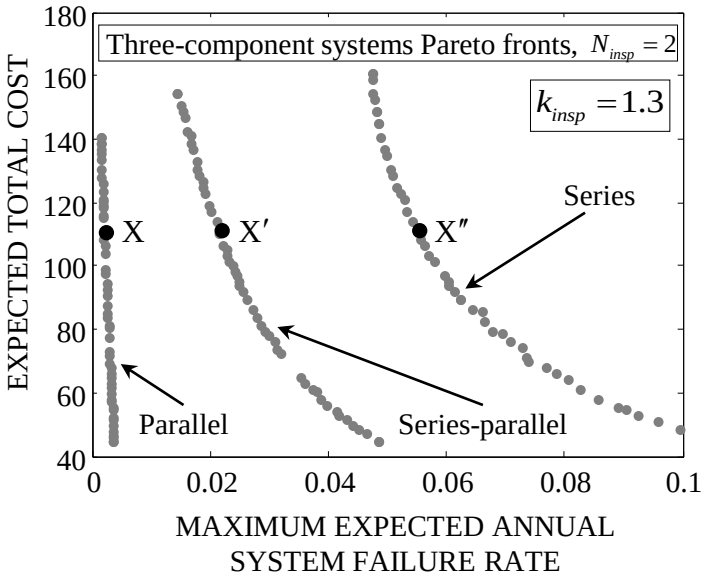

(b)

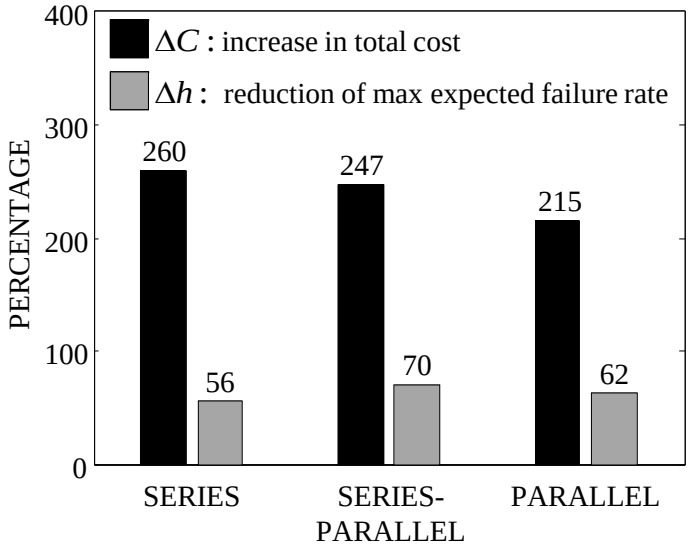

Figure 8.8 (a) Pareto front of optimal solutions for series, series-parallel and parallel systems, considering two in-depth inspections; (b) percentage of increase in total cost and percentage of maximum expected annual system failure rate reduction between the cheapest and the most expensive optimal solutions for each system

(a)

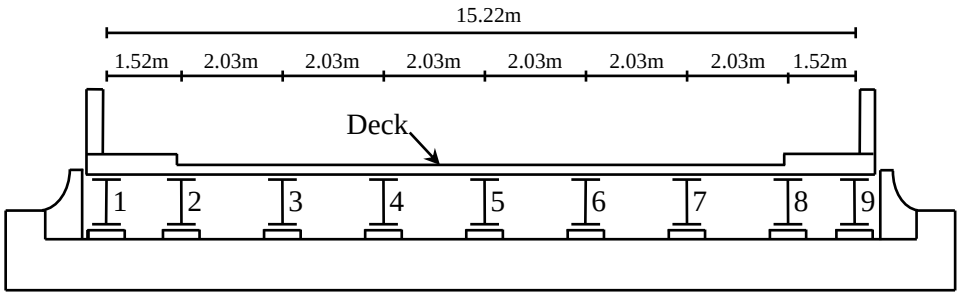

(b)

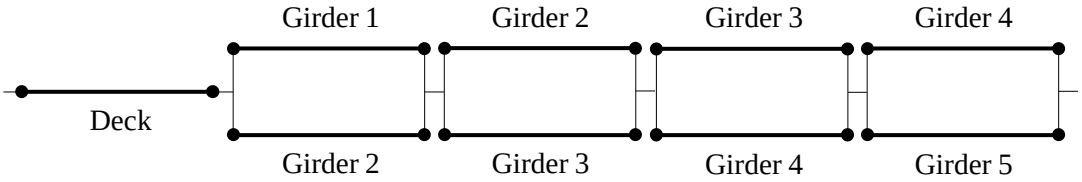

Figure 8.9 Colorado State Highway Bridge E-17-AH: (a) superstructure cross-section; (b) series-parallel model

(a)

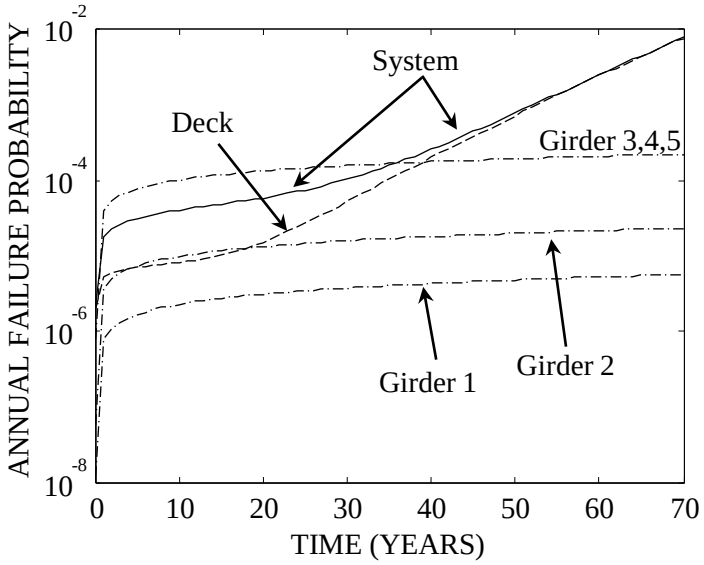

(b)

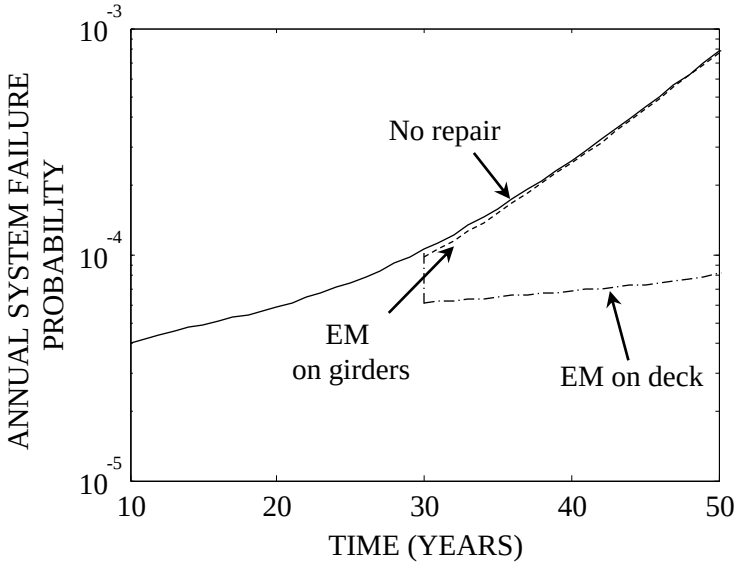

Figure 8.10 (a) annual failure probability of single components and system; (b) annual system failure probability considering no repair, EM on girders and EM on deck

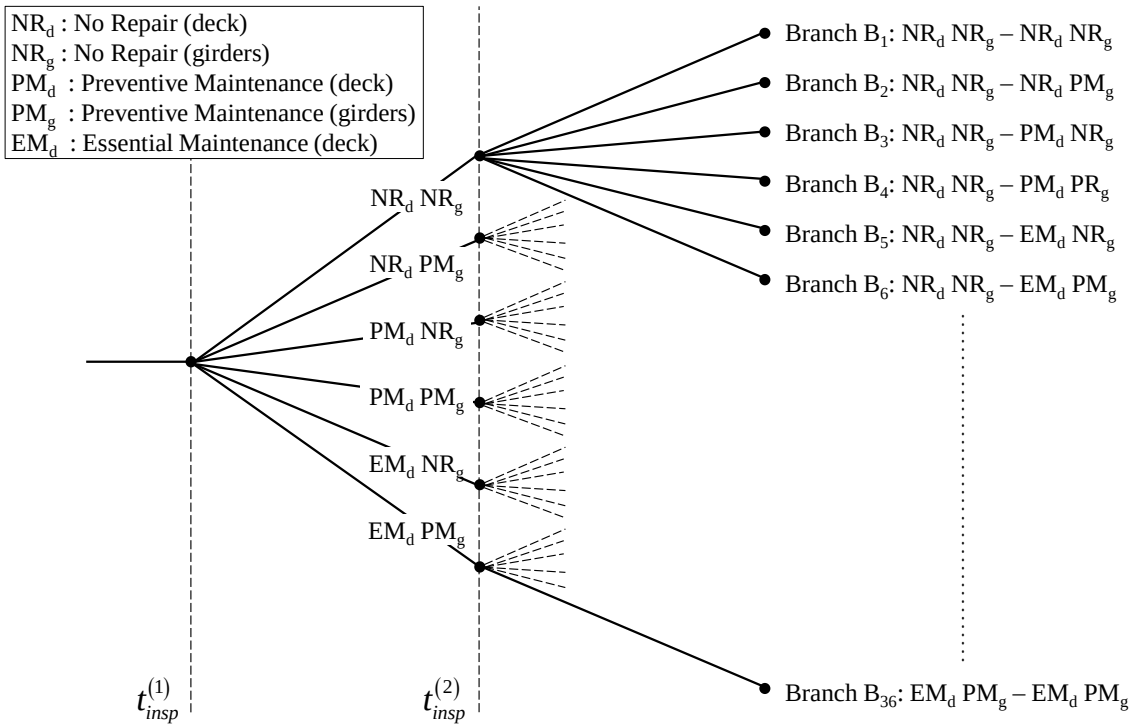

Figure 8.11 Event tree associated with the Colorado State Highway Bridge E-17-AH superstructure considering two in-depth inspections, three different repair options for the deck and two for girders

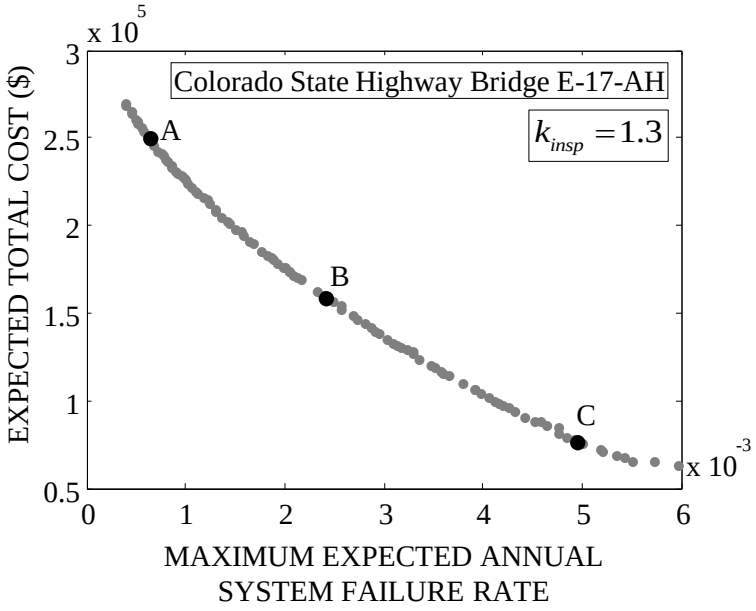

Figure 8.12 Pareto front associated with optimal maintenance plans considering two in-depth inspections for the Highway Bridge E-17-AH

(a)

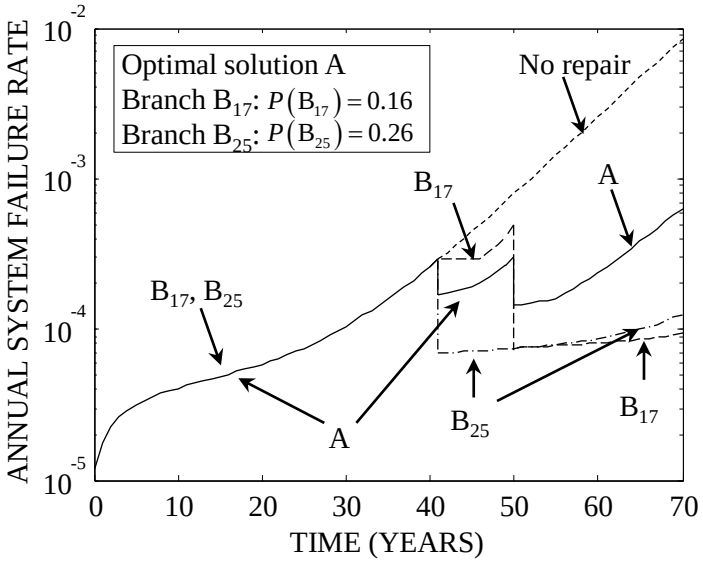

(b)

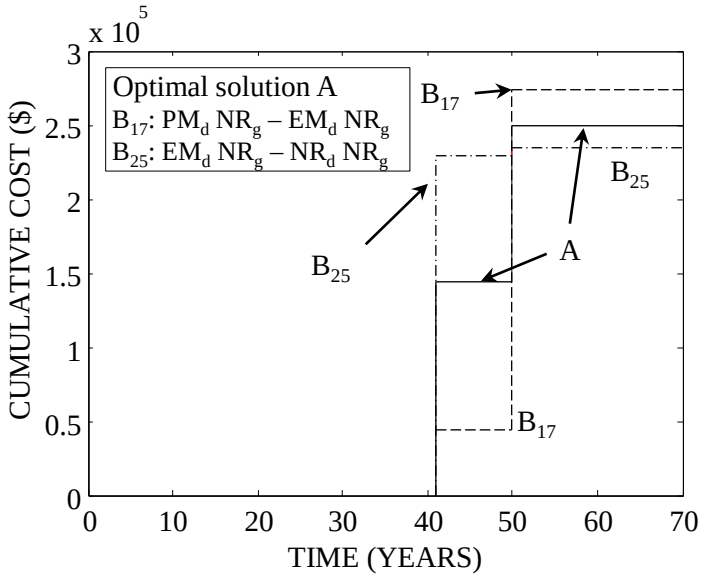

Figure 8.13 (a) Annual system failure rate and (b) cumulative cost profiles for the two branches with highest occurrence probability, compared with corresponding expected values for optimal solution A

(a)

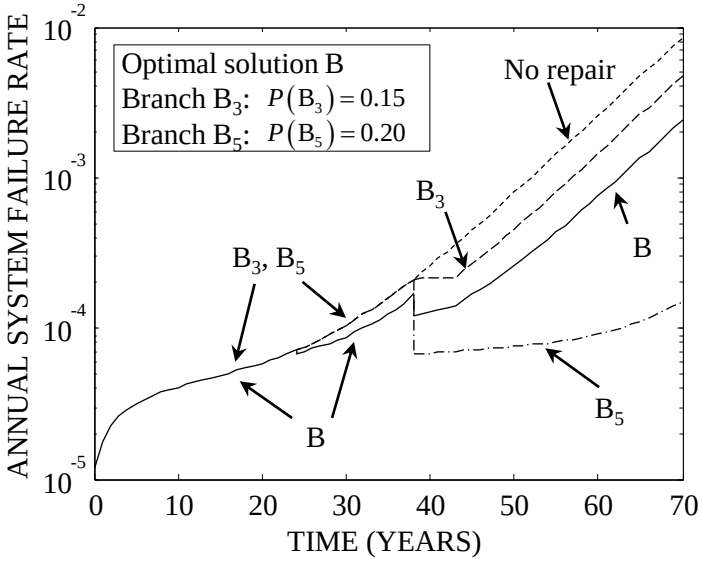

(b)

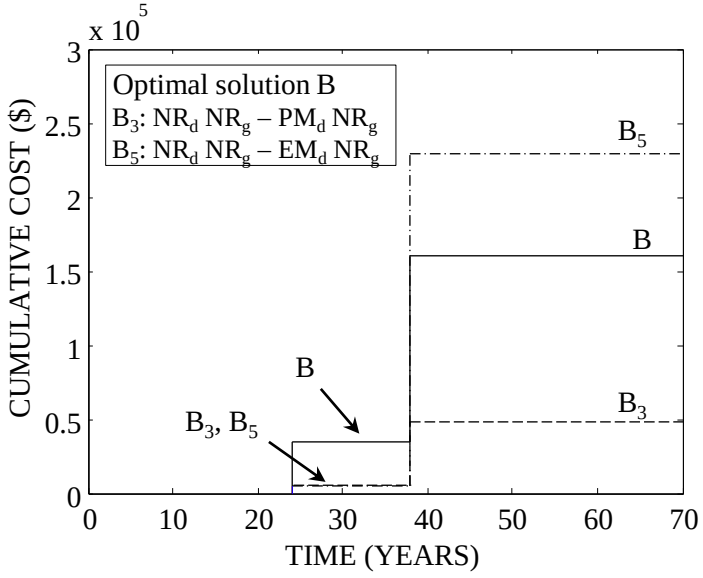

Figure 8.14 (a) Annual system failure rate and (b) cumulative cost profiles for the two branches with highest occurrence probability, compared with corresponding expected values for optimal solution B

(a)

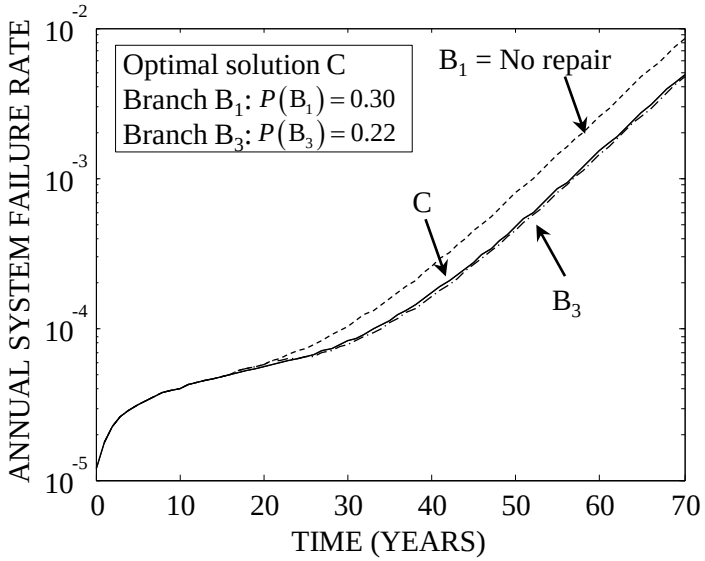

(b)

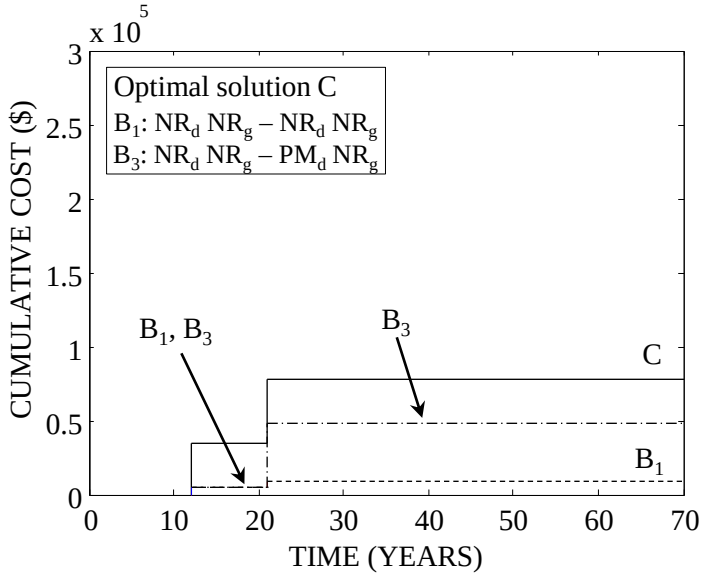

Figure 8.15 (a) Annual system failure rate and (b) cumulative cost profiles for the two branches with highest occurrence probability, compared with corresponding expected values for optimal solution C

(a)

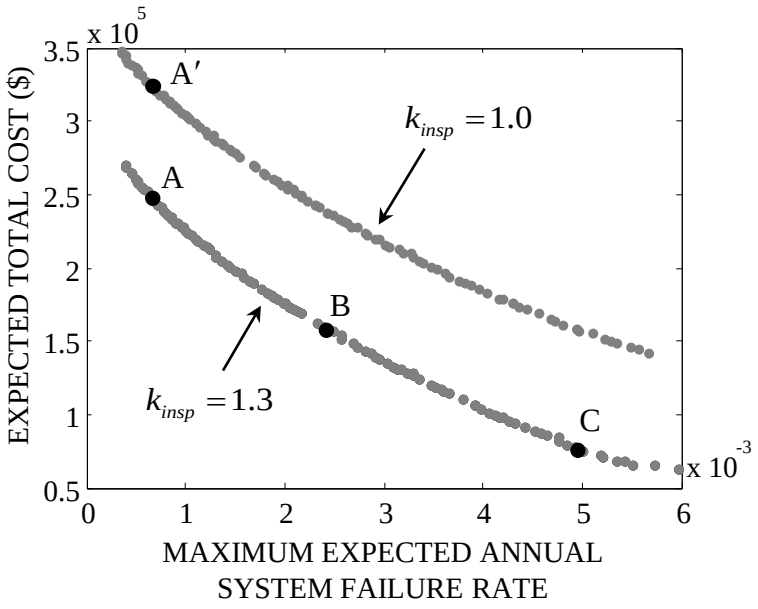

(b)

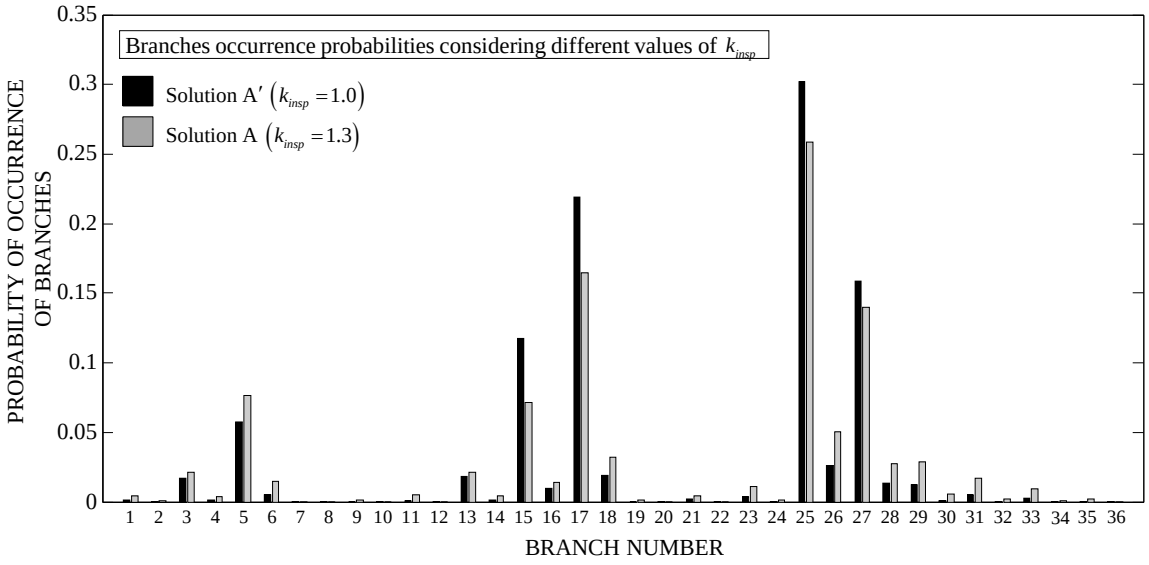

Figure 8.16 (a) Pareto fronts associated with optimal maintenance plans for the Colorado State Highway Bridge E-17-AH, considering and ; (b) branches occurrence probabilities for two solutions of the two Pareto fronts having same maximum expected system failure rate

CHAPTER 9 LIFE-CYCLE COST CONSIDERATIONS FOR DETERIORATING STEEL BRIDGES

9.1 Overview

Steel bridges under severe chloride exposure, due to de-icing salts or marine environmental effects, require frequent maintenance and repair activities to extend their service life and maintain an adequate performance level. In the previous chapters of this study, only the direct costs of interventions (e.g., materials and labor cost for maintenance) are included in the life-cycle cost computations. In addition to these direct costs, maintenance actions may lead to indirect costs associated with traffic delays and environmental effects, which can significantly increase the life-cycle cost of the bridge under consideration. The use of more sustainable materials, such as maintenance-free steel, may increase the initial cost of the structure; however, the life-cycle cost, including the maintenance actions along the service life and their associated indirect effects, can be significantly reduced.

This chapter presents a computational approach to quantify the total life-cycle cost of steel bridges including direct and indirect maintenance costs. This approach can also aid in evaluating different material alternatives for bridge construction. The life-cycle cost of a steel bridge constructed using conventional painted carbon steel is computed and compared to that of the same bridge constructed using maintenance-free steel. Indirect environmental, social, and economic impacts of maintenance actions are computed to quantify the sustainability metrics associated with steel bridges during their

life-cycle. The approach is illustrated using an existing bridge located in Pennsylvania. This chapter is based on the technical note Soliman & Frangopol (2014b).

9.2 Background

Bridges represent a critical component of our transportation infrastructure system. Steel bridges represent more than 30% of the total number of highway bridges in the United States (FHWA 2012). These bridges, if placed in highly corrosive environment, due to de-icing salts or marine exposure, may require frequent maintenance and repair actions along their service life. Bridge maintenance activities can cause delays on the transportation network which, in turn, will lead to other indirect effects in addition to the direct cost of maintenance. These indirect effects include social, economic, and environmental impacts which are directly connected to the sustainability measures of the bridge and the bridge network to which the bridge belongs. However, in the previous chapters of this study, indirect cost were not included in the life-cycle cost computations. This chapter addresses this issue by presenting an approach to compute the total life-cycle cost of steel bridges constructed using conventional carbon steel. The life-cycle cost includes the initial construction cost of girders, in addition to the repainting maintenance actions performed during the service life of the bridge.

However, several steel types offering better corrosion resistance have been introduced by steel manufacturers to reduce the need for maintenance in corrosive environments. Examples are the weathering steel and the corrosion-resistant steel codified as ASTM A1010. Although weathering steel provides maintenance-free operation in low chloride environments, it is unsuitable for bridges under heavy chloride exposure. In such cases, coated carbon steel is used and multiple repainting maintenance

actions are performed along the service life of the bridge to ensure its acceptable performance. The A1010 steel, as a maintenance-free alternative, is superior in such applications; however, it has considerably higher initial cost when compared to the painted carbon steel. Therefore, there exists a need to quantify the life-cycle cost of both alternatives such that bridge managers can rationally select the appropriate material which suits their needs.

A recent study by Okasha *et al.* (2012) computed the life-cycle cost of a steel bridge girder constructed using conventional painted steel and compared it to that of the same girder constructed using the A1010 steel. The life-cycle cost included the initial cost of materials as well as the direct cost of repainting actions. However, other indirect user and environmental costs of life-cycle maintenance actions were not included in that study. In this chapter, the life-cycle cost of a representative steel bridge constructed using painted conventional carbon steel and compare it to that of the same bridge constructed using the A1010 corrosion-resistant steel while considering different direct and indirect effects of life-cycle maintenance actions.

9.3 Life-cycle Cost Analysis

The effect of bridge maintenance on the life-cycle cost and cost-oriented bridge maintenance planning was addressed in several studies including Frangopol (1999), Estes & Frangopol (2001), Kong & Frangopol (2003b), and Neves *et al.* (2006a, 2006b), among others. In this chapter, the life-cycle cost of the bridge under investigation is considered to be composed of the initial cost of materials and fabrication, in addition to the direct and indirect costs of life-cycle maintenance actions. The initial cost of conventional carbon steel bridges consists of the material, fabrication, initial painting,

shop inspection, and the transportation costs. Actions performed to maintain/repair corroded bridge elements include spot repair, zone painting, spot repair and overcoat, and complete painting of the bridge; the choice of the repair type depends on several factors such as the degree of corrosion, budgetary limits, other ongoing maintenance tasks, and appearance to the public, among others (MnDOT 2014). Since complete painting will have the highest impact on the total life-cycle cost of a bridge, it is used for the life-cycle cost evaluation in this investigation.

A model of a real bridge located in Pennsylvania is used to illustrate the life-cycle cost computational procedure. The bridge, which carries the state route SR 987 over the SR 22, was built in 1973 and has a deck area of 3047.22m^2 (32800ft^2) with an estimated weight of 498 metric tons. In 2013, after 40 years of service life, a complete bridge repainting maintenance was performed to the bridge. In order to compute the initial cost of the model bridge constructed using both types of steel, the purchase price of carbon steel is considered deterministically to be $975 per metric ton, whereas that of the A1010 steel is considered to be $2265 per metric ton (Okasha *et al.* 2012). Other initial cost items also include the cost of fabrication, initial painting, shop inspection, and transportation total cost are assumed, for carbon steel, to be $2400 per metric ton. For the A1010 steel, since the steel does not require initial painting, this cost is reduced by 5% yielding $2280 per metric ton (Okasha *et al.* 2012).

For conventional carbon steel, maintenance actions are considered to have direct and indirect cost components. The direct component C_R represents the cost of removing the old paint, repairing corroded areas, and applying new paint. Additionally, this cost covers the traffic control expenses during the maintenance period. Information about the

cost of repainting maintenance was given by Pennsylvania Department of Transportation (PennDOT) to be ranging from \$215.28/m^2 (\$20/ft^2) to \$376.74/m^2 (\$35/ft^2) of the bridge deck area (PennDOT 2013). This cost depends on the location of the bridge, the bridge type, and the capacity of the road below the bridge, among others. In order to properly consider the variability in this cost, the direct maintenance cost is considered to be a random variable following a triangular distribution with a lower limit of \$215.28/m^2 (\$20/ft^2), an upper limit of \$376.74/m^2 (\$35/ft^2), and a most probable value of \$322.92/m^2 (\$30/ft^2) [i.e., Tri(215.28, 322.92, 376.74)].

The indirect cost of maintenance can also affect the life-cycle cost and sustainability considerations of the bridge. Within the new direction towards more sustainable infrastructure systems, different social, environmental, and economic sustainability aspects must be considered to evaluate various designs and material alternatives. Social and environmental aspects can be rationally integrated into the life-cycle analysis by evaluating their monetary value (Bocchini *et al.* 2014, Dong *et al.* 2013, Adey *et al.* 2014). These costs arise due to the delays associated with the maintenance, in addition to the environmental impact resulting from the maintenance actions.

In the case of repainting steel girder bridges and in order to access the steel beams, maintenance activities are implemented on the underside of the bridge. This requires traffic control procedures for the road under the bridge. Depending on many factors such as the average daily traffic (*ADT*), road conditions, and the number of lanes, different traffic control procedures, ranging from only reducing the speed limit to the complete closure of the road and directing the traffic through a detour, may be adopted. For the bridge under consideration, it is assumed that the traffic control procedure is

performed by reducing the speed limit within an effective distance. Therefore, traffic delays may occur, along with their associated social, environmental, and economic dimensions. As the traffic speed is reduced on the road below the bridge, an increase in the travel time will occur leading to time losses, which can be expressed, based on Shiraki *et al.* (2007), as

$$TL = d \cdot ADT \cdot [\frac{l}{S_D} - \frac{l}{S_o}] \tag{9.1}$$

where *ADT* is considered as 40,000 vehicle/day; *d* is the duration of maintenance and is assumed 15 days; *l* is the length of the traffic control region considered to be 1.609 km (one mile); S_o is the un-restricted traffic speed considered to be 88.51 km/h (55 mph); and S_D is the restricted traffic speed which is assumed as 32.19 km/h (20 mph).

The cost associated with the time loss C_{TL} for users and goods is (Stein *et al.* 1999)

$$C_{TL} = \left[c_w O_c (1-T) + (c_c O_t + c_g) T \right] \cdot TL \tag{9.2}$$

where c_w is the average wage per hour (USD/*h*) considered as a random variable following a lognormal distribution with mean 23.36 USD/h and a coefficient of variation of 0.28 [i.e., LN(23.36, 0.28)]; c_c is average compensation per hour for truck drivers (USD/*h*) following a lognormal distribution LN(29.28, 0.31); c_g is time value of the goods transported in a cargo (USD/*h*) considered as LN(3.81, 0.2); O_c and O_t are the average occupancies for cars and trucks, respectively, assumed to follow the respective distributions LN(1.5, 0.15) and LN(1.05, 0.15); and *T* represents the ratio of the average daily truck traffic to the average daily traffic and is considered as LN(0.12, 0.2). The

parameters of the random variables in Equation (9.2) are assumed based on Decò & Frangopol (2011).

The environmental impact of traffic delays due to maintenance includes an increase in air pollutants and emissions, energy consumption, and potential for global warming (Dong *et al.* 2013, 2014). The increase in the carbon dioxide emissions is used herein as the environmental impact of maintenance. Based on Kendall *et al.* (2008), this environmental impact is

$$E = ADT \cdot l \cdot d \cdot \left[En_{d,c} \cdot (1-T) + En_{d,t} \cdot T \right] \frac{En_{S_D} - En_{S_o}}{En_{S_o}} \tag{9.3}$$

where $En_{d,c}$ and $En_{d,t}$ represent the environmental metric per unit distance for cars and trucks, respectively, and it is quantified as the carbon dioxide emissions per kilometer (i.e., carbon dioxide kg/km). The environmental metrics $En_{d,c}$ and $En_{d,t}$ are assumed to follow the lognormal distributions LN(0.22, 0.2) and LN(0.56, 0.2), respectively (Gallivan *et al.* 2010, Dong *et al.* 2013). En_{S_D} and En_{S_o} represent the carbon dioxide emissions per kilometer at speeds S_D and S_o, respectively, and are considered herein 0.416 kg/km and 0.298 kg/km, respectively (Gallivan *et al.* 2010). The costs of carbon dioxide emissions can be transferred into monetary value by

$$C_E = E \cdot c_{Env} \tag{9.4}$$

where c_{Env} is cost value of environmental metric (e.g., carbon dioxide USD/*t*). The cost value c_{Env} of carbon dioxide emissions is assumed to follow the lognormal distribution LN(26, 2.93) (Kendall *et al.* 2008). Similarly, the cost of other pollutants due to maintenance, such as the carbon monoxide, can be computed.

The total cost of a maintenance action C can be found as the summation of the repainting cost, time loss cost, and environmental cost as

$$C = C_R + C_{TL} + C_E \tag{9.5}$$

The cost of maintenance is subjected to a discount rate of money at the application time t. The present cost of the kth maintenance action at time t is

$$C_{PV,k} = \frac{C}{(1+r)^t} \tag{9.6}$$

where $C_{PV,k}$ is the present cost of the kth maintenance action performed at time t, C is the cost of the maintenance at the application time, and r is the discount rate of money. As can be seen from Equations (9.1) and (9.3), the indirect maintenance cost depends, to a great extent, on the *ADT*. Since the *ADT* may be subjected to an annual increase rate, the maintenance cost will also be time-dependent. Assuming a constant rate of increase, the *ADT* at time t can be calculated as

$$ADT_t = ADT(1+v)^t \tag{9.7}$$

in which ADT_t is the *ADT* at time t, and v is the annual increase rate in the average daily traffic.

In order to evaluate the total cost of a single maintenance, a Monte Carlo simulation is performed with 100,000 samples. For the studied case, Figure 9.1 (a) shows the probability density function (PDF) of the total cost of a single maintenance including direct and indirect components at time = 0, 20, 40, 60, 80, and 100 years and considering the annual increase in *ADT* to be 0.5%. Figure 9.1 (b) shows the mean value and the standard deviation of the time-variant total maintenance cost for v = 0.5% and an annual discount rate of money r = 0.00. Figure 9.2 (a) depicts the PDF of the maintenance costs

at various times with v = 1.0% and r = 0.00, while Figure 9.2 (b) shows the mean and standard deviation of the time-variant maintenance cost for the same values of v and r. Figure 9.3 presents the mean value of the time-variant total maintenance cost for v = 0.5%, 1.0%, and 1.5%. As shown in Figure 9.3, the present value of the maintenance cost is significantly affected by the increase rate of the average daily traffic. An increase in v from 0.5% to 1.5% will lead to a corresponding increase of 88% in the present value of a maintenance performed after 100 years. This also shows that the indirect maintenance cost cannot be neglected in the life-cycle cost evaluation.

The cost values presented in Figures 9.1 – 9.3 illustrate only the total cost of one maintenance action performed at different times along the service life. However, depending on the environmental conditions at the bridge location, multiple maintenance actions may be needed throughout the service life of the structure to maintain an acceptable performance level. As previously indicated, the bridge under consideration was constructed in 1973 and the first complete painting maintenance was performed after 40 years of service life. Personal communication with PennDOT (2013) revealed that the time for the first complete maintenance can go to as high as 50 years, while some other bridges may be required to be repainted after 30 years (PennDOT 2013). Therefore, to compute the total life-cycle cost, the time for the first maintenance was assumed as a random variable following a triangular distribution Tri(30, 40, 50). However, the repainting maintenance may not be as effective as the initial painting for protecting the bridge from corrosion. This is mainly due to the effect of site conditions on the quality of the repainting. This quality is affected by multiple factors, such as the weather conditions,

bridge location, and the layout of the bridge. Thus, it is assumed that the time interval between subsequent maintenance actions follow a triangular distribution Tri(20, 25, 30).

In order to determine the total life-cycle cost of the bridge, a Monte Carlo simulation with 100,000 samples is also adopted. Figure 9.4 (a) shows the life-cycle cost profile for the carbon steel and the A1010 steel considering discount rate of money r = 0.00. Similarly, Figure 9.4 (b) presents the life-cycle cost profiles considering r = 0.03. The results in Figures 9.4 (a) and (b) assume no annual increase in the *ADT* (i.e., v = 0.0%).

Figure 9.5 (a) depicts the life-cycle cost profiles considering the discount rate of money to be a random variable following a uniform distribution with values ranging from 0.00 to 0.03 [i.e., U(0.00,0.03)]. Finally, Figure 9.5 (b) shows the life-cycle cost of the bridge for the case of carbon steel and the A1010 steel considering the rate of increase in traffic v = 1.0%. As shown in Figures 9.4 and 9.5, the life-cycle cost of the bridge constructed using the corrosion-resistant steel A1010 is constant throughout the service life of the bridge. Moreover, although the A1010 provides higher initial cost than the carbon steel, the life-cycle cost of the bridge constructed using carbon steel is significantly higher and can reach a value up to two times that of the same bridge constructed using the A1010 steel after 100 years of service life. It should also be noted that including other frequent corrosion-related maintenance actions such as zone panting will further increase the life-cycle cost of the bridge constructed using conventional carbon steel.

9.4 Conclusions

This chapter presents the computational results of a probabilistic study to evaluate the life-cycle cost of steel bridges constructed using conventional painted carbon steel and corrosion-resistant A1010 steel. The life-cycle cost consisted of the initial cost, in addition to the cost of repainting maintenance performed along the service life. The initial cost includes the cost of materials, fabrication, initial painting, shop inspection, and transportation. The cost of maintenance covers the repainting and traffic control costs, in addition to the indirect costs arising from the traffic delays and their social and environmental impacts.

The cost of a single maintenance action was computed for various values of average daily traffic increase rate and it was shown that this rate has significant effect on the indirect cost of maintenance. Moreover, the total life-cycle cost of the bridge considering multiple maintenance actions along the service life was computed for the conventional steel and the corrosion-resistant alternative. It was shown that, although the corrosion-resistant steel has higher initial cost, its life-cycle cost is less than that of the conventional steel, even when using a discount rate of money of 0.03. This indicates that the A1010 steel represents a more sustainable alternative to the conventional carbon steel for the bridge under consideration.

It is also observed that by including the indirect maintenance cost, the cost of a single maintenance action increases with time due to the increase in the *ADT* associated with the bridge. This increase can reach up to 20% after 40 years of service life. Therefore, it is expected that including the indirect effect of maintenance in the life-cycle cost computations associated with intervention optimization may affect the optimal

management solutions. Therefore it is crucial to integrate these indirect effect into the life-cycle cost computations in the future studies.

(a)

(b)

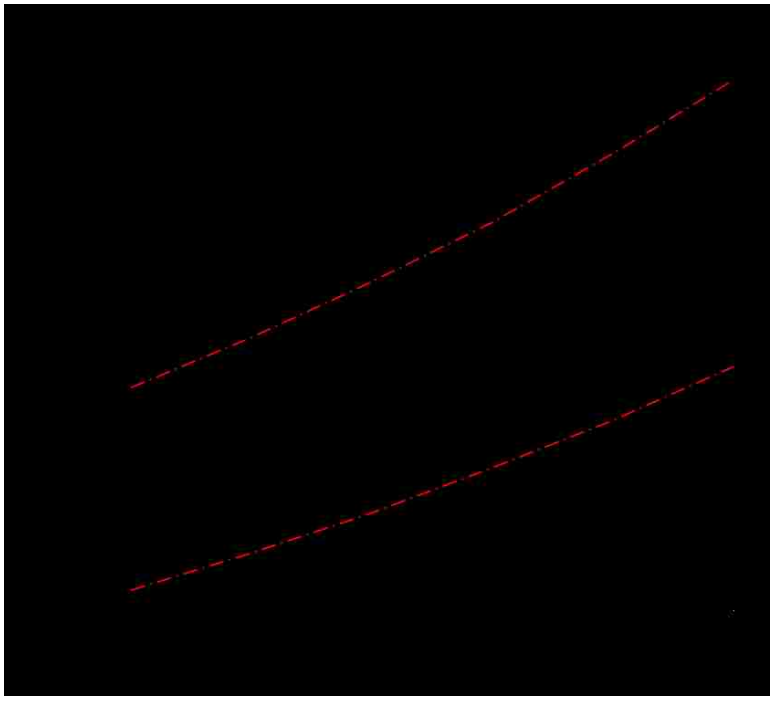

Figure 9.1 Present value of the total cost of a single repainting maintenance with v = 0.5% and r = 0.00; (a) PDF of the cost at t = 0, 20, 40, 60, 80, and 100 years, and (b) time-variant mean and standard deviation of the present value of the maintenance cost

(a)

(b)

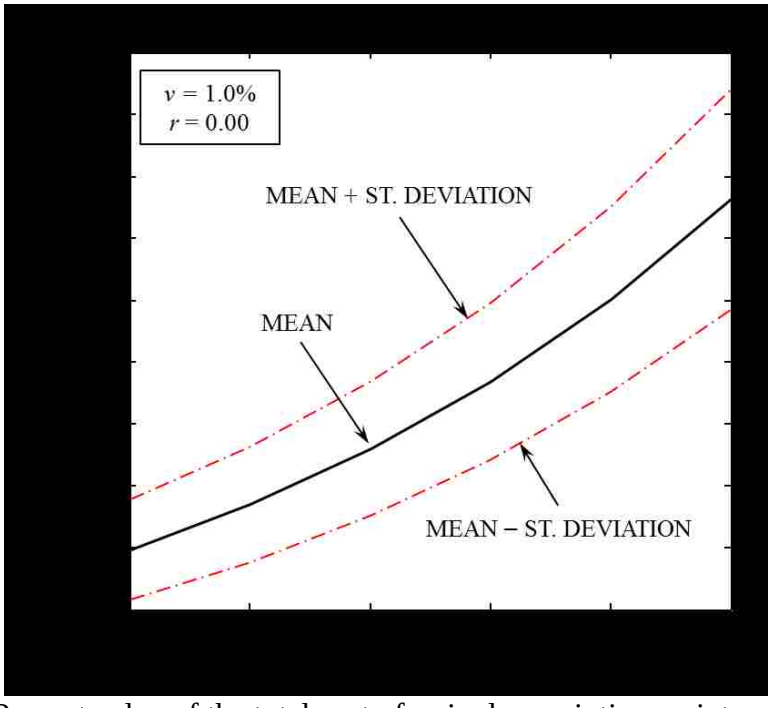

Figure 9.2 Present value of the total cost of a single repainting maintenance with v = 1.0% and r = 0.00; (a) PDF of the cost at t = 0, 20, 40, 60, 80, and 100 years, and (b) time-variant mean and standard deviation of the present value of the maintenance cost

Figure 9.3 Time-variant mean of the present value of the cost of a single maintenance for v = 0.5%, 1.0%, and 1.5%

(a)

(b)

Figure 9.4 Life-cycle cost of the bridge constructed using conventional steel and A1010 steel with v = 0.0%; (a) r = 0.00, and (b) r = 0.03

(a)

(b)

Figure 9.5 Life-cycle cost of the bridge constructed using conventional steel and A1010 steel; (a) r = U(0.00, 0.03) and v = 0.0%, and (b) r = U(0.00, 0.03) and v = 1.0%

CHAPTER 10 CONCLUSIONS

10.1 Summary

In this study, probabilistic methodologies for predicting the service life and scheduling inspection, monitoring, and maintenance actions for deteriorating civil and marine structures were proposed. The study presented different approaches suited for component- and system-level LCM of bridges and ships under fatigue and corrosion deterioration. Additionally, effective incorporation of SHM and inspection information to enhance the LCM process was addressed. The main outputs of the study are the time-variant performance profiles and the optimum intervention times and types which fulfil the management needs. The proposed methodologies enhance the life-cycle decision making process and enable the effective budget allocation.

The study employed multi-objective optimization techniques to obtain the optimum trade-offs between conflicting LCM criteria such as minimizing the life-cycle cost and maximizing the expected service life. Although multiple probabilistic performance indicators exist, the focus has been placed on estimating the structural performance in terms of the reliability index, probabilistic damage level (i.e., time-variant crack size, or corrosion depth), and lifetime functions. In the proposed intervention optimization approaches, the probabilistic damage level has been implemented as the performance measure to facilitate the decision making and interpretation of the results.

The main reliability and probabilistic performance prediction concepts were introduced in Chapter 2. Additionally, the adopted methodologies for predicting corrosion initiation and propagation in steel structures and the reinforcement of RC

structures were discussed. Fatigue life prediction approaches were also presented. The role of SHM and inspection information in the LCM was explained and a brief discussion on the use of optimization in the LCM was also provided.

Chapters 3 and 4 presented probabilistic approaches which aid in the fatigue assessment and service life estimation for fatigue prone details in steel bridges and high speed aluminum vessels, respectively. Chapter 3 investigated the gain in the fatigue life resulting from using the bi-linear *S-N* approach for different detail categories. It also investigated the relationship between the second slope of the *S-N* lines and the fatigue life while making use of bridge monitoring data. The work in Chapter 4 proposed a reliability-based approach for estimating fatigue life in aluminum ship details based on SHM data. The computational method for fatigue life prediction is flexible to accommodate any combination of operational conditions or any future change in the operational profile of the ship.

Chapter 5 provided a methodology for scheduling inspections, monitoring, and maintenance actions along the life-cycle of structures under time-dependent deteriorating actions. The approach considered various uncertainties associated with the damage occurrence and propagation, relationship between inspection/monitoring quality and the probability of damage detection, and the effect of maintenance on the structural performance and the service life. Several examples of intervention scheduling for ships and bridges subjected to corrosion and fatigue have been provided. The concept of maintenance delay has been introduced. Additionally, multiple objectives for optimizing the interventions have been considered simultaneously. These objectives are minimizing

the total life-cycle cost including the failure cost, maximizing the expected service life, and minimizing the maintenance delay.

In Chapter 6, emphasis has been placed on the incorporating the information obtained during inspections and evaluating its effect on the scheduled intervention schedule. Accordingly, an approach for integrating the damage level measured by NDI actions into the LCM framework has been proposed. The approach utilized a Bayesian updating scheme to draw samples from the damage propagation model parameters given the information obtained through an inspection. The main outputs of such approach are the updated intervention schedules given the measured damage level during inspection.

Chapter 7 provided an approach for scheduling NDI actions for structures with multiple critical locations. These locations can be fatigue prone details and/or specific locations under corrosion damage. The approach provided the optimum inspection times and the optimum NDI method to be used at each location. In Chapter 8, a system-based approach for scheduling inspections and maintenance actions has been provided. The approach aims to find the optimum intervention schedule which minimizes the maximum expected failure rate and the total intervention cost. Finally, Chapter 9 presented a discussion on computing the life-cycle cost of steel bridges while considering sustainability measures. It has been shown that these measures have a significant effect on the life-cycle cost; thus, they should be included in future LCM studies involving life-cycle cost. The presented study enhance the capabilities of the general integrated LCM framework and assist the informed decision making for deteriorating structures. Moreover, the approaches presented in Chapters 4 and 6 enable the near real-time decision making regarding future interventions on deteriorating structures.

10.2 Conclusions

Several conclusions can be drawn based on the investigations performed in this study. Significant conclusions related to the probabilistic fatigue life estimation for bridges and naval vessels are:

- Increasing the value of the slope below the CAFT (i.e., m_2) from 3 to 5 results in a significant increase in the remaining life especially for target reliability indices ranging from 2.0 to 3.5.
- Increasing the value of m_2 also yields an increase in the reliability index of the detail and an upward shift in the time-variant reliability profile. For a low number of stress cycles, the increase in the reliability index may not be significant; however, for higher numbers of stress cycles, this increase is significant and in some cases the reliability index can be doubled.
- For assessing fatigue life of critical bridge details, using recorded vehicle count and SHM data provide additional information that can assist in improving the accuracy of the fatigue reliability assessment.
- For structural details in naval vessels, some combinations of speeds, sea states, and wave headings have a significant effect on fatigue damage accumulation. These operational conditions should be identified and they should be avoided to prevent the accelerated damage to ship structures.
- Since the approach proposed for assessing the fatigue life of aluminum ship details provides the fatigue damage with respect to the individual operational conditions, it enables the active integration of fatigue aspects in the LCM framework in which inspection and maintenance optimization can be performed,

as well as the active route planning to minimize the fatigue damage accumulation at critical details during voyages.

- Specific properties of the vessel under investigation have to be considered when assessing the fatigue damage. For instance, with respect to the vessel analyzed in Chapter 2 and equipped with a T-foil to reduce vibrations at high speeds, it was found that at speeds 30 and 15 knots, the damage accumulation is larger when the T-foil is deployed. However, for a speed of 35 knots, the T-foil deployment reduces the damage accumulation by 30%.

With respect to the intervention optimization approaches proposed in this study, the following conclusions can be drawn:

- Minimizing the maintenance delay, maximizing the service life, and minimizing the life-cycle cost are conflicting objectives. Minimizing the maintenance delay tends to increase the life-cycle cost. Additionally, maximizing the service life yields higher expected life-cycle cost. In order to find a well-balanced solution, tri-objective optimization which simultaneously maximizes the expected service life, minimizes the total life-cycle cost, and minimizes the expected maintenance delay has to be solved. Through comparison among the Pareto-optimal solutions obtained from this multi-objective optimization, the effects of inspection/monitoring quality, number of inspections, damage criteria for determining maintenance types on the expected service life, maintenance delay, and total life-cycle cost are revealed.
- The optimum solution of the multi-objective optimization problem (i.e., optimum intervention types and times) depends on the cost of different intervention

options. For the investigated examples, it was found that for low values of ultrasonic inspection cost compared to that of acoustic emission monitoring, the optimization scheme suggests that only management plans where ultrasonic inspections are performed are optimal. This is also due to the lower probability of damage detection associated with the acoustic emission crack monitoring, However, if the cost of ultrasonic inspection increases due to the additional time required to perform the inspection, solutions with acoustic emission monitoring appear in the optimal solution front.

- Since the multi-objective optimization performed in this study provides a set of optimal solutions and not a single solution, the presence of constraints related to maximum allowable life-cycle cost and system performance (i.e., expected service life or maintenance delay) are crucial for selecting an optimal strategy.
- The monetary value associated with structural failure has a significant effect on the optimum solutions. A higher value yields solutions which have higher overall probability of performing repairs and lower probability of failure.
- The results of the proposed framework depend on the accuracy of damage propagation and service life prediction models. Information from each inspection should be used to update the damage propagation and service life. The efficient use of this information can lead to more accurate and reliable inspection and maintenance scheduling.

Based on the updating methodology proposed in this study, the following conclusions can be drawn:

- By using the proposed intervention optimization and performance updating, management plans allowing for real-time decisions based on future inspection outcomes are possible to be developed. The outcomes of such plans are the next inspection times and the damage level-based thresholds for re-assessment and repair decisions.
- The updated time-variant performance profiles are significantly affected by the inspection information. Therefore, the updating process enhances the accuracy of the performance estimation and is crucial for the successful LCM.
- Lifetime reliability measures such as the survivor function and the cumulative probability of failure can be effectively integrated into the LCM to assist the decision making process regarding future inspection and maintenance actions.
- The proposed LCM and performance updating scheme can be used in conjunction with different optimization techniques for inspection scheduling. The optimization may include extending the service life as an objective; however, care should be taken in selecting the optimization technique as it may affect the computational effort.

For scheduling inspections for structures with multiple deteriorating locations and system-based intervention optimization, the following conclusions can be drawn:

- For structures with multiple critical locations, establishing the inspection schedule that provides optimal inspection times and selects the best NDT technique for each location can be achieved using the proposed probabilistic optimization process. In this process, the different deterioration rates at each location can be

accounted for. Moreover, performance indicators based on lifetime functions and point-in-time probability of failure can be included.

- Based on the studied bridges, it was found that higher quality NDI methods do not have to be performed routinely throughout the lifetime of the structure. A limited number of optimally planned inspections can be enough to yield an acceptable probability of damage detection before failure of damaged components. In fact, some inspection techniques can provide a considerably higher probability of damage detection after a relatively small number of inspections when compared to methods with lower quality. The number of inspections, as well as their application times, can be provided by the solution of the optimization process.
- Including a realistic discount rate of money is essential to obtain an accurate Pareto-optimal solution front. Multiple solutions on this front may be associated with the same inspection method; however, each solution corresponds to unique cost and probability of damage detection pair allowing bridge managers to select the best solution which fits the management constraints.
- For system-based intervention scheduling of structures with different configurations of the same set of components, optimal inspection and maintenance plans for a given configuration may not be optimal for a different one. This is due to the fact that the expected total cost is component-dependent, while the system performance depends on both the system configuration and component failure rate.
- For the system-based intervention optimization approach discussed in this study, it was found that low cost maintenance plans are mainly associated with no repair

or preventive maintenance, providing a small reduction of the expected system failure rate. In these cases, in-depth inspections should be concentrated in the early life of the structure. Maintenance plans with the highest impact on the structural performance are generally associated with in-depth inspections distributed along the last part of the life-cycle of the system. For these strategies, essential maintenance options on critical components are dominant.

- Improving the inspection accuracy reduces the risk of occurrence of false alarms. Therefore, the most appropriate management decisions are more likely to be selected.

From the sustainability-based life-cycle cost computation approach, the following conclusions can be drawn:

- Sustainability measures for life-cycle cost computations include social, economic, and environmental aspects, which are dependent on the traffic volume. Therefore, the cost of a single maintenance action is significantly affected by the average daily traffic and the average daily traffic increase rate.
- Based on the results of the life-cycle cost comparison between the two steel alternatives, it was shown that, although the corrosion-resistant steel has higher initial cost, its life-cycle cost is less than that of the conventional steel, even when using a discount rate of money of 3%. This indicates that the corrosion-resistant steel represents a more sustainable alternative to the conventional carbon steel for the bridges in highly corrosive environments.

10.3 Suggestions for Future Work

- The performance prediction process is the foundation of the LCM. This prediction process depends to a great extent on the accuracy of the performance prediction model and the descriptors of its probabilistic parameters. However, in some cases, the accurate information on some model parameters does not exist. Therefore, future efforts to quantify these parameters are crucial. An example of these parameters are the descriptors of the slope m_2 (see Chapter 3). The accurate estimation of the characteristics of these parameters can be achieved by making use of the available bridge inspection and monitoring results and will help improving the reliability assessment process of bridges.
- The effect of maintenance on the structural performance is generally difficult to quantify, especially when using probabilistic performance indicators. In the maintenance optimization approach presented in this study, two types of maintenance have been considered, namely, the maintenance which stops the further damage propagation and the one which results in the restoration of structural performance to the initial level. These two types represent the lower and upper extremes for the extent of maintenance (i.e., degree of performance restoration); however, in real world situations, maintenance can yield other levels of performance restoration (e.g., 90% performance restoration). Therefore, further research is needed to (a) establish the relationship between various maintenance types and the associated performance restoration, and (b) incorporate these maintenance types into the intervention optimization approaches presented in this study.

- The approach for monitoring scheduling presented in this study provides the optimum monitoring times and types for monitoring methods employed for damage detection. However, conventional monitoring activities which use strain gauges and accelerometers to assess the performance cannot be optimized by using this approach. Since these monitoring activities yield a large amount of data whose analyses and interpretation may require significant financial resources, establishing the optimum monitoring plan is a crucial aspect, especially for structures equipped with long-term monitoring hardware (e.g., the high speed naval vessel analyzed in Chapter 4). A rational approach is to find the optimum monitoring schedule which minimizes the error arising from using multiple short term monitoring actions compared to the continuous long-term monitoring. Such an approach does not exist for naval vessels.
- In this study, the reliability of naval vessels was only computed with respect to fatigue damage. Although fatigue is a major aspect affecting the ship safety, other aspects, such as the serviceability, crew comfort, and ultimate strength should also be studied. Therefore, an integrated approach for estimating the overall ship reliability and safety is still required.
- The proposed LCM approach in its current format can be only applied to structures under time-dependent deterioration. However, the approach can be extended to a risk-based intervention optimization methodology where the damage induced by extreme events, such as earthquakes and hurricanes, can be assessed and the risk-based decision making process can be included.

- The proposed LCM and performance updating scheme presented in Chapter 6 can be used in conjunction with other intervention optimization and scheduling techniques. The use of SHM information in updating the parameters of load and resistance prediction models for ships and bridges is another interesting topic which will also improve the accuracy of the performance prediction.

- For intervention optimization, the accurate estimation of the *PoD* parameters is crucial for the accuracy of the optimum solutions. However, more research is needed to establish the *PoD* for different NDI and monitoring methods. Further research aiming to establish other models for quantifying the inspection effectiveness are required. The approach presented in Chapter 8 uses a novel inspection accuracy parameter; however, more research is still needed to quantify the descriptors of this parameter for different inspection and monitoring methods.
- From the life-cycle cost computations procedure presented in Chapter 9, it is evident that including the social and environmental aspects arising from the maintenance of a bridge affect the cost estimation. Therefore, an integrated approach which performs the LCM while considering these aspects is required. A risk-based approach can be well suited to address this integration.
- The intervention optimization approaches presented in this study for ship structures assumes that the loading conditions of the ship are constant over time. A system-based approach which can provide the optimum intervention schedule as a function of the operational profile of the ship is required.

REFERENCES

American Association of State Highway and Transportation Officials (AASHTO). (2002). *AASHTO standard specifications for highway bridges and interim specifications*. Seventeenth Edition, HB-17. American Association of State Highway and Transportation Officials, Washington, D.C.

American Association of State Highway and Transportation Officials (AASHTO). (2014). *AASHTO LRFD Bridge Design Specifications*. Seventh Edition, American Association of State Highway and Transportation Officials, Washington, D.C.

ABAQUS. (2009). *ABAQUS/Standard Version 6.9 User's Manuals*. Hibbit, Karlsson, and Soreson, Inc., Pawtucket, Rhode Island.

ABS. (2010) *Spectral-based fatigue analysis for floating production, storage and offloading (FSPO) installations*. American Bureau of Shipping, Houston, TX

Adey, B.T, Lethanh, N., Hartmann, A., and Francesco, V. (2014) Evaluation of Intervention Strategies for a Road Link in the Netherlands. *Built Environment Project and Asset Management*, Emerald Group Publishing Limited, 4(2), in press.

Ahmad, S. (2003). Reinforcement corrosion in concrete structures, its monitoring and service life prediction – a review. *Cement and Concrete Composites*, Elsevier, 25(4-5), 459, 471.

Akgül, F. (2002). *Lifetime system reliability prediction for multiple structure types in a bridge network*. PhD Thesis, Department of Civil, Environmental, and Architectural Engineering, University of Colorado, Boulder, Colorado.

Akgül, F., and Frangopol, D.M. (2004). Lifetime performance analysis of existing steel girder bridge superstructures. *Journal of Structural Engineering*, 130(12), 1875–1888.

Akgül, F., and Frangopol, D.M. (2005a). Lifetime performance analysis of existing reinforced concrete bridges. I: Theory. *Journal of Structural Engineering*, 11(2), 122–128.

Akgül, F., and Frangopol, D.M. (2005b). Lifetime performance analysis of existing reinforced concrete bridges. II: Application. *Journal of Structural Engineering*. 11(2), 129–141.

Akiyama, M., Frangopol, D.M., and Suzuki, M. (2012). Integration of the effects of airborne chlorides into reliability-based durability design of reinforced concrete structures in a marine environment, *Structure and Infrastructure Engineering*, 8(2), 125-134.

Akpan, U.O., Koko, T.S., Ayyub, B., and Dunbar, T. E. (2002). Risk assessment of aging ship hull structures in the presence of corrosion and fatigue. *Marine Structures*, 15(3), 211-231.

Albrecht P., Naeemi A. (1984). *Performance of weathering steel in bridges*. NCHRP Report 272, National Cooperative Highway Research Program, Transportation Research Board, National Research Council, Washington D.C.

Albrecht, P., and Yamada, K. (1977). Rapid calculation of stress intensity factors, *Journal of the Structural Division*, ASCE, 103, 377-389.

Anastasopoulos, A., Kourousis, D., Botten, S., and Wang, G. (2009), Acoustic emission monitoring for detecting structural defects in vessels and offshore structures. *Ships and Offshore Structures*, 4(4), 363–372.

Anderson, T.W., and Darling, D.A. (1952). Asymptotic theory of certain, goodness-of-fit criteria, based on stochastic processes. *The Annals of Mathematical Statistics*, 23(2):193–212, 1952.

Ang, A.H.-S., and Tang, W.H. (1984). *Probability concepts in engineering planning and design: decision, risk and reliability*. Vol II. New York: Wiley.

Ang, A.H.-S., and Tang, W. (2007). *Probability concepts in engineering: emphasis on applications to civil and environmental engineering*. Second Edtion. John Wiley & Sons, New Jersey.

Ang, A.H-S., and De Leon, D. (2005). Modeling and analysis of uncertainties for risk-informed decisions in infrastructures engineering, *Structure and Infrastructure Engineering*, 1(1), 19-31.

Arora, J. (2012). *Introduction to Optimum Design*. Third Edition, Elsevier Academic Press, NY, 896p.

Ayyub. B.M., Akpan, U.O., DeSouza, G.F., Koto, T.S., and Luo, X. (2000). *Risk-based life cycle management of ship structures*. Ship Structure Committee Report SSC-416, Ship Structure Committee, Washington, D.C.

Ayyub, B.M., Assakkaf, I.A., Kihl, D.P., and Sieve, M.W. (2002). Reliability-Based Design Guidelines for Fatigue of Ship Structures. *Naval Engineers Journal*, 114(2), 113-138.

Baran, I., Nowak, M., Jagenbrein, A., and Buglacki, H. (2012). Acoustic emission monitoring of structural elements of a ship for detection of fatigue and corrosion damages. *Proceedings of 30th European Conference on Acoustic Emission Testing & 7th International Conference on Acoustic Emission*, University of Granada.

Barone, G., and Frangopol, D.M. (2013a). Hazard-based optimum lifetime inspection and repair planning for deteriorating structures. *Journal of Structural Engineering*, 139(12), 04013017.

Barone, G., and Frangopol, D.M. (2013b). Reliability, risk and lifetime distributions as performance indicators for life-cycle maintenance of deteriorating structures. *Reliability Engineering & System Safety*, 123, 21-37.

Barone, G., Frangopol, D.M., and Soliman, M. (2014). Optimization of life-cycle maintenance of deteriorating bridges considering expected annual system failure

rate and expected cumulative cost. *Journal of Structural Engineering*, 140(2), 04013043

Barsom, J.M., and Rolfe, S.T., (1999). *Fracture and fatigue control in structures: applications of fracture mechanics*. Third Edition, American Society for Testing and Materials, West Conshohocken, PA.

Berens, A.P. (1989). *NDE reliability analysis*. Metal handbook, Ninth Edition, Vol. 17, ASM International, Material Park, Ohio, 689-701

Berens, A.P., and Hovey, P.W. (1981). *Evaluation of NDE reliability characterization*. Air Force Wright-Aeronautical Laboratory, Wright-Patterson Air Force Base, Dayton, Ohio.

Biondini, F., and Frangopol, D.M. (2008). Probabilistic limit analysis and lifetime prediction of concrete structures, *Structure and Infrastructure Engineering*, 4(5), 399-412.

Biondini, F., Bontempi, F., Frangopol, D.M. and Malerba, P.G. (2006). Probabilistic service life assessment and maintenance planning of concrete structures, *Journal of Structural Engineering*, 132(5), 810-825.

Bocchini, P., and Frangopol, D.M. (2011). A probabilistic computational framework for bridge network optimal maintenance scheduling, *Reliability Engineering & System Safety*, 96(2), 332-349.

Bocchini, P., Frangopol, D.M., Ummenhofer, T. and Zinke, T. (2013). Resilience and sustainability of the civil infrastructure: Towards a unified approach, *Journal of Infrastructure Systems*, 20(2), 0414004.

Brady T.F. (2004a). *Wave impact loading response measurement and analysis for HSV-2 from JLOTS and blue game rough water trials*. NSWCCD-65-TR- 2004/32, Naval Surface Warfare Center, Carderock Division, West Bethesda, MD.

Brady T.F. (2004b). *HSV-2 Swift instrumentation and technical trials plan*. NSWCCD-65-TR- 2004/18, Naval Surface Warfare Center, Carderock Division, West Bethesda, MD.

Brady T.F. (2004c). *Global structural response measurement of SWIFT (HSV-2) from JLOTS and blue game rough water trials*. NSWCCD-65-TR- 2004/33, Naval Surface Warfare Center, Carderock Division, West Bethesda, MD.

British Standards Institute (BSI). (1980). *Steel, concrete, and composite bridges: code of practice for fatigue*. 5400-Part 10. British Standards Institute, London, UK.

British Standards Institute (BSI). (2005). *Guide to methods for assessing the acceptability of flaws in metallic structures*. BS7910, British Standards Institute, London, UK.

Brooks, S., and Gelman, A. (1998). General methods for monitoring convergence of iterative simulations. *Journal of computational and Graphical Statistics*, 7, 434-455.

Caldeira Duarte, J.A., Craveiro, J.C.T.A., and Trigo, T.P. (2006). Opmitization of the preventive maintenance plan of a series components system. *International Journal of Pressure Vessels and Piping*, 83, 244-248.

Carino, N.J. (1999). Nondestructive techniques to investigate corrosion status in concrete structures. *Journal of Performance of Constructed Facilities*, 13(3), 96-106.

Catbas, N.F., Zaurin, R., Frangopol, D.M., and Susoy, M. (2007). System Reliability-Based Structural Health Monitoring with FEM Simulation, *Proceedings SHMII-3*, Vancouver, B.C., Canada.

Chaker, V., ed. (1992). *Corrosion forms & control for infrastructure*. *ASTM STP 1137*, Philadelphia.

Chan, T.H.T., Li, Z.X and Ko, J.M. (2001). Fatigue analysis and life prediction of bridges with structural health monitoring data – Part II: application. *International Journal of Fatigue*, 23 (1), 55-64.

Chung, H., Manuel, L. and Frank, K. (2006). Optimal inspection scheduling of steel bridges using nondestructive testing techniques, *Journal of Bridge Engineering*, 113, 305-319.

Clark, M.R., McCann, D.M., and Forde, M.C. (2003). Application of infrared thermography to the non-destructive testing of concrete and masonry bridges. *NDT&E International*, 36, 265-275.

Cho, H., and Lissenden, C.J. (2012). Structural health monitoring of fatigue crack growth in plate structures with ultrasonic guided waves. *Structural Health Monitoring*, 11(4), 393-404.

Collette, M. (2005). *Strength and reliability of aluminum stiffened panels*. 139-198, A Thesis submitted for the Degree of Doctor of Philosophy, School of Marine Science and Technology, Faculty of Science, Agriculture and Engineering, University of Newcastle, UK.

Collette, M., and Incecik, A., (2006). An approach for reliability-based fatigue design of welded joints in aluminum high-speed vessels. *Journal of Ship Research*, 50(3), 85-98.

Connor, R.J., and Fisher, J.W. (2001). *Report on Field Measurements and Assessment of the I-64 Kanawha River Bridge at Dunbar, West Virgini.* ATLSS Report No. 01-14, Lehigh University's Center for Advanced Technology for Large Structural Systems (ATLSS), Bethlehem, PA.

Connor, R.J., and Fisher, J.W. (2006). Identifying effective and ineffective retrofits for distortion fatigue cracking in steel bridges using field instrumentation. *Journal of Bridge Engineering*, 11(6), 745–52.

Connor, R.J., Hodgson, I.C., Mahmoud, H.N. and Bowman, C.A. (2005). *Field testing and fatigue evaluation of the I-79 Neville Island Bridge over the Ohio River*. ATLSS Report No. 05-02, Lehigh University's Center for Advanced Technology for Large Structural Systems (ATLSS), Bethlehem, PA.

Cramer, E.H., and Bea, R.G. (1991). Fatigue reliability model for inspection, updating and repair of welded geometries. *Paper presented at the Marine Structural Inspection, Maintenance, and monitoring Symposium*. Ship Structure Committee. Arlington, VA.

Cramer, E.H., and Friis-Hansen, P. (1994). Reliability-based optimization of multi-component welded structures. *Journal of Offshore Mechanics and Arctic Engineering*, 116(4), 223-238.

Crank, J. (1975). *The mathematics of diffusion*. Oxford University Press, Oxford, UK.

Crawshaw, J., and Chambers, J. (1984). *A Concise Course in A-Level Statistics*. Stanley Thornes (Publishers) Ltd., Surrey, UK.

Cremona, C. (1996). Reliability updating of welded joints damaged by fatigue. *International Journal of Fatigue*, 18(8), 567-575.

Crudele, B.B. and Yen, B.T. (2006). Analytical examination of *S-N* curves below Constant Amplitude Fatigue Limit. *Proceedings of the First International Conference on Fatigue and Fracture in the Infrastructure*, Philadelphia, PA.

Deb, K. (2001). Multi-objective optimization using evolutionary algorithms. John Wiley & Sons, New Jersey.

Deb, K., Pratap, A., Agarwal, S., and Meyarivan, T. (2002). A fast and elitist multiobjective genetic algorithm: NSGA-II. *IEEE Transactions on Evolutionary Computation*, 6(2), 182- 197.

Decò, A., and Frangopol, D.M. (2011). Risk assessment of highway bridges under multiple hazards. *Journal of Risk Research*, 14(9), 1057-1089.

Decò, A, Frangopol, D.M., and Okasha, N.M. (2011). Time-variant redundancy of ship structures. *Journal of Ship Research*. 55(3), 208–219.

Decò, A, Frangopol, D.M., and Zhu, B. (2012), Reliability and redundancy of ships under different operational conditions. *Engineering Structures* 42, 457 – 471.

Ditlevsen, O., and Madsen, H.O., (2007). *Structural reliability methods*, Deparment of Mechanical Engineering, Technical University of Denmark, http://od-website.dk/books/OD-HOM-StrucRelMeth-Ed2.3.7.pdf <accessed July, 7, 2014>

Det Norske Veritas (DNV). (1997). *Fatigue analysis of high speed and light craft*, Det Norske Veritas Classification A.S., CN 30.9, Høvik, Norway.

Det Norske Veritas (DNV). (1998). *Type approval program for protective coating systems*. No. 1-602.1, DNV, Oslo, Norway.

Det Norske Veritas (DNV). (1999). *Corrosion prevention of tanks and holds*. Classification Notes No. 33.1, DNV, Oslo, Norway.

Det Norske Veritas (DNV). (2010). *Fatigue methodology of offshore ships*, Recommended Practice DNV-RP-C206, October 2010. DNV: Høvik, Norway

Dobson, W.G., Brodrick, R.F., Wheaton, J.W., Giannotti, J., and Stambaugh, K.A. (1983). *Fatigue considerations in view of measured load spectra.* SSC-315, Ship Structure Committee.

Dong, Y., Frangopol, D.M., and Saydam, D. (2013). Time-variant sustainability assessment of seismically vulnerable bridges subjected to multiple hazards. *Earthquake Engineering and Structural Dynamics*, 42(10), 1451-1467.

Dong, Y., Frangopol, D.M., and Saydam, D. (2014). Sustainability of highway bridge networks under seismic hazard, *Journal of Earthquake Engineering*, 18, 41-66.

Downing, S.D., and Socie, D.F. (1982). Simple rainflow counting algorithms. *International Journal of Fatigue*, 4(1), 31-40.

Ellingwood, B.R. (2005). Risk-informed condition assessment of civil infrastructure: state of practice and research issues, *Structure and Infrastructure Engineering*, 1(1), 7-18.

Enright, M.P. and Frangopol, D.M. (1999). Maintenance planning for deteriorating concrete bridges. *Journal of Structural Engineering*, 125(12), 1407-1414.

Enright, M. and Frangopol, D.M., (2000). RELTSYS: A computer program for life prediction of deteriorating system. *Structural Engineering and Mechanics*, 9(6), 557–568.

Estes, A.C. (1997). *A system reliability approach to the lifetime optimization of inspection and repair of highway bridges*. PhD Thesis, Department of Civil, Environmental, and Architectural Engineering, University of Colorado, Boulder, Colorado.

Estes, A.C., and Frangopol, D.M. (1998), RELSYS: A computer program for structural system reliability analysis. *Structural Engineering Mechanics*, 6(8), 901-919.

Estes, A.C. and Frangopol, D.M. (1999). Repair optimization of highway bridges using system reliability approach. *Journal of Structural Engineering*, 125(7), 766-775.

Estes, A.C., and Frangopol, D.M. (2001). Minimum expected cost-oriented optimal maintenance planning for deteriorating structures: Application to concrete bridge decks. *Reliability Engineering & System Safety*, 73(3), 281-291.

Estes, A.C., and Frangopol D.M. (2003), Updating bridge reliability based on bridge management systems visual inspection results. *Journal of Bridge Engineering*, 8(6), 374-382.

Eurocode 9. (2009). *Design of Aluminium Structures Part 1-3, Additional rules for structures susceptible to fatigue*. CEN – European committee for Standardisation, Brussels, Belgium.

Eurocode 3. (2010). *Design of Steel Structures Part 1-9, Fatigue strength*. CEN – European committee for Standardisation, Brussels, Belgium

Fatemi, A., and Yang, L. (1998). Cumulative fatigue damage and life prediction theories: a survey of the state of the art for homogeneous materials. *International Journal of Fatigue*, 20(1), 9-34.

Federal Highway Administration (FHWA). (2001). *Reliability of visual inspection for highway Bridges*, Volume I, Final Report, FHWA Report No. FHWA-RD-01-

020, Federal Highway Administration, U.S. Department of Transportation, Washington, DC.

Federal Highway Administration (FHWA). (2012). *Material Type of Structure by State*, 2012, online: http://www.fhwa.dot.gov/bridge/nbi/no10/mat12.cfm, accessed December 2013.

Federal Highway Administration (FHWA). (2012). *National bridge inspection standards*, NBIS, Federal Highway Administration, U.S. Department of Transportation, Washington, DC.

Fisher, J.W. (1984). *Fatigue and Fracture in Steel Bridges, Case Studies*. John Willey & Sons, New Jersey.

Fisher, J.W., Kulak, G.L., and Smith, I.F. (1998). *A fatigue primer for structural engineers*, National Steel Bridge Alliance, Chicago, IL

Fisher, J.W., Jin, J., Wagner, D.C., and Yen, B.T., (1990). *Distortion-induced fatigue cracking in steel bridges*. National Cooperative Highway Research Program, Report 366, Transportation Research Board, National Research Council, Washington D.C.

Forsyth, D.S. and Fahr, A. (1998). An Evaluation of probability of detection statistics. *Paper presented at the RTO-AVT Workshop on Airframe inspection reliability under field/depot conditions*, Brussels, Belgium.

Frangopol, D.M. (1999). *Life – cycle cost analysis for bridges*, Chapter 9 in Bridge Safety and Reliability, D.M. Frangopol, ed., ASCE, 210-236.

Frangopol D.M. (2011). Life-cycle performance, management, and optimization of structural systems under uncertainty: accomplishments and challenges. *Structure and Infrastructure Engineering*, 7(6), 389-413.

Frangopol, D.M., Lin, K.Y., and Estes, A.C. (1997a). Reliability of reinforced concrete girders under corrosion attack. *Journal of Structural Engineering*, 123(3), 286-297.

Frangopol, D.M., Lin, K.Y., and Estes, A.C. (1997b). Life-cycle cost design of deteriorating structures. *Journal of Structural Engineering*, 123(10), 1390-1401.

Frangopol, D.M., Strauss, A., and Kim, S. (2008a). Use of monitoring extreme data for the performance prediction of structures: General approach. *Engineering Structures*, 30 (12), 3644–3653.

Frangopol, D.M., Strauss, A., Kim, S. (2008b). Bridge reliability assessment based on monitoring. *Journal of Bridge Engineering*, 13(3), 258–270.

Frangopol, D.M., Bocchini, P., Decò, A., Kim, S., Kwon, K., Okahsa, N.M., and Saydam, D. (2012) Integrated life-cycle framework for maintenance, monitoring, and reliability of naval ship structures. *Naval Engineers Journal*, 124(1): 89–99.

Frangopol, D.M., and Soliman, M. (2013). Integration of structural health monitoring in system-based life-cycle infrastructure management under uncertainty.

Proceedings of the 6th International Conference on Structural Health Monitoring if Intelligent Infrastructure (SHMII-6 2013), Hong Kong, December 9-11, 2013.

Frangopol, D.M., and Soliman, M., (2014a). Evaluation and prediction of damage to ship structures under uncertainty. in *Handbook of Nano to Macro Damage Mechanics* (G.Z. Voyiadjis, ed.), Springer Dordrecht-Heidelberg-London-New York (in press).

Frangopol, D.M., and Soliman, M., (2014b). Life-cycle of structural systems: recent achievements and future directions. *Structure and Infrastructure Engineering*, (submitted).

Frangopol, D.M., and Soliman, M. (2014c). Structural life-cycle management of ships under uncertainty. *Naval Engineers Journal* (in press).

Gallivan, F., Ang-Olson, J., Papson, A., and Venner, M. (2010). Greenhouse gas mitigation measures for transportation construction, maintenance, and operations activities. *AASHTO Standing Committee on the Environment*, San Francisco, CA.

Garbatov, Y., and Guedes Soares, C. (2001). Cost and reliability based strategies for fatigue maintenance planning of floating structures. *Reliability Engineering & System Safety*, 73(3), 293-301.

Gelman, A. (1996). Inference and monitoring convergence. In *Markov chain Monte Carlo in practice*, W.R. Gilks, S. Richardson and D. T. Spiegelhalter, eds., London: Chapman and Hall, 131-143.

Giovanni, B. and Sorrentino, R. (2007). *Electronic filter simulation & design*. McGraw-Hill, New York.

Glen, I.F., Paterson, R.B., and Luznik, L., (1999a). *Sea operational profiles for structural reliability assessment*. Ship Structure Committee Report No SSC-406, Ship Structure committee, Washington, DC

Glen, I.F., Dinovitzer, A., Paterson, R.B., Luznik, L., and Bayley, C., (1999b). *Fatigue-resistant detail design guide for ship structures*. Ship Structure Committee Report No SSC-405, Ship Structure committee, Washington, DC

Gonzalez, J.A., Andrade, C., Alonso, C., and Feliu, S. (1995). Comparison of rate of general corrosion and maximum pitting penetration on concrete embedded steel reinforcement. *Cement and Concrete Research*, 25(2), 257-264.

Guedes Soares, C., and Garbatov, Y. (1999a). Reliability of maintained, corrosion protected plate subjected to non-linear corrosion and compressive loads. *Marine Structures*, 12, 425–445

Guedes Soares, C., and Garbatov, Y. (1999b). Reliability based fatigue design of maintained welded joints in the side shell of tankers. *European Structural Integrity Society*, 23, 13-28.

Guedes Soares, C., Garbatov, Y., Zayed, A., and Wang, G. (2005). Nonlinear corrosion model for immersed steel plates accounting for environmental factors. *SNAME Maritime Technology Conference & Expo*, Houston, TX.

Hasting, W.K., (1970). Monte Carlo sampling methods using Markov chains and their applications. *Biometrika*, 57 (1), 97–109.

Heredia-Zavoni, E. and Montes-Iturrizaga, R. (2004). A Bayesian model for the probability distribution of fatigue damage in tubular joints. *Journal of Offshore Mechanics and Arctic Engineering*, 126(3), 243-249.

Hess, P.E. (2007). Structural health monitoring for high-speed naval ships. *In: Proceedings of the 6th international workshop on structural health monitoring. Quantification, validation, and implementation*, 11–14 September 2007, Stanford, CA. Lancaster, PA: DEStech Publishing, 3–15.

Huang, N.E., and Shen, S.S. (2005). *Hilbert-Huang transform and its applications*. Vol. 5. World Scientific, Singapore.

Hughes, O.F. (1988). *Ship Structural Design*. The Society of Naval Architects and Marine Engineers, Jersey City, New Jersey.

Hutter, W., and Donnelly D.E. (1977), Rate of deterioration of concrete bridge decks in Colorado. *Final Rep. No. CDOH-P&R-R-77-6*, Colorado Division of Highways, Denver.

IACS. (2003). *Renewal criteria for side shell frames and brackets in single side skin bulk carriers not build in accordance with UR S12*. Rev.1 or subsequent revisions, International Association of Classification Societies, London

Incat. (2012). *98 Metre wave piercing catamaran*. 3 Dec. 2012, < http://www.incat.com.au/domino/incat/incatweb.nsf/0/76457AADD2C1A987CA2571AF0019EC66?OpenDocument >

ISSC. (2006). *Condition assessment of aged ships*. International Ship and Offshore Structures Congress, Committee V.6, Volume 2

ISSC. (2009). *Condition assessment of aged ships and offshore structures*. Committee V.6, 17th International Ship and Offshore Structures Congress, August 16–21, Seoul, Korea.

Jensen, J.J., (2001). *Load and Global Response of Ships*. Elsevier Ocean Engineering Series, ed. R. Bhattacharyya and M.E. McCormick. Vol. 4, Elsevier, Oxford.

Kale, A.A and Haftka, R.T. (2008). Tradeoff of weight and inspection cost in reliability-based structural optimization. *Journal of Aircraft*, 45(1), 77-85.

Kendall, A., Keoleian, G. and Helfand, G. (2008). Integrated life-cycle assessment and life-cycle cost analysis model for concrete bridge deck applications. *Journal of Infrastructure Systems*, 14(3), 214-222.

Kim, S., and Frangopol, D.M. (2011a). Cost-based optimum scheduling of inspection and monitoring for fatigue sensitive structures under uncertainty. *Journal of Structural Engineering*, 137(11), 1319-1331.

Kim, S., and Frangopol, D.M. (2011b). Inspection and monitoring planning for RC structures based on minimization of expected damage detection delay. *Probabilistic Engineering Mechanics*, 26(2), 308-320.

Kim, S., and Frangopol, D.M. (2011c). Optimum inspection planning for minimizing fatigue damage detection delay of ship hull structures. *International Journal of Fatigue,* 33(3), 448-459.

Kim, S., and Frangopol, D.M. (2012). Probabilistic bicriterion optimum inspection/monitoring planning: Application to naval ships and bridges under fatigue. *Structure and Infrastructure Engineering,* 8(10), 912-927.

Kim, S., Frangopol, D.M., and Zhu, B. (2011). Probabilistic optimum inspection / repair planning to extend lifetime of deteriorating RC structures. *Journal of Performance of Constructed Facilities,* 25(6), 534-544.

Kim, S., Frangopol, D.M., and Soliman, M. (2013). Generalized probabilistic framework for optimum inspection and maintenance planning. Journal of Structural Engineering 139(3), 435–447 .

Kong, J.S., and Frangopol, D.M. (2003a). Life-cycle reliability-based maintenance cost optimization of deteriorating structures with emphasis on bridges. *Journal of Structural Engineering*, 129(6), 818-828.

Kong, J.S., and Frangopol, D.M. (2003b). Evaluation of expected life-cycle maintenance cost of deteriorating structures. *Journal of Structural Engineering*, 129(5), 682-691.

Kosteas, D. (1999*). Design example in fatigue based on European Standard ENV 1999-2 (Eurocode 9)*, Training in Aluminium Application Technologies (TALAT), 2712:1-14.

Kwon, K., Frangopol, D.M. (2010). Bridge fatigue reliability assessment using probability density functions of equivalent stress range based on field monitoring data. *International Journal of Fatigue*, 32, 1221–1232.

Kwon, K., Frangopol, D.M. (2011) Bridge fatigue assessment and management using reliability-based crack growth and probability of detection models. *Probabilistic Engineering Mechanics* 26(3, 471–480.

Kwon, K., and Frangopol, D.M. (2012a) System reliability of ship hull structures under corrosion and fatigue. *Journal of Ship Research*, 95(4), 234–251.

Kwon, K., and Frangopol, D.M. (2012b) Fatigue life assessment and lifetime management of aluminum ships using life-cycle optimization. *Journal of Ship Research*, 56(2), 91–105.

Kwon, K., Frangopol, D.M., and Soliman, M. (2012). Probabilistic Fatigue Life Estimation of Steel Bridge Based on a Bi-linear S-N Approach. *Journal of Bridge Engineering*, 17(1), 58-70.

Kwon, K., Frangopol, D.M., and Kim, S., (2013). Fatigue performance assessment and service life prediction of high-speed ship structures based on probabilistic lifetime sea loads. *Structure and Infrastructure Engineering*, 9(2), 102-115.

Lamtenzan D., Washer G., and Lozev M., (2000). *Detection and sizing of cracks in structural steel using the eddy current method*, FHWA-RD-00-018, McLean, VA 22101-2296.

Leemis, L.M. (1995). *Reliability, Probabilistic Models and Statistical Methods.* Prentice Hall, New Jersey.

Li, Z., Zhang, Y., and Wang, C. (2013). A sensor-driven structural health prognosis procedure considering sensor performance degradation, *Structure and Infrastructure Engineering*, 9(8), 764-776.

Li, Z.X, Chan, T.H.T. and Ko, J.M. (2001). Fatigue analysis and life prediction of bridges with structural health monitoring data – Part I: methodology and strategy. *International Journal of Fatigue*, 23 (1), 45-53.

Liu, M., Frangopol, D.M., Kwon, K. (2010). Fatigue reliability assessment of retrofitted steel bridges integrating monitored data. *Structural Safety*, 32(1), 77-89.

Liu, P.L., Lin, H.Z., and Der Kiureghian, A., (1989). *CalREL User Manual*, Department of Civil Engineering. University of California, Berkeley, CA.

Luki, M., and Cremona, C., (2001). Probabilistic optimization of welded joints maintenance versus fatigue and fracture. *Reliability Engineering & System Safety*. 72(3), 253-264.

Ma, K-T., Orisamolu, I.R., and Bea, R.G. (1999). *Optimal strategies for inspection of ships for fatigue and corrosion damage*. Ship Structure Committee Report *No. SSC – 407*, Ship Structure Committee, Washington DC.

Maddox, S.J. (2003). Review of fatigue assessment procedures for welded aluminum structures. *International Journal of Fatigue*, 25, 1359-1378.

Madsen, H.O., Skjong, R.K., Tallin, A.G., and Kirkemo, F. (1987). Probabilistic fatigue crack growth analysis of offshore structures, with reliability updating through inspection. *Paper presented at the marine Structural Reliability Symposium*, Arlington, VA.

Madsen, H.O., Torhaug, E., and Cramer, E.H. (1991). Probability-based cost benefit analysis of fatigue design, inspection, and maintenance. *Paper presented at the Marine Structural Inspection, Maintenance, and monitoring Symposium*. Ship Structure Committee. Arlington, VA.

Mahmoud, H.N., Connor, R.J., Bowman, C.A. (2005). *Results of the Fatigue Evaluation and Field Monitoring of the I-39 Northbound Bridge over the Wisconsin River*. ATLSS Report No. 05-04, Lehigh University's Center for Advanced Technology for Large Structural Systems (ATLSS), Bethlehem, PA.

Mansour, A.E., Wirsching, P.H., White G.J., and Ayyub B.M. (1996). *Probability-based ship design: implementation of design guidelines*. Ship Structures Committee Report SSC 392. Ship Structures Committee. Washington D.C.

Marsh, P.S. and Frangopol, D.M. (2008), Reinforced concrete bridge deck reliability model incorporating temporal and spatial variations of probabilistic corrosion rate sensor data. *Reliability Engineering and System Safety*, 93 (3), 394–409

Martinez, W.L, and Martinez A.R. (2002). *Computational Statistics handbook with MATLAB*. Boca Raton: Chapman & Hall/CRC.

MathWorks Inc. (2010). *Optimization toolbox™ user's guide*. Version 5.0, MathWorks Inc, Natick, MA.

MathWorks Inc. (2011a). *Global optimization toolbox™ user's guide*. Version 3.1.1, MathWorks Inc., Natick, MA.

MathWorks Inc. (2011b). *Optimization toolbox™ user's guide*. Version 6.0. MathWorks, Inc., USA.

MathWorks Inc. (2011c). *Statistics toolbox™ user's guide*. Version 7.5, MathWorks, Inc., Natick, MA.

MathWorks Inc. (2012). *Signal processing toolbox™ user's guide*. Version 6.17, MathWorks Inc, Natick, MA.

MathWorks Inc. (2013). *Global optimization toolbox™ user's guide*. Version 3.2.4, MathWorks Inc., Natick, MA.

MathWorks Inc. (2014a). *Global optimization toolbox™ user's guide*. Version 3.2.5, MathWorks Inc., Natick, MA.

MathWorks Inc. (2014b). *MATLAB Programming Fundamentals*. Version 8.3. MathWorks Inc., Natick, MA.

Mattson, S.G., and Pandit, S.M. (2006). Statistical moments of autoregressive model residuals for damage localisation, *Mechanical Systems and Signal Processing*, 20(3), 627-645.

McCuen, R.H., and Albrecht, P. (1995). *Composite modeling of atmospheric corrosion penetration data*. Application of accelerated corrosion tests to service life prediction of materials, *ASTM STP 1194*, Philadelphia, 65–102.

Melchers, R.E. (1999). *Structural Reliability Analysis and Prediction*, Second Edition, John Wiley & Sons Ltd., Chichester, England.

Melchers, R.E. (2002). Effect of temperature on the marine immersion corrosion of carbon steels. *Corrosion* (NACE) 58(9): 768–782.

Melchers, R.E. (2003a). Modeling of marine immersion corrosion for mild and low alloy steels – Part 1: phenomenological model. *Corrosion* (NACE), 59(4), 319– 334

Melchers, R.E. (2003b). Probabilistic models for corrosion in structural reliability assessment - Part 2: Models based on mechanics. *Journal of Offshore Mechanics and Arctic Engineering*, 125(4), 272–280.

Melchers, R.E. (2004a). Pitting corrosion of mild steel in marine immersion environment – Part 1: maximum pit depth. *Corrosion* (NACE), 60(9), 824–836.

Melchers, R.E. (2004b). Pitting corrosion of mild steel in marine immersion environment – Part 2: variability of maximum pit depth. *Corrosion* (NACE) 60(10), 937–944.

Melchers, R.E. (2004c) Mathematical modeling of the effect of water velocity on the marine immersion corrosion of mild steel coupons. *Corrosion* (NACE), 60(5), 471–478.

Melchers, R.E. (2006). Recent progress in the modeling of corrosion of structural steel immersed in seawaters. *Journal of Infrastructure Systems*, 12(3), 154–162.

Metropolis, N., Rosenbluth, A., Rosenbluth, M., Teller A., and Teller E., (1953). Equation of state calculations by fast computing machines. *The Journal of Chemical Physics*, 21 (6), 1087–1092.

Miner, M.A. (1945). Cumulative damage in fatigue. *Journal of Applied Mechanics*, 12(3), 159–164.

Minnesota Department of Transportation (MnDOT). (2014). *Transportation agency practices currently employed for bridge maintenance painting operations: Findings from a National Survey*. *Transportation Research Synthesis TRS1404*, Minnesota Department of Transportation, available online http://www.dot.state.mn.us/research/TRS/2014/TRS1404.pdf

Miyamoto, A., Kawamura, K., and Nakamura, H. (2000). Bridge management system and maintenance optimization for existing bridges. *Computer-Aided Civil and Infrastructure Engineering*, Blackwell Publishers, 15(1), 45-55.

Moan, T., and Song, R. (2000). Implications of inspection updating on system fatigue reliability of offshore structures, *Journal of Offshore Mechanics and Arctic Engineering*, 122(3), 173-180.

Mori, Y., and Ellingwood, B.R. (1993). Reliability-based service-life assessment of aging concrete structures. *Journal of Structural Engineering*, 119 (5), 1600–1621.

Mori, Y., and Ellingwood B.R. (1994). Maintaining reliability of concrete structures. II: optimum inspection/repair. *Journal of Structural Engineering*, 120(3), 846-862.

Moses, F., Schilling C. G., and Raju K.S. (1987). *Fatigue Evaluation Procedures for Steel Bridges*, NCHRP Report 299, National Cooperative Highway Research Program, Washington, DC.

Munse, W.H., Wilbur, T.W., Tellalian, M.L., *et al*. (1982). Fatigue Characterizations of Fabricated Ship Details for Design. *Ship Structure Committee* Report No. SSC-318, Ship Structure Committee, Washington, DC.

Neal, R.M. (2003). Slice sampling. *The Annuals of Statistics*, Institute of Mathematical Statistics, 31(3), 705-767.

Neves, L.A.C., Frangopol, D.M., and Cruz, P.J.S. (2006a). Probabilistic lifetime-oriented multi-objective optimization of bridge maintenance: single maintenance type. *Journal of Structural Engineering*, 132(6), 991-1005.

Neves, L.A.C., Frangopol, D.M., and Petcherdchoo, A. (2006b). Probabilistic lifetime-oriented multi-objective optimization of bridge maintenance: combination of maintenance types. *Journal of Structural Engineering*, 132(11), 1821-1834.

Ni, Y.Q., Ye, X.W. and Ko, J. M., (2010). Monitoring-Based Fatigue Reliability Assessment of Steel Bridges: Analytical Model and Application. *Journal of Structural Engineering*, 136(12), 1563-1573.

Niemi, E., (1995). *Stress Determination for Fatigue Analysis of Welded Components*, 53-65, International Institute of Welding, Abington Publishing, Abington, Cambridge.

O'Rourke, R. (2012). *Naval littoral combat ship (LCS) program: background and issues for congress*, CRS Report for Congress, Congressional Research Service, Washington, D.C.

Okasha, M.N., and Frangopol D.M. (2009). Time-variant redundancy of structural systems. *Structure and Infrastructure Engineering*, 6(1-2), 279-301.

Okasha, N.M., and Frangopol, D.M. (2010a). Novel approach for multi-criteria optimization of life-cycle preventive and essential maintenance of deteriorating structures. *Journal of Structural Engineering*, 136(8), 1009-1022.

Okasha, N.M. and Frangopol, D.M., (2010b). Redundancy of structural systems with and without maintenance: An approach based on lifetime functions. *Reliability Engineering & System Safety*, 96(5), 520-533.

Okasha, N.M. and Frangopol, D.M., (2010c). Advanced modeling for efficient computation of life-cycle performance prediction and service-life estimation of bridges. *Journal of Computing in Civil Engineering*, 24(6), 548-556.

Okasha, N.M. and Frangopol, D.M., (2011). Computational platform for the integrated life-cycle management of highway bridges. *Engineering Structures*, 33(7), 2145-2153.

Okasha, N.M., Frangopol D.M. (2012). Integration of structural health monitoring in a system performance based life-cycle bridge management framework. Structure and Infrastructure Engineering 8(11): 999–1016.

Okasha, N.M., Frangopol D.M., Decò A. (2010). Integration of structural health monitoring in life-cycle performance assessment of ship structures under uncertainty, Marine Structures 23(3): 303–321.

Okasha, N.M., Frangopol D.M., Saydam D., Salvino L.W. (2011). Reliability analysis and damage detection in high speed naval crafts based on structural health monitoring data. Structural Health Monitoring 10(4): 361–379.

Okasha, N.M, Frangopol, D.M., Fletcher, F., and Wilson, A. (2012). Life-cycle cost analyses of a new steel for bridges. *Journal of Bridge Engineering*, 17(1), 168–172.

Orcesi, A.D., and Cremona, C.F. (2009). Optimization of management strategies applied to the national reinforced concrete bridge stock in France. *Structure and Infrastructure Engineering*, 5(5), 355 – 366.

Orcesi A.D., and Frangopol D.M. (2011a). A stakeholder probability-based optimization approach for cost-effective bridge management under financial constraints. *Engineering Structures*, 33, 1439-1449.

Orcesi A.D., and Frangopol D.M. (2011b). Use of lifetime functions in the optimization of nondestructive inspection strategies for bridges. *Journal of Structural Engineering*, 137, 531-539.

Orcesi, A., and Frangopol, D.M. (2013). "Bridge Performance Monitoring Based on Traffic Data." *Journal of Engineering Mechanics*, 139(11), 1508-1520.

Paik, J.K. and Frieze, P.A., (2001). Ship structural safety and reliability. *Progress in Structural Engineering and Materials*, 3, 198-210.

Paik, J.K., and Wang, G. (2003). Time-dependent risk assessment of ageing ships accounting for general/pit corrosion, fatigue cracking and local dent damage. *World Maritime Technology Conference*, San Francisco, CA.

Paik, J.K., Lee, J.M., Hwang, J.S., and Park, Y.I. (2003a). A time-dependent corrosion wastage model for the structures of single and double hull tankers and FSOs and FPSOs. *Marine Technology*, 40(3), 201–217.

Paik, J.K., Lee, J.M., Park, Y.I., Hwang, J.S., and Kim, C.W. (2003b). Time-variant ultimate longitudinal strength of corroded bulk carriers. *Marine Structures*, 16, 567–600.

Paris, P.C., and Erdogan**,** F.A. (1963). Critical analysis of crack propagation laws. *Journal of Basic Engineering*, 85(Series D), 528–534.

Pennsylvania Department of Transportation (PennDOT) (2013). District 5-0, Bridge Inspection Unit, personal communication

Perrin, F., Sudret, B., and Pendola, M. (2007). Bayesian updating of mechanical models-application in fracture mechanics. *18 ème Congrès Françes de Mèçanique*, Grenoble, 27-31.

Pollock, A. (2007). Probability of Detection for Acoustic Emission. *Journal of Acoustic Emission*, 25, 231-237.

Pollock, A. (2010). A POD Model for Acoustic Emission-Discussion and Status. CP1211 *In Review of Progress in Quantitative Nondestructive Evaluation, Vol. 209, eds. D.O. Thompson and D.E. Chimenti*, AIP Publishing, Melville, NY, 1927-1933.

Radaj, D., Sonsino, C.M., and Fricke, W., (2006). *Fatigue assessment of welded joints by local approaches*. Second Edition, 33-90, Woodhead Publishing and Maney Publishing on behalf of The Institute of Materials, Minerals & Mining, CRC Press, Boca Raton Boston, New York, Washington DC.

Ramirez, C.M., Liel, A.B., Mitrani-Reiser, J., Haselton, C.B., Spear, A.D., Steiner, J., Deierlein, G. G., and Miranda, E. (2012), Expected earthquake damage and repair costs in reinforced concrete frame buildings, *Earthquake Engineering & Structural Dynamics*, 41, 1455-1475.

Rausand, M., and Høyland, A. (2004). *System Reliability Theory: Models, Statistical Methods, and Applications*, John Wiley & Sons, New York.

Righiniotis, T.D. (2004). Influence of management actions on fatigue reliability of a welded joint. *International Journal of Fatigue*, 26(3), 231-239.

Robert, C.P., and Cassella, G. (1999). *Monte Carlo Statistical Methods*, Springer Texts in Statistics, Springer, Verlag, New York, USA.

Salvino, L.W., and Brady, T.F. (2008). Hull monitoring system development using hierarchical framework for data and information management. *Proceedings of the 7th International Conference on Computer and IT Applications in the Marine Industries (COMPIT'08)*, Liège, Belgium.

Schijve, J. (2003). Fatigue of structures and materials in the 20th century and the state of the art. *International Journal of Fatigue*, 25(8), 679-702.

Shiraki, N., Shinozuka, M., Moore, J.E., Chang, S.E., Kameda, H., and Tanaka, S. (2007). System risk curves: probabilistic performance scenarios for highway networks subject to earthquake damage. *Journal of Infrastructure Systems*, 213(1), 43–54.

Sielski, R.A. (2007). Research needs in aluminum structure. *Proceedings of the 10th International Symposium on Practical Design of Ships and Other Floating Structures*, American Bureau of Shipping, Washigton, D.C.

Sielski, R.A., Nahshon, K., Salvino, L.W., Anderson, K., and Dow, R. (2012). The ONR ship structural reliability program. *Proceedings of the 2012 ASNE Day*, Arlington, VA

Sohanghpurwal, A.A. (2006). Manual on service life of corrosion-damaged reinforced concrete bridge superstructure elements. NCHRP Report 558, *Transportation Research Board, National Cooperative Highway Research Program*, Washington D.C.

Soliman, M., and Frangopol, D.M., (2012). Inspection planning for steel bridges subjected to fatigue and corrosion. *Proceedings of the IABSE Conference, Global Thinking in Structural Engineering: Recent Achievements*, Sharm El-Sheikh, Egypt, May 7-9, 2012.

Soliman, M., and Frangopol, D.M., (2013a). Fatigue assessment of high-speed naval vessels based on structural health monitoring. *Proceedings of the 11th International Conference on Structural Safety & Reliability* (ICOSSAR 2013), Columbia University, NY, June 16-20, 2013.

Soliman, M., and Frangopol, D.M., (2013b). Reliability and remaining life Assessment of fatigue critical steel structures: Integration of inspection and monitoring information. *Proceedings of the ASCE Structures 2013 Congress*, Pittsburgh, PA, May 2-4, 2013.

Soliman, M., and Frangopol, D.M. (2014a). Life-cycle management of fatigue sensitive structures integrating inspection information, *Journal of Infrastructure Systems*, 20(2), 04014001.

Soliman, M., and Frangopol, D.M., (2014b). Life-cycle cost evaluation of conventional and corrosion-resistant steel for bridges. Technical Note, *Journal of Bridge Engineering*, ASCE, 10.1061/(ASCE)BE.1943-5592.0000647, 06014005 (in press).

Soliman, M., and Frangopol, D.M., (2014c). Reliability quantification and service life prediction of high-speed naval vessels based on SHM data. *Proceedings of the*

IMAC XXXII Conference and Exposition on Structural Dynamics, Orlando, Florida, USA, February 3-6, 2014.

Soliman, M., Frangopol, D.M., Kim, S. (2013a). Probabilistic optimum inspection planning of steel bridges based on multiple fatigue sensitive details. *Engineering Structures*, 49, 996–1006.

Soliman, M., Frangopol, D.M., and Kim, S. (2013b). Optimum inspection and maintenance planning for steel bridges under uncertainty. *Proceedings of the 11th International Conference on Structural Safety & Reliability* (ICOSSAR 2013), Columbia University, NY, June 16-20, 2013.

Soliman, M., Frangopol, D.M., and Kwon, K. (2013c). Fatigue assessment and service life prediction of existing steel bridges by integrating SHM into a probabilistic bi-Linear S-N approach. *Journal of Structural Engineering*, 139(10), 1728-1740

Soliman, M., Barone, G., and Frangopol, D.M., (2014a). Fatigue reliability and service life prediction of aluminum high-speed naval vessels based on structural health monitoring. *Structural Health monitoring*, doi:10.1177/1475921714546059.

Soliman, M., Frangopol, D.M., and Modoro, A., (2014b). A probabilistic approach for optimizing inspection, monitoring, and maintenance actions on fatigue critical ship details. *Journal of Ship Research*, (Submitted).

Stanish, K.D., Hooton, R.D., and Thomas, M.D.A. (1997). Testing the chloride penetration resistance of concrete: a literature review. FHWA contract DTFH61 (1997): 19-22.

Stein, S., Young, G., Trent, R. and Pearson, D. (1999). Prioritizing scour vulnerable bridges using risk. *Journal of Infrastructure Systems*, 5(3), 95-101.

Stewart, M.G. (2004). Spatial variability of pitting corrosion and its influence of structural fragility and reliability of RC beams in flexure. *Structural Safety*, 26(4), 453-470.

Stewart, M.G. (2006). Spatial variability of damage and expected maintenance costs for deteriorating RC structures. *Structure and Infrastructure Engineering*, 2(2), 79 – 90.

Swartz, R.A., and Lynch, J.P., (2008). Damage characterization of the Z24 Bridge by transfer function pole migration. *Proceedings of the International Modal Analysis Conference (IMAC) XXVI*, February 4-6, Orlando, Florida, USA.

T.S.K., (2013). *Microwave type wave height meter WM-2*. The Tsurumi-Seiki Co. Ltd. 9 April 2013 < http://www.tsk-jp.com/upload/product/pdf/WM2_E.pdf >

Tada, H., Paris, P.C., Irwin, G.R. (2000). *The stress analysis of cracks handbook*. Third Edition, The American Society of Mechanical Engineers, Three Park Avenue, New York.

Torres-Acosta, A.A., and Martinez-Madrid. M. (2003). Residual life of corroding reinforced concrete structures in marine environment. *Journal of Materials in Civil Engineering*, 15(4), 344-353.

Tscheliesnig, P. (2006). Detection of corrosion attack on oil tankers by means of acoustic emission (AE). *Proceedings of the 12th A-PCNDT 2006 – Asia-Pacific Conference on NDT*, Auckland, New Zealand.

Tveiten, B.W., (1999). *Fatigue Assessment of Welded Aluminium Ship Details*, A Thesis submitted for the Degree of Doctor of Philosophy, Department of Marine Structures, Norwegian University of Science and Technology.

Val, D.V., and Melchers, R.E. (1997). Reliability of deteriorating RC slab bridges. *Journal of Structural Engineering*, 123(12), 1638-1644.

Maslouhi, A. (2011). Fatigue crack growth monitoring in aluminum using acoustic emission and acousto-ultrasonic methods. *Structural Control and Health Monitoring*, 18(7), 790-806.

Violette, F.L.M., Polezhayeva, H.A., and Chung, H.W. (1998). Basic Parameters Governing the Fatigue of Aluminum Ships. *In 3rd International Forum on Aluminium Ships*. Haugesund, Norway.

VisualScript, (2006), *Design integration toolkit, version 5.2, getting started manual*. Vanderplaats R&D, Colorado Springs, CO.

Wang, G., Lee, A., Ivanov, L., Lynch, T., Serratella, C., Basu, R. (2008). A statistical investigation of time-variant hull girder strength of aging ships and coating life. *Marine Structures*, 21(2-3), 240–256.

Wang, G., Michael, L., Serratella, C., Botten, S., Ternowchek, S., Ozevin, D., Thibault, J., and Scott, R. (2010). Testing of acoustic emission technology to detect cracks and corrosion in the marine environment. *Journal of Ship Production and Design* 26(2), 106–110

Wang, Z.W., Zhou, M., Slabaugh, G.G., Zhai, J., and Fang, T. (2011). Automatic detection of bridge deck condition from ground penetrating radar images. *IEEE Transactions on Automation Science and Engineering*, 8(3), 633-640.

Wirsching, P.H. (1984). Fatigue reliability for offshore structures. *Journal of Structural Engineering*, 110(10), 2340-2356.

Yang, S.-I., Frangopol, D.M. and Neves, L.C. (2004). Service life prediction of structural systems using lifetime functions with emphasis on bridges. *Reliability Engineering and System Safety*, 86 (1), 39–51

Yazdani, N. and Albrecht, P. (1987). Risk Analysis of Fatigue Failure of Highway Steel Bridges. *Journal of Structural Engineering*, 113(3), 483-500.

Yazdani, N. and Albrecht, P. (1990). Probabilistic fracture mechanics application to highway bridges. *Engineering Fracture Mechanics*, 34, 969-985.

Ye, X.W., Ni, Y.Q., Wong, K.Y., and Ko, J.M. (2012). Statistical analysis of stress spectra for fatigue life assessment of steel bridges with structural health monitoring data. *Engineering Structures*, 45(12), 166-176.

Ye, N., and Moan, T. (2008). Improving fatigue life for aluminium cruciform joints by weld toe grinding. *Fatigue and Fracture of Engineering materials and structures*, 31(2), 152-163.

Yen, B.T., Hodgson, I.C., Zhou, E. and Crudele, B.B. (2009). Estimation of fatigue life below CAFL. *Proceedings of the second International Conference on Fatigue and Fracture in the Infrastructure,* Philadelphia, PA.

Yen, B.T., Hodgson, I.C., Zhou, Y.E. and Crudele, B.B. (2013). Bilinear S-N curves and equivalent stress ranges for fatigue life estimation. *Journal of Bridge Engineering*, 18(1), 26–30.

Yu, J., Ziehl, P., Zárate, B., and Caicedo, J. (2011). Prediction of fatigue crack growth in steel bridge components using acoustic emission. *Journal of Constructional Steel Research*, 67(8), 1254-1260.

Zayed, T.M., Chang, L.-M., and Fricker, J.D. (2002). Life-cycle cost based maintenance plan for steel bridge protection systems. *Journal of Performance of Constructive Facilities*, 16(2), 55-62.

Zheng, R. and Ellingwood, B.R. (1998). Role of non-destructive evaluation in time-dependent reliability analysis. *Structural Safety*, 20, 325-339.

Zhu, B., and Frangopol, D.M. (2013a). Reliability assessment of ship structures using Bayesian updating. *Engineering Structures*, 56, 1836-1847

Zhu, B., and Frangopol, D.M. (2013b). Incorporation of structural health monitoring data on load effects in the reliability and redundancy assessment of ship cross-sections using Bayesian updating, *Structural Health Monitoring,* 12(4), 377-392.

APPENDIX A: LIST OF NOTATIONS

Chapter 2

A = Fatigue detail coefficient for each S-N category

a = Crack size

A_1 = Area representing the time to failure CDF

A_2 = Area representing the survivor function

$A_r(t)$ = Remaining cross sectional area of reinforcement

$A_s(t)$ = The reinforcement area at time t

b_1 = Slope of the logarithmic transformation

b_o = Corrosion losses after one year

C = Crack growth material parameter

$C(x, t)$ = Chloride concentration at a distance x from the surface and time t

C_0 = Chloride concentration on concrete surface

C_c = Concentration of chloride ions

C_{cr} = Threshold level of chloride concentration

D = Miner's damage accumulation index

$d(t)$ = Time dependent corrosion depth

$D(t)$ = Miner's time dependent damage accumulation index

D_c = Effective chloride diffusion coefficient

d_∞ = Model parameters of corrosion wastage prediction model

d_o = Initial diameter of rebars

$F_T(t)$ = Time to failure CDF

$F_R(x,t)$ = Instantaneous CDF of resistance at time t

$f_S(x,t)$ = Instantaneous PDF of the load effects at time t

$f_T(t)$ = Time to failure PDF

$f_S(s)$ = PDF of the stress range

g = Performance function

$g(t)$ = Time-variant performance function

g_i = Performance function of the *i*th component

K = Stress intensity factor

m = The slope of the *S*-*N* line

N = Number of cycles

N_{avg} = Average annual number of cycles

N_i = Number of cycles to failure under the stress range S_i

N_T = Total number of cycles in the stress range histogram

n_i = Number of stress cycles in the ith bin with stress range S_i

n_s = Number of rebars subjected to corrosion

n_{ss} = Number of stress range bins in a stress-range histogram

$P(\cdot)$ = Probability of event between parenthesis

P_f = Probability of failure

P_{fsys} = System probability of failure

$PT(t)$ = Maximum penetration of pitting corrosion time t

p = Corrosion losses after t years

Q = Demand random variable

$Q(t)$ = Time-variant demand random variable

R = Resistance random variable

$R(t)$ = Time-variant resistance random variable

R_c = Ratio of maximum pit depth to average pit depth

r_{corr} = Rate of corrosion

S = Stress range

$S_T(t)$ = Survivor function

S_i = Stress range in the ith bin of the stress range histogram

S_{re} = Equivalent constant amplitude stress range

S_{ro} = Mode of the Rayleigh distribution

s_c = Distribution threshold

T = Time to failure random variable

T_I = Corrosion initiation time

t	=	Time
t_i	=	Fatigue life in years
t_L	=	Time period for load effects following Poisson's process
x	=	Distance from outer surface of the solid
$Y(a)$	=	Correction factor for crack growth model
α	=	Scale parameter of the Weibull distribution
β	=	Reliability index
Δ	=	Miner's critical damage accumulation index
ΔK	=	Range of the stress intensity factor
Δt	=	Time interval
ζ	=	Scale parameters of the lognormal distribution
κ	=	Shape parameters of the Weibull distribution
λ	=	Location parameter of the lognormal distribution
λ_o	=	mean occurrence rate of load effects following Poisson's process
μ_i	=	Mean value of random variable i
σ_i	=	Standard deviation of random variable i
τ_c	=	Model parameters of corrosion wastage prediction model
$\Phi^{-1}(\cdot)$	=	Inverse standard normal CDF
$\bigcup$	=	Union
$\bigcap$	=	Intersection

CHAPTER 3

A	=	Fatigue detail coefficient for each category
A_1	=	Fatigue detail coefficients above the CAFT
A_2	=	Fatigue detail coefficients below the CAFT
$D(t)$	=	Miner's damage accumulation index
$f_s(s)$	=	PDF of the distribution of the stress range
$g(t)$	=	Performance function for fatigue reliability
m	=	Value of the single slope of the *S*-*N* line
m_1	=	Slopes of the *S*-*N* lines above the CAFT
m_2	=	Slopes of the *S*-*N* lines below the CAFT
N	=	Number of cycles
$N(t)$	=	Number of cycles at time t
N_{avg}	=	Average daily number of cycles
n_i	=	Number of cycles in the predefined stress range bin S_{ri}
n_{total}	=	Total number of cycles in the stress range bin histogram
n_i^o	=	Number of cycles in the stress range bin S_{ri} greater than CAFT
n_j^o	=	Number of cycles in the stress range bin S_{rj} less than CAFT
P_f	=	Probability of violating a certain limit state
S	=	Stress range random variable
S_r	=	Variable amplitude stress range
S_{re}	=	Equivalent constant amplitude stress range
S_{ri}	=	Stress range associated with the i-th bin in the histogram
S_{re}^L	=	Equivalent constant amplitude stress ranges calculated using the linear *S*-*N*
S_{re}^B	=	Equivalent constant amplitude stress ranges calculated using the bi-linear *S*-*N*
s_c	=	Cut-off threshold
T_{rem}	=	Remaining fatigue life
t	=	Time
t_s	=	Number of elapsed service years of the bridge
β	=	Reliability index

$\beta\,(t)$	=	Reliability index at time t
Δ	=	Miner's critical damage accumulation index
ΔF	=	Fatigue resistance (stress range)
ζ	=	Scale parameters of the lognormal distribution
λ	=	Location parameter of the lognormal distribution
$\Phi^{-1}(\cdot)$	=	Inverse standard normal CDF

CHAPTER 4

A	=	Fatigue coefficient dependent on the type of the detail
$D(t)$	=	Miner's damage accumulation index
D^*	=	Approximate damage accumulation index
D_j	=	Annual damage accumulation index for the detail associated with the *j*th operational condition
D_T	=	Total damage accumulation index
m	=	Slope of the *S*-*N* lines in logarithmic scale
N_{avg}	=	Average annual number of cycles
$N_{avg\,j}$	=	Average number of cycles acting on the detail during one year of exposure to the *j*th operational condition
n_o	=	Number of operational conditions encountered by the ship during the reference time T_r
o_r	=	Annual ship operation rate
P_f	=	Probability of violating a certain limit state
p_j	=	Probabilities of occurrence of different sea states, speeds, and heading angles
S	=	Stress acting on the detail
S_{re}	=	Equivalent constant amplitude stress rang
S_{re_j}	=	Constant equivalent stress range acting on the detail at the *j*th operational condition
T_r	=	Reference time for computing fatigue life
T_{rem}	=	Remaining fatigue life
t_f	=	Fatigue life
t_{f_j}	=	Fatigue life under the *j*th operational condition
t_p	=	Plate thickness
t_s	=	Already spent service life
β_{target}	=	Fatigue reliability threshold
Δ	=	Miner's critical damage accumulation index
ζ	=	Scale parameters of the lognormal distribution
λ	=	Location parameter of the lognormal distribution

$\Phi^{-1}(\cdot)$ = Inverse standard normal CDF

CHAPTER 5

a	=	Crack size
a_{min}	=	Minimum detectable crack size
a_o	=	Initial crack size
a_r	=	Critical crack size for repair
C	=	Crack growth parameter
$C^{(insp)}$	=	Cost of a single inspection
$C^{(insp,d)}$	=	Cost of a single in-depth inspection action
$C^{(m_A)}$	=	Cost of a single maintenance A
$C^{(m_B)}$	=	Cost of a single maintenance B
$C^{(mon)}$	=	Cost of a single monitoring
C_1^{mon}	=	Initial monitoring cost
C_2^{mon}	=	Monitoring cost depending on the monitoring duration
C_f	=	Monetary loss associated with the failure of the damaged location
C_{insp}	=	Total cost of inspection
$C_{insp,d}$	=	Total cost of in-depth inspection
C_k	=	Total cost associated with branch k
C_{main}	=	Total cost of maintenance action
C_{mon}	=	Total cost of monitoring action
D_k	=	Maintenance delay associated with the *k*-th branch
d_A	=	First damage criterion for determining a maintenance type
d_B	=	Second damage criterion for determining a maintenance type
d_o	=	Initial diameter of the reinforcement
$E[C_{total}]$	=	Expected total life-cycle cost
$E[D]$	=	Expected maintenance delay
$E[T]$	=	Expected service life
$F_T(t)$	=	Time to failure CDF
$f_T(t)$	=	Time to failure PDF
m	=	Crack growth exponent

N_A = Number of maintenance A associated with the *k*-th branch

N_{avg} = Average annual number of cycles

N_B = Number of maintenance B associated with the *k*-th branch

N_I = Number of interventions

N_{insp} = Number of inspections associated with the *k*-th branch

$N_{insp,d}$ = Number of in=depth inspections associated with the *k*-th branch

N_{mon} = Number of monitoring associated with the *k*-th branch

$P(\cdot)$ = Probability of event between parenthesis

P_f = Probability of failure

PoD = Probability of damage detection

PT = Maximum pit depth for reinforcement corrosion

R_{tmd} = *PoD* reduction factor depending on the monitoring duration

r_d = Annual discount rate of money

r_{ins} = Constant to determine the cost of inspection

S_{re} = Stress range

T = Time to failure

T_k = Service life associated with the *k*-th branch

T^A = Service life extension associated with the application of maintenance A

T^B = Service life extension associated with the application of maintenance B

T^o = Initial service life with no maintenance

$t_{insp,d}^{(j)}$ = *j*-th in-depth inspection time

$t_{insp}^{(l)}$ = *l*-th inspection time

$t_{mon}^{(m)}$ = *m*-th monitoring time

$t_A^{(n)}$ = *n*-th maintenance A time

$t_B^{(y)}$ = *y*-th maintenance B time

t^* = Required service life

t_{eff} = Effective duration of maintenance

t_i = Time of *i*-th intervention

t_{md} = Monitoring duration

t_{occ}	=	Damage occurrence time
$Y(a)$	=	Correction factor for crack growth model
α	=	*PoD* function parameter
α_δ	=	Damage intensity at which the given inspection method has 50% *PoD*
β	=	*PoD* function parameter
δ	=	Damage intensity
Δt	=	Time interval
δ_{thres}	=	Threshold of damage intensity
λ	=	Scale parameter
$\Phi[\cdot]$	=	Standard normal CDF

CHAPTER 6

a	=	Crack size
a_I	=	Lower crack size threshold for determining the appropriate management actions
a_{II}	=	Upper crack size threshold for determining the appropriate management actions
$a_{insp,i}$	=	Crack size measured at the *i*th inspection
a_o	=	Initial crack size
$a_{p,i}$	=	Predicted data at the *i*th inspection
C	=	Crack growth material parameter
C_{fail}	=	Monetary losses as a result of the crack reaching it critical size
$\mathbf{C}_{insp}$	=	Vector consisting of the cost of performing a single inspection using each of the available inspection types
$C_{insp,i}$	=	Cost of performing the *i*th inspection
C_{insp}^{T}	=	Total inspection cost
c	=	Surface half-length of a surface crack
$\mathbf{d}$	=	Vector of observed data
d_i	=	Observed data at the *i*th inspection
$E(a_p(t_{insp,1}))$	=	Mean of the predicted crack size at the first inspection
$E(C_{\text{fail}})$	=	Expected failure cost
$E(C_{total})$	=	Expected total cost
$E(k)$	=	Complete elliptical integral of the second kind
F_e	=	Correction factor taking into account the effect of the elliptical crack shape,
F_g	=	Correction factor taking into account the effect of non-uniform stress acting on the crack
F_s	=	Correction factor taking into account the effect of free surface
F_w	=	Correction factor taking into account the effect of finite width (or thickness)
$F_T(t)$	=	Cumulative probability of failure
K_{tm}	=	Maximum stress concentration factor at the weld toe
m	=	Crack growth exponent
n	=	Number of scheduled inspections
n_b	=	Number of samples that may not represent the posterior distribution

(i.e., burn-in period)

$P(\cdot)$	=	Probability of event between parenthesis
$P(\mathbf{d}\|\boldsymbol{\theta})$	=	Likelihood function of obtaining information **d** conditioned by $\boldsymbol{\theta}$
$P(\boldsymbol{\theta})$	=	Prior distribution of model parameters
$P(\boldsymbol{\theta}^*\|\boldsymbol{\theta}_t)$	=	Proposal distribution
$P(\boldsymbol{\theta}\|\mathbf{d})$	=	Posterior distribution of model parameters
PD	=	Probability of detecting the crack before failure
P_{fail}	=	Probability of failure
$\overline{PoD}(t_{insp,i-1})$	=	Probability of not detecting the crack at the $(i-1)$ th inspection
$PoD(t_{insp_i})$	=	Probability of crack detection at the *i*th inspection
r	=	Annual discount rate of money
$\hat{R}$	=	Potential scale reduction factor
S_{re}	=	Stress range
$S_T(t)$	=	Survivor function
T	=	Time to failure
t_a	=	Time associated with crack growth
t_{insp_1}	=	Time of application of the first inspection
t_w	=	Web thickness
$\hat{\text{var}}(\nu)$	=	Overall variance
W	=	Within-sequence variance
$Y(a)$	=	Geometry function for crack growth model
Z	=	Weld leg size
β	=	Scale parameters of the cumulative lognormal *PoD* curve
ζ	=	Gaussian noise parameter
$\boldsymbol{\theta}$	=	Vector of model parameters
$\boldsymbol{\theta}^*$	=	Candidate vector
λ	=	Location parameters of the cumulative lognormal *PoD* curve
σ_e	=	Single error term combining the measurement and modeling errors
υ	=	Scalar summary of interest

$\Phi(\cdot)$	=	Standard normal CDF
$\boldsymbol{\Psi}$	=	Matrix consisting of the *PoD* parameters different available inspection types

CHAPTER 7

$A_s(t)$	=	Reinforcement area at time t
a	=	Crack size
a_f	=	Critical crack size
a_o	=	Initial crack size
a_t	=	Crack size at time t
C	=	Crack growth material parameter
$\mathbf{C}_{insp}$	=	Vector consisting of the cost of performing a single inspection using each of the available inspection types
C_{insp}	=	Cost of a single inspection
C_o	=	Surface chloride concentration
C_{th}	=	Threshold limit of chloride concentration for reinforcement
C_{insp}^T	=	The present cost of n inspections
D	=	Effective chloride diffusion coefficient
d_o	=	Initial diameter of rebars
F_e	=	Correction factor taking into account the effect of the elliptical crack shape,
F_g	=	Correction factor taking into account the effect of non-uniform stress acting on the crack
F_s	=	Correction factor taking into account the effect of free surface
F_w	=	Correction factor taking into account the effect of finite width (or thickness)
L	=	Total number of inspected details
N	=	Number of cycles
N_{avg}	=	Average daily number of cycles
n	=	Number of scheduled inspections
n_s	=	Number of rebars subjected to corrosion effect
$P(\cdot)$	=	Probability of event between parenthesis
PD	=	Probability of detecting the crack before failure
$\overline{PoD}\left(t_{insp_{i-1}}, \rho_{i-1}\right)$	=	Probability of not detecting the crack at the $(i-1)$th inspection using the inspection method ρ_{i-1}
$PoD\left(t_{insp_j}, \rho_j\right)$	=	Probability of crack detection at the jth inspection using the inspection method ρ_j

r	=	Annual discount rate of money
r_{corr}	=	Rate of corrosion
S_{re}	=	Stress range
T	=	Time to failure
T_I	=	Corrosion initiation time
x	=	Depth of steel reinforcement from the concrete surface
$Y(a)$	=	Generalized stress intensity factor
$\delta(t)$	=	Time-dependent corrosion damage intensity
$\delta_{0.5}$	=	Damage intensity at which the inspection method has 50% probability of detection
ΔK	=	Range of the stress intensity factor
ζ	=	Scale parameters of the cumulative lognormal *PoD* curve
λ	=	Location parameters of the cumulative lognormal *PoD* curve
ρ	=	Inspection method identifier
σ_δ	=	Standard deviation of the damage intensity $\delta_{0.5}$
$\Phi(\cdot)$	=	Standard normal CDF
$\boldsymbol{\Psi}$	=	Matrix consisting of the *PoD* parameters different available inspection types

CHAPTER 8

$A(t)$	=	Time-variant cross-sectional area
$C_j^{(EM)}$	=	Costs of the *j*-th essential maintenance actions
$C^{(insp)}$	=	Inspection cost
$C_j^{(PM)}$	=	Cost of the *j*-th preventive maintenance actions
C^*	=	Cost of an *ideal* inspection
d_0	=	Initial diameter
$d_{bar}(t)$	=	Bar diameter at time t
DR	=	Deterioration rate
$E[\ ]$	=	Mean value of the quantity between parenthesis
f_y	=	Yield strength of the component material
F_y	=	Yield strength of the steel girders
$g_i(t)$	=	Performance function
$h_{sys}(t)$	=	System failure rate
I	=	Impact factor of girders
i_{corr}	=	Represents the rate of corrosion parameter
k_{insp}	=	Index of the inspection accuracy
$L(t)$	=	Time-variant axial load
$M_{deck}(t)$	=	Moments acting on the deck
$M_{gir,i}(t)$	=	Moments acting on the girder *i*
N_b	=	Number of branches
N_C	=	Number of components in a system
N_{insp}	=	Number of inspections
N_O	=	Possible repair options for each component
n_{bar}	=	Number of reinforcement bars in the deck
$P(\mathrm{B}_k)$	=	Probability of occurrence of branch *k*
$P_{EM,i}$	=	Probability of essential maintenance
$P_{NR,i}$	=	Probability of no repair
$P_{PM,i}$	=	Probability of preventive maintenance

$P_{sys}(t)$	=	Point-in-time annual failure probability of the system
$R_i^{(est)}$	=	Estimated capacity of the component i immediately after inspection
$R_i(t)$	=	Structural capacity of the components over time
r_d	=	Annual discount rate of money
$S_{sys}(t)$	=	Structural system survivor function
t	=	Time
TDP_{sys}	=	Cumulative distribution function of the system time-to-failure
T_{ini}	=	Initiation time of corrosion
t_{insp}	=	Inspection time
$t_j^{(EM)}$	=	j-th essential maintenance times
$t_{insp}^{(i)}$	=	The i-th inspection time
$t_j^{(PM)}$	=	j-th preventive maintenance times
t_{tot}	=	Observation time window
$Z_i(t)$	=	Plastic section modulus of the girder i
γ_d	=	Modeling uncertainty factors of the resistance of deck
γ_g	=	Modeling uncertainty factors of the resistance of girders
ΔC	=	Difference in cost
$\delta_{EM,i}$	=	Essential maintenance threshold
Δh	=	Difference in the maximum expected annual system failure rate
$\delta_{PM,i}$	=	Preventive maintenance threshold
ΔT_{PM}	=	Effective time period of preventive maintenance
Δt	=	Time interval
η_i	=	Traffic load distribution factor
$\mu_A(t)$	=	Mean value of A at time t
$\mu_{R_i}(t_{insp})$	=	Mean value of the estimated capacity at time t_{insp}
$\sigma_A(t)$	=	Standard deviation of A at time t
σ_{insp}	=	Standard deviation of the estimated capacity at time t_{insp}
σ_{R_i}	=	Standard deviation of resistance accounting for the imperfections associated with the predictive model

CHAPTER 9

ADT = Average daily traffic

ADT_t = Average daily traffic at time t

C = Total cost of a maintenance action

C_E = Costs of carbon dioxide emissions

$C_{PV,k}$ = Present value of the cost of the kth maintenance action performed at time t

C_R = Direct cost of maintenance actions

C_{TL} = Cost associated with the time loss

c_{En} = Cost value of environmental metric

c_g = Time value of the goods transported in a cargo

c_w = Average wage per hour

d = Duration of maintenance

E = Environmental impact

$En_{d,c}$ = Environmental metric per unit distance for cars

$En_{d,t}$ = Environmental metric per unit distance for trucks

En_{S_D} = Carbon dioxide emissions per kilometer at speeds S_D

En_{S_o} = Carbon dioxide emissions per kilometer at speeds S_o

l = Length of the traffic control region

O_c = Average occupancy for cars

O_t = Average occupancy for trucks

S_D = restricted traffic speed

S_o = Un-restricted traffic speed

T = Ratio of the average daily truck traffic to the average daily traffic

t = Time

v = Annual increase rate in the average daily traffic

APPENDIX B: LIST OF ACRONYMS

AASHTO	:	American association of state highway and transportation officials
ADT	:	Average daily traffic
ADTT	:	Average daily truck traffic
AE	:	Acoustic emission
ASCE	:	American society of civil engineers
ATLSS	:	Engineering research center for advanced technology for large structural systems
CAFT	:	Constant amplitude fatigue threshold
CDF	:	Cumulative distribution function
COV	:	Coefficient of variation
DOT	:	Department of transportation
EC3	:	Eurocode 3
ECI	:	Eddy current inspection
EM	:	Essential maintenance
FAD	:	Failure assessment diagram
FEA	:	Finite element analysis
FHWA	:	Federal highway administration
FORM	:	First order reliability method
GA	:	Genetic algorithm
LEFM	:	Linear elastic fracture mechanics
LPI	:	Liquid penetrant inspection
LRFD	:	Load and resistance factor design

MCMC	:	Markov chain Monte Carlo
MPI	:	Magnetic particle inspection
NDI	:	Nondestructive inspection
NDT	:	Nondestructive testing
PD	:	Probability of damage detection before failure
PDF	:	Probability density function
PM	:	Preventive maintenance
PoD	:	Probability of damage detection
RC	:	Reinforced concrete
SHM	:	Structural health monitoring
S-N	:	Stress-life
SORM	:	Second order reliability method
UI	:	Ultrasonic inspection
USD	:	United States Dollar

VITA

Mohamed Soliman was born on May 05, 1981 in Alexandria, Egypt to Soliman E. Soliman and his wife Soheir Hassan. He received his Bachelor of Science Degree in Civil Engineering from Alexandria University, Egypt, in 2003. In 2008 he received his Masters of Science degree in the field of Structural Engineering also from Alexandria University, Egypt. In 2009, he was awarded the University Fellowship from Lehigh University to pursue his Ph.D. degree. During his Ph.D. work at Lehigh University, he was awarded the Lehigh University P.C. Rossin Fellowship in 2012, in addition to the 2014 J. James R. Croes Medal awarded by the American Society of Civil Engineers (ASCE) for co-authoring the paper "Generalized Probabilistic Framework for Optimum Inspection and Maintenance Planning", which was published in the March 2013 issue of the Journal of Structural Engineering. The Croes Medal is one of the two most prestigious awards given by the ASCE to one of more than 7,000 papers published in all of its 34 journals in the preceding year.